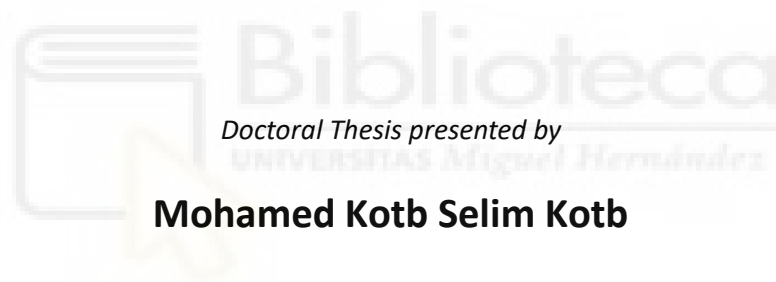




**Characterising White Matter Disruption in Alcohol Use Disorder:
A Deep TMS Intervention Study**



Doctoral Thesis presented by

Mohamed Kotb Selim Kotb

Thesis Director

Dr. Santiago Canals Gamoneda

Thesis Co-Director

Dr. Silvia De Santis

Doctoral Programme in Neurosciences

Miguel Hernández University of Elche

—2024—



This Doctoral Thesis, entitled "*Characterising White Matter Disruption in Alcohol Use Disorder: A Deep TMS Intervention Study*" is presented as a compendium of the following publications:

- Selim, M. K., Harel, M., De Santis, S., Perini, I., Sommer, W. H., Heilig, M., ... & Canals, S. (2024). Repetitive deep TMS in alcohol dependent patients halts progression of white matter changes in early abstinence. *Psychiatry and Clinical Neurosciences*, 78(3), 176-185.
DOI <https://doi.org/10.1111/pcn.13624>
- De Santis, S., Selim, M. K., & Canals, S. (2023). Brain Microstructure in Alcohol Addiction: Characterization of Diffusion-Based MRI Biomarkers, Neuropathological Substrates, and Functional Consequences. In *Alcohol and Alcohol-related Diseases* (pp. 493-508). Cham: Springer International Publishing.
DOI https://doi.org/10.1007/978-3-031-32483-3_27



Sant Joan d'Alacant, July 2024

Dr. Santiago Canals Gamoneda as Director, and Dr. Silvia De Santis as Co-Director of the doctoral thesis entitled: "*Characterising White Matter Disruption in Alcohol Use Disorder: A Deep TMS Intervention Study*"

INFORM:

That Mr. Mohamed Kotb Selim Kotb has carried out under our supervision the work entitled "*Characterising White Matter Disruption in Alcohol Use Disorder: A Deep TMS Intervention Study*" in accordance with the terms and conditions defined in his Research Plan and in accordance with the Code of Good Practice of the Miguel Hernández University of Elche, satisfactorily fulfilling the objectives foreseen for its public defence as a doctoral thesis.

We sign for appropriate purposes, in **Sant Joan d'Alacant** on **July** of **2024**.



Thesis director

Dr. Santiago Canals Gamoneda

Thesis Co-Director

Dr. Silvia De Santis



Sant Joan d'Alacant, July 2024

Dr. Maria Cruz Morenilla Palao, Coordinator of the Neurosciences PhD programme at the Institute of Neurosciences in Alicante, a joint centre of the Miguel Hernández University (UMH) and the Spanish National Research Council (CSIC),

INFORM:

That Mr. Mohamed Kotb Selim Kotb has carried out under the supervision of our PhD Programme the work entitled "*Characterising White Matter Disruption in Alcohol Use Disorder: A Deep TMS Intervention Study*" in accordance with the terms and conditions defined in its Research Plan and in accordance with the Code of Good Practice of the University Miguel Hernández of Elche, fulfilling the objectives satisfactorily for its public defence as a doctoral thesis.

Which I sign for the appropriate purposes, in **Sant Joan d'Alacant** on **of July of 2024**.

And for the record, for all due purposes, I sign this certificate.

Dr. Maria Cruz Morenilla Palao

Coordinator of the PhD Programme in Neurosciences



The Doctoral thesis entitled “*Characterising White Matter Disruption in Alcohol Use Disorder: A Deep TMS Intervention Study*”, carried out by me, Mohamed Kotb Selim Kotb, at the Institute of Neurosciences in Alicante (UMH-CSIC), has been supported by” la Caixa” Foundation (ID 100010434), INPhINIT doctoral fellowship (code: LCF/BQ/DI18/11660067) and Marie Skłodowska-Curie- COFUND agreement (Grant No. 713673).



يٰۤاَيُّهَا الَّذِيْنَ ءَامَنُوْا اِنَّمَا الْخَمْرُ وَالْمَيْسِرُ وَالْاَنْصَابُ وَالْاَزْلَامُ رِجْسٌ
مِّنْ عَمَلِ الشَّيْطٰنِ فَاَجْتَنِبُوْهُ لَعَلَّكُمْ تُفْلِحُوْنَ

سورة المائدة - الآية ٩٠

O you who have believed! Intoxicants, gambling, idolatry, and divination are abominations and Satan's doing. Shun them, so that you may prosper.

Quran, 5-90

¡Oh, creyentes! Los estupefacientes, juegos de azar, idolatría y adivinación son abominaciones y obra del Demonio. Aléjense de todo ello, que así podáis triunfar y prosperar.

Corán, 5-90

To my father's soul, whose wisdom and love continue to guide me,
and to my son, Harún, whose presence fills my life with joy and purpose.
This work is a tribute to both past inspirations and future hopes.



Acknowledgement

First and foremost, I want to express my gratitude to my thesis director, Prof. Santiago Canals, and my co-director, Dr. Silvia De Santis, for their invaluable guidance over the years.

Santiago, thank you for giving me the opportunity to grow within your team. Your mentorship has taught me how to critically analyse my work and harness my abilities to their fullest potential. I also appreciate your ability to dismantle my hypotheses in mere seconds, which has been both humbling and enlightening. Your impact on my development has been profound, both scientifically and personally, as you have guided me to become a better version of myself.

Silvia, I vividly remember your bit-by-bit guidance on navigating the path into academia. Despite your demanding schedule, you have always been there for me. Thank you for introducing me to the world of diffusion MRI. Without your effort, I would not have reached this point in my journey.

Santiago and Silvia, thank you both for always having your doors open and for your unhesitant support.

Even though they are far away, I must acknowledge my family for their unparalleled support. To my mom, my two brothers, Sameh and Abdelhamid, and my sister, Heba—thank you for being there when I needed you the most. Special thanks to my wife, Yamán, for enduring the ups and downs of my doctoral journey and for dedicating more time to our child while I focused on my research. I am also grateful to her family for their support. I love you all.

A big thank you to my friend, Amr, who helped me navigate the PhD process and answered my many questions about paperwork and science beforehand.

To all the Canals and De Santis lab members, past and present, thank you for sharing unforgettable moments. I am incredibly grateful for the technical support from our dedicated technicians in both labs and the MRI facility—without you, this work wouldn't have been possible.

I also want to thank the many collaborators who contributed to this work and the funding agencies. Special thanks to our institute manager, Maite, and the entire community at the Institute of Neurosciences. To my friends at the Islamic Centre of Alicante, especially Sheikh Mohamed Hager, and to everyone who has crossed my path and wished me well—thank you.

Finally, I want to thank myself for making it this far.

Acronyms

A

ACC - Anterior Cingulate cortex
AD - Axial Diffusivity
AMG - Amygdala
ANTs - Advanced Normalization Tools
ASD - Autism Spectrum Disorder
AUD - Alcohol Use Disorder
AX - Axonal Diameter

B

BBB - Blood Brain Barrier
BC - Before Christ
BNST - Bed Nucleus of the Stria Terminalis
BOLD - Blood Oxygenation Level Dependent

C

CC - Corpus Callosum
CHARMED - The Composite Hindered and Restricted Model of Diffusion
CNS - Central Nervous System
CSF - Cerebrospinal Fluid
CT - Computed Tomography

D

DAN - Dorsal Attention Network
Deep TMS - Deep Transcranial Magnetic Stimulation
dIPFC - dorsolateral Prefrontal Cortex
DMN - Default Mode Network
dmPFC - dorsomedial Prefrontal Cortex
DS - Dorsal Striatum
DSM-V - Diagnostic and Statistical Manual of Mental Disorders (fifth edition)

E

EEG - Electroencephalography
EPI - Echo Planar Imaging

F

FA - Fractional Anisotropy
FDA - Food and Drug Administration
FLAIR - Fluid-Attenuated Inversion Recovery
fMRI - functional Magnetic Resonance Imaging
FR - Restricted Fraction (refers to axonal density)
FEF - Frontal Eye Field

G

GABA - Gamma-Aminobutyric Acid
GFAP - Glial Fibrillary Acidic Protein
GLM - General Linear Model
GM - Grey matter
GP - Globus Pallidum

H

HARDI - High Angular Resolution Diffusion Imaging
HDR - Haemodynamic Response
Hippo - Hippocampus
HRF - Haemodynamic Response Function

L

LFP - Local Field Potential

LTP - Long Term Potentiation

M

MBP - Myelin Basic Protein

MD - Mean Diffusivity

MDD - Major Depressive Disorder

MEG - Magnetencephalography

MNI - Montreal Neurological Institute

mPFC - medial Prefrontal Cortex

MRI - Magnetic Resonance Imaging

MS - Multiple Sclerosis

N

NAc - Nucleus Accumbens

NF - Neurofilament

NIFTI - Neuroimaging Informatics Technology Initiative

NODDI - Neurite Orientation Dispersion and Density Imaging

O

OCD - Obsessives Compulsive Disorder

OFC - Orbitofrontal Cortex

OPCs - Oligodendrocyte Precursor Cells

P

PCC - Posterior Cingulate Cortex

PD - Proton Density

PET - Positron Emission Tomography

PFC - Prefrontal Cortex

PNS - Peripheral Nervous System

R

RD - Radial Diffusivity

RESTORE - Robust Estimation of Tensors by Outlier Rejection

RMT - Resting Motor Threshold

rs-fMRI - resting-state functional Magnetic Resonance Imaging

rTMS - repetitive Transcranial Magnetic Stimulation

S

SM - Standard Model

SNC - Substantia Nigra compacta

STEM - Scanning Transmission Electron Microscopy

SUDs - Substance Use Disorders

T

Thal - Thalamus

TMS - Transcranial Magnetic Stimulation

V

VTA - Ventral Tegmental Area

W

WMHs - White Matter Hyperintensities

WHO - World Health Organization

WM - White Matter

WMTI - White Matter Tract Integrity



Abstract

Alcohol use disorder (AUD) is the most prevalent form of addiction, imposing a substantial societal burden and offering limited treatment options. The intricate effects of AUD on the brain, particularly on white matter, are challenging to understand due to the disorder's complexity and associated comorbidities. This work aims to: (1) utilise advanced non-invasive diffusion MRI on a rat model of AUD to reveal the alcohol-induced effects on white matter microstructure; (2) translationally explain, through multimodal imaging, the clinical benefits of a recent trial on Deep Transcranial Magnetic Stimulation (Deep TMS) as a novel treatment for AUD; and (3) elucidate the potential mechanisms by which Deep TMS exerts therapeutic effects, reflected as preserved white matter structure, reduced craving, and relapse in treated patients. For the animal studies, we used the alcohol-preferring rat line (msP) and a two-bottle free choice paradigm for alcohol drinking. Advanced diffusion-weighted MRI techniques, combined with histology, were employed to investigate the effects of alcohol on white matter. Human studies involved AUD patients admitted to detoxification programmes and participating in a Deep TMS clinical trial. White matter integrity was compromised in the AUD rat model and patients relative to controls, as reflected by a widespread reduction in fractional anisotropy (FA). In AUD rats, advanced diffusion MRI revealed altered structure in the axonal bundles, with enlarged axonal diameter, decreased axonal density, and decreased myelin content. These findings were confirmed by histological analysis showing increased neurofilament and reduced myelin basic protein staining. In AUD patients, FA reduction progressed during early abstinence (3 weeks) in the absence of Deep TMS. However, stimulation of midline frontocortical areas halted the progression of FA changes, which was associated with decreased craving and relapse scores. Reconstruction of axonal tracts from white matter regions showing preserved FA values identified cortical regions in the posterior cingulate and dorsomedial prefrontal cortices, where functional connectivity was persistently modulated in the direction of healthy controls. These effects were not present in the sham-stimulated group. Advanced diffusion MRI has demonstrated sensitivity in non-invasively revealing distinctive alterations in axonal structure within the white matter induced by alcohol consumption. By integrating brain structure and function, this study characterises the alcohol-dependent brain and offers mechanistic insights into the therapeutic effects of Deep TMS, highlighting the potential role of rescuing axonal structure through adaptive myelination. These findings suggest the potential application of Deep TMS as a treatment to correct white matter microstructure alterations in general, and for AUD in particular.

Resumen

El Trastorno por Consumo de Alcohol (TCA) es la forma más prevalente de adicción, imponiendo una carga sustancial a la sociedad y ofreciendo opciones de tratamiento limitadas. Los efectos del TCA en el cerebro, particularmente en la sustancia blanca, son difíciles de entender debido a la complejidad del trastorno y las comorbilidades asociadas. Este trabajo tiene como objetivo: (1) utilizar técnicas avanzadas de imagen por resonancia magnética pesada en difusión (RM-D) en un modelo de rata de TCA para investigar de forma no invasiva los efectos producidos por el alcohol en la microestructura de la sustancia blanca; (2) explicar de manera traslacional, a través de imágenes multimodales, los beneficios clínicos de un ensayo reciente sobre Estimulación Magnética Transcraneal Profunda (EMT Profunda) como tratamiento para el TCA; y (3) dilucidar los posibles mecanismos por los cuales EMT Profunda ejerce efectos terapéuticos, reflejados en la preservación de la estructura de la sustancia blanca, la reducción del ansia por el consumo y la recaída en pacientes tratados. Para los estudios con animales, utilizamos la línea de ratas con preferencia por el alcohol (msP) y un paradigma de libre elección con dos botellas para el consumo de alcohol. Se emplearon técnicas avanzadas de RM-D, combinadas con histología, para investigar los efectos del alcohol en la sustancia blanca. Los estudios en humanos involucraron a pacientes con TCA admitidos en programas de desintoxicación y que participaron en un ensayo clínico de EMT Profunda. La integridad de la sustancia blanca se vio comprometida en el modelo de rata y en los pacientes con TCA en comparación con los controles sanos, reflejada por una reducción generalizada de la anisotropía fraccional (AF). En las ratas con TCA, la RM-D avanzada reveló una alteración en la estructura de los haces axonales, con un aumento del diámetro axonal, una densidad axonal disminuida y un contenido de mielina reducido. Estos hallazgos fueron confirmados por el análisis histológico que mostró un aumento de neurofilamentos y una reducción de la tinción de proteína básica de mielina. En los pacientes con TCA, la reducción de AF progresó durante la abstinencia temprana (3 semanas) en ausencia de la EMT Profunda. Sin embargo, la estimulación de áreas frontocorticales en la línea media detuvo la progresión de los cambios en AF en esa región, lo que se asoció con una disminución del ansia por el consumo y la probabilidad de recaída. La reconstrucción de los tractos axonales cuya sustancia blanca mostró valores de AF preservados, identificó regiones corticales en la corteza cingulada posterior y la corteza prefrontal dorsomedial, donde la conectividad funcional se moduló en la dirección de los controles sanos, de manera persistentemente. Ninguno de estos efectos se observó en el grupo de estimulación simulada. La RM-D avanzada ha demostrado sensibilidad para revelar alteraciones en la integridad de los axones en la sustancia blanca, de forma no invasiva, producidas por el consumo de alcohol. Al integrar la estructura y función cerebral, este estudio caracteriza el cerebro dependiente del alcohol y ofrece información mecanicista sobre los efectos terapéuticos de la EMT Profunda, destacando el papel potencial del rescate de la estructura axonal a través de la plasticidad de la mielina. Estos hallazgos sugieren la posible aplicación de la EMT Profunda como un tratamiento para corregir las alteraciones de la microestructura de la sustancia blanca en general, y para el TCA en particular.

List of Figures

- Figure 1.1 **Cartoon for a typical myelinated neuron.**
- Figure 1.2 **Addiction neurocircuitry.**
- Figure 1.3 **Theory of MR.**
- Figure 1.4 **Relaxation times.**
- Figure 1.5 **Tensor illustration.**
- Figure 1.6 **Diffusion-weighted MRI pipeline, from acquisition and processing to visualization.**
- Figure 1.7 **Different elements contribute to the observed diffusion signal.**
- Figure 1.8 **Proceedings on the development of fMRI.**
- Figure 1.9 **Temporal and spatial resolutions of different brain mapping techniques.**
- Figure 1.10 **FDA-approved TMS coils.**
- Figure 3.1 **Preclinical study design.**
- Figure 3.2 **Clinical study design.**
- Figure 3.3 **Preclinical data preprocessing pipeline.**
- Figure 3.4 **TMS power distribution.**
- Figure 4.1 **Alcohol intake and preference.**
- Figure 4.2 **White matter alteration assessed by different dw-MRI maps.**
- Figure 4.3 **Statistical tests conducted on the mean value per ROI extracted from atlas-based analysis.**
- Figure 4.4 **Histological analysis of brain slices.**
- Figure 4.5 **White matter alterations progress during early abstinence.**
- Figure 4.6 **Progression of white matter alterations is arrested by Deep TMS.**
- Figure 4.7 **Statistics of the Deep TMS protected spot (FroL).**
- Figure 4.8 **Deep TMS decreases alcohol craving.**
- Figure 4.9 **White matter tracts protected by Deep TMS define terminal fields in the grey matter that show persistent changes in functional connectivity.**
- Figure 5.1 **Cartoon of the blistering within the axon-myelin unit.**

Index

I. INTRODUCTION	1
1.1 BRAIN WHITE MATTER	1
1.1.1 Structure and function	1
1.1.2 White matter pathology	3
1.2 ALCOHOL	4
1.2.1 History of alcohol as a beverage	4
1.2.2 Alcohol Use Disorder (AUD): Definition, prevalence, and consequences	5
1.2.3 Addiction cycle and brain circuits	7
1.2.4 Animal models of AUD	11
1.3 MAGNETIC RESONANCE IMAGING (MRI)	13
1.3.1 Foundation	13
1.3.2 Methods for studying the white matter with MRI	16
1.3.3 MRI strengths and limitations	27
1.3.4 Relevance of MRI in studying AUD	29
1.4 TRANSCRANIAL MAGNETIC STIMULATION	30
1.4.1 Basics and application of Transcranial Magnetic Stimulation	30
1.4.2 TMS relevance in AUD	32
II. AIMS AND OBJECTIVES.....	35
III. MATERIALS AND METHODS	37
3.1 PRECLINICAL STUDY	38
3.1.1 AUD rat model	38
3.1.2 Anaesthesia and preparation	39
3.1.3 Image acquisition	39
3.1.4 Imaging data analysis	40
3.1.5 Immunohistochemistry and histological analysis	41
3.2 CLINICAL STUDY	42
3.2.1 Participants	42
3.2.2 Image acquisition	43
3.2.3 TMS protocol	43
3.2.4 Imaging data analysis	44
IV. RESULTS.....	47
4.1 PRECLINICAL RESULTS	47
4.1.1 Alcohol consumption	47
4.1.2 Imaging	47
4.1.3 Histology	51
4.2 CLINICAL RESULTS	53
4.2.1 Imaging	53
4.2.2 Psychiatric measures and clinical outcomes	55
V. DISCUSSION.....	59
5.1 CONTRIBUTION TO UNDERSTANDING WHITE MATTER ALTERATIONS IN AUD	59
5.1.1 Preclinical framework	59
5.1.2 Clinical framework	62
5.2 TRANSLATIONAL FINDINGS AND THEIR SIGNIFICANCE	64
5.2 POTENTIAL APPLICATIONS AND FUTURE RESEARCH DIRECTIONS	66
5.3 LIMITATIONS	67
5.5 FINAL REMARKS	68
VI. CONCLUSIONS.....	69
VII. CONCLUSIONES.....	71

VIII. REFERENCES	72
IX. APPENDICES	95
A. SUPPLEMENTARY DATA	95
B. ETHICAL CONSIDERATIONS AND APPROVALS	97
C. PEER-REVIEWED PUBLICATIONS INTEGRATED INTO THE THESIS:	99



I. Introduction

1.1 Brain White Matter

1.1.1 Structure and function

The human brain's complex structure depends on the harmonious interaction between Grey Matter (GM, throughout this text, both will be used interchangeably) and White Matter (WM, throughout this text, both will be used interchangeably). While grey matter primarily includes neuronal cell bodies and dendrites, white matter comprises the extensive network of myelinated and nonmyelinated axons that connect and synchronise activity among remote brain regions. These "information superhighways" of the brain, featuring myelin-insulated fibres, facilitate the swift, efficient transmission of signals throughout the nervous system, and ensure synchronous connections between specialised brain areas (Schmahmann et al., 2008); these connections enable the integration of sensory input, motor output, and cognitive processes (Fields, 2008; Sampaio-Baptista et al., 2013). For instance, white matter tracts connecting brain regions involved in emotional processing (e.g., amygdala, prefrontal cortex) contribute to emotional regulation, decision-making, and social cognition (van der Horn et al., 2021), while the arcuate fasciculus that connects Broca's and Wernicke's areas is important in language processing (Catani et al., 2005).

White matter tracts form an elaborate system of interconnected pathways, where their integrity is crucial for typical brain functioning. Numerous studies demonstrate a robust association between white matter integrity and core higher-order brain functions (Borghesani et al., 2013), including processing speed, executive functions, working memory, and attentional control (Charlton et al., 2006; Filley and Fields, 2016).

Within white matter structure, in addition to axons, glial cells play an essential role in maintaining the homeostasis and microstructural environment of white matter. For example, the microglia cells serve as the immune cells of the CNS (Central Nervous System); they are involved in inflammation, repair, and synaptic pruning (Salter and Stevens, 2017). While star-shaped cells, known as astrocytes, provide structural support, regulate the extracellular environment, and play a role in synaptic transmission (Verkhratsky and Nedergaard, 2018). Oligodendrocytes are responsible for wrapping their plasma membranes around axons, forming the myelin sheathes within the CNS; at the peripheries, the same role is carried out by Schwann cells. A single oligodendrocyte can myelinate segments of multiple axons (Nave and Werner, 2014). Nonetheless, their contribution to WM structure and function goes beyond myelination, as they may also play a role in axonal support by secreting neurotrophic factors that promote axonal growth, metabolism, survival, and repair (Boulanger and Messier, 2014; Wilkins et al., 2003). Furthermore, oligodendrocytes interact with immune cells and may influence inflammatory responses within CNS (Madsen et al., 2020). Also studies showed

that they could potentially contribute to the dynamic remodelling of synapses, which is critical for learning and memory (Munyeshyaka and Fields, 2022).

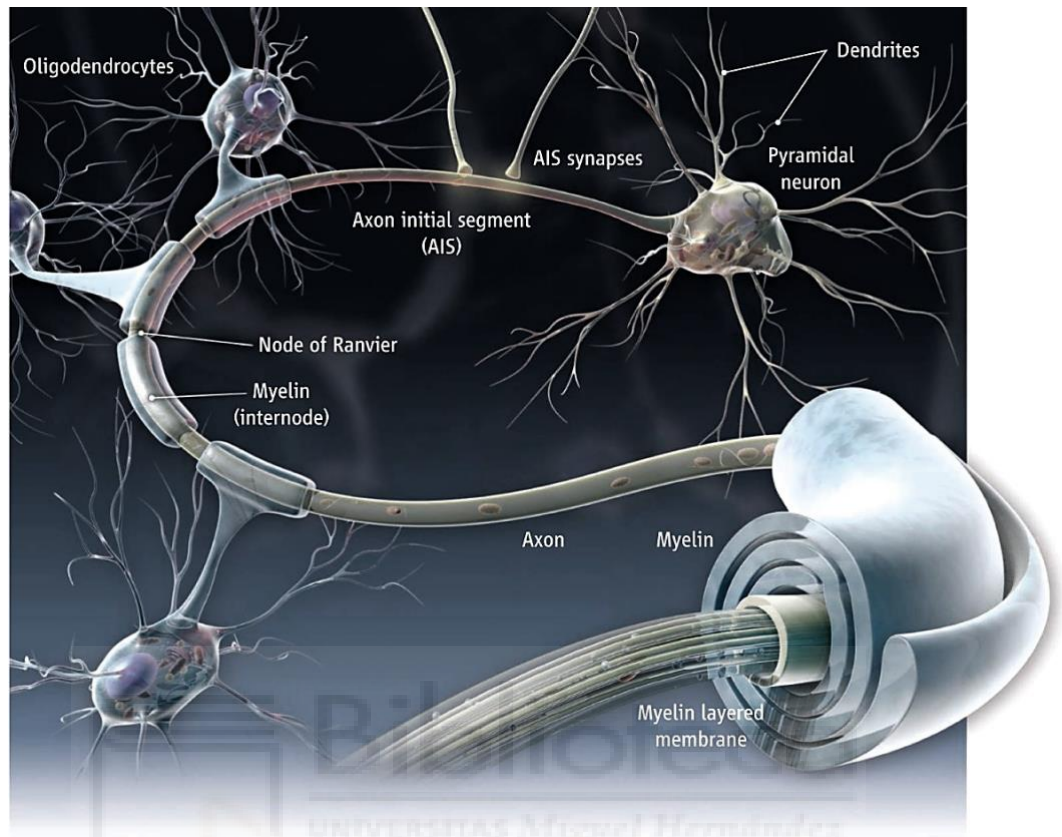


Figure 1.1 Cartoon for a typical myelinated neuron. Structure of myelinated pyramidal neuron comprises the cell body (soma) and its dendrites, axon initial segment, oligodendrocytes myelinating distant axon segments, and myelinated layered membrane, figure adapted from (Fields, 2014).

In the context of myelin, where WM's distinctive white hue stems from, myelin is an insulating substance that covers the axons of neurons in the central and peripheral nervous systems (CNS and PNS). Myelin is composed primarily of lipids (about 70-80%) and proteins (Kister and Kister, 2023), where the unique protein composition of myelin (e.g., proteolipid protein (PLP) and myelin basic protein (MBP) in the CNS) provides structural integrity and stability (Kister and Kister, 2023). As mentioned, myelin formation involves the spiral wrapping of an oligodendrocyte around an axon (see Figure 1.1), resulting in a multi-layered sheath that is interrupted periodically by gaps known as nodes of Ranvier. A major function of myelin is to increase the speed of action potential transmission along neuronal axons. Myelin presents a high-resistance barrier, preventing ion leakage across the axonal membrane. Hence, depolarisation 'jumps' from one node of Ranvier to the next through a process known as saltatory conduction (from the Latin *saltare*, to jump). This allows action potentials to propagate at dramatically increased speeds compared to their unmyelinated counterparts (Nave, 2010). Myelin has been found to serve purposes beyond its traditional role in facilitating rapid impulse transmission, studies suggest that myelin offers metabolic support to axons, with oligodendrocytes playing a crucial role in this process by providing lactate, as

an energy source for axons (Fünfschilling et al., 2012; Lee et al., 2012). While myelinated axons dominate white matter, a significant population of nonmyelinated axons also exists (Li et al., 2016). These unmyelinated axons typically conduct slower but may play important roles in local communication within brain regions. Studies suggest that they might be involved in early brain development, forming temporary connections before being replaced by myelinated pathways (Buyanova and Arsalidou, 2021). The corpus callosum, connecting the brain hemispheres, is an example of a region containing both myelinated and nonmyelinated axons, making it valuable for studying the functional differences between these two types (Li et al., 2016).

Existing myelin sheaths are not fixed; they can be remodelled, with segments being added, removed, or altered in response to the firing of action potentials in the neurons (Fields, 2015; Kato and Wake, 2019), that triggers signalling cascades within oligodendrocytes, leading to increased myelin production and metabolic transfer (Foster et al., 2019). This dynamic adaptation, which is known as myelin plasticity, supports high-activity neurons with the resources they need to function (Yeung et al., 2014), with profound implications for the fine-tuning of neural circuits. Study showed an increase in myelination in brain areas associated with motor skill acquisition, and this suggests that myelin plasticity helps strengthen the neural circuits involved in new motor learning (McKenzie et al., 2014). Similar changes in myelin are observed during complex cognitive tasks, indicating myelin's involvement in the encoding of new memories and adaptations of cognitive abilities (Sampaio-Baptista and Johansen-Berg, 2017).

Oligodendrocyte precursor cells (OPCs), the progenitors of myelinating oligodendrocytes, have emerged as key players in myelin plasticity process. OPCs are distributed throughout the adult brain and act as a reservoir of potential myelinating cells. In response to neuronal stimuli (Gibson et al., 2014), OPCs can differentiate into mature oligodendrocytes and generate new myelin segments (Dimou and Gallo, 2015; Hughes et al., 2013), similar observation can be achieved by external stimulation (Braun et al., 2016). OPCs are not merely passive progenitors of oligodendrocytes; they also release signalling molecules that modulate neuronal excitability and synaptic transmission (Thornton and Hughes, 2020). Ongoing research is exploring the molecular mechanisms underlying OPC-neuron interactions, and the potential of targeting OPCs for therapeutic interventions in demyelinating diseases (Skaper, 2019).

1.1.2 White matter pathology

Deviations in white matter structure or function can result from various factors, including genetics, epigenetics, environmental factors, diseases, injuries, and unhealthy habits or lifestyles. These factor-induced disruptions in WM have been implicated in a range of neurological and psychiatric conditions (Charlton et al., 2006; De Santis et al., 2019; Fields, 2008; Van Velzen et al., 2020), leading to impairments in both functional and cognitive domains. Damage to white matter tracts involved in motor control can lead to weakness, spasticity, gait disturbances, balance issues, and altered sensory processing (Bohnen and

Albin, 2011; Zhai et al., 2020). Such impairments can potentially affect an individual's daily functioning, social interactions, decision-making, problem-solving abilities, and overall quality of life. Demyelination, or damage to the myelin sheath, disrupts nerve impulses' rapid, saltatory conduction (Love, 2006). This disruption can lead to a broad range of neurological symptoms depending on the affected nerves. For example, Multiple Sclerosis (MS), a recurrent autoimmune ailment, is characterised by the destruction of the myelin sheath, which impedes nerve impulse transmission and leads to diverse neurological manifestations. Similarly, other demyelinating diseases may impact white matter (Compston and Coles, 2008), including but not restricted to leukoencephalopathy (Cortese et al., 2021), or traumatic axonal injury (Bruggeman et al., 2021).

Recent research indicates that white matter changes are prevalent in both mood and anxiety disorders, such as major depressive disorder (Van Velzen et al., 2020), as well as Parkinson's disease (Bohnen and Albin, 2011), and Alzheimer's disease (Nasrabad et al., 2018). Moreover, studies reveal white matter abnormalities in conditions like Autism Spectrum Disorder (ASD) (Ohta et al., 2020), and schizophrenia (Kubicki et al., 2005). These findings suggest that atypical white matter development might play a role in the underlying pathophysiology of these complex disorders (Fields, 2008).

Ultimately, a recent systematic review conducted on Substance Use Disorders (SUDs) revealed both convergent and divergent patterns in the impact of substance use on brain regions and volume (Pando-Naude et al., 2021). The severity of consumption patterns and the type of substance used played a significant role in determining the extent of these effects. It was observed that certain brain regions, including the internal capsule bundle and thalamic radiation in the white matter, exhibited convergent pathology across different substances. On the other hand, there was divergent pathology between occasional use and addiction, suggesting a possible top-down neuroadaptation. These findings shed light on specific brain morphometry alterations in SUDs and have the potential to inform therapeutic approaches and improve our understanding of disease progression (Pando-Naude et al., 2021). Among these substances alcohol was prominent to induce brain changes (Chanraud et al., 2007; Segobin et al., 2014), loss of white matter fibre integrity (De Santis et al., 2019; Pérez-Cervera et al., 2023; Pfefferbaum and Sullivan, 2005; Wang et al., 2019), that progresses even during early abstinence (De Santis et al., 2019; Selim et al., 2023).

1.2 Alcohol

1.2.1 History of alcohol as a beverage

Alcohol beverages have an important role in the modern human lifestyle, often accompanying social events or even principal meals during the day. While the origins of recreational alcohol consumption date back thousands of years, the exact moment of its discovery remains elusive. Nonetheless, evidences suggest multiple independent origins of alcoholic beverages around 7000 BC. From China, in a 7,000-year-old Neolithic village called Jiahu, the chemical analysis

of pottery shards revealed residues of a fermented beverage made with rice, honey, and fruits (McGovern et al., 2004). In the Middle East where evidence of barley beer and grape wine production dates to 7000-5000 BC, with sites like Hajji Firuz Tepe in Iran and Godin Tepe showcasing ancient alcoholic legacies. It remains unclear whether alcohol production was intentional or accidental, but some argue that fruit juices naturally ferment, leading to unintentional consumption (McGovern, 2009). However, the complexity of some early alcoholic beverages suggests deliberate production. Early texts from ancient Egypt (2100 BC) mention alcohol's medicinal use, indicating an understanding of its psychoactive effects beyond mere intoxication (McGovern et al., 2009). Collectively, Alcoholic beverages appear to have developed independently across various regions and cultures, where alcohol likely played a role in early social bonding and community formation. Understanding the motivations and contexts surrounding early alcohol consumption requires more research on cultural and social practices. Ongoing archaeological research constantly uncovers new evidence, potentially altering our understanding of the timeline and geographic spread of alcoholic beverages.

1.2.2 Alcohol Use Disorder (AUD): Definition, prevalence, and consequences

Alcohol addiction is a considerable issue for public health on a global scale, which has severe implications. As per the World Health Organization (WHO), excessive alcohol consumption ranks among the primary causes of mortality and disability across the world, resulting in more than 3 million fatalities each year (World Health Organization, 2018). It has substantial economic and social impacts, costing billions in healthcare costs, lost productivity, and social welfare expenses (Laramee et al., 2013). Some research suggests moderate alcohol consumption might offer some benefits, such as a lower likelihood of developing heart disease, stroke, and type 2 diabetes, although the mechanisms are still under investigation, and individual factors play a crucial role (Chiva-Blanch and Badimon, 2019). However, the notion of "moderate" consumption of alcohol being safe is a contentious issue, as evidenced by a substantial study involving approximately 600,000 participants (Wood et al., 2018). According to this study, there is no entirely safe level of alcohol consumption, and any level of consumption comes with several risk factors. According to a subset of this data involving 37 thousand participants, the brain is one of the organs that are particularly vulnerable to damage. It was revealed that even light alcohol consumption, which consists of one to two daily units (1 unit is equivalent to 12g of pure alcohol), can lead to changes in both the macrostructure and microstructure of the brain. (Daviet et al., 2022), which indicates that there is no level of consumption that is risk-free for brain health (Topiwala et al., 2022). Alcohol, in its nature, is a neurotoxin, which means it can harm brain cells and interfere with their function. This damage can occur at multiple levels, impacting neurotransmitters, cell membranes, and brain structures (Crews and Nixon, 2009).

The aetiology of Alcohol Use Disorder (AUD, henceforth) is attributed to various factors, including environmental elements such as family-home lifestyle, peer interaction, hereditary

elements, and cognitive performance. The Diagnostic and Statistical Manual of Mental Disorders, Fifth Edition (DSM-5) sets the standard diagnostic criteria for AUD; it is defined as a maladaptive pattern of alcohol consumption that leads to significant distress or impairment in social, occupational, or other important areas of functioning (American Psychiatric Association, 2013). To meet the diagnostic criteria for AUD, an individual must exhibit two or more of the eleven specific criteria within a 12-month period. These criteria encompass a range of aspects, including the individual's inability to control their alcohol consumption, the presence of social or interpersonal problems, engaging in hazardous drinking behaviours, and the development of tolerance and withdrawal symptoms (see Table 1). AUD has a widespread global occurrence; according to the WHO, approximately 283 million people worldwide are affected by AUD (World Health Organization, 2018). As such, AUD is considered a highly prevalent mental health condition with its characteristics of loss of control over alcohol intake, compulsive alcohol use, and a negative emotional state upon abstinence. Individuals affected by AUD also experience numerous physical and psychiatric comorbidities, resulting in significant impairment in productivity and interpersonal functioning. This ultimately leads to substantial financial burdens for society as a whole. The impact of AUD extends beyond the affected individual and their immediate social circle, affecting entire communities through vehicle accidents, gender-based violence, and crime.

The adverse consequences of AUD extend across multiple domains, negatively impacting both individual well-being and societal structures:

- Health-wise, AUD significantly increase an individual's risk for a wide range of physical health conditions, including but not limited to liver cirrhosis, various cancers, cardiovascular disease, neurological impairment, accidental injuries, and comorbid mental health disorders like depression and anxiety (Baan et al., 2007; Boden and Fergusson, 2011; O'Keefe et al., 2014; Rehm et al., 2019). Alcohol abuse is a contributing factor to over 200 diseases and injuries, as reported by the WHO, and other studies (Im et al., 2023).
- Socially and economically, AUD often disrupt interpersonal relationships, contribute to occupational difficulties, financial hardship, and involvement in the legal system (Malathesh et al., 2021). Moreover, society as a whole, bears the burden of increased healthcare expenditures, lost productivity, and elevated crime-related costs.

Additionally, AUD can have intergenerational effects, with progeny of parents with AUD facing an increased likelihood of developing substance use disorders themselves, contributing to the perpetuation of addiction cycles (Esser et al., 2021).

DSM-5	
In the past year, have you:	
1	Had times when you ended up drinking more, or longer, than you intended?
2	More than once wanted to cut down or stop drinking, or tried to, but couldn't?
3	Spent a lot of time drinking? Or being sick or getting over other aftereffects?
4	Wanted a drink so badly you couldn't think of anything else?
5	Found that drinking – or being sick from drinking- often interfered with taking care of your home or family? Or caused jobs troubles? Or school problems?
6	Continued to drink even though it was causing trouble with your family or friends?
7	Given up or cut back on activities that were important or interesting to you, or gave you pleasure, in order to drink?
8	More than once gotten into situations while or after drinking that increased your chances of getting hurt (such as driving, swimming, using machinery, walking in a dangerous area, or having unsafe sex)?
9	Continued to drink even though it was making you feel depressed or anxious or adding to another health problem? Or after having had a memory blackout?
10	Had to drink much more than you once did to get the effect you want? Or found that your usual number of drinks had much less effect than before?
11	Found that when the effects of alcohol were wearing off, you had withdrawal symptoms, such as trouble sleeping, shakiness, restlessness, nausea, sweating, a racing heart, or a seizure? Or sensed things that were not there?

The presence of at least 2 of these symptoms indicates Alcohol Use Disorder (AUD).

The severity of the AUD is defined as:

Mild: the presence of 2 to 3 symptoms.

Moderate: the presence of 4 to 5 symptoms.

Severe: the presence of 6 or more symptoms.

Table 1 **Diagnostic criteria for Alcohol Use Disorder.** AUD criteria according to the Diagnostic and Statistical Manual of Mental Disorders, Fifth Edition (DSM-5) (American Psychiatric Association, 2013).

1.2.3 Addiction cycle and brain circuits

Drug addiction is typically a persistent and disabling disorder characterised by an uncontrollable craving for a specific substance, an inability to regulate the amount consumed, and the emergence of negative emotional states during periods of abstinence. Each drug has distinct mechanisms of action, such as cocaine, which inhibits dopamine reuptake in the synaptic cleft, and alcohol, which acts on inhibitory GABAergic channels. Despite these differences, addiction to any substance is believed to progress through a three-stage cycle (Koob et al., 2014). The first stage involves the initial attraction to the drug, “i.e., intoxication”; the second stage involves continued use despite negative consequences, “i.e., withdrawal negative effect”, and the third stage involves a loss of control and compulsive drug-seeking behaviour, “i.e., craving”.

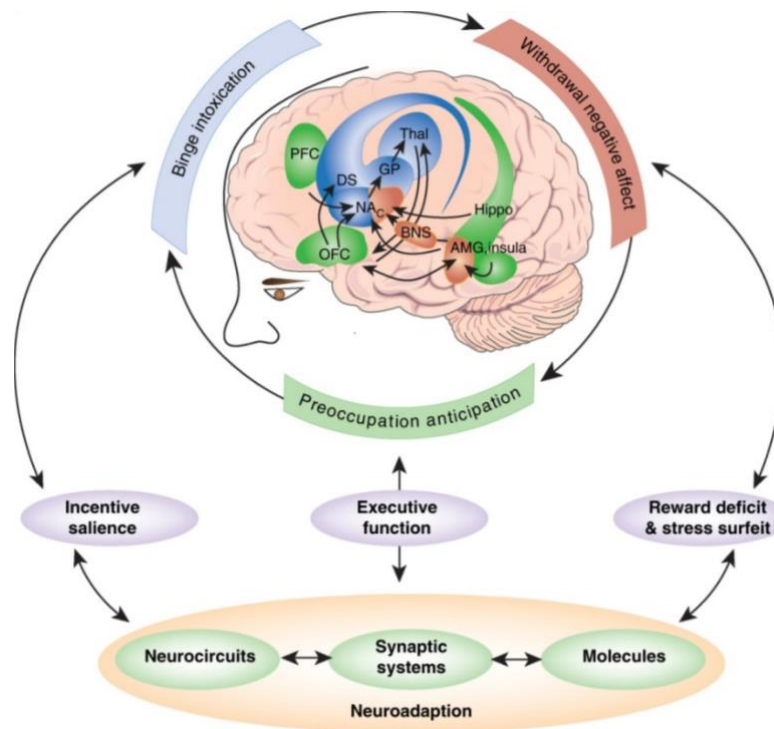


Figure 1.2 **Addiction neurocircuitry**. A diagram depicts the neurocircuitry of addiction, which is comprised of three phases within the addiction cycle, divided as: binge/intoxication phase (in blue), withdrawal/negative affect phase (in red), and preoccupation/anticipation phase (in green). Adapted from (Wise and Koob, 2014).

In the case of alcohol, after ingestion, alcohol translocates to the bloodstream via absorption in the gastrointestinal canal; it circulates all over the body, reaching distant organs; due to its lipophilic nature, it possesses the capacity to cross the Blood-Brain Barrier (BBB). Once inside the brain, it exerts effects at various levels, including molecular, cellular, and systemic, leading to neuroadaptations that can result in addiction. The following lines will elaborate on the three-stage addiction cycle in the context of AUD:

Intoxication

This stage of alcohol addiction during which the alcohol enters the body and permeates various tissues and organs, with the brain being the primary target, where the initial euphoric effects are primarily driven by alcohol's ability to enhance dopamine release in the mesolimbic pathway (Gonzales et al., 2004), dopamine generates conditioned alcohol-related reinforcement, as such all brain regions involved in reward become sensitised to alcohol cues, leading to intense cravings that can be difficult to resist. The regions involved in this stage are highlighted in Figure 1.2 in blue, with the basal ganglia, including the Dorsal Striatum (DS) and Nucleus Accumbens (NAc), both structures are necessary for and contributing to the formation of habits and the development of compulsive drug-seeking (Everitt et al., 2008). Globus Pallidum (GP), through its connections with NAc serves as a hotspot for reward and motivation, associating the drug consumption hedonics with external cues (K. S. Smith et al., 2009). Then the Thalamus (Thal), which serves as a central hub for transmitting information between the basal ganglia and cortical structures (Sherman, 2016), furthermore plays a critical role in drug-induced emotional and motivational states (McFarland et al., 2003; Neumann et

al., 2016), and cognitive control (Halassa and Kastner, 2017). Other two major areas that are not shown in Figure 1.2 are the Ventral Tegmental Area (VTA) and Substantia Nigra compacta (SNc) as key players in the dopamine-mediated rewarding effects of the alcohol and the development of habits through their dopaminergic connections to the DS. Additionally, at a brain-wide level, alcohol acts as a potent “positive allosteric modulator” of GABA receptors, which means that it binds to these receptors and enhances the effects of GABA (Olsen, 2018), a key inhibitory neurotransmitter in the brain. This results in a state of sedation and reduced anxiety, which also reinforces drinking behaviours. Alcohol also stimulates the release of endogenous opioids, also known as endorphins, in the brain. This opioid activity enhances alcohol's pleasurable effects, leading to a reinforcement of alcohol-seeking behaviour (Oswald and Wand, 2004).

Withdrawal negative effect

When alcohol consumption is ceased, withdrawal effects emerge, which are the brain's response to the sudden absence of alcohol. These effects, commonly referred to as "withdrawal symptoms," include anxiety, agitation, irritability, insomnia, headaches, nausea, vomiting, and tremors. In severe cases, these symptoms may be accompanied by seizures and even hallucinations. These symptoms are a result of neuroadaptation, which occurs in specific regions of the brain. These brain areas, highlighted in Figure 1.2 in red, include the extended amygdala, which consists of the bed Nucleus of the Stria Terminalis (BNST), the central nucleus of the Amygdala (AMG), and a transition area in the shell of the NAc, as key regions involved in the withdrawal/negative affect stage (Koob and Volkow, 2010). When the individual experiences such emotions, negative reinforcement comes into play. This differs from the positive reinforcement discussed in the previous stage, as the individual's motivation to seek and consume alcohol is now driven by the desire to avoid this anxiety-induced mood. This is due to a decrease in mesolimbic activity, contrary to what normally occurs at the intoxication phase (Wise and Koob, 2014).

Craving

The preoccupation/anticipation phase, also known as craving, of the addiction process is defined by an intense urge to resume alcohol drinking, which is characterised by a deficiency in executive function. This dysregulation is associated with the disruption of significant afferent projections from the prefrontal cortex and insula to the basal ganglia and extended amygdala. The brain regions that are involved in this stage are shown in green in Figure 1.2, which comprise the frontal cortices, including the Prefrontal Cortex (PFC) and Orbitofrontal Cortex (OFC), the Insula, and the Hippocampus (Hippo).

The PFC, which plays a pivotal role in executive function, is the primary region in this stage. It is responsible for the loss of control and subsequent relapse upon alcohol exposure or alcohol-associated cues; as such, it is crucial in the perpetuation of addiction. Neuroimaging studies showed that addicted individuals display alterations in the activity of PFC during the performance of tasks requiring inhibitory control, which they tend to perform more poorly

than non-addicted individuals (Goldstein and Volkow, 2011). Another study demonstrated that the PFC activity (combined with other mesocorticolimbic areas, i.e., striatum, ventral tegmental area/substantia nigra) tends to be higher in alcohol dependant patients when exposed to the taste of their preferred alcoholic beverage, compared with the activity induced by another appetitive cue (i.e., sugary drink) (Filbey et al., 2008). The OFC, with its major role in decision-making and reward valuation, during the phase of craving, the OFC's function is compromised, resulting in the prioritisation of immediate alcohol rewards over long-term negative consequences. Studies suggest that individuals with alcohol dependence exhibit a reduction in the volume of grey matter in the OFC. This reduction in the OFC is a significant predictor of heavy relapse in detoxified patients at the six-month mark, where the risk of relapse increases with decreased grey matter volume (Zois et al., 2017). A Key element in the neurocircuitry at this stage is the Insula: its role in decision-making- processes that precipitate in relapsing action (Naqvi and Bechara, 2009), maladaptive engagement and impulsivity (Belin-Rauscent et al., 2016), and the integration of interoceptive information, where addictive behaviours are associated with reduced interoceptive signalling, makes it a fundamental structure for drug craving (Droutman et al., 2015).

The Hippocampus is crucial for declarative memory (facts and events) and contextual learning (Burwell et al., 2004; Tulving and Markowitsch, 1998), and the formation of reward-associated representations (i.e., reward learning), which is the association of explicit cues with alcohol consumption; this reward learning is considered a form of associative long-term memory (Hyman, 2005). The effects of alcohol on the hippocampus are prominent. Studies suggest that alcohol-induced hippocampal damage impairs spatial learning abilities and disrupts the ability to associate environmental cues with alcohol-related memories (White, 2003). Hippocampal dysfunction may contribute to a dysregulated stress response, making individuals with AUD more prone to relapse triggered by stress (Spanagel, 2009). A recent translational study from our research group demonstrated that, by combining quantitative MRI, immunohistochemistry and electrophysiological recordings, alcohol induces alteration in the microstructural integrity of the fimbria-fornix, concurrently with disrupted communication from the hippocampus to the PFC; such communication may impede the extinction of maladaptive memories of alcohol consumption, and consequently increasing relapse. This same study also showed an association between the extent of alterations in the fimbria-fornix and the reduction in cognitive flexibility among patients with AUD (Pérez-Cervera et al., 2023).

Furthermore, and not depicted in the summary Figure 1.2, comes the Anterior Cingulate Cortex (ACC) as a pivotal brain region implicated in diverse functions, including attention, error detection, and emotional regulation. This region plays a substantial role in AUD, as its activity is important for craving and salience attribution. Due to its close integration with brain reward centres, the ACC becomes increasingly sensitive to alcohol-related cues, resulting in hypersensitivity that contributes to intense craving and the salience of alcohol-related stimuli over other reinforcers. This, in turn, influences behaviour towards drinking (Myrick et al.,

2004). Alcohol-induced deficits in ACC function hinder the ability to evaluate conflicting internal states (i.e., the desire to drink vs. choosing sobriety); this impairment can undermine an individual's efforts to resist alcohol and increases the risk of relapse (Marinkovic et al., 2012).

Finally, the progression from recreational alcohol use to a state of addiction is characterised by four essential elements, which are facilitated by neuroadaptations at the molecular, synaptic, and neurocircuitry levels (lower part of Figure 1.2). These elements incorporate increased incentive, increased stress, decreased reward, and decreased executive function (Wise and Koob, 2014).

1.2.4 Animal models of AUD

Animal models hold a crucial place in basic and translational neuroscientific research; they play a significant role in understanding the complex neurobiological and behavioural underpinnings of major psychiatric disorders (Koob and Zimmer, 2012). AUD is not an exception. Animal models are present heavily in AUD diagnosis and prognosis studies; while those models cannot fully replicate the human experience, they offer valuable insights into AUD development, susceptibility factors, and potential therapeutic targets. Rodents, i.e., rats (*Rattus rattus*) and mice (*Mus musculus*), are the most widely used species due to their genetic tractability, short lifespan for studying generational effects, and availability of behavioural paradigms.

Animal AUD models can be categorised into two groups: first, the “genetically modified” where animal lines are selected by selective breeding for high alcohol preference or sensitivity. Examples of this category include the alcohol mouse model of the National Institute on Alcohol Abuse and Alcoholism (NIAAA) (Bertola et al., 2013), and the widely used alcohol-preferring msP rat line (Ciccocioppo et al., 2006). These genetically selected models contribute to understanding the pathophysiology of AUD and identifying genetic risk factors associated with it (Crabbe et al., 2009). On the other hand, “environmental models” are models where alcohol consumption is a consequence of manipulating the environmental settings; for example, in the alcohol vapour exposure model, animals are exposed to alcohol vapour for prolonged periods, leading to physical dependence. This model is particularly useful for studying withdrawal symptoms and changes associated with chronic heavy alcohol use. Operant conditioning models, in which animals are trained to self-administer alcohol in response to cues (lights, levers), investigate the role of reward mechanisms and cue-induced craving in driving alcohol-seeking behaviour. Recently, using the operant choice procedure, rats chose alcohol over social reward (Marchant et al., 2023). Models of chronic intermittent ethanol exposure to induce dependence-like behaviours and neuroadaptation, as well as binge drinking and relapse models to capture withdrawal phenotypes, are pertinent to the human experience of AUD (Becker and Lopez, 2004).

Paradigms for alcohol administration are also important to understand AUD. In the oral self-administration, animals are given access to alcohol solutions alongside water, allowing the study of individual differences in alcohol preference, drinking patterns, and the development of escalated intake. These models provide translational relevance for human consumption behaviours (Carnicella et al., 2014). A popular consumption paradigm for self-administration is the two-bottle free choice (Huynh et al., 2019), where animals are given continuous access to both water and alcohol solutions, allowing the study of consumption preference, and the progress of alcohol intake. Whereas in the drinking in the dark (DID) model (Thiele and Navarro, 2014), animals have limited access to alcohol for a few hours during their active (dark) cycle. This paradigm can induce binge-like drinking patterns relevant to human consumption. In addition, alcohol may be administered through various other means, such as gavage (Chandler et al., 2022), or liquidised into the diet (Guo et al., 2018). Animals are generally exposed to these paradigms individually (i.e., the animal is single-housed), which leaves a gap in addressing alcohol consumption under socially influenced, human-like conditions. However, recent advances in administration paradigms have aimed to capture the intrinsic complexity of alcohol consumption within different social contexts (Frie and Khokhar, 2024).

Rats are commonly considered a better model organism than mice for studying addictive conducts based on genetic and behavioural considerations (Spanagel, 2017). For example, the results obtained from a glutamate magnetic resonance spectroscopy study were found to be consistent during alcohol withdrawal, as both rats and humans displayed hyperglutamatergic activity in various brain regions. The observed activity, however, decreased once the withdrawal symptoms subsided (Hermann et al., 2012). Furthermore, both alcoholic rats and humans showed similar alteration of brain microstructure as revealed by diffusion magnetic resonance study (De Santis et al., 2019).

Besides rodents, non-human primate models are also involved in studying AUD; for instance, vervet monkeys and other primates exhibit voluntary alcohol consumption patterns surprisingly similar to humans, offering translational value for studying social and environmental factors that contribute to AUD (Grant et al., 2008). Studying alcohol consumption within the hierarchy of social interactions among these models offers crucial insights into peer-influence and individual differences towards AUD vulnerability (Vivian et al., 2001). Also, non-human primates provide a preclinical platform closer to human biology than rodents, but they are costly and require specialised facilities, often limiting their widespread use compared to rodent models. Whether rodents or non-human primates, ethical standards are important, and it's vital to uphold them in animal research, employing refinement, replacement, and reduction (3Rs) strategies when possible.

To this end, we can say that animal models have shaped our current understanding of the basis of AUD; they have helped elucidate alcohol's effects on key neurotransmitter systems (e.g., dopaminergic, GABAergic, glutamatergic), unrevealing the mechanisms involved in addictive behaviours, such as the transition to dependence and withdrawal (Koob, 2009). At

the forefront of treatments, animal models are used for screening new compounds for AUD treatment, investigating mechanisms of action, and evaluating their efficacy in reducing alcohol consumption, craving, and withdrawal symptoms (Litten et al., 2012). Nevertheless, animal models cannot fully capture the complex psychosocial elements contributing to human AUD due to inherent species differences.

1.3 Magnetic Resonance Imaging (MRI)

1.3.1 Foundation

Magnetic resonance imaging (MRI) is an indispensable tool in neuroscience research, providing exceptional *in vivo* visualization of brain tissues. Its exceptional sensitivity to water content and variations in tissue composition makes MRI particularly well-suited for the detailed examination of brain structure and potential pathology. In theory, MRI scans employ powerful magnetic fields and radio frequency waves (RF-pulse) to evaluate the arrangement of protons ^1H , as subatomic particles in biological samples attached to water and fat. Protons possess the quantum mechanical property called (*spin*, spin and proton may be used alternately), representing the particle's angular momentum (\mathbf{s}). MRI is also employed in other species that possess non-zero angular momentum, such as ^{13}C and ^{31}P . However, for the purposes of this theoretical introduction, we will exclusively focus on proton MRI, as this is both practical and pertinent to the research presented. Classically, a spin can be visualized as

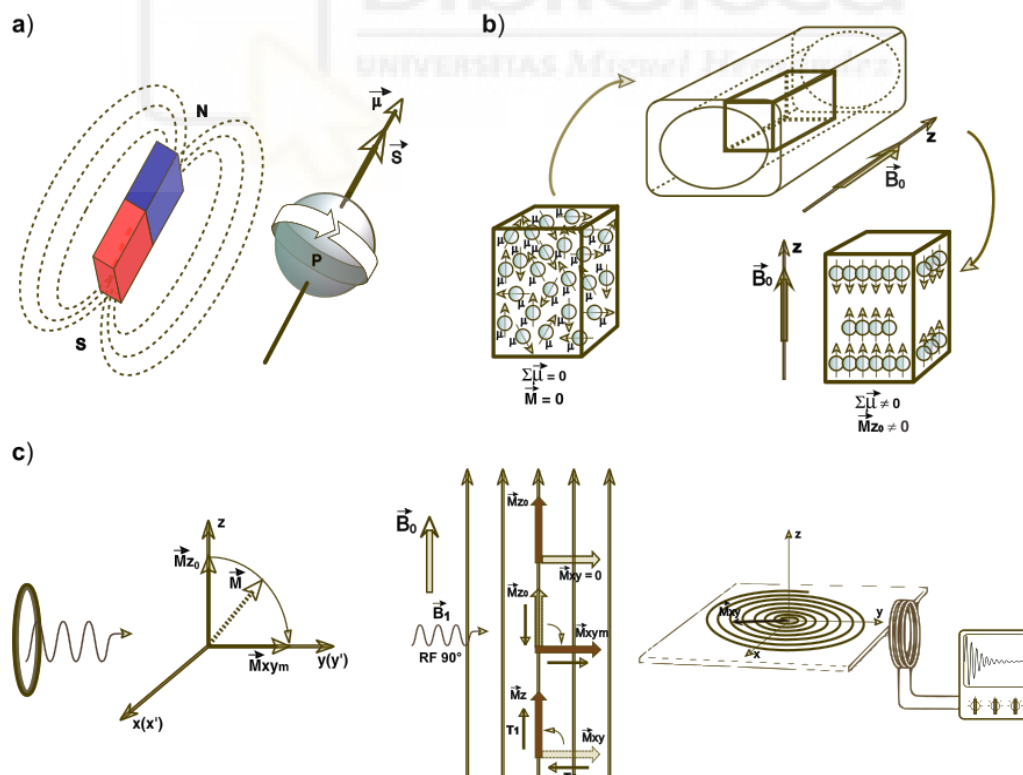


Figure 1.3 **Theory of MR.** (a) Magnetic moment μ of a rotating charged particle. (b) Influence of external magnetic field on the magnetic moment orientations, with two arrangements: spin-up and spin-down. (c) Application of RF pulse leads to the occurrence of resonance, which results in the rotation of the net magnetizing momentum, M , into the transverse plane, that will be detected as MR signal subsequently. Figure is adapted from (Kastler and Anstett, 2011).

a particle rotating on its axis. When a charged particle spins, it produces an electric current and consequently induces a magnetic field characterised by a magnetic moment (μ). Hence, each spin can be thought of as a tiny magnet, see panel (a) in Figure 1.3.

Based on the magnetic and mass properties of protons, along with their non-zero spin, it is possible to calculate the spin magnetic moment as $\mu_s = \gamma S$, where γ is the gyromagnetic ratio and for a proton $S = \frac{1}{2}$. This ratio, typically expressed in units of ($\text{rads}^{-1}\text{T}^{-1}$) and often reported as (MHzT^{-1}), represents the relationship between the angular momentum and the magnetic moment of a particle. When an external static magnetic field is applied (see Figure 1.3-b), the protons within the field experience a torque, which is proportional to the strength of the magnetic field. The resultant torque causes the protons to align or anti-align themselves with the magnetic field, this arrangement is also known as spin-up ($E\uparrow$) or spin-down ($E\downarrow$). Despite the torque exerted by the magnetic field, the spin angular momentum prevents the protons from aligning precisely with the magnetic field. Instead, they *precess* around the main axis of the magnetic field, with a precession frequency that is known as the Larmor frequency (ω_0). Larmor frequency is determined by the gyromagnetic ratio and the applied magnetic field strength (in the case of proton $\gamma \approx 42.58 \text{ MHzT}^{-1}$), as shown in Equation 1.

$$\omega_0 = \gamma B_0 \quad \text{Eq. (1)}$$

Overall, once an external magnetic field is applied, a macroscopic magnetization appears due to the contribution of all spins present in the sample. This magnetization can be decomposed in a transverse (M_{xy}) and longitudinal magnetization (M_z), the transverse magnetization M_{xy} is zero due to the spins having a random phase for their precession movement resulting in the magnetic moments adding non coherently. The longitudinal magnetization M_z is non-zero, with the net magnetization $M = M_z$ pointing towards the external magnetic field B_0 . However, the biological magnetization is small in comparison, making the signal hardly measurable. In order to obtain a measurable signal, the magnetization has to be moved away from the direction of the external magnetic field. This is achieved through the use of a time-varying Radiofrequency pulse (RF-pulse) that oscillates at the same Larmor frequency, it carries an energy equal to ΔE , and the induction of such energy causes the phenomenon of *resonance*. The RF-pulse induces transitions from the energy level $E\uparrow$ to $E\downarrow$ causing the longitudinal magnetization to switch its orientation. Moreover, the transition from one state to the other causes the spins to get in phase resulting in transverse magnetization, which later will be detected as the MR signal (panel c in Figure 1.3).

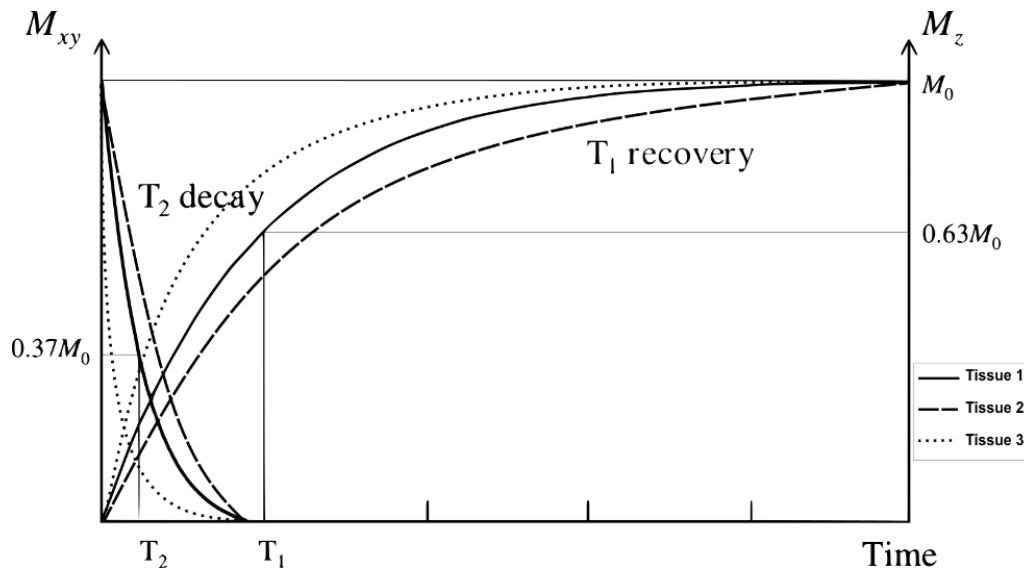


Figure 1.4 **Relaxation times.** Longitudinal (T_1) and transverse (T_2) relaxation times. Theoretical case of three tissues that exert different relaxation times in correspondence to their protons' compositions.

Once the RF-pulse is turned off, the spins de-phase to return to the equilibrium status, resulting in a diminishing of transverse magnetization (M_{xy}) and recovery of longitudinal one (M_z). Two key relaxation times, longitudinal relaxation (T_1) and transverse relaxation (T_2), determine how long it takes for excited protons within tissues to return to that state of equilibrium after absorbing energy from the RF-pulse. T_1 relaxation describes the time it takes for the net longitudinal magnetization (aligned with the external magnetic field, B_0) to recover to 63% of its original value. T_1 varies significantly across tissues due to differences in their molecular composition and mobility, also known as spin-lattice relaxation time. Tissues with higher water content and fewer large molecules generally exhibit longer T_1 values. While T_2 relaxation describes the time it takes for the magnetization in the transverse plane (perpendicular to B_0) to decay to 37% of its initial value following an RF-pulse. T_2 relaxation is primarily influenced by interactions between water molecules and their local environment, also known as spin-spin relaxation time. The presence of macromolecules, restricted water diffusion, and susceptibility variations can all contribute to shorter T_2 values.

Hence, the net magnetization, which subsequently determines the MR signal, depends on the biochemical makeup of the tissue being scanned. Consequently, the contrast between distinct tissues is determined by their compositions. For example, as depicted in Figure 1.4, which represents theoretically different 3 tissues with different T_1 and T_2 times. The objective is to acquire the signal at the optimal time that maximizes the distinguishability between the three tissues. In the context of brain MRI, these three tissues could represent white matter, grey matter, and cerebrospinal fluid (CSF).

Through MR, the signal can be spatially labelled so that a 3D image of the sample can be obtained. By incorporating an additional magnetic field, it is possible to manipulate the Larmor frequency of protons in a sample to get spatially varying frequencies. By applying an RF-pulse at the adjusted Larmor frequency, usually in the form of a band of frequencies, we

can selectively excite protons in a specific region. For instance, a linear function of z , such as $G_z = f(z)$, can be used to create a magnetic field gradient along the z dimension. This gradient in turn leads to a variation in Larmor frequencies along the z -axis. During the application of the gradient magnetic field, an RF-pulse can excite a spatially localized group of protons along z . This concept can be extended to the x and y axes using additional orthogonal gradient magnetic fields; G_x and G_y . In turn, every point in the 3 dimensions will have a frequency that is a function of all: B_0 , G_x , G_y , and G_z ; making it possible to excite and receive MR signals in an independent spatial manner.

Using a receiver coil tuned to the Larmor frequency, via electromagnetic induction theory, it is possible to measure the electrical voltage induced in the coil by the transverse plane net magnetization (right part of panel c in Figure 1.3). The resulting voltage is proportional to the frequency of the alternating current and the inductance of the coil. The detected signal is then “digitalised” and processed by the MRI console, the word digitalised refers to extensive processes before getting an actual MR image, including but not limited to Analog-to-Digital conversion (ADC), k -space and k -space sampling, Fourier-transformation and reconstruction before landing to visualization (Lipton, 2008).

1.3.2 Methods for studying the white matter with MRI

Relaxometry MRI techniques

Relaxometry MRI refers to the contrasts that are based on the basic phenomena of magnetic resonance of water molecules, primarily the longitudinal (T_1) or transverse (T_2) relaxations, as depicted in Figure 1.4. Different tissues usually exhibit distinct T_1 and T_2 times. Sequences that are designed to be sensitive to either T_1 or T_2 relaxations are known as T_1 -weighted or T_2 -weighted contrasts, respectively. Both types of contrasts capture a single instance of brain tissue at the scanning time. In T_1 -weighted images, the brain’s white matter appears brighter than grey matter due to the shorter T_1 (longitudinal relaxation) times of lipids within myelin. At a magnetic field strength of 3 Tesla, grey matter exhibits a T_1 time of 1331 ms, whereas white matter demonstrates a T_1 of 832 ms (Wansapura et al., 1999). Additionally, for T_2 time, grey and white matter display values of 80 ms and 110 ms, respectively (Wansapura et al., 1999). The T_1 contrast is particularly effective at depicting overall WM anatomy and gross structural lesions, such as multiple sclerosis plaques; however, it provides limited specificity for distinct pathologies. In contrast, T_2 -weighted contrasts exhibit longer T_2 (transverse relaxation) times in white matter compared to grey matter, making white matter appear relatively darker on T_2 -weighted images. This contrast is particularly sensitive to water content changes associated with oedema, inflammation, demyelination, or axonal loss (Barkhof and Scheltens, 2002). Fluid-attenuated Inversion Recovery (FLAIR) sequences are particularly effective in suppressing the signal from CSF, thus increasing the contrast between lesions and surrounding tissues. FLAIR is commonly used to detect white matter hyperintensities (WMHs), indicative of various pathologies, including vascular diseases, inflammation, and demyelination (Filippi et al., 2018). In addition to T_1 and T_2 -weighted

contrasts, Proton Density (PD) images reflect the concentration of protons (primarily in water). These images provide excellent anatomical delineation, but subtle white matter pathology may be less noticeable than on T2-weighted or FLAIR images.

Conventional MRI is pivotal in the diagnosis and monitoring of demyelinating disorders like multiple sclerosis. T2-weighted and FLAIR sequences are used to visualize and characterise white matter lesions associated with multiple sclerosis and monitor changes in lesion burden over time (Wattjes et al., 2015). White matter changes, which may precede grey matter atrophy, can be detected with conventional MRI in neurodegenerative conditions like Alzheimer's disease and frontotemporal dementia. Moreover, ischemic changes and chronic small vessel disease within white matter are prominently visible on T2-weighted and FLAIR images, offering insights into cerebrovascular health and its association with cognitive decline (Wen and Sachdev, 2004). Nonetheless, conventional contrasts often lack specificity for differentiating the exact nature of white matter pathology. Combining MRI sequences, clinical context, and possibly additional advanced techniques (e.g., diffusion-weighted imaging, to be introduced next) is essential for accurate diagnosis. Collectively, multimodal MR imaging will be better suited to provide greater sensitivity and specificity, by probing specific white matter properties like myelination and axonal integrity (Filippi et al., 2016).

Diffusion-weighted MRI (dw-MRI) and Diffusion Tensor Imaging (DTI)

Water molecules exhibit constant motion at temperatures above absolute zero due to their inherent thermal energy. This motion is referred to as a "random walk" as the trajectories of the motion are completely random. This constant motion is known also as Brownian motion, as it was named after the botanist Robert Brown who was the first to observe it back in 1827, and subsequently, mathematically detailed by Albert Einstein in 1905 (Einstein, 1905). Random walk, or Brownian motion, refers to the random translational motion or diffusion of molecules. Where in a free medium, the average diffusion displacement of water molecules is zero, while the variance of the displacement is given by:

$$\langle r^2 \rangle = 2D\Delta \quad \text{Eq. (2)}$$

where $\langle r^2 \rangle$ represents the mean-squared distance, D is the diffusion coefficient and Δ is the time of diffusion.

In an environment free of barriers, this random motion is isotropic with displacement variance that is equal in all directions. Whereas in a non-free environment as in living organisms, water molecules are abundant in soft tissues (e.g. the brain), and the displacement trajectory of the molecules will be influenced by the shape and orientation of the structures they are embedded in, such as axons, cell bodies, and glia. In areas filled with cerebrospinal fluid, like the ventricular system, water molecules diffusion is nearly identical to that in a medium without barriers, resulting in a form of isotropic diffusion. Grey matter, which primarily consists of cell bodies, neurites and axon terminals in the brain cortex and subcortical structures, has a roughly isotropic diffusion profile. This is due to the lack of a preferred

displacement direction in the grey matter, since diffusion is equally likely to occur in all orientations, resulting in a low magnitude of diffusion anisotropy. In the context of white matter, diffusion is more facilitated along the elongated axis of a neuronal bundle than along its cross-section, and for this reason, white matter is an anisotropic structure.

Detecting diffusion in MRI scanning, in simple terms, is achieved through a label that is assigned to hydrogen nuclei by manipulating the phase of the transverse magnetization. The displacement of water molecules is determined by checking this label after a certain period of time (diffusion time). The greater the signal attenuation, the greater the motion that has occurred, or in other words the displacements that the nuclei had undergone. The contrast between diffusion patterns exhibited by different microstructural environments forms the basis of dw-MRI, which uses the measured diffusion pattern to indirectly inform about the underlying microstructure of the media being scanned (Stejskal and Tanner, 1965).

Diffusion imaging provides fine details of WM anatomy, as mentioned, by sensitizing the random motion of water trapped inside its substructures. One of the major advantages of diffusion imaging is its ability to highlight the degree of diffusion anisotropy, which is the difference in diffusion properties along different directions. The most parsimonious mathematical construct that is capable of accounting for anisotropic diffusion in a three-dimensional environment is a tensor. Hence, in the context of Diffusion Tensor Imaging (DTI), the diffusion tensor D , which is a 3×3 matrix, is employed to model water diffusion in each individual voxel (volume-element) (Basser et al., 1994).

$$D = \begin{bmatrix} D_{xx} & D_{xy} & D_{xz} \\ D_{yx} & D_{yy} & D_{yz} \\ D_{zx} & D_{zy} & D_{zz} \end{bmatrix} \quad Eq. (3)$$

D is made up of nine terms, but only six of them are independent due to the symmetry of the tensor. Consequently, in order to measure the diffusion tensor, a minimum of six measurements along different orientations, in addition to one measurement without diffusion weighting, are required, although a higher signal-to-noise ratio can be achieved by using more measurements (Jones and Basser, 2004). From the eigendecomposition of D , various scalar indices may be obtained, the most utilized indices are mean diffusivity (MD) and fractional anisotropy (FA), as defined by the following expressions:

$$MD = \frac{\lambda_1 + \lambda_2 + \lambda_3}{3} \quad Eq. (4)$$

$$FA = \sqrt{\frac{(\lambda_1 - \lambda_2)^2 + (\lambda_2 - \lambda_3)^2 + (\lambda_3 - \lambda_1)^2}{2(\lambda_1^2 + \lambda_2^2 + \lambda_3^2)}} \quad Eq. (5)$$

MD is the average value of the three diffusivities measured along the eigenvectors, i.e., the average water diffusivity within the measured volume (the voxel in MRI), MD is expressed in square meters per second (m^2/s). FA instead measures the degree of diffusion anisotropy of

the tissue. Anisotropic tissues have fractional anisotropy values closer to 1 (unitless), indicating that the diffusion of water molecules occurs predominantly in one orientation and can be visualized as a cigar-shaped ellipsoid (see Figure 1.5). In contrast, isotropic tissues have fractional anisotropy values closer to 0, indicating that the diffusion is similar in all directions and can be visualized as a sphere (Beaulieu, 2002). These scalars are translationally invariant, which means that they do not depend on the specific orientations along which the diffusion is measured. This makes them ideal as quantitative biomarkers of brain microstructure, to provide valuable information for diagnosing various pathologies.

For instance, among the diffusion-based indices extracted from dw-MRI, FA has probably become the most popular in neurology and psychiatry, with its reduction commonly interpreted as a marker of loss of white matter integrity (Jones et al., 2013).

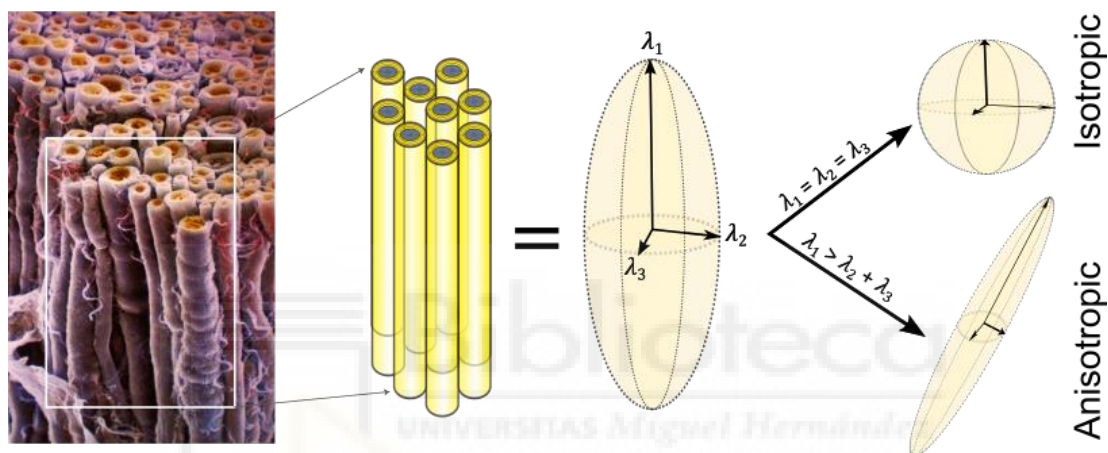


Figure 1.5 Tensor illustration. The concept of a tensor to capture the underlying microstructures. Left section represents an electron microscopy for axonal bundles that is modelled as cylinders. From tensor characteristics we could infer the degree of isotropy; complete isotropic were the tensor's eigenvectors all are equal $\lambda_1 = \lambda_2 = \lambda_3$, and anisotropic when $\lambda_1 > \lambda_2 + \lambda_3$.

From the tensor eigenvalues, we can obtain the Axial Diffusivity (AD), which is defined as the diffusion magnitude along the principal (longitudinal) axis of the tensor:

$$AD = \lambda_1 \quad Eq.(6)$$

In addition to AD, the radial diffusivity (RD) is the average diffusion in the tensor transverse directions (second and third eigenvalues):

$$RD = \frac{\lambda_2 + \lambda_3}{2} \quad Eq.(7)$$

These indices, alongside MD and FA, are widely used in the field of medical imaging to quantify brain microstructure and provide valuable information for diagnosing various pathologies (Baijot et al., 2022; Budde et al., 2009; Weston et al., 2020; Winklewski et al., 2018; Zanon Zotin et al., 2023).

Tractography

In white matter fibres, we could infer that the highest diffusivity, which represents the direction of the principal eigenvector, can serve as a proxy for the main fibre orientation. This inference assumes that the alignment of multiple neuronal axons along a shared axis results in greater resistance to the diffusion of water molecules across this axis compared to along it (Johansen-Berg and Behrens, 2014). By integrating these estimates across the whole brain white matter, it is possible to generate a three-dimensional representation of the major axonal bundles. These are the basis of the technique called *tractography*, which offers a powerful, non-invasive method for mapping white matter pathways (fibre tracts) within the brain, sometimes referred to as the “computational anatomy”, permitting to perform brain dissection in a “virtual” fashion (Oishi, 2011). Reconstructing fibre bundles by following the principal axis of this tensor in a stepwise manner is known as tensor-based tractography. This procedure can be achieved by applying concepts from field vector calculus to the fibre orientations extracted from dw-MRI datasets (Basser et al., 2000). Fibre-tracking starts from a specific point “seed” and is directed towards the path of least-hindered diffusivity, which equals maximum anisotropy, which represents the primary fibre orientation. The path followed in this direction continues until it reaches the next designated point, as defined by the predetermined step-length, where it then follows an interpolated streamline. This process is performed repeatedly until one or more termination criteria are met, such as reaching an area with a chosen threshold for FA, a way to restrict fibre tracking to WM only, or terminating upon entering “stop” region. Tractography methods are typically categorized into two groups: deterministic and probabilistic. In the first group, a single curve is reconstructed for each starting point, which serves as a point estimate of the underlying pathway. On the other hand, the probabilistic approach involves repeating fibre tracking from the same starting point and stochastically sampling the modelled fibre orientation distribution, which generates a spatial distribution of streamlines that represents the uncertainty in estimation. In simpler terms, this approach reflects the probability that a reconstructed fibre pathway passes through a given voxel.

Indeed, FA driven from DTI has become a powerful basis for tractography since its origin. Despite this utility, DTI indices suffer from some limitations, as they lack specificity with respect to the intricate structure of brain tissue within a single voxel; we will expand on that in the next section. Emergent methods try to overcome such drawbacks, by going beyond modelling the dw-MRI with just a tensor. For instance, High Angular Resolution Diffusion Imaging (HARDI), HARDI methods acquire diffusion data in more directions, allowing better modelling of complex fibre orientations. Such acquisition schemes allow techniques like Q-ball imaging and constrained spherical deconvolution (Tournier et al., 2008; Tuch, 2004) to resolve multiple fibre populations within a voxel. Overall, advances in diffusion modelling methods are an active research area (Canales-Rodríguez et al., 2015; Dela Haije et al., 2020; Herberthson et al., 2021; Morez et al., 2023; Sotiropoulos et al., 2013). Despite these developments, still, an inherent limitation of these tractography methods, and diffusion data

in general, is the inability to handle the noisy nature of diffusion, which implies extensive preprocessing steps before any useful information can be obtained. Preprocessing, in general, includes sophisticated methods to deal with artifacts and noise based on their origins, whether it is sequence-specific noise or subject motion, techniques such as denoising, skull-stripping, motion and eddy-current corrections are crucial components of any diffusion pipeline analysis. An appreciation of these methods and their significance can be found in Figure 1.6, which it, in a broader term, explains dw-MRI from design to analysis and visualization. Nevertheless, tractography, whether based on DTI or other advanced methods, is capable of mapping the connectome of the brain, setting the basis for the investigation of white matter organization in health, ageing and disease. Beyond scientific research, it has great potential in neurosurgical planning by delineating critical white matter tracts, tractography maps reduce the risk of inflicting damage during tumour resection, epilepsy surgery, or deep brain stimulation. Identifying the relationship between tracts and lesions aids in patient selection and surgical decision-making (Nimsky et al., 2005).



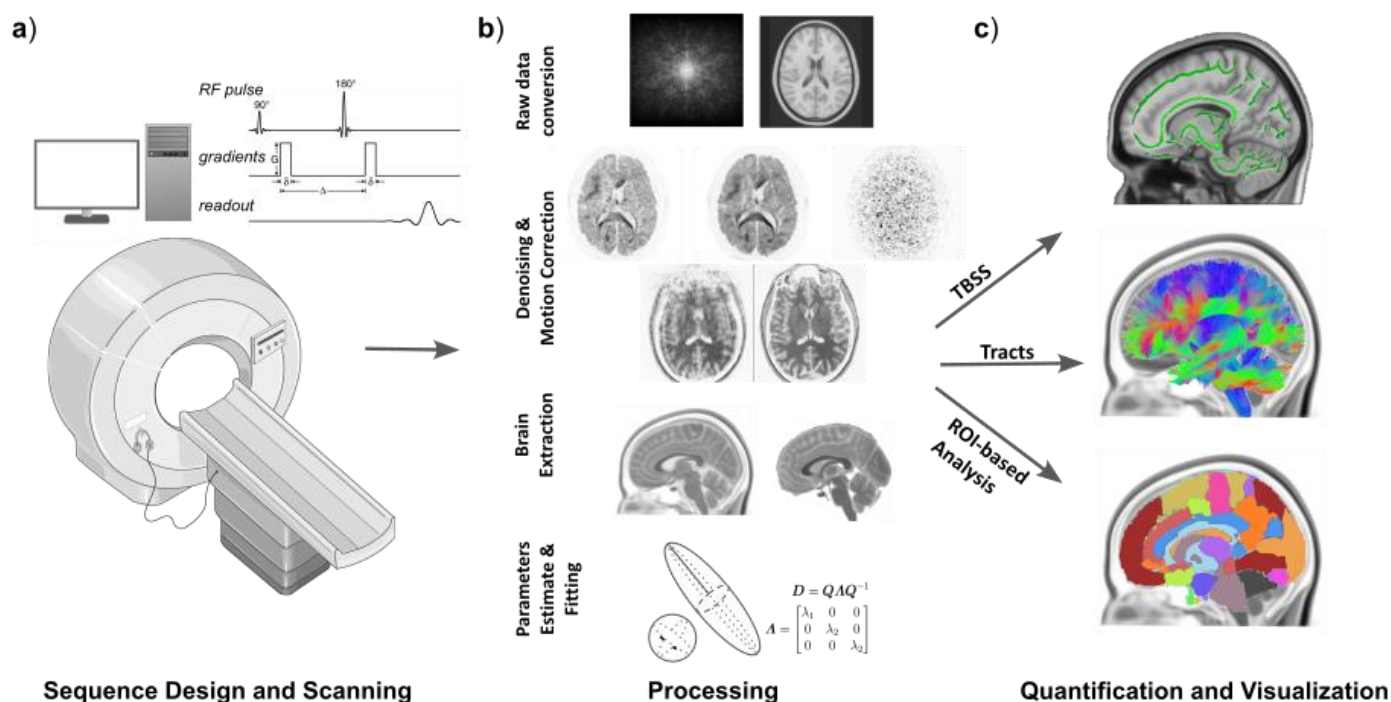


Figure 1.6 Diffusion-weighted MRI pipeline, from acquisition and processing to visualization. (a) Diffusion-weighted MRI experiments normally include several acquisition and processing steps. The diffusion weighted MRI sequence is adjusted based on the particular requirements of the experiment regarding diffusion weighting (measured by the b -value) which, by defining the time allowed for the labelled water molecule to diffuse and the range of diffusivities on which the sequence focuses, weights the contribution of the different tissue compartments to the diffusion measurement (e.g., diffusion in the intracellular vs. extracellular space). Other important parameters to define are the number of diffusion gradient directions, which define the orientations in which diffusion will be quantified; or the image resolution, which is a compromise between the capabilities of the MRI system to acquire data with good signal-to-noise ratio and the time devoted to acquiring them, and which determines the voxel size. (b) Once the appropriate diffusion-weighted MRI sequence has been identified and acquired, preprocessing steps may include denoising, motion and distortion corrections, brain extraction, and normalization to other contrasts. Afterwards, the desired diffusion model is applied, and the data are visualised, prepared for the statistical analysis of choice. (c) Statistical analysis normally involves voxel-wise approaches like the widely adopted tract-based spatial statistics (Smith et al., 2006), or region-of-interest approaches like those based on parcellated brains in standard space (Mori et al., 2008), or on tractography in single subject space (Chamberland et al., 2021).

Biophysical modelling

In the tensor framework (DTI), each voxel represents a single tensor with a single Gaussian profile, considering the scale of neuronal cells and their axons in (μm) relative to typical MRI voxel sizes (mm), many factors would be contributing to the resulting FA value, such as the amount of myelin, axonal density, axonal diameter, and fibre distribution. A single diffusion tensor would represent the average over tens of thousands of cells and/or axons, therefore, it is not straightforward to assign a specific tissue configuration or biological state to a measured FA change (see Figure 1.7-a for orientation). In the absence of this beyond

information DTI is unable to distinguish between diverse processes, whether cellular or subcellular, such as loss of structural integrity, inflammation, or neural remodelling, and thus leads to limited and an inherently vague representation of the underlying tissue compartments or neuroanatomy in general (De Santis et al., 2014). Consequently, more advanced dw-MRI acquisition schemes and reconstruction methods have been developed to surpass the constraints of DTI. “Biophysical modelling” provides the tools to translate the intricacies of water diffusion into detailed information about brain tissue properties and their potential changes due to disease or development. Biophysical models of dw-MRI seek to bridge the gap between the diffusion signal and underlying tissue properties, they can be framed into two categories:

- 1- Compartment models: These models aim to partition the complex diffusion signal into distinct components representing various biological environments:
 - The Ball-and-Stick Model: Represents intracellular diffusion as restricted within 'sticks' and extracellular diffusion as free ('ball') diffusion (Behrens et al., 2003). This model is useful for characterising the properties of white matter fibre bundles.
 - Multicompartment models: Such models address DTI's shortcomings by incorporating separate compartments for intra- and extracellular diffusions, enhancing the characterisation of complex tissue structures. An example is the Composite Hindered and Restricted Model of Diffusion (CHARMED) (Assaf and Basser, 2005), where the diffusion's signal is fitted into two compartments, one intracellular represents the restricted diffusion and one extracellular represents the hindered part, look at panel (b) of Figure 1.7 for illustration. Another example is the Neurite Orientation Dispersion and Density Imaging (NODDI) which is similar to CHARMED in modelling two distinct compartments for diffusion signal (intra and extra) but it adds an extra third compartment separately for the cerebrospinal fluid (Zhang et al., 2012).
- 2- Tissue models: These models offer a more intricate representation of brain tissue, explicitly incorporating parameters that describe cellular structures known to influence diffusion patterns:
 - AxCaliber: Estimates the distribution of axon diameters within an imaging voxel (Assaf et al., 2008). It offers information about axonal health and remodelling after injury or during pathophysiological status.
 - ActiveAx: Models white matter with realistic representations of axon properties, including varying orientations, diameters, and myelin content, it provides detailed insights into white matter pathology (Alexander et al., 2010).
 - White Matter Tract Integrity (WMTI): Models water diffusion in and around white matter axons, including axon diameter distribution (Fieremans et al., 2011). This model helps quantify white matter changes related to disease or development.

- Standard Model (SM): Represents brain tissue as a complex composition of cells, axons, and dendrites, facilitating the investigation of diffusion in highly complex environments like the grey matter (Novikov et al., 2019).

In summary, biophysical models extract valuable information from dw-MRI data, including fibre orientation mapping, quantification of axonal density, diameter, and myelination, all of which provide sensitive biomarkers for various neurological and psychiatric conditions. Moreover, biophysical models can detect subtle changes in tissue structure, enabling the investigation of disease progression or treatment effects, for instance, a recent study showed the capability of multicompartment modelling of diffusion to map activation of microglia and astrocytes independently, their activation, a complex process involving morphological and molecular changes, is a hallmark of the brain's response to various stimuli (Garcia-Hernandez et al., 2022). Despite these promising insights, there are challenges to face when it comes to bio-modelling brain microstructures in a fine detail. These include model validation where developing methods to directly validate these biophysical models against actual tissue remains an ongoing challenge. Many models are computationally demanding, making clinical translation and large-scale studies more difficult. Additionally, advanced models may need specialized MRI sequences, often at the cost of increased scan times and complexity, making it restricted to research settings and far from direct application. An elegant summary, yet comprehensive, of the microstructural modelling of brain tissue using dw-MRI can be found in the work of Alexander et al. (Alexander et al., 2019).

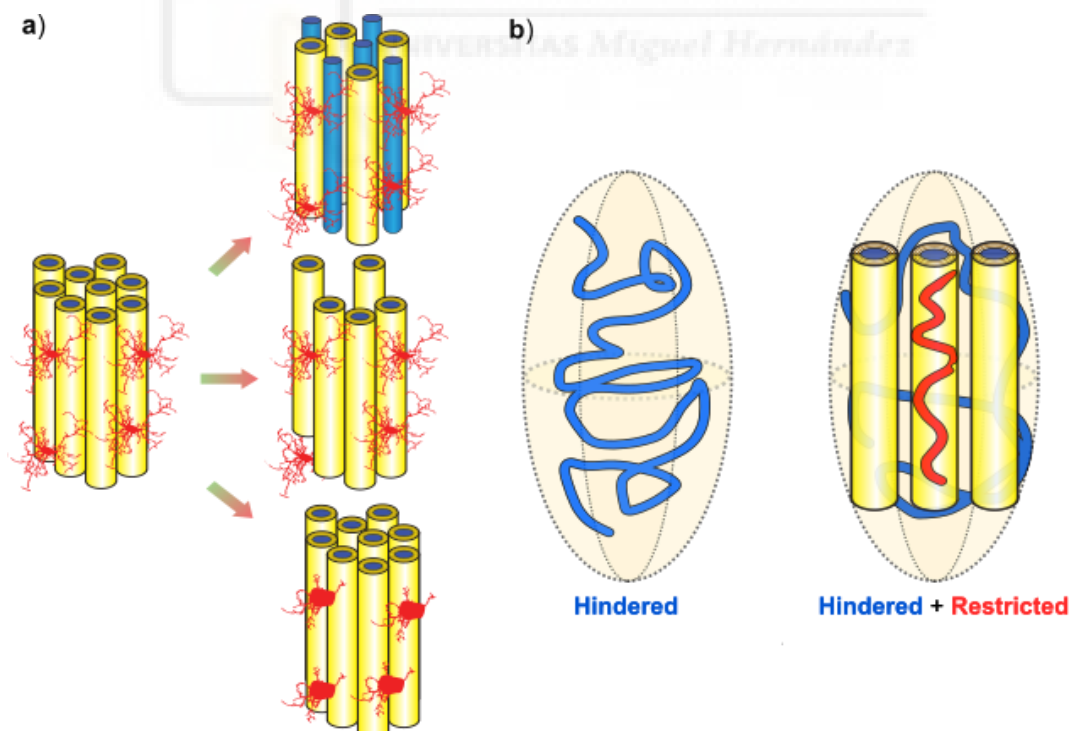


Figure 1.7 Different elements contribute to the observed diffusion signal. (a) Potential biological substrates drive the observed changes in fractional anisotropy, from an ideal scenario on the left to demyelination, axonal loss, or glia morphological changes on the right side. (b) Representation of modelling diffusion signal as single hindered compartment (DTI) vs Two compartments modelling; intra-axonal with restricted diffusion and extra-axonal as hindered signal (CHARMED). Myelin is shown in yellow, axons in blue and microglial cells in red.

Functional MRI (fMRI) and resting-state functional MRI (rs-fMRI)

Functional MRI, often abbreviated as fMRI, is a major modality derived from MRI for investigating brain activity and communication between different brain regions. The term "functional" highlights its relevance to neuronal activity and its pertinence to multiple levels of brain function, such as cognitive and sensory processing. Although fMRI is not specifically designed to study white matter, it has been used to investigate diseases where the primary pathology occurs in the white matter (Rocca et al., 2022). Considering the importance of white matter as the brain's highways, any damage to the WM can have a significant impact on communication between brain regions. Such induced damage will result in altered internal signalling and, eventually, affect overall brain function.

In essence, fMRI is based on a biophysical property of blood haemoglobin (Hb), where oxygenated haemoglobin (Hb) is regarded as diamagnetic, i.e., very weakly repelled, while deoxygenated haemoglobin (dHb) was reported to be paramagnetic, i.e., weakly attracted to magnetic fields, displaying a considerable magnetic moment. The existence of paramagnetic material within a homogenous magnetic field will induce a form of susceptibility, in such a scenario protons will precess at marginally different frequencies, as a consequence the MR signal will attenuate faster than usual, such phenomenon was postulated in the work of Ogawa in 1990, where he showed upon acquisition of T_2^* contrast, which has a particular sensitivity to proton inhomogeneities, the appearance of dark lines in the images of a deceased rodent that had not been presented previously, became evident. These lines were no longer apparent when the animal was breathing pure oxygen and became visible once again when the animal was experiencing asphyxiation (see Figure 1.8-a). Consequently, he and his colleagues confirmed that deoxygenated blood leads to a faster decay of transverse magnetization of the MRI signal and this decay is more evident at stronger magnetic strengths (Ogawa et al., 1990). The term Blood-Oxygenation-Level Dependent (BOLD) was named after Ogawa's discovery, BOLD contrast, or BOLD signal is the core of modern-day fMRI work. When neurons fire upon activity, they require increased energy, this triggers a localized increase in blood flow to the activated region, a process known as the Haemodynamic Response (HDR). HDR brings oxygen-rich blood to the active area. However, oxygen consumption by active neurons increases at a slower rate than oxygen delivery, leading to a relative excess of oxygenated haemoglobin (oxyhaemoglobin) in that region, changes in the ratio of oxyhaemoglobin to deoxyhaemoglobin alter the magnetic field inhomogeneities which leads to a detectable BOLD signal (Thulborn et al., 1982). The dynamics of such events are described by a waveform that is known as the Haemodynamic Response Function (HRF), shown in panel (b) of Figure 1.8, HRF is usually described by the canonical double gamma function.

BOLD signal is an indirect measure of neural activity, influenced by several factors including baseline blood flow, vascular reactivity, and the intricacies of “neurovascular coupling”, a term that refers to the correlation between, both vascular and neuronal activities. Early evidence of such a relationship comes from the landmark study conducted by Logothetis et al. (Logothetis et al., 2001), researchers recorded single-, multi-unit activity, and Local Field Potential (LFP) in addition to BOLD fMRI in the visual cortex of anesthetized monkeys. The study concluded that, the LFP responses were found to provide the most accurate estimate of the BOLD signal compared to the other measures. These findings postulated that the BOLD signal unambiguously reflects the neural responses upon receiving a stimulus.

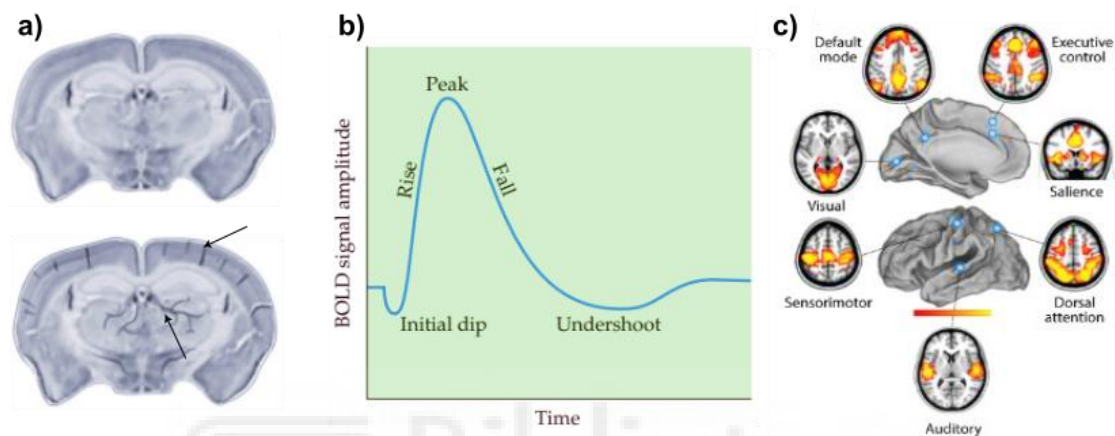


Figure 1.8 Proceedings on the development of fMRI. (a) Ogawa’s work showing dark lines on rodent T2 contrast with lack of oxygen supply. (b) Haemodynamic response function. (c) Different resting-state networks. a and b are adapted from (Huettel et al., 2014) and c from (Raichle, 2015).*

Consequently, numerous studies investigating different brain mechanisms have taken advantage of the fMRI potential, alone or in conjunction with direct activity manipulators, such as electrical brain stimulation (Canals et al., 2008) or optogenetics (Christie et al., 2013). The goal of these joint approaches is to reach the brain’s deep structures that cannot be recruited by simple sensory protocols. These experimental paradigms have significantly advanced our understanding of the connectivity between different brain areas at a circuit level, particularly by examining the transmission of signals triggered by stimulation application. For instance, stimulating the perforant pathway using glass-coated iridium electrodes revealed the first fMRI evidence of Long-Term Potentiation (LTP), a complex process of synapse strengthening implicated in learning and memory (Canals et al., 2009).

The term fMRI in common practice, is perceived usually as the task-based fMRI which involves an individual lying inside the scanner and being exposed to an external stimulus, such as a visual stimulus, or engaging in a task, like finger-tapping or pronouncing specific words, following a predetermined scheme. The aim of this technique is to localize different brain functions in response to executed tasks. Another type of fMRI is resting-state fMRI (rs-fMRI), which seeks to understand the general network structure of the brain and how these networks interact with one another. The “rest” in the resting-state term, is an operational definition in which the individual is not exposed to a particular stimulus or behavioural task, but rather

maintains a constant condition. This concept is characterised by synchronized fluctuations in brain activity even, as mentioned, in the absence of an explicit task. Examining the temporal correlations within these fluctuations provides insights into the brain's intrinsic functional organization. Studies have shown that these connectivity patterns are highly conserved across species, as demonstrated by research on anesthetized rats (Pawela et al., 2008) and on monkeys (Vincent et al., 2007). While conducting early fMRI studies centred on task-based activation, researchers discovered that specific regions of the brain showed a paradoxical deactivation when a task was executed. These areas, comprising the medial prefrontal cortex and posterior cingulate cortex, were collectively referred to as the Default Mode Network (DMN) (Raichle et al., 2001). Several networks, each with their distinct pattern of fluctuations, were identified later. These networks (see panel (c) in Figure 1.8) include those involved in sensory processing (visual, auditory), motor control, attention, and higher cognitive functions (S. M. Smith et al., 2009). The consistent activities observed within networks imply the presence of functional connectivity. In this context, connectivity is not determined by direct anatomical connections, but rather by the synchronization of BOLD oscillations over time, reflecting a coordinated function among spatially distributed regions.

In brief, functional magnetic resonance imaging, whether used for task-based or resting-state analysis, is a valuable instrument for offering remarkable insights into the brain's intrinsic activity. It has the potential to serve as an impartial diagnostic tool and clinical biomarker for numerous neurological conditions (Hohenfeld et al., 2018; Paulsen et al., 2004; Rocca et al., 2022; Sperling, 2011). For a comprehensive review of fMRI theory and practice please refer to this source (Huettel et al., 2014).

1.3.3 MRI strengths and limitations

MRI, with its multiple Nobel Prize-backed advancements, represents a cornerstone for clinical diagnostics, surgical planning, and treatment monitoring. MRI excels at differentiating between different types of tissues in the brain. This is crucial for identifying subtle induced changes in the brain parenchyma, such as those associated with early-stage diseases or injuries. Its superior contrast resolution allows clear visualization of white matter, grey matter, cerebrospinal fluid, and blood vessels, aiding in diagnosing various brain abnormalities. Unlike Computed Tomography (CT) scans, which use X-rays, or Positron Emission Tomography (PET) which uses radioactive tracers to image molecular-level processes, MRI employs powerful magnetic fields and radiofrequency waves. This non-invasive approach eliminates the risk of radiation exposure, making it exceptionally safe and suitable for repeated imaging and longitudinal studies. MRI scanners can acquire images in various geometrical planes (i.e., sagittal, coronal, and axial), which provide a comprehensive three-dimensional view of the brain. This flexibility is crucial for pinpointing the exact location of abnormalities and for surgical planning. Also, it comes with diverse imaging capabilities including the previously explained diffusion and functional MRI. Other existing methods to record brain activity, like electrical ones in the case of Electroencephalography or Magnetoencephalography for

neuromagnetic activity, offer insights into brain function in health and disease. However, they lack the spatial resolution of MRI to pinpoint the exact source of activity. Figure 1.9 represents an appreciation of where MRI and its different modalities stand among the other conventional neuroscience methods in terms of both spatial and temporal resolutions.

While MRI has revolutionized our understanding of brain structure, it's important to acknowledge some limitations, including artifacts from patient motion (Andre et al., 2015), or magnetic field inhomogeneities (Wang and Doddrell, 2005). Both dw-MRI and fMRI are sort of Echo Planar Imaging (EPI), which means inherent noise, susceptibility artifacts, and partial volume effects in the data (Buonocore and Gao, 1997). All can undesirably influence subsequent results. Hence, the interpretation of MRI findings in the context of white matter must be conducted with care, given the potential for WM changes to occur in various pathologies, in addition to insufficient validation of the biophysical models against actual tissue. The adoption of standardized MRI acquisition protocols and analysis pipelines would significantly improve the reliability and comparability of such findings (George et al., 2020). Furthermore, the development of innovative MRI techniques, such as advanced diffusion modelling and myelin-specific contrast agents, holds great promise for enhancing the sensitivity and specificity of WM investigations in both healthy and diseased states.

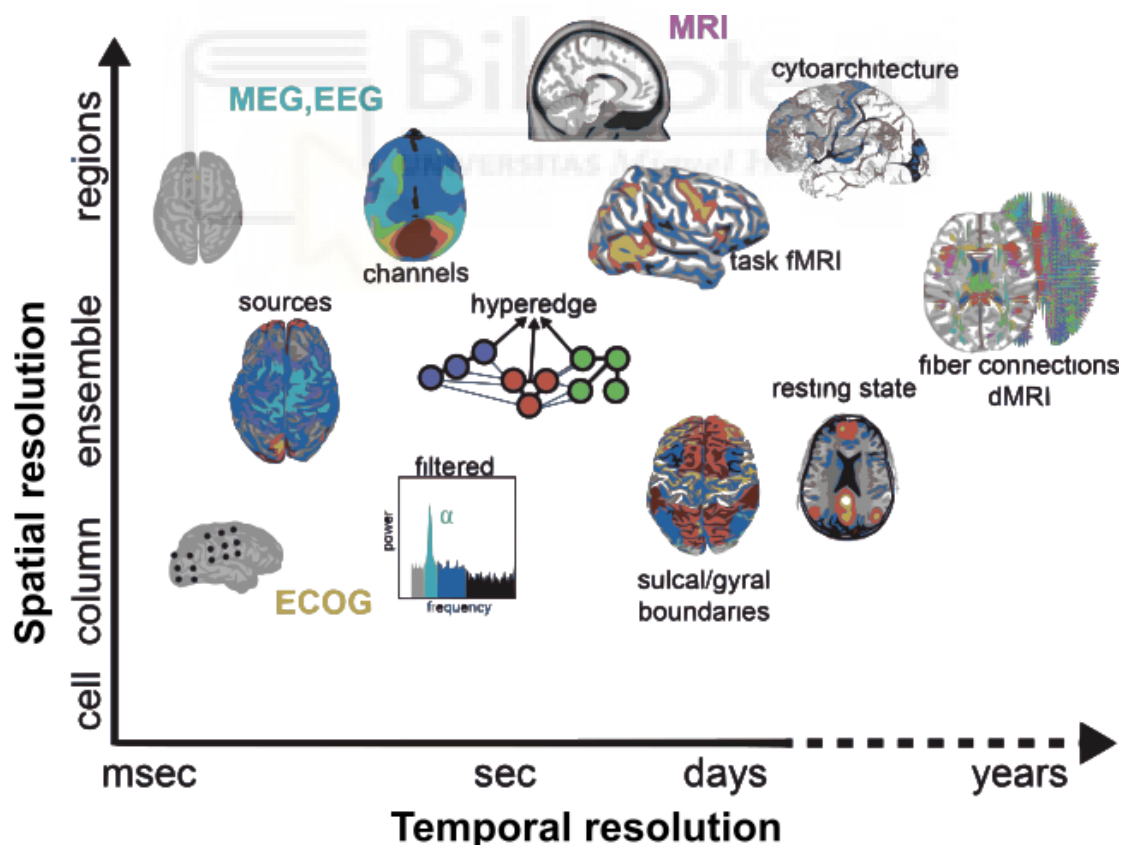


Figure 1.9 Temporal and spatial resolutions of different brain mapping techniques. MRI techniques occupy a unique place in the spatio-temporal resolution space, compared to the rest of the tools. Acronyms: ECOG, electrocorticography; EEG, electroencephalography; MEG, magnetoencephalography; dMRI, diffusion MRI; fMRI, functional MRI. Figure is adapted from (Garcia et al., 2018).

1.3.4 Relevance of MRI in studying AUD

Different modalities of MRI have been used since the beginning to study AUD, to understand the underlying pathophysiology, and to highlight brain-induced alterations. Studies have shown that individuals with AUD exhibit reduced grey matter volumes in regions such as the prefrontal cortex, hippocampus, and cerebellum, which are crucial for decision-making, memory, and motor coordination, respectively (Bühler and Mann, 2011; Li et al., 2021). Structural MRI studies on hippocampal volume highlighted significant atrophy of the hippocampus in individuals with alcohol dependence relative to healthy controls, which has been found to have a detrimental effect on memory and learning capabilities (Agartz et al., 1999; Sullivan et al., 1995).

In addition, diffusion tensor imaging has revealed microstructural alterations in white matter tracts of patients with AUD, suggesting compromised neural connectivity within key brain networks (Pfefferbaum et al., 2009). Widespread microstructural alterations have been observed throughout the whole white matter skeleton (De Santis et al., 2023, 2019; Pfefferbaum and Sullivan, 2005; Yeh et al., 2009), while some other studies focused on certain bundles, such as the corpus callosum, the fimbria-fornix, internal and external capsules, and cingulate and longitudinal fasciculi (Bühler and Mann, 2011; Pérez-Cervera et al., 2023; Pfefferbaum et al., 2014, 2009; Yeh et al., 2009). A notable study that contrasted relapsers and abstainers after six- to nine months of detoxification indicated that the former exhibited lower white matter integrity in the corpus callosum and the right stria terminalis/fornix, as indicated by DTI metrics. This difference was associated with their relapse scores and persisted despite comparable lifetime and recent drinking histories. This suggests a direct correlation between the preservation of white matter and relapse risk (Zou et al., 2018). Employing MRI in animal models of AUD yielded comparable outcomes to human subjects. In a four-day binge protocol involving intragastric gavage, wild-type rats exhibited transient changes in white matter, as detected by DTI (Pfefferbaum et al., 2015). Furthermore, a longitudinal study conducted on an alcohol-preferring rat line revealed altered white matter in the rats, which persisted even after alcohol cessation and was comparable in magnitude to the changes observed in human subjects (De Santis et al., 2019).

A More elaborative content on the usage of dw-MRI in AUD, with a particular emphasis on DTI utility is published as a chapter of the Alcohol and Alcohol-related Diseases book (Mueller and Heilig, 2023). The Brain Microstructure in Alcohol Addiction chapter (De Santis et al., 2023) forms part of the quality criteria for the current thesis, which is appended in Appendix (C).

Moreover, aberrant functional connectivity in networks like the default mode network highlights the long-term impact of alcohol on intrinsic brain organization, even in the absence of immediate alcohol use (Chanraud et al., 2011). Activation patterns during reward, inhibition, or decision-making tasks expose dysfunctions in relevant circuits in individuals with AUD, often linked to impulsivity and heightened craving (Bach et al., 2020; Bordier et al., 2022; Zilverstand et al., 2018). Pharmacotherapies can benefit from tools like fMRI to evaluate their

efficacy for AUD (Grodin and Ray, 2019), or to define a lesion-based alcohol addiction remission network, for a better localized intervention (Joutsa et al., 2022). In such a way MRI may be used to assess brain changes associated with treatment response or as potential biomarkers for evaluating the efficacy of novel therapeutic interventions. In general, MRI studies help identify brain structural and functional patterns associated with vulnerability to developing AUD, potentially aiding in early interventions (Whelan et al., 2014). Changes in brain structure and function over time with abstinence can inform on recovery processes and potential neuroplasticity.

1.4 Transcranial Magnetic Stimulation

1.4.1 Basics and application of Transcranial Magnetic Stimulation

Transcranial Magnetic Stimulation (TMS) is a non-invasive brain stimulation technique that has emerged as a potential tool for modulating neuronal activity through targeting and stimulating specific brain regions. TMS utilizes brief, high-intensity magnetic pulses delivered through a coil positioned over the scalp. These pulses generate a focused electric current within the brain tissue, influencing the firing of neurons in the targeted region (Lefaucheur et al., 2020). The specific effects of TMS depend on various factors, including stimulation parameters (frequency, intensity, duration) and the targeted brain region. Custom-made of each stimulation protocol depends on tuning and modifying these parameters, in order to achieve specific activity levels or tissue coverage, for example:

1. Stimulation frequency:
 - Low-frequency TMS (≤ 1 Hz): Suppresses activity in the targeted area, potentially mimicking the effects of certain inhibitory neurotransmitters (Chen et al., 1997). This can be useful for dampening overactive brain regions implicated in conditions like epilepsy or chronic pain.
 - High-frequency TMS (≥ 5 Hz): Enhances activity in the targeted area, possibly mimicking the effects of excitatory neurotransmitters (Huang et al., 2005). This approach may be used to stimulate underactive regions associated with depression or stroke recovery.
2. Stimulation intensity: Determines the depth and extent of neural activation. Higher-intensity pulses can reach deeper brain structures, while lower intensities stimulate more superficial regions.
3. Coil placement: To target specific brain regions based on their known functions. Precise coil positioning is crucial for maximizing the desired effects and minimizing unintended consequences.


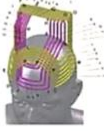


	TRADITIONAL rTMS		DEEP rTMS or DEEP TMS	
COIL DESIGN	Figure-8 coil	H1-coil Bilateral PFC & DLPFC	H7-coil Medial PFC & ACC	H4-coil Bilateral Insula and PFC
				
DEPTH	0.7cm subdural	1.8cm subdural 2.5x deeper	3cm subdural 4x deeper	1.5cm subdural 2.1x deeper
BREADTH	3cm ³ volume	18cm ³ volume millions of more neurons	40.3cm ³ volume millions of more neurons	15.2cm ³ volume millions of more neurons
INDICATION	MDD	MDD	OCD	Smoking Cessation

Figure 1.10 **FDA-approved TMS coils**. Technical specifications of various FDA-approved TMS coils, figure is adapted from (Harmelech et al., 2021).

While TMS can influence the brain in a multifaceted fashion, the precise mechanisms remain under investigation. Nevertheless, research shows some keyways where TMS affects brain structure and function, for instance by altering cortical excitability; as mentioned earlier, TMS can increase or decrease the firing rate of neurons in the targeted area. This can impact the local processing of information and influence communication with other brain regions involved in various cognitive functions. For instance, stimulating the motor cortex can evoke muscle twitches, while stimulating language regions may alternate speech production (Devlin and Watkins, 2007). Repetitive TMS (rTMS) protocols delivered over multiple sessions can induce neuroplastic changes. Neuroplasticity refers to the brain's remarkable ability to reorganize its connections and adapt to stimulation, potentially leading to lasting improvements in function. rTMS protocols can be tailored to either strengthen or weaken specific neural connections, depending on the desired outcome (Gordon et al., 2022). Moreover, TMS can be used as a probing tool to map the functional organization of the brain by studying the behavioural effects of stimulating specific regions. This can help us understand how different brain areas contribute to various cognitive processes like decision-making, memory, or motor control. By observing how TMS disrupts or enhances these functions, researchers can gain valuable insights into the underlying neural mechanisms (Jannati et al., 2023).

Advances in coil engineering have led to the development of new coils capable of achieving better stimulation power and tissue coverage. This advance has resulted in the emergence of a new term, "Deep" TMS, which refers to a category of coils capable of reaching profound brain regions in both width and depth. This leads to the activation of a larger neural population, resulting in widespread stimulation effects. One example of a state-of-the-art deep TMS coil is the H7-coil, which is capable of reaching up to four times deeper than the conventional 8-shaped coil, reaching up to three centimetres beneath the brain dura matter. As illustrated in Figure 1.10, the H7 coil is capable of recruiting neurons within a volume of more than 40 cubic centimetres. It has been approved recently for the treatment of Obsessive-Compulsive Disorders (OCD) (Harmelech et al., 2021). A growing body of research indicates

the therapeutic possibilities of TMS, as mentioned in the case of OCD, but also several examples demonstrate this potential:

- Major Depressive Disorder (MDD): Repetitive TMS protocols targeting specific brain regions associated with mood regulation have shown promising results in alleviating symptoms of depression in individuals who haven't responded well to traditional medications (Tendler et al., 2021).
- Stroke recovery: TMS can be used to stimulate healthy brain tissue near the lesion site after a stroke, potentially promoting neuroplastic changes and facilitating functional recovery in motor skills or language abilities (Hoyer and Celnik, 2011).
- Chronic pain: TMS may offer a non-invasive approach to managing chronic pain by modulating activity in brain regions involved in pain perception (Nardone et al., 2017; Olechowski et al., 2023).
- Nicotine dependence: TMS demonstrated positive results in treating patients with nicotine dependence, promoting smoking cessation. A study showed that rTMS applied to the lateral prefrontal and insular cortices was sufficient to induce a significant reduction in cigarette consumption and nicotine craving (Zangen et al., 2021).

TMS is a well-tolerated intervention with a good safety profile. Most reported adverse effects are transient and mild, including, and most frequently, scalp discomfort or pain at the stimulation spot, it is usually described as a tapping or tingling sensation. Proper coil placement and adjusting stimulation parameters can minimize such discomfort. Besides, headaches can occur after TMS sessions, but they are typically mild and short-lived, resolving on their own or with over-the-counter pain medication (Rossi et al., 2009).

1.4.2 TMS relevance in AUD

Over the last two decades, several attempts have been made on the usage of TMS to study (Kähkönen et al., 2003) or treat AUD (Mishra et al., 2010). Several studies have suggested potential modes of action by which TMS may influence brain structures in individuals with AUD. For instance, neuroplasticity, TMS may induce long-lasting changes in synaptic strength and neuronal circuitry (Hoogendam et al., 2010). Additionally, TMS may act as an antidepressant and modulate neurotransmitter systems, particularly glutamate and GABA, which play crucial roles in the pathophysiology of addiction (Brunoni et al., 2019; Dubin, 2017). TMS may lead to improved function by normalizing dysfunctional neural activity in regions involved in reward processing, decision-making, and impulse control, which are all associated with AUD (Hanlon et al., 2015).

However, clinical studies on TMS for AUD have yielded inconclusive results, with some demonstrating significant reductions in craving and alcohol consumption, while others report more modest effects. For instance, a repetitive TMS study on treating alcohol dependence by targeting the dorsolateral prefrontal cortex (dlPFC) has shown promise in reducing alcohol

cravings, in individuals with AUD (Belgers et al., 2022). Another study targeting the same brain area had no relevant clinical outcome, showing no significant difference between treated and non-treated groups regarding alcohol craving (Höppner et al., 2011). Controversial findings have caused TMS as AUD treatment to remain largely confined to experimental settings. Various factors such as stimulation frequency, intensity, coil design (e.g. Deep TMS), and coil positioning can influence the outcomes of TMS. Therefore, optimizing these parameters and implementing advances in coil design are essential to maximize its therapeutic benefits. Moreover, many studies have been conducted on a small scale or without the use of multiparametric approaches (e.g. imaging techniques) to evaluate TMS efficacy. To date, many efforts have been made to standardise the application of TMS under a community consensus (McClintock et al., 2018; Perera et al., 2016), but larger, well-controlled, multidisciplinary studies are needed to fully assess its effectiveness. Thus, one objective of the present work is to overcome these constraints and introduce a multiparametric, multimodal MRI-supported method for evaluating the effectiveness of Deep TMS in treating AUD.





II. Aims and Objectives

The central goal of this PhD thesis was to investigate alcohol-induced alterations to the microstructure of brain white matter and to analyse the progression of these changes during the early stages of abstinence. Moreover, the thesis aimed to propose Deep Transcranial Magnetic Stimulation as a potential non-invasive treatment for individuals with Alcohol Use Disorder. To achieve this goal, a translational research design was implemented, involving both human subjects with AUD and a rat model of AUD. Specifically, the study focused on advanced diffusion MRI techniques, which facilitated the translation of findings between humans and rats, and were validated through invasive histological methods in the animal model. Ultimately, the research sought to elucidate the specific effects of AUD on compromising axonal integrity and to identify potential mechanisms through which TMS may interact with this pathology to produce positive therapeutic outcomes.

The specific objectives of this thesis were:

1. To probe the integrity of white matter in AUD employing diffusion-weighted MRI in both human subjects diagnosed with AUD and an AUD rat model.
2. To investigate the evolution of the structural alterations during abstinence.
3. To introduce the utility of advanced diffusion models to characterise the damage induced by alcohol consumption.
4. To validate MRI findings with gold-standard histological analysis.
5. To test the hypothesis that Deep TMS may recover white matter microstructure based on the concept of myelin plasticity, and therefore improve brain function in patients with AUD.



III. Materials and Methods

This thesis comprises two independent yet connected investigations, one of which has already been published in (Selim et al., 2023), and is appended in Appendix (C). The experimental designs for both studies are outlined in Figures 3.1 & 3.2.

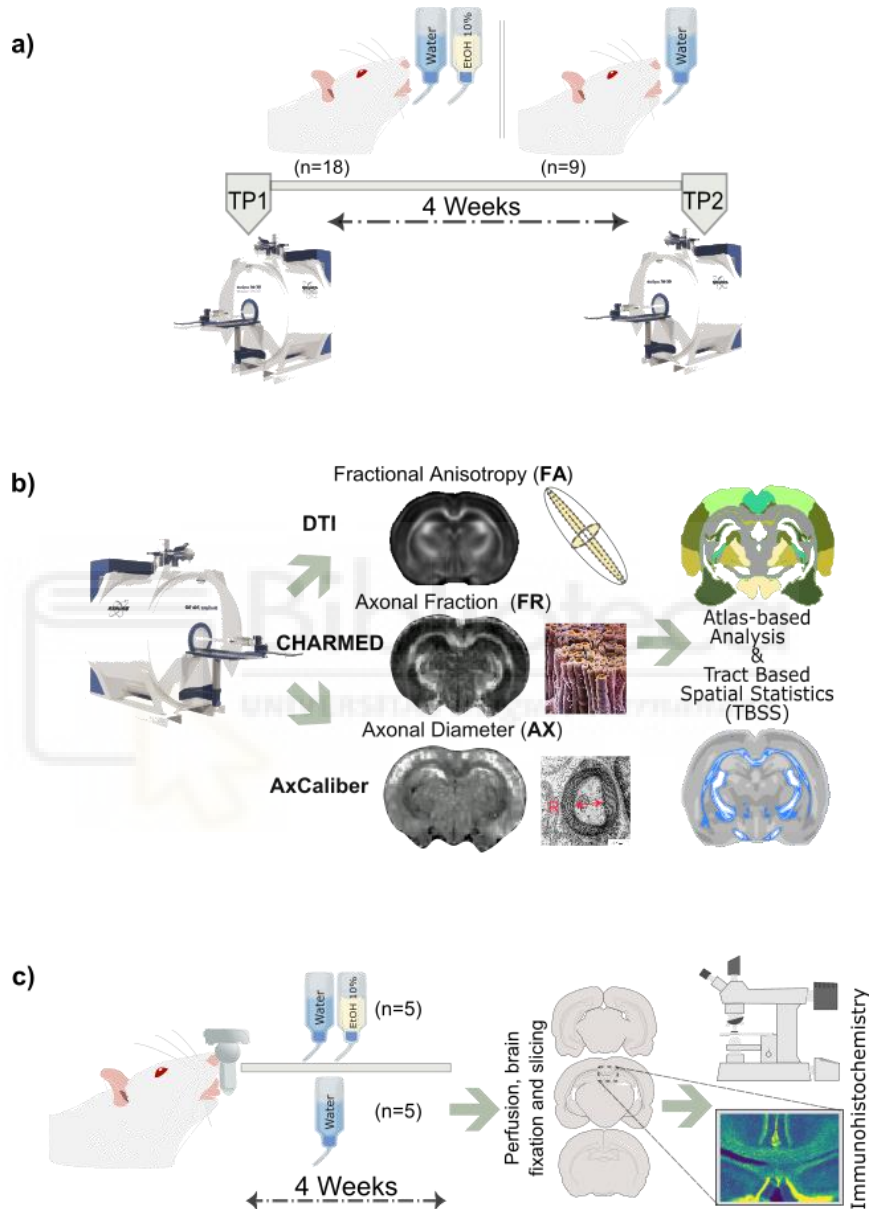
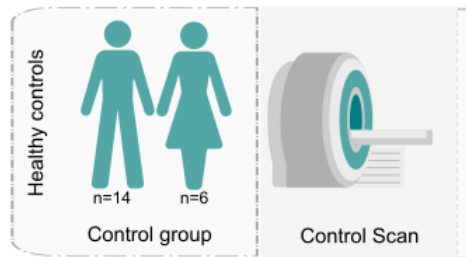


Figure 3.1 Preclinical study design. (a) Preclinical MRI group, 18 experimental male msP rats were exposed to a two-bottle free choice paradigm with 10% alcohol. Another 9 controls had access to water only, both groups were scanned at baseline (TP1) and after 4 weeks of consumption (TP2). (b) Multimodal maps extracted from diffusion data, include Fractional Anisotropy (FA) from the DTI model as a global metric for white matter integrity, Axonal Fraction (FR, which also represents axonal density) from CHARMED, and Axonal Diameter (AX) from AxCaliber model. Both AX and FR are generated through multicompartiment diffusion modelling. All maps are extracted after conversion and processing of diffusion data, results and statistics are performed using atlas-based and tract-based spatial statistics methods. (c) Preclinical histology group. 10 msP rats underwent the same alcohol consumption protocol, then were perfused and brain sliced for immunohistochemistry.

a)



b)

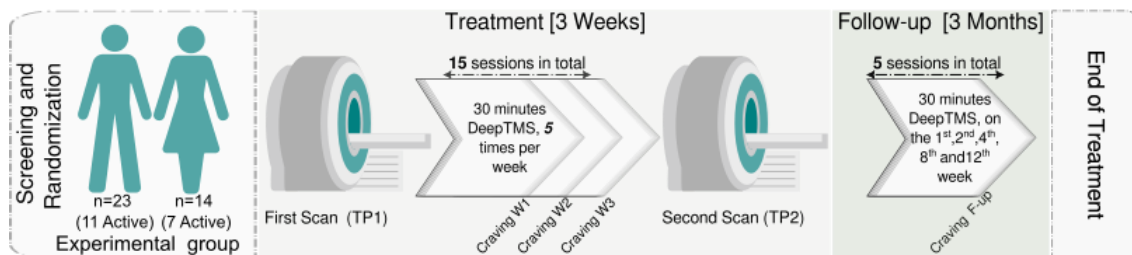


Figure 3.2 **Clinical study design.** (a) Control group from the clinical study, 20 healthy controls were scanned using the same scanner and scanning protocols for comparison with patients with AUD in the experimental group. (b) Scanning and stimulation for the experimental clinical group, patients with AUD are randomly assigned to sham- or active-stimulated groups. All patients receive two MRI sessions (TP1 and TP2) separated by three weeks of Deep TMS (active or sham) treatment (5 daily sessions per week). MRI sessions included functional, anatomical, and diffusion-weighted imaging sequences. Additional Deep TMS sessions were applied during the follow-up visits taking place 1, 2, 4, 8, and 12 weeks after the end of the acute daily treatment period. Craving and relapse were monitored every week during the acute treatment period and every visit during the follow-up period.

3.1 Preclinical study

3.1.1 AUD rat model

We used the marchigian sardinian alcohol-preferring rat line (msP), a line that was created by selective breeding for high alcohol preference and voluntary alcohol consumption (Ciccocioppo et al., 2006), these rats exhibit anxiety-like behaviours and are sensitive to stress, which makes them an ideal model for studying the mechanisms underlying excessive alcohol intake (Economidou et al., 2008) and withdrawal symptoms (Economidou et al., 2011), or for developing new medications for AUD (Cannella et al., 2019).

A total of 37 male msP rats (weighing between 370–480 grams with 8 weeks of age), distributed into 3 groups were used in our experiments; MRI experimental (n=18), MRI control (n=9), and immunohistochemistry group (n=10). Rats were ordered from the host breeding facility at the School of Pharmacy, University of Camerino, Camerino, Italy. When they arrived at our university facility, the rats were housed in groups for five days for habituation, then they were distributed individually in transparent polycarbonate cages with bedding material and were provided with a wooden stick and nesting material as enrichment.

The temperature and humidity in the facility were kept at 22±2 °C and 55±10 percent, respectively, under a 12-hour light/dark cycle, with free access to food and water for the animals. The rats were provided with *ad libitum* access to two drinking bottles, one filled with

water and the other with 10 percent (volume/volume) EtOH (ethanol absolute pure, Panreac Química SLU) in water, for four weeks. The fluids were renewed, each bottle's position switched to not create side-preference, and the animals' weight and fluid consumption were recorded every 2-3 days.

3.1.2 Anaesthesia and preparation

Imaging experiments were carried out under isoflurane anaesthesia, which was induced using 4-5% isoflurane in oxygen (0.8-1L/min). Animals were kept held in a custom-made holding apparatus featuring a tooth bar and a nose cone. Throughout scanning, isoflurane concentration was maintained at 1.2%, while body temperature was monitored and kept constant at 37 ± 0.5 °C using a heating pad. The physiological parameters, including oxygen saturation, pulse, and breathing rate, were observed (MouseOx, Starr Life Sciences, Oakmont, PA, USA). Following the experiment, the animals were euthanized, and their brains were processed for histological analysis.

3.1.3 Image acquisition

MRI data acquisition was performed on a horizontal 7 T scanner with a 30 cm diameter bore (Biospec 70/30, Bruker Medical, Ettlingen, Germany) at the Institute of Neurosciences in Alicante (CSIC-UMH). We used a receive-only phase array coil with an integrated combiner and preamplifier, combined with an actively detuned transmit-only resonator. Diffusion-weighted data were acquired using an EPI spin-echo diffusion sequence. We scanned a protocol with 30 uniformly distributed gradient directions, b-value = 1000 and 2500 s/mm², with three non-diffusion weighted images (b₀), repetition time (TR) = 8000 ms, and echo time (TE) = 29 ms. Sixteen coronal slices were planned for each subject (field of view [FOV] = 32 × 32 mm², matrix size = 110 × 110 × 16, in-plane resolution = 0.225 × 0.225 mm², slice thickness = 1 mm). Additionally, we repeated the same protocol using a stimulated-echo sequence (Frahm et al., 1985) at four diffusion times: 15, 30, 60, and 100 ms. T1-weighted and T2-weighted maps were also acquired, using the same geometry as the diffusion scans. The control group was acquired at a later stage due to the interference with scanner maintenance and a technical upgrade of the managing software. The Bruker Paravision software was upgraded from the fifth to the sixth version. All acquisition schemes were kept the same for the control animals, except for the number of diffusion directions, which was increased to 40 uniformly distributed gradient directions.

3.1.4 Imaging data analysis

All raw data were converted from Paravision format to NIfTI (The Neuroimaging Informatics Technology Initiative) format, and then reoriented and augmented by multiplying the voxel size by ten. Skull stripping was done using a common built template using the *buildtemplateparallel.sh* script implemented in Advanced Normalization Tools (ANTs) (Avants et al., 2009), a method that has been previously described (Martínez-Tazo et al., 2024). Registration was used to get brain mask in native space, then each data was manually checked and corrected, to ensure that the brain had been successfully extracted and a binary mask created, as required for the following preprocessing steps. All data were pre-processed in accordance with the recent community recommendation (Jelescu et al., 2022), that include denoising, Eddy current, motion distortions, and bias field corrections. The DTI fitting was performed using a Robust Estimation of Tensors by Outlier Rejection (RESTORE) approach, which involves iteratively reweighted least-squares regression to identify potential outliers and excludes them from the fit (Chang et al., 2005). Pre-processed multi-shell acquisition data with b-values of 1000 and 2500 were used to fit the CHARMED model (Assaf and Basser, 2005) using an in-house MATLAB script (The Mathworks Inc., Natick, MA). For fitting the AxCaliber model (Assaf et al., 2008) diffusion data with multiple diffusion times acquired on a STEAM sequence were fed, after preprocessing, into a separate in-house MATLAB script.

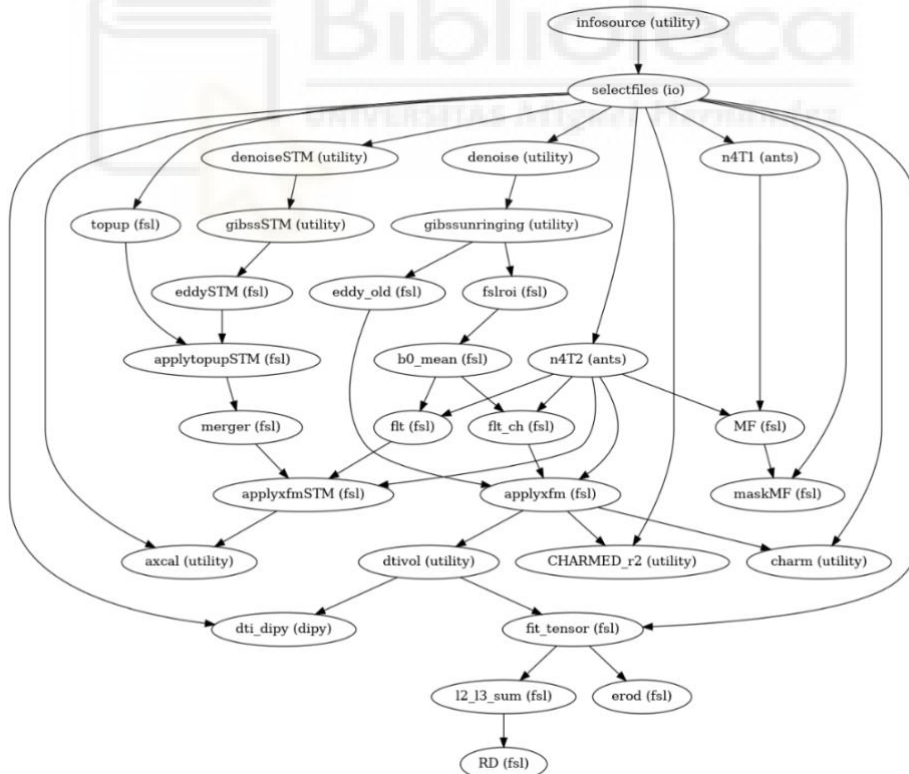


Figure 3.3 *Preclinical data preprocessing pipeline. Rats' diffusion data preprocessing steps including denoising motion correction and model fitting.*

Preprocessing steps were built on a custom-made pipeline using the Nipype package (Gorgolewski et al., 2011) in combination with tools from DIPY package (Garyfallidis et al., 2014), and was made publicly available through GitHub repository hosted on this link

(https://github.com/mokselim/Preprocessing_msP_diffusion), pipeline steps are shown in Figure 3.3.

Extracted Fractional Anisotropy (FA) maps from the tensor model, Axonal Fraction (FR) from CHARMED model as a surrogate for axonal density, and Axonal Diameter (AX) maps from the AxCaliber model were used to test the differences between alcohol exposed and control animals.

For conducting ROI-based analyses, each animal FA map was registered linearly from TP2 to itself at TP1. This was done to reduce the non-biological variance of the same brain that was acquired at two time points. Maps at TP1 were then registered nonlinearly to the SIGMA rat template (Barrière et al., 2019). Finally, both registrations were applied to the other FR and AX maps using the *antsApplyTransforms* command as part of the ANTs package. Corpus callosum, fimbria and fornix correspondent ROIs from the SIGMA atlas were used to mask the data to extract the mean value per ROI. These mean values will subsequently be tested using a paired-sample t-test.

The whole-brain statistical analysis of group differences was carried out using a modified version of tract-based spatial statistics (TBSS) (Smith et al., 2006), in combination with an advanced normalization approach, to adapt for animal data. A general linear model (GLM) was utilized within a voxel-wise, non-parametric permutation-based statistical framework to test for significant differences between the alcohol exposed and control animals, while accounting for multiple comparisons across clusters using Threshold Free Cluster Enhancement. We performed 10,000 permutations, and a voxel-wise p-value corrected for multiple comparisons was considered statistically significant if it was less than 0.05. Cluster locations were achieved using a white matter FA-driven skeleton by averaging all subjects using the *tbss_skeleton* routine in FSL (FMRIB Software Library) (Jenkinson et al., 2012).

3.1.5 Immunohistochemistry and histological analysis

After alcohol protocol had been completed, rats within the immunohistochemistry group were administered with a lethal dose of sodium pentobarbital, 46 mg/kg, which was injected intraperitoneally (E.V.S.A. laboratories, Madrid, Spain) to induce deep anaesthesia. Following this, the rats were perfused intracardially with 100 ml of 0.9% phosphate saline buffer (PBS) and 100 ml of ice-cold 4% paraformaldehyde (PFA, BDH, Prolabo, VWR International, Louvain, Belgium). The brains were subsequently removed from the skull and fixed in 4% PFA for 1 hour. Afterwards, the brains were embedded in 3% agarose/PBS (Sigma-Aldrich, Madrid, Spain) and cut into 50- μ m-thick serial coronal sections using a vibratome (VT 1000 S, Leica, Wetzlar, Germany). Coronal sections underwent three rinses in 1 x PBS containing 0.5% Triton X-100 (Sigma-Aldrich, Madrid, Spain) for 10 minutes each, followed by a 2-hour blockade in the same solution with 4% bovine serum albumin (Sigma-Aldrich, Madrid, Spain) and 2% goat serum (Sigma-Aldrich) at room temperature. Subsequently, the slices were incubated overnight at 4 °C with primary antibodies against neurofilament 160 kD medium (1:250, Abcam Cat# ab134458) and myelin basic protein (1:250, Millipore Cat# MAB384-1ML) to label axonal

processes and myelin, respectively. Then, secondary antibodies conjugated to fluorescent probes (Molecular Probes Cat# A-11029; Molecular Probes Cat# A-11042) were added to the sections at a concentration of 1:500 and incubated for 2 hours at room temperature. Following this, the sections were treated with 15 mM 4',6-Diamidino-2'-phenylindole dihydrochloride (DAPI, Sigma-Aldrich) for 15 minutes at room temperature. Subsequently, the sections were mounted on slides and covered with an anti-fading medium made from a 1:10 solution comprising Propyl-gallate and Mowiol (P3130, Sigma-Aldrich; 475904, MERCK-Millipore, Massachusetts, United States). For myelin labelling, antigen retrieval was performed using 1% citrate buffer (Sigma-Aldrich) and 0.05% Tween 20 (Sigma-Aldrich) warmed to 80 °C to unmask its proteins.

The slides were subsequently analysed using a computer-assisted morphometry system that included a Leica DM4000 fluorescence microscope equipped with a QICAM Qimaging camera (model 22577, Biocompare, San Francisco, USA) and Neurolucida morphometric software (MBF, Biosciences, VT, USA). Myelin and neurofilament fluorescent analyses were performed using Icy software (De Chaumont et al., 2012), and the ImageJ program (Schneider et al., 2012). Two rectangular ROIs of 400x300 μm^2 were placed, one per the midsection of corpus callosum, and one per fimbria-fornix bundle per hemisphere in at least 2 slices per rat to obtain the corresponding intensity values. Intensity of fluorescence was determined considering the ROI area (Integrated density = mean fluorescence * area) and the background. In this way, we obtained the corrected total fluorescence (CTF) with this formula: $\text{CTF} = \text{Integrated density} - (\text{area} * \text{mean background fluorescence})$. We reduced the variability in the measurement by averaging the mean intensity of two consecutive slices per animal, and later averaging values across the two hemispheres of the same rat. Afterwards, significant differences between alcoholic and control rats were calculated using an unpaired t-test on fluorescence mean intensity, besides additional Icy's software parameters including texture contrast, homogeneity, and entropy. A p-value of less than 0.05 was considered statistically significant. All statistical analyses were done using the Pingouin statistical package (Vallat, 2018) in Python or GraphPad Prism version 8.00 for Windows (GraphPad Software, La Jolla, CA, USA).

3.2 Clinical study

3.2.1 Participants

This was a double-blind, sham-controlled, randomized clinical trial performed at the Ben-Gurion University and the Soroka Medical Centre. Recruitment occurred between July 2016 and December 2019, participants were recruited via social media and local newspaper advertisements. All participants provided written informed consent and their anonymity was preserved. This clinical trial conforms to the provisions of the Declaration of Helsinki. The study was approved by local health authorities and was registered at ClinicalTrials.gov under the following identifier (NCT02691390). The main clinical outcomes of the original study have been reported previously, where the full recruitment protocol is also described (Harel et al.,

2022), however, the initial results included psychiatric measurements and resting state fMRI data only. This work features a unique, yet complementary, portion that was not reported previously, which is resembled by the inclusion of diffusion data and the interplay between structure and function to explain the observed clinical outcome, in addition to analysis of a control cohort. Both AUD patients (n=40) and age-matched controls (n=20) were included in the trial. Functional (fMRI) and structural (DTI) data were not available for all subjects in the trial. The clinical assessment of the subjects included in the DTI analysis is reported in tables 1 and 2 in (Selim et al., 2023); for AUD vs. control, and sham vs. active Deep TMS, respectively, see Appendix (C) for details. More details on the exclusion criteria are provided in the supplementary methods of Appendix (A) as well.

3.2.2 Image acquisition

Imaging protocols were harmonised across the SyBil-AA (Systems Biology of Alcohol Addiction) Horizon 2020 Consortium. Data acquisition utilised a Philips Ingenia 3 Tesla MRI scanner (Philips Healthcare, Best, Netherlands) equipped with a 32-channel Philips dS Head head coil. A multi-shell diffusion MRI protocol was employed, encompassing images with 30 uniformly distributed diffusion directions acquired at a b-value of 1000 s/mm², alongside 60 directions acquired at a b-value of 2000 s/mm². A non-diffusion weighted image (b₀) was also acquired. An EPI spin-echo diffusion sequence was used with the following parameters: repetition time (TR) = 7 ms, echo time (TE) = 108 ms, matrix size = 224 x 224 x 125, and a spatial resolution of 1.75 x 1.75 x 2.5 mm. BOLD data were acquired using a separate EPI sequence: TR = 2000 ms; TE = 30 ms; flip angle = 77°; field-of-view (FOV) = 220 x 220 mm; in-plane resolution = 3.4 x 3.4 mm; slice thickness = 4 mm; no slice gap; number of axial slices (angled with the AC-PC line) = 32; number of volumes = 360. Two resting-state runs, each lasting 12 minutes, were collected (baseline and follow-up). A high-resolution 3D T1-weighted Turbo Field Echo scan was acquired prior to the EPI data collection (TR = 7.0 ms; TE = 3.2 ms; flip angle = 8°; FOV = 256 x 256 x 170 mm; voxel resolution = 1 x 1 x 1 mm; no slice gap; plane: sagittal; number of sagittal slices = 170). All acquisition information are reported in the original publications (Harel et al., 2022; Selim et al., 2023).

3.2.3 TMS protocol

Active and sham Deep TMS were administered using a Magstim Rapid2 TMS stimulator (Magstim Co. Ltd.) equipped with an H7 coil (BrainsWay). In each session, the optimal spot on the scalp for stimulation of the leg motor cortex was localised, and the Resting Motor Threshold (RMT) was defined according to a previously described method (Roth et al., 2014). The coil was then moved four centimetres anterior to the motor spot and aligned symmetrically over the medial prefrontal cortex (mPFC). Each daily stimulation session following localization over the mPFC lasted approximately 30 minutes and included 3000 pulses using the intensity of the leg RMT measured for that individual patient (100% of leg RMT). The session included 100 trains of pulses (3 seconds per train) at 10Hz, with an inter-

train interval of 15 seconds. Placebo treatment was performed using a sham coil located within the same helmet as the active coil. The sham coil is capable of producing similar acoustic artifacts and scalp sensations as the active coil, it induces only negligible electric fields in the brain (Roth et al., 2014). Figure 3.4 illustrates the stimulation power distribution in an anteroposterior direction across the brain.



Figure 3.4 **TMS power distribution**. Stimulation power distribution in V/m, and the central focus of Deep TMS over the midline of the mPFC (green cross).

3.2.4 Imaging data analysis

Resting-state fMRI processing and statistics

The Analysis of Functional Neuro Images (AFNI) software v18.3.16 (Cox, 1996) was employed for preprocessing and statistical analysis of resting-state data. Initially, Freesurfer-based parcellation was performed on T1-weighted data using the *recon-all* function. This parcellation was subsequently utilised for tissue-based regression to account for signal fluctuations not attributable to the BOLD signal. The BOLD signal underwent de-spiking, slice-time and motion correction. Subsequently, it was spatially transformed to Montreal Neurological Institute (MNI) template space using a combination of linear and non-linear transformations. Motion censoring excluded volumes exceeding a 3 mm displacement or 0.05 outlier fraction. The *3dDeconvolve* function within AFNI performed a regression on BOLD time-series data. Head motion effects were incorporated by adding motion parameters and their derivatives as regressors of no interest. Finally, the data-driven *APPLECOR* method (Marx et al., 2013) removed covarying signals from grey and white matter regions within the residuals.

Microstructural data processing and statistics

Eight subjects from the original study (Harel et al., 2022) lacked diffusion-weighted data and were excluded. Additionally, one subject did not complete the treatment sessions, resulting in their removal from the analysis. All raw data underwent denoising using a statistically independent method (Fadnavis et al., 2022) before conversion to ExploreDTI format (Alexander Leemans et al., n.d.). Each dataset was corrected for subject motion and eddy-current distortions, followed by brain extraction to isolate brain tissue. Images were then categorised based on their b-value. Diffusion-weighted data with a b-value of 1000 (30

directions) was utilised for diffusion tensor-DTI estimation, using the robust model fitting (Chang et al., 2005). Following tensor fitting, voxel-wise FA maps were generated for statistical analysis.

Both cross-sectional and longitudinal analyses employed TBSS (Smith et al., 2006). For the cross-sectional analysis, FA maps from the AUD cohort at baseline (TP1) and healthy controls were co-registered to the MNI standard template using a combination of linear and non-linear registration implemented in ANTs (Klein et al., 2009). The FA maps in standard space were then used to generate the white matter skeleton, onto which the FA images were projected. In the longitudinal analysis, FA maps for each subject in the AUD cohort at the second time point (TP2) were first registered linearly to their corresponding FA maps at TP1. These were then transformed into standard space using the same transformation and field warping obtained from the non-linear registration at TP1. Finally, the FA maps at TP1 in standard space were used to generate the white matter skeleton, where the difference in FA images between the two time points was projected. Statistical testing of the skeletonised FA images was performed using the permutation testing tool, *randomise*, within the FSL package (Jenkinson et al., 2012). A general linear model (GLM) design with threshold-free cluster enhancement was employed for the statistical analysis. Three types of statistical comparisons were conducted. To identify baseline FA differences between the AUD and control cohorts, a GLM model compared FA maps between groups while controlling for age and gender. To assess the longitudinal changes in FA between TP1 and TP2, a separate GLM model tested for significant positive or negative differences in FA maps between time points. Finally, to highlight group-specific changes in FA progression between sham and active Deep TMS, a GLM model compared the interaction effect of group (sham vs. active) and time (TP2 - TP1) on FA progression, again controlling for age and gender. All information about rs-fMRI and DTI processing are reported in (Selim et al., 2023), see Appendix (C).

Tractography and DTI-based functional connectivity analysis

Whole-brain tractography was performed for each participant in the AUD group using the constrained spherical deconvolution algorithm (Tournier et al., 2007) implemented within ExploreDTI software. Diffusion-weighted data with a b-value of 2000 and 60 directions was employed. Voxel-wise analysis revealed a significant cluster of voxels within the Deep TMS stimulation area, where FA demonstrated differential changes between the sham and active groups. Based on this finding, a seed region was defined within this Deep TMS-sensitive area and white matter tracts traversing this region were selected. Individual subject tractography data was then registered to a standard space and averaged. A threshold was applied to retain tracts present in at least 70% of the participants. These averaged tracts were subsequently masked using a standard grey matter mask to define four cortical targets connected by the tracts passing through the Deep TMS-sensitive region. These targets were used to define the seed regions for the functional connectivity analysis at post-treatment. Seeds were

constructed as 5 mm radius spheres centred on the MNI coordinates of the DTI-derived targets. Seed-to-whole-brain and grey matter connectivity analyses were performed for each participant who passed motion censoring criteria (sham, N=19; active, N=21 at pre-treatment; sham, N=19; active, N=20 at post-treatment). This involved entering the seed time course as a predictor variable within a regression analysis implemented using *3dDeconvolve* method. Resulting 3D volumes containing beta coefficients for each seed location were compared between groups at post-treatment using the AFNI function *3dttest++*. A per-voxel p-threshold of 0.002 was applied, followed by multiple comparison correction at alpha = 0.05 (Cox et al., 2017). To account for spatial smoothness of the residuals, the cluster size threshold for correction was estimated using the *3dClustsim* simulation function. The simulation mask employed was a grey matter mask, constructed from the union of 80% of the subjects' censored EPI masks. To assess potential time effects, beta coefficients from significant clusters were extracted and analysed using a 2x2 repeated measures ANOVA with factors of time (pre/post) and group (sham/active Deep TMS) (sham, N=18; active, N=19).



IV. Results

4.1 Preclinical results

4.1.1 Alcohol consumption

In the two-bottle free choice paradigm administered for four weeks, msP rats showed an escalating pattern of alcohol consumption compared to water. Initially, the rats consumed approximately 3 grams of alcohol per kilogram of body weight per day, as illustrated in Figure 4.1-a. Over time, the rats' alcohol intake escalated to 5-7 grams per kilogram per day, as indicated in the same figure. Notably, the increased alcohol consumption was accompanied by a growing preference for alcohol. Since the rats were naive to alcohol, they initially consumed water at similar levels of 10% alcohol (EtOH) or higher. However, over the first three days, the animals' preference shifted towards alcohol, which comprised 80% of the total liquid consumed, as depicted in Figure 4.1-b. After eight days in the two-bottle free choice paradigm, the rats' preference for alcohol over water reached a plateau, similar to findings reported previously (Cosa et al., 2017).

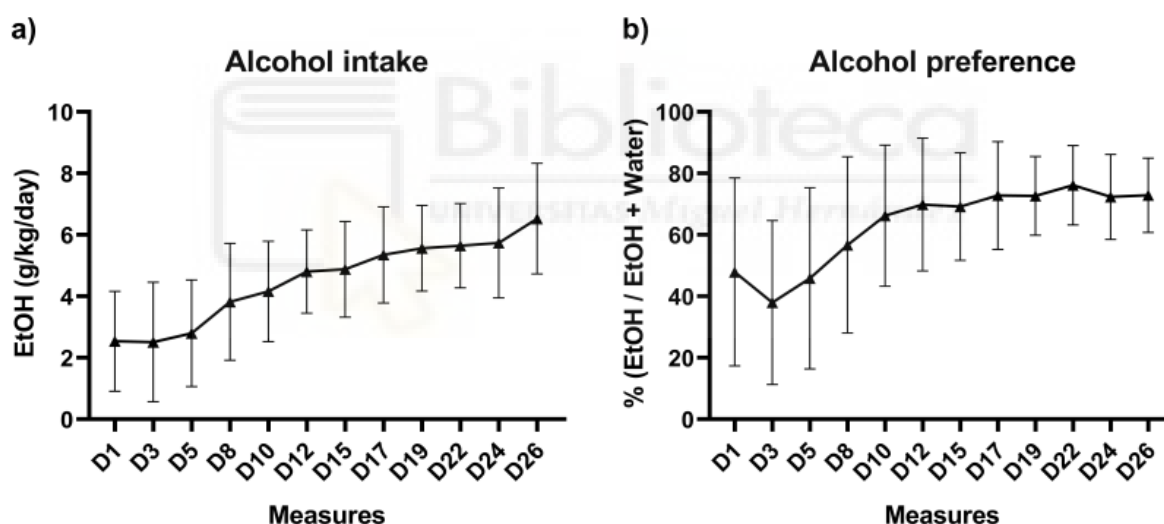


Figure 4.1 **Alcohol intake and preference.** (a) Alcohol intake is calculated over recording days (measures) and averaged for all rats; alcohol intake is measured in grams adjusted for kilogram of body weight per day. (b) Alcohol preference is calculated over recording days and measured as the percentage of the consumed 10% alcohol (EtOH) over the total liquid consumed (EtOH+Water) per rat, averaged across all rats. Symbols show mean \pm standard deviation.

4.1.2 Imaging

Alcohol induces white matter alteration

When comparing the fractional anisotropy (FA) of alcohol-drinking rats at time point 1 (TP1), i.e., before alcohol consumption, to themselves at time point 2 (TP2), after 4 weeks of alcohol drinking, we found a significant reduction in the entire white matter skeleton using TBSS analysis with threshold-free cluster enhancement (Figure 4.2-a). We considered a total of three regions of interest (ROIs), known to be the principal targets of alcohol effects (Pérez-

Cervera et al., 2023): the corpus callosum, fimbria, and fornix. Instead of confining this analysis to the centre of the tract, we employed an atlas-based approach to assess the mean value extracted per ROI. All ROIs demonstrated significant reductions in mean FA values in alcohol-drinking rats compared to their naive state, as shown in Figures 4.2-b (statistical maps) and 4.3-a (scatter plots).

Paired t-tests revealed significant differences in the three ROIs: for the CC, $t(17) = 10.2$, $p = 1e-6$, Cohen's $d = 1.06$; for the fimbria, $t(17) = 3.18$, $p = 5e-3$, Cohen's $d = 0.81$; and for the fornix, $t(17) = 2.54$, $p = 0.02$, Cohen's $d = 0.28$ (Figure 4.3-a). In contrast, the control group exhibited no significant differences in FA between TP1 and TP2 (Figure 4.3-b): for the CC, $t(8) = 1.40$, $p = 0.20$, Cohen's $d = 0.69$; for the fimbria, $t(8) = 0.67$, $p = 0.52$, Cohen's $d = 0.38$; and for the fornix, $t(8) = 0.55$, $p = 0.60$, Cohen's $d = 0.23$.

The restricted fraction of diffusion (FR) obtained from the CHARMED model, a surrogate marker for axonal density, exhibited a pattern comparable to FA with a decrease observed between TP1 and TP2 in both TBSS and ROI-based analyses (Figures 4.2-a and 4.2-b, respectively). Paired t-tests revealed significant differences in the three ROIs: for the CC, $t(17) = 5.40$, $p = 1e-5$, Cohen's $d = 0.90$; for the fimbria, $t(17) = 3.32$, $p = 4e-3$, Cohen's $d = 0.63$; and for the fornix, $t(17) = 2.12$, $p = 0.04$, Cohen's $d = 0.42$ (Figure 4.3-c). In contrast, the control group exhibited no significant differences between TP1 and TP2 (Figure 4.3-d): for the CC, $t(8) = 0.16$, $p = 0.88$, Cohen's $d = 0.09$; for the fimbria, $t(8) = 1.15$, $p = 0.55$, Cohen's $d = 0.28$; and for the fornix, $t(8) = 1.92$, $p = 0.09$, Cohen's $d = 0.80$.

In contrast, the axon diameter (AX) obtained from the AxCaliber model, which serves as an approximation of *in vivo* axon diameter measured in micrometres, exhibited a divergent pattern compared to FA and FR. Specifically, it displayed an increase between TP1 and TP2 in the alcohol group but not in the control group. Both TBSS and ROI-based analyses yielded comparable results, as shown in Figures 4.2-a and 4.2-b, respectively. Paired t-tests (Figure 4.3-e) revealed a significant increase between TP1 and TP2 for the CC ($t(17) = 3.69$, $p = 1e-3$, Cohen's $d = 0.93$), but not for the fimbria and fornix ($t(17) = 1.20$, $p = 0.25$, Cohen's $d = 0.37$, and $t(17) = 1.55$, $p = 0.14$, Cohen's $d = 0.33$, respectively; Figure 4.3-e). No significant differences were observed in the control group ($t(8) = 1.57$, $p = 0.16$, Cohen's $d = 0.69$ for the CC; $t(8) = 1.96$, $p = 0.09$, Cohen's $d = 0.76$ for the fimbria; and $t(8) = 1.01$, $p = 0.34$, Cohen's $d = 0.36$ for the fornix; see Figure 4.3-f for clarification).

It is noteworthy that the range of acquired AX measurements was greater in the control group than in the experimental group. The control group was scanned using an updated MRI console software version (Paravision 6.0.1), while the alcohol group was scanned with the previous version. A thorough examination revealed that the newer software performs internal compensation when diffusion times are altered in STEAM sequences, a crucial step for AxCaliber analysis. This unintended adjustment resulted in an overestimation of b-values. As a consequence, the magnitude of the axonal calibres estimated with the two protocols cannot be compared (De Santis et al., 2016). Nevertheless, the extracted values from the three ROIs

demonstrated a pattern consistent with those observed in the alcohol cohort. Taken together, these findings suggest global alterations in white matter, characterised by a concomitant decrease in axonal density and an increase in axonal diameter.

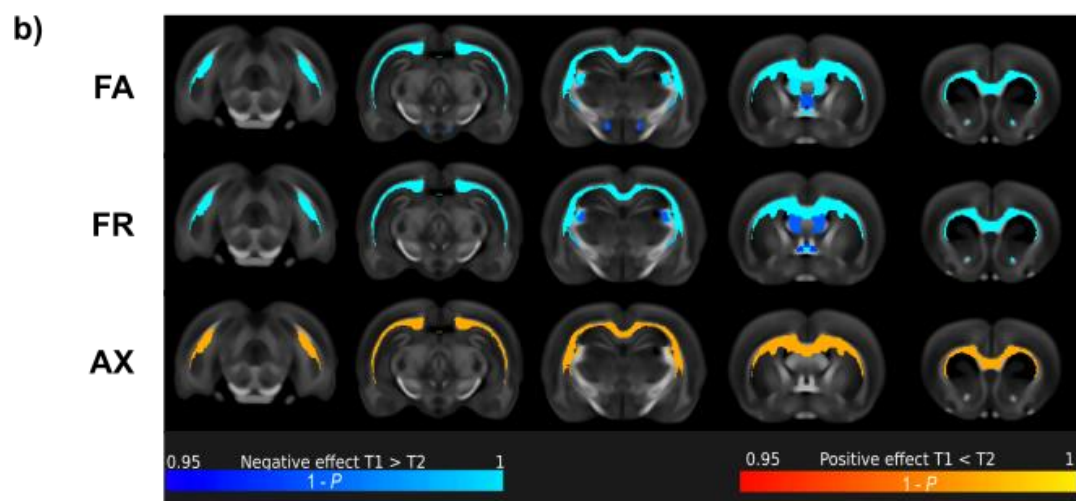
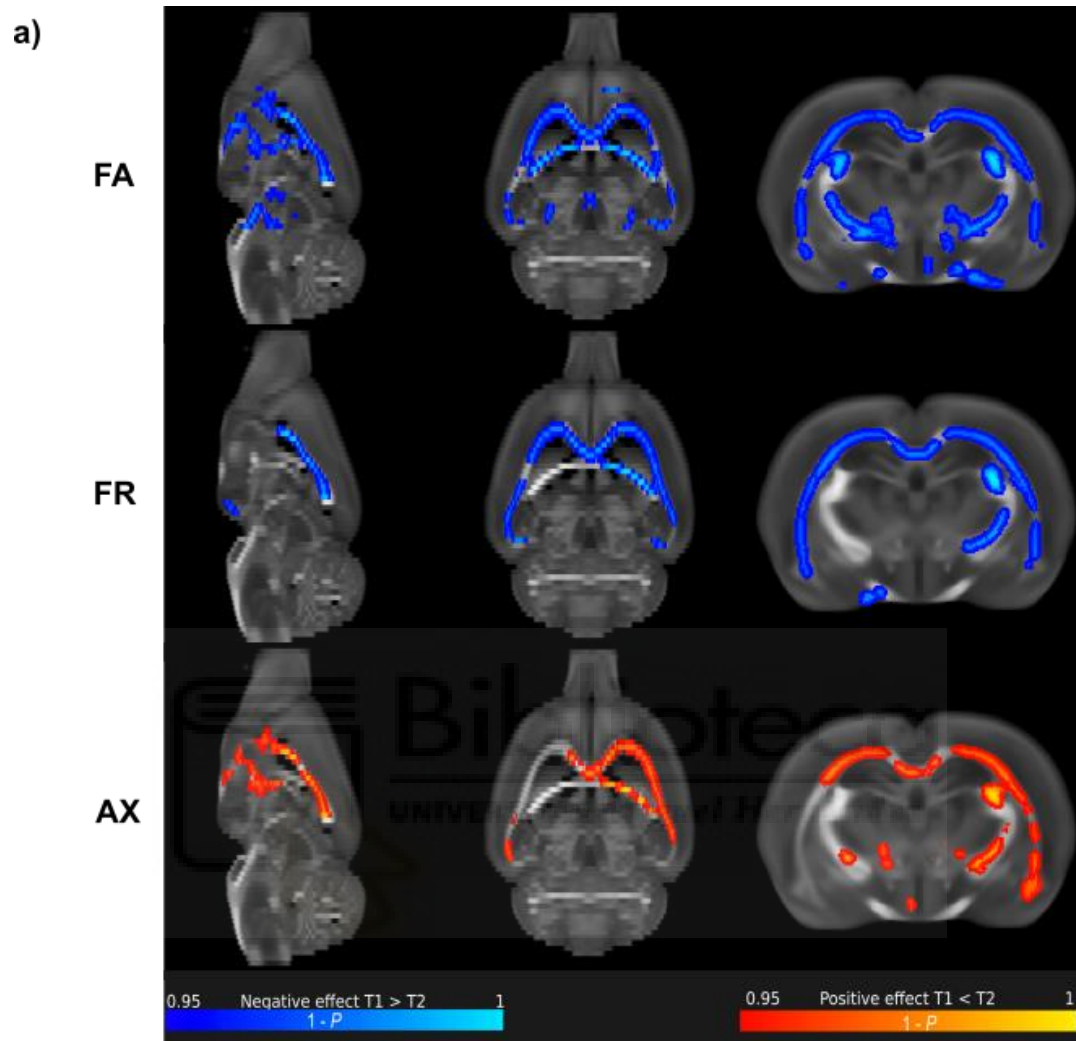
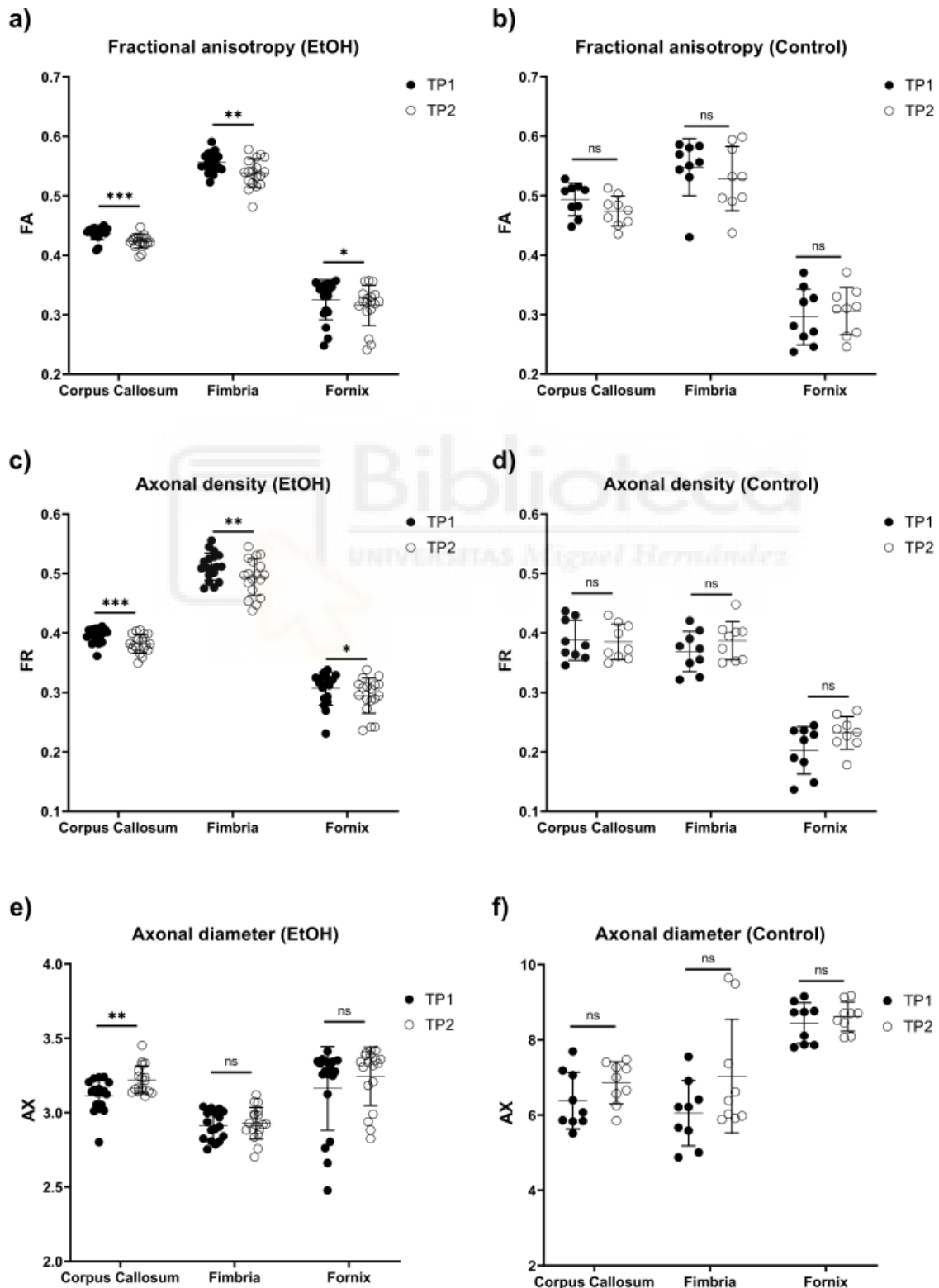


Figure 4.2 **White matter alteration assessed by different dw-MRI maps.** (a) Tract-based spatial statistics performed at the centre of the white matter skeleton, voxel-wise with free cluster correction, demonstrate a longitudinal reduction in both fractional anisotropy (FA) and restricted fraction (FR) in the alcohol-exposed group, accompanied by an increase in axonal diameter (AX). (b) Anatomical ROIs that show significant change after alcohol consumption were extracted by atlas-based analysis using the SIGMA rat template. The colour-coding indicates the p-value, with blue denoting a reduction in value between TP1 and TP2, and orange indicating an increase in value. It is important to note that the control group is not depicted in the plot as no significant findings were identified.



*Figure 4.3 Statistical tests conducted on the mean value per ROI extracted from atlas-based analysis. Scatter plots of the mean values of FA (a), FR (c) and AX (e) of the three considered ROIs (corpus callosum, fimbria and fornix) in all animals in the alcohol-drinking experiment at baseline (TP1) and after alcohol drinking (TP2). The respective control experiment in water-drinking animals with longitudinal measurements at TP1 and TP2 is shown for FA (b), FR (d) and AX (f), for the three ROIs. ns = non-significant, * $p < 0.05$, ** $p < 0.01$, and *** $p < 0.001$ denote the levels of statistical significance. All data were checked for normality and homoscedasticity. The individual data points reflect the results shown in Figure 4.2-b. Horizontal lines and Whiskers denote the mean \pm standard deviation, respectively, $n=18$ for the EtOH group and $n=9$ for the control group.*

4.1.3 Histology

Signature of altered axonal structure

When comparing immunofluorescence staining in histological preparations of alcohol-exposed rats versus controls, we found higher mean fluorescence intensity for neurofilament staining in the corpus callosum (unpaired t-test, $t(8) = 2.91$, $p = 0.02$, Cohen's $d = 1.36$) and the fimbria-fornix ($t(8) = 2.60$, $p = 0.03$, Cohen's $d = 1.28$). Interestingly, the corpus callosum showed significant alterations in texture parameters, with an increase in contrast ($t(8) = 3.33$, $p = 0.01$, Cohen's $d = 1.45$) and a reduction in homogeneity ($t(8) = 3.32$, $p = 0.01$, Cohen's $d = 1.44$). The same analysis yielded no significant results in the fimbria-fornix, although there was a trend towards significance ($t(8) = 2.22$, $p = 0.057$, Cohen's $d = 1.17$, and $t(8) = 2.023$, $p = 0.08$, Cohen's $d = 1.10$ for contrast and homogeneity, respectively). No significant differences were observed in texture entropy in either area ($t(8) = 1.269$, $p = 0.24$, Cohen's $d = 0.78$, $t(8) = 2.050$, $p = 0.08$, Cohen's $d = 1.11$ for corpus callosum and fimbria-fornix, respectively), as shown in panels (b) and (e) of Figure 4.4. These results support the AX findings and suggest microstructural alterations in these axonal bundles.

Regarding MBP staining, lower mean staining intensity was observed in the fimbria-fornix bundle of alcohol-drinking rats (unpaired t-test, $t(8) = 3.04$, $p = 0.02$, Cohen's $d = 1.39$), but not in controls. Additionally, there was a tendency towards reduced texture contrast and increased texture homogeneity, although these did not reach significance ($t(8) = 2.04$, $p = 0.08$, Cohen's $d = 1.11$, and $t(8) = 1.56$, $p = 0.16$, Cohen's $d = 0.91$ for contrast and homogeneity, respectively, as shown in Figure 4.4-f). There were no significant results for texture entropy ($t(8) = 0.65$, $p = 0.53$, Cohen's $d = 0.42$). Conversely, the corpus callosum did not display any significant differences in mean intensity ($t(8) = 0.60$, $p = 0.56$, Cohen's $d = 0.40$) or in texture quantification ($t(8) = 0.37$, $p = 0.72$, Cohen's $d = 0.25$ for contrast; $t(8) = 0.42$, $p = 0.69$, Cohen's $d = 0.28$ for homogeneity; and $t(8) = 0.14$, $p = 0.89$, Cohen's $d = 0.10$ for entropy), as illustrated in panel (c) of Figure 4.4. Collectively, these results suggest that under these conditions and at the studied time point, the total myelin content was significantly altered in the fimbria-fornix bundle, but possibly remained preserved within the corpus callosum.

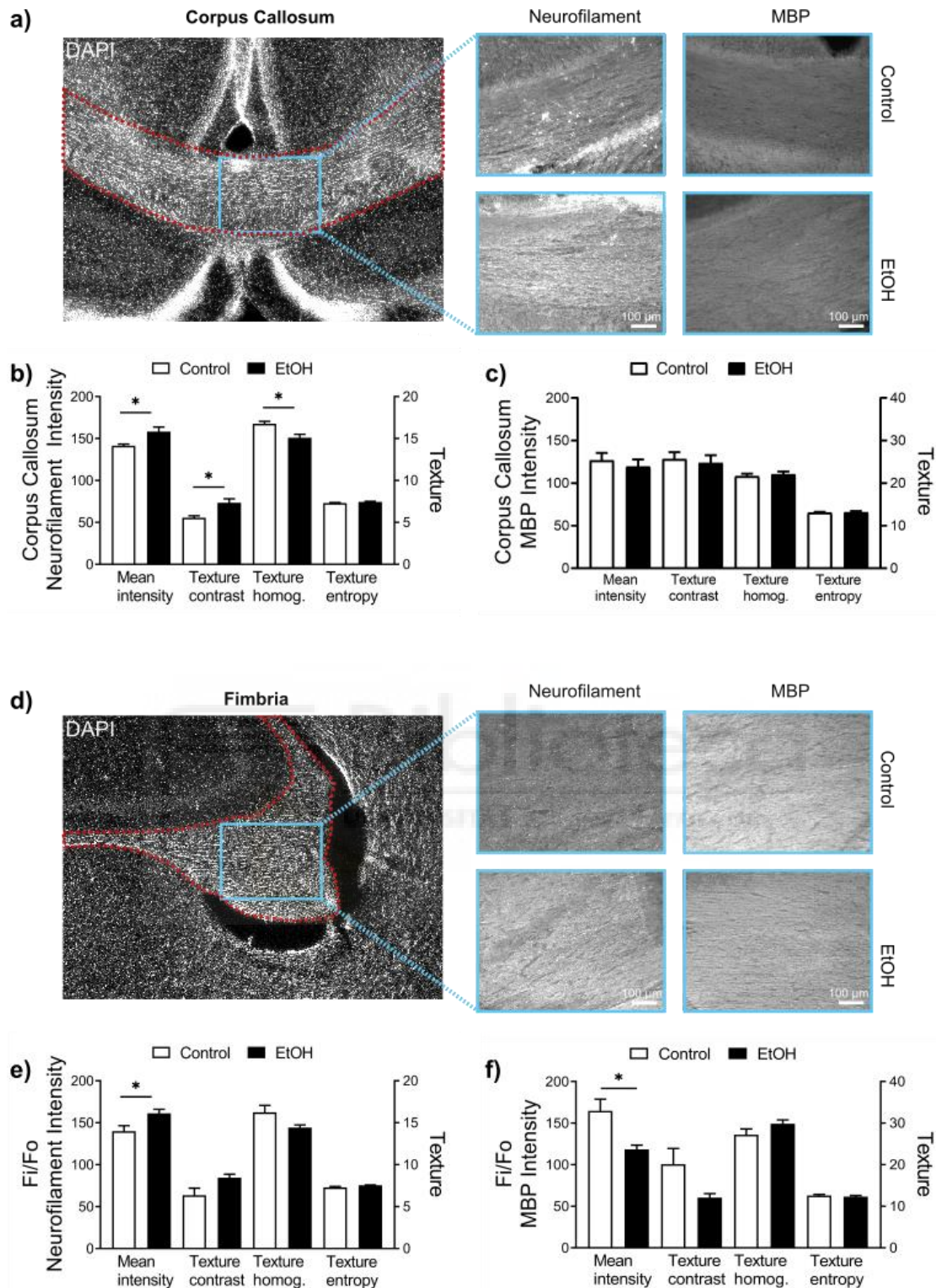


Figure 4.4 Histological analysis of brain slices. (a) Representative DAPI-stained coronal section of the corpus callosum, and enlarged representative ROIs of both groups stained for neurofilament and MBP. (b) Unpaired *t*-test of the different ROI statistics of the Neurofilament staining in the corpus callosum. (c) ROI statistics of the MBP staining in the corpus callosum. (d) Representative DAPI-stained coronal section of the fimbria-fornix (Fi/Fo) bundle. (e) Unpaired *t*-test of the different ROI statistics of the Neurofilament staining of the fimbria-fornix bundle. (f) ROI statistics of the MBP staining in the fimbria-fornix bundle. Dashed red lines delineate the anatomical ROI and light-blue boxes representative areas for image analysis. * $p < 0.05$ denotes the statistical significance. Prior to conducting the test, all data distributions were checked for normality and homoscedasticity.

4.2 Clinical results

4.2.1 Imaging

FA decline progresses in early abstinence

When analysing the FA maps of the control group and the age- and gender-matched AUD cohort before Deep TMS treatment, we found significantly lower FA values in the AUD patients ($p < 0.05$, mean effect size $d = 1.0$) in most areas of the white matter skeleton (Figure 4.5-a). In addition, when examining the progression of FA changes between time points TP1 and TP2 in the AUD cohort receiving sham treatment only, we observed a significant reduction in FA in most regions of the white matter skeleton ($p < 0.05$, mean effect size $d = 0.317$), as shown in Figure 4.5-b. These findings replicate previous findings on white matter alterations in AUD (De Santis et al., 2019; Pfefferbaum et al., 1995; Yeh et al., 2009), and its progression during early abstinence (De Santis et al., 2019).

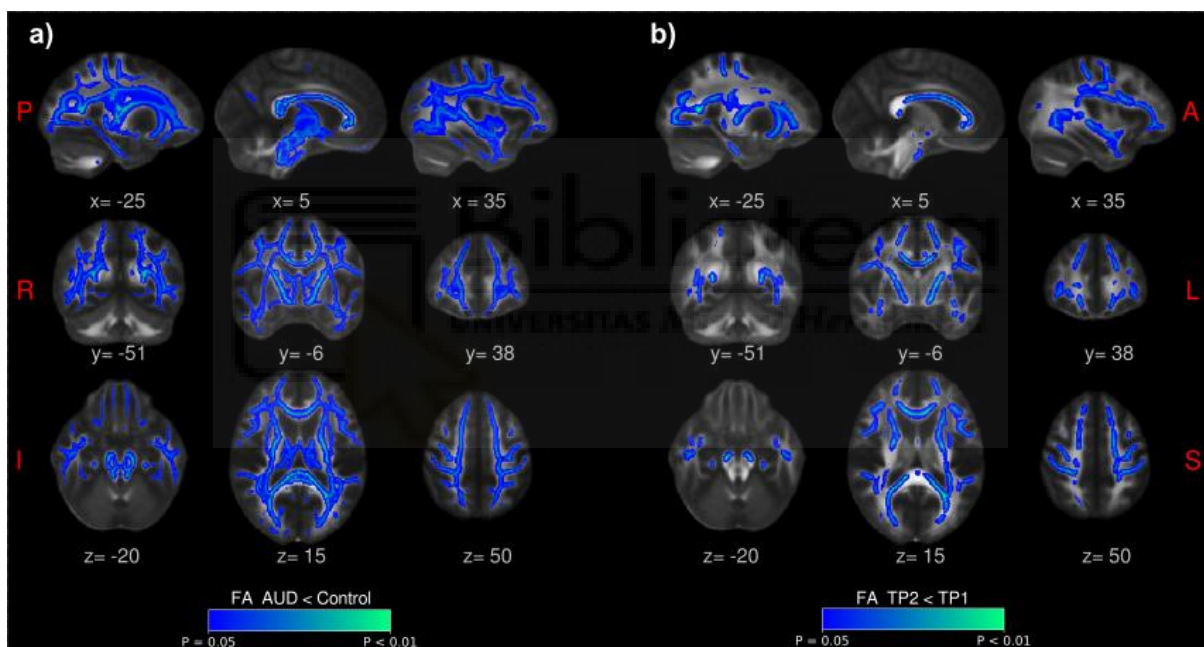


Figure 4.5 White matter alterations progress during early abstinence. Tract-based spatial statistics showing in blue the white matter skeleton where FA is reduced in the following conditions: (a) AUD at TP1 ($n = 20$) compared to group-matched healthy controls ($n = 20$; see Table-1 in (Selim et al., 2023) for demographic characteristics), (b) AUD at TP2 compared to TP1 ($n = 19$; longitudinal comparison) from the sham-stimulated group of patients.

Deep TMS halts the progression of FA decline in early abstinence

When comparing the longitudinal changes in FA between the two groups (active Deep TMS vs. sham Deep TMS) independently, we observed a strong reduction in the extension of white matter affected by the progression of FA changes, particularly in the active Deep TMS group, and involving the right frontal lobe (Figure 4.6-a). We then compared the change in FA (TP2-TP1) between the sham and active Deep TMS groups and found a significant difference in a white matter region belonging to the right frontal lobe (FroL), as depicted in Figure 4.6-b. In both cases, the regions with preserved FA values in the active group were entirely contained within the volume of brain tissue targeted by the Deep TMS with voltage intensities above 100 V/m, known to be suprathreshold for action potential firing (the orange shading in Figure 4.6). We then used the mask of the TBSS-defined spot to calculate the mean FA values for each subject and compare the distributions across groups. As shown in Figure 4.7-a, FA reduction during abstinence is significant in the sham group ($p < 0.002$), as expected for the progression of microstructural changes, while in the active Deep TMS group, FA is stable after three weeks of treatment ($p = 0.82$), indicating that Deep TMS successfully prevented progression. This result remained significant even when controlling for baseline differences in FA values.

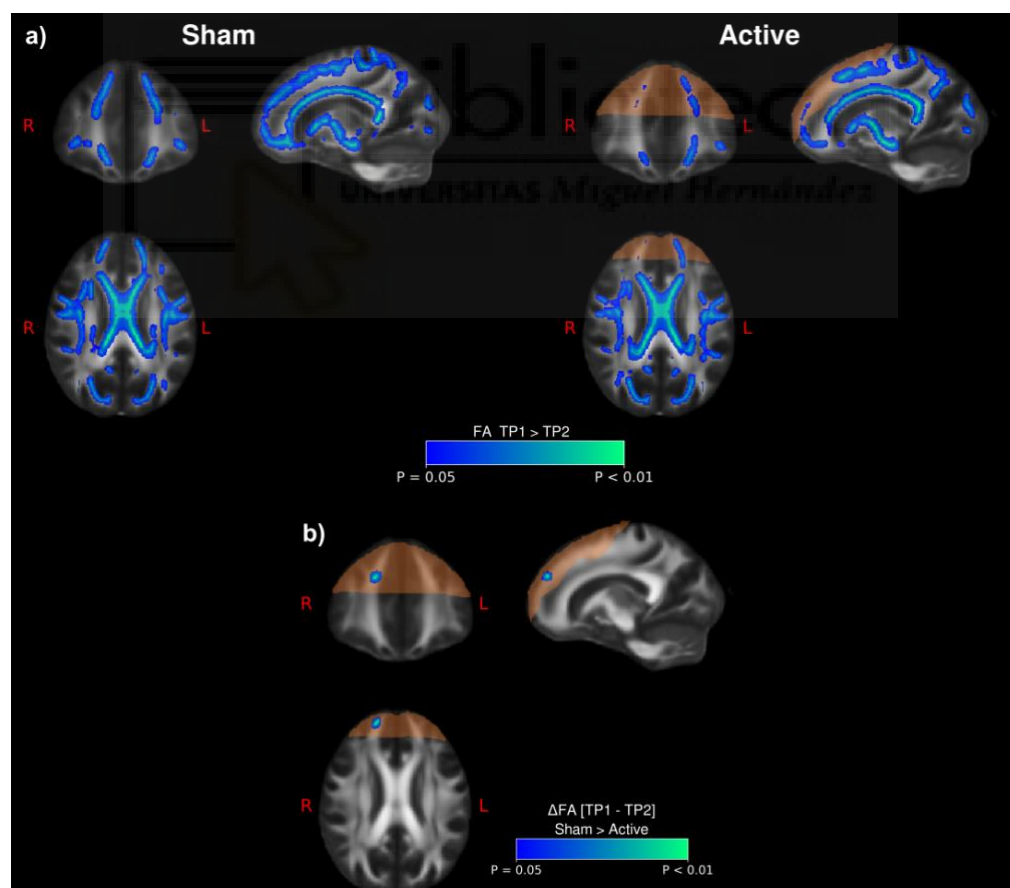


Figure 4.6 Progression of white matter alterations is arrested by Deep TMS. (a) Progression of FA between time points was calculated separately for sham (left) and active (right) groups. The portion of the brain within the theoretical Deep TMS field intensity above the average threshold for action potential firing is highlighted in orange. (b) Tract-based spatial statistics showing regions of the white matter skeleton with significant differences between active and sham Deep TMS groups in the FA change between TP2 and TP1.

To gain insights into the impact of Deep TMS on lateralization, we analysed the maximal statistical significance areas in the right FroL and their counterparts in the left hemisphere (Figure 4.7-b) to calculate the effect size (Cohen's *d*) of FA reduction in AUD versus healthy controls. Our findings revealed significantly higher effect sizes in the right FroL compared to the left, indicating a greater susceptibility of white matter microstructure in this hemisphere, particularly in the frontal region.

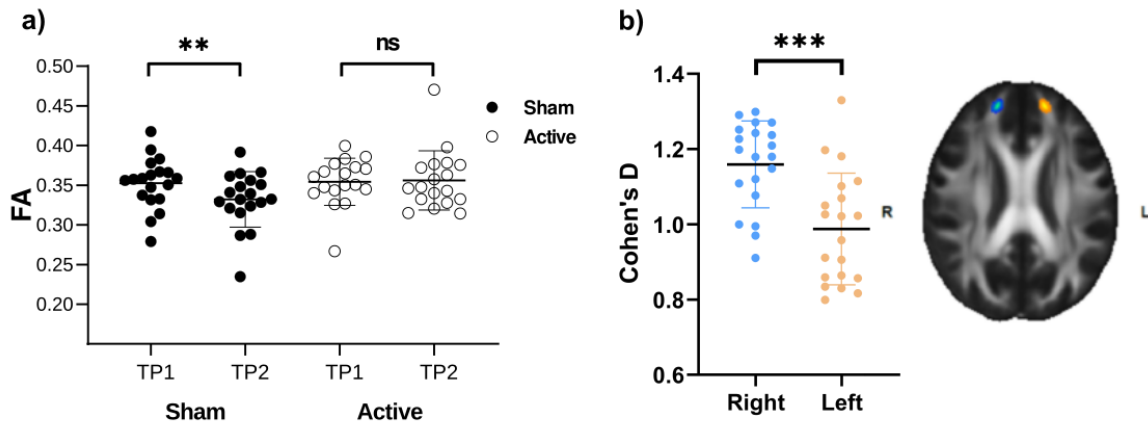


Figure 4.7 Statistics of the Deep TMS protected spot (FroL). (a) Mean FA was calculated for the two time points and for the two groups in the area of significant time \times group interaction according to tract-based spatial statistics (shown in Figure 4.6-b). Two-way ANOVA yielded significant time \times group interaction $F_{1,35} = 5.3$, $p = 0.027$, then Sidak's multiple comparisons test showed significant change in the Sham group only ($p = 0.008$). ns: not statistically significant, $**p < 0.01$. (b) Comparison of effect sizes in the AUD vs. healthy control contrast, measured by Cohen's-*d* metric at the significant spot (FroL right) and its contralateral counterpart (FroL left), Anatomical presentation of both clusters. unpaired *t*-test $*** p < 0.001$.

4.2.2 Psychiatric measures and clinical outcomes

Microstructural changes are paralleled by significant clinical outcome

The subjects in this study differ slightly from the original cohort reported by Harel et al. (Harel et al., 2022), due to the quality requirements of the diffusion-weighted images. As a result, we reanalysed the clinical outcomes of Deep TMS for the current active and sham Deep TMS groups. Consistent with previous findings (Harel et al., 2022), the active group experienced a reduction in craving levels after three weeks of Deep TMS treatment (Figure 4.8-a). Additionally, craving levels remained lower in the active group three months post-treatment,

while the sham group experienced an increase in craving over the follow-up period (Figure 4.7-b), similarly a significant reduction in the consumption was observed (Figure 4.7-c).

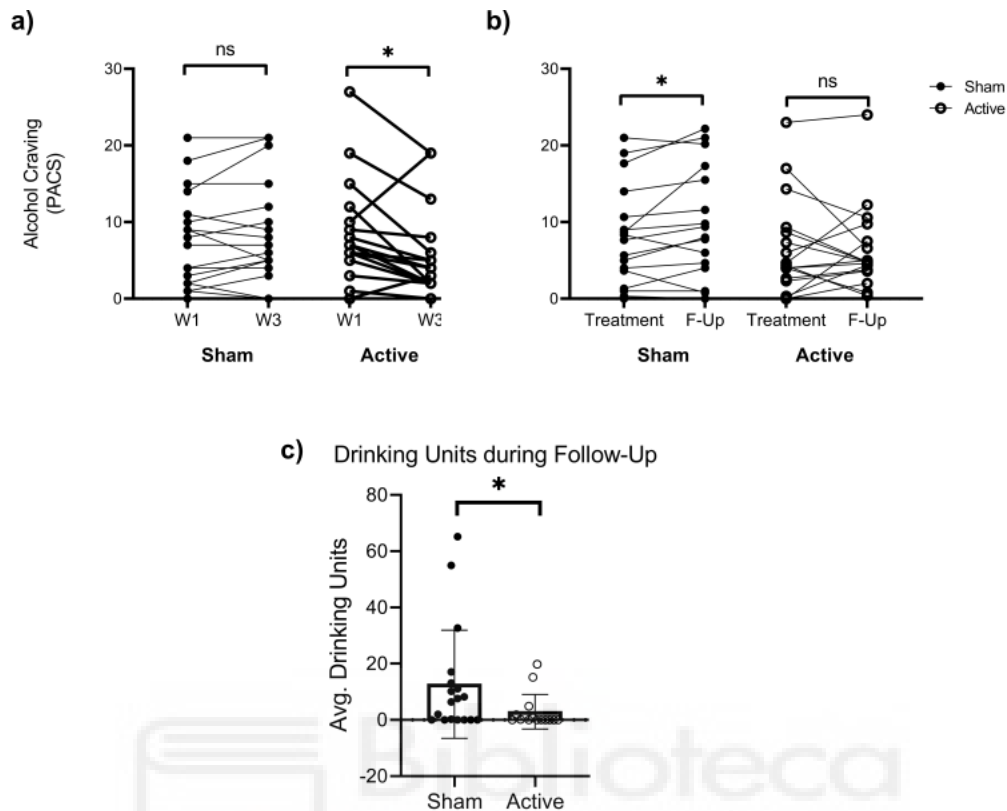


Figure 4.8 Deep TMS decreases alcohol craving. (a) Evolution of PACS (Penn Alcohol Craving Scale) values across groups (sham and active) and treatment time points (weeks 1 and 3). (b) Average PACS values were measured during the 3 weeks treatment (“Treatment”) and at 3 months follow-up (“F-Up”) for sham and active Deep TMS groups. Wilcoxon rank test. ns: not statistically significant, $*p < 0.05$. (c) Comparison of alcohol consumption during the follow-up period, average drinking units (DU) in the follow-up period was lower for active vs. sham Deep TMS-treated patients. One DU=12g of ethanol. Mann-Whitney test $*p < 0.05$.

Functional connectivity is modulated in the cortical regions specified by the Deep TMS-sensitive axonal tracts

Tractography was employed to trace streamlines passing through the white matter region sensitive to Deep TMS. Two fibre tracts were consistently identified across subjects: one association and one commissural. These tracts were present in at least 70% of the subjects and were identified as the green and red tracts shown in Figure 4.9-a. The terminals of these tracts defined four regions of interest in the grey matter: the posterior cingulate cortex (PCC; MNI: 12, -50, 40) and the dorsomedial prefrontal cortex (dmPFC; MNI: 11, 62, 28), defined by the association fibres and located in the posterior and anterior portions of the default mode network, respectively (Figure 4.8-a); and bilateral regions of the dorsolateral prefrontal cortex (dlPFC; MNI: 10, 56, 42 and -13, 55, 34), connected by the commissural fibres. Functional connectivity analysis using these regions as seeds showed significant main effects of the group at post-treatment. Follow-up ANOVAs on extracted beta coefficients revealed time x group interactions driven by between-group differences at post-treatment. Specifically, we found

increased negative connectivity in active vs. sham Deep TMS groups between the PCC and the middle frontal gyrus in the premotor cortex (MNI: -32, -2, 58; 6 voxels; main effect of group $F_{(1,35)} = 16.5$, $p < 0.001$, $\eta^2 = 0.32$; time x group interaction $F_{(1,35)} = 10.9$, $p = 0.002$, $\eta^2 = 0.24$; between-group difference at post-treatment, $p < 0.001$, pre-treatment $p = 0.33$). The results were not affected by the removal of one outlier (between-group difference at post-treatment, $p < 0.001$, pre-treatment $p = 0.09$; Figure 4.9-b).

Additionally, we found increased positive connectivity in active vs. sham Deep TMS groups between the dmPFC seed and the posterior portion of the superior temporal sulcus (pSTS; MNI: 43, -59, 13; 6 voxels; main effect of group $F_{(1,35)} = 12.5$, $p = 0.001$, $\eta^2 = 0.26$; time x group interaction $F_{(1,35)} = 5.3$, $p = 0.028$, $\eta^2 = 0.13$; between-group difference at post-treatment, $p < 0.001$, pre-treatment $p = 0.17$). The results were not affected by the removal of one outlier (between-group difference at post-treatment, $p < 0.001$, pre-treatment $p = 0.33$; Figure 4.9-c).

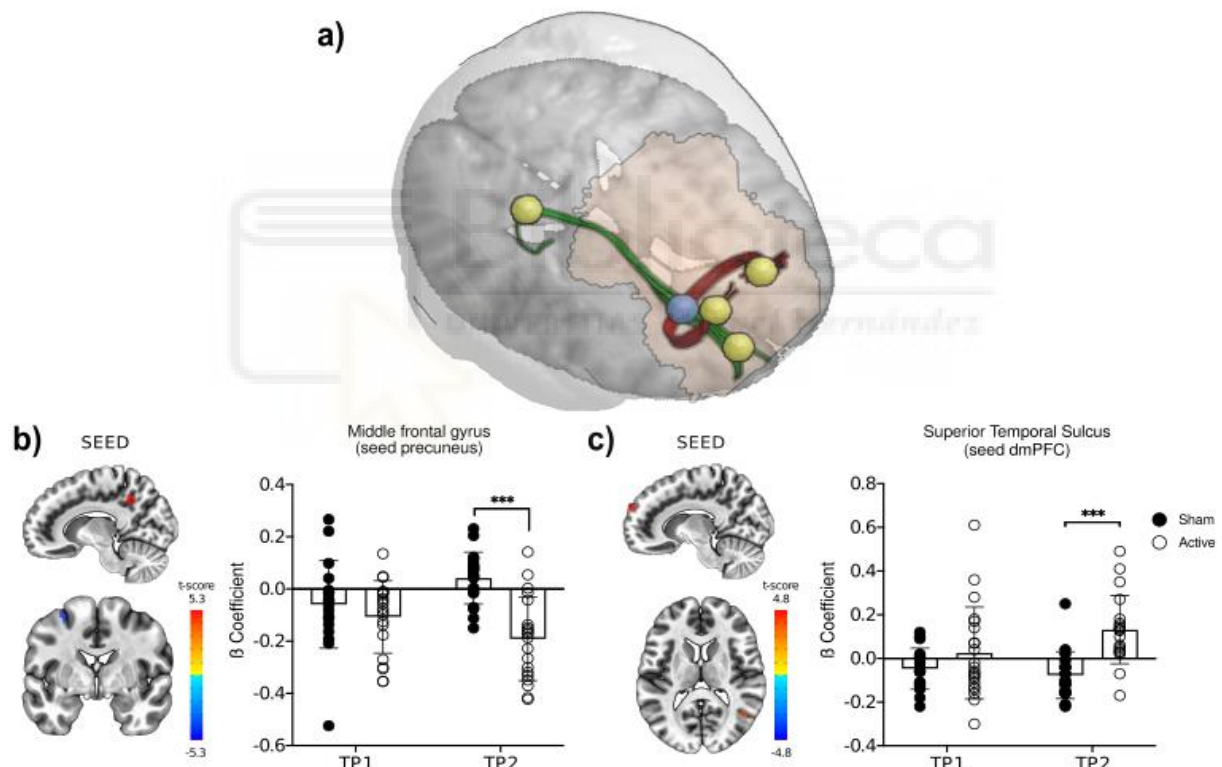


Figure 4.9 White matter tracts protected by Deep TMS define terminal fields in the grey matter that show persistent changes in functional connectivity. (a) Cortical targets (yellow spheres) are defined by the terminations of white matter streamlines (green: ipsilateral/association; red: bilateral/commissural) passing through the Deep TMS-sensitive spot (blue sphere). Two fibre tracts were consistently identified. (b) Increased negative functional connectivity in the active group at TP2 between the PCCs (defined by the green tract) and middle frontal gyrus. (c) Increased positive functional connectivity in active Deep TMS vs. sham at TP2 between the dmPFC (defined by the green tract) and the pSTS.



V. Discussion

5.1 Contribution to understanding white matter alterations in AUD

Probing the specific alterations in white matter that occur in individuals with AUD provides valuable insights into the underlying mechanisms of the disorder, potentially facilitating the development of personalized treatment plans. Moreover, examining the effects of alcohol on white matter in animal models can provide further information on the long-term consequences of alcohol use on brain health. In this work, we employed diffusion MRI to detect alcohol-induced alterations in the white matter of both patients with AUD and an AUD rat model, yielding findings consistent with previous studies. Our methods extended beyond traditional approaches by incorporating advanced multicompartment diffusion techniques specific to the axonal structure. Translationally, this approach aimed to deepen our understanding of white matter pathology in the context of AUD, position it as a therapeutic target for Deep TMS, and provide insights into the mechanistic actions by which Deep TMS acts as a novel treatment for AUD.

5.1.1 Preclinical framework

Results from the preclinical section demonstrate several key findings. Alcohol consumption disrupts the white matter microstructures in a rat model of AUD, as revealed by diffusion MRI. This disruption appears to alter the axonal structure, as measured by neurofilament staining, and myelination, as revealed by MBP staining.

In the presented preclinical setup, msP rats reached an alcohol intake level of 7 g/kg/day, this consumption level aligns with those observed in individuals with AUD and meets the criteria for an AUD model (Ciccocioppo et al., 2006). The four-week alcohol protocol was sufficient to induce global alteration in the brain parenchyma that was revealed by both diffusion MRI and immunohistochemistry procedures. Group comparisons within diffusion MRI analysis indicated a reduction in fractional anisotropy (FA), suggesting altered white matter integrity. This reduction was observed throughout the entire white matter, consistent with previous reports (De Santis et al., 2023, 2019; Pfefferbaum and Sullivan, 2005; Yeh et al., 2009). The observed FA reduction was corroborated by both tract-based and atlas-based approaches. Furthermore, the same rat line exhibited a consistent pattern of FA reduction, which persisted for at least six weeks into abstinence (De Santis et al., 2019).

Changes in FA indicate alterations in tissue integrity that could result from several factors, such as changes in myelin thickness, axonal density, or axonal diameter (Assaf et al., 2019). Advanced multicompartment modelling, which separates intra- and extracellular compartments in the diffusion signal, surpassed the inherent non-specificity of FA and yielded more precise results. These results were primarily localized within major white matter tracts, with particular emphasis on the corpus callosum and fimbria-fornix, regions previously shown to be more susceptible to alcohol-induced damage (Huang et al., 2012; Pérez-Cervera et al.,

2023). Within these tracts, there was evidence of axonal thickening, as indicated by an increase in AX maps, a proxy for axonal diameter. Meanwhile, the reduction in the restricted water fraction (FR) indicated decreased axonal density.

Immunohistochemistry performed within these two major white matter bundles, i.e., corpus callosum and fimbria-fornix connection, revealed hallmarks of altered axonal structure, where the mean neurofilament staining intensity was significantly higher in alcohol-drinking rats compared to controls. Additionally, staining texture parameters exhibited significant differences in the corpus callosum of alcohol-exposed rats, with higher texture contrast and lower homogeneity, indicating global changes in the overall axonal structure (Haralick et al., 1973; Lopes and Betrouni, 2009). A similar trend was observed in the fimbria-fornix but did not reach statistical significance. Both texture contrast and homogeneity provide valuable insights into the underlying tissue structure, with homogeneity measuring the similarity of pixel values within the stained area, while contrast quantifies the difference in intensity between adjacent pixels within that area. These two factors are qualitatively opposite, with lower homogeneity indicating a more granular and irregular texture (De Chaumont et al., 2012).

Elevated levels of neurofilament peptides have been linked to the progression of various chronic neurodegenerative diseases and nerve disorders, such as multiple sclerosis, Huntington's disease, and Alzheimer's disease (Gafson et al., 2020). Due to their role in maintaining neuron structural integrity, neurofilament peptides have been regarded as biomarkers for neuronal injury (Yuan and Nixon, 2021). Notably, recent research has unveiled a significant positive correlation between the intensity of neurofilament staining and a proxy for axonal diameter in an animal model of induced neurodegeneration (Cerdán Cerdá et al., 2024). In humans, a study on white matter lesions detected by diffusion MRI, sensitive to axonal pathology, revealed an association between these lesions and serum neurofilament levels in the entire patient cohort (Rahmanzadeh et al., 2021).

Myelin basic protein staining revealed a contrasting pattern compared to neurofilament staining, indicating a significant reduction in the fimbria-fornix bundle in alcohol-exposed rats compared to controls. This reduction was accompanied by a trend in texture parameters towards increased homogeneity, suggestive of myelin breakdown. However, the lack of significant changes in MBP staining in the corpus callosum could be attributed to the position of the region of interest in the segmented plane. In the fimbria-fornix, analysis was conducted on transverse sections, while in the corpus callosum, longitudinal sections were examined due to brain slicing in the anteroposterior axis. Transverse sections are generally preferred for examining myelin, this preference is because of the detailed and quantifiable information that transverse sections provide about the structure and organization of myelin around axons. Conversely, longitudinal sections are better suited for visualizing axonal continuity (Hildebrand and Hahn, 1978). Moreover, given the increased susceptibility of the fimbria-fornix connection to alcohol damage (Pérez-Cervera et al., 2023), demyelination may onset more rapidly in fimbria-fornix axons compared to those in the corpus callosum.

It has been demonstrated that the loss of MBP can trigger myelin vesiculation and subsequent breakdown in animal models of demyelinating diseases (Weil et al., 2016). MBP also serves as a biomarker for the pathogenesis of multiple sclerosis (Martinsen and Kursula, 2022). Intriguingly, MBP immunofluorescence was positively correlated with FA in white matter coherent fibres (Chang et al., 2017).

Together, the combined MRI and histology results presented here, where histology mirrored the advanced diffusion-based discoveries, reveal a series of alcohol-induced changes in axonal structure and myelination.

Biological substrate of the observed neurodegenerative pattern

The notion that there is an increased axonal diameter, and a decreased number of axons is illusive. However, a recent extensive study on axonal morphology in the normal-appearing white matter of MS patients revealed that an early event in axonal degeneration is the blistering-like alteration of the axon-myelin unit (Luchicchi et al., 2021), as depicted in Figure 5.1. Additionally, diffusion MRI acquired from MS patients who were scanned in a period less than 5 years from the disease's onset have preferentially increased axonal diameter compared to controls (Cerdán Cerdá et al., 2024).

Consequently, the presence of these blisters may offer an explanation for the observed thickening detected by diffusion MRI and the granular texture evident in neurofilament staining. Both phenomena are compatible with the hypothesis of alcohol-induced neurodegeneration.

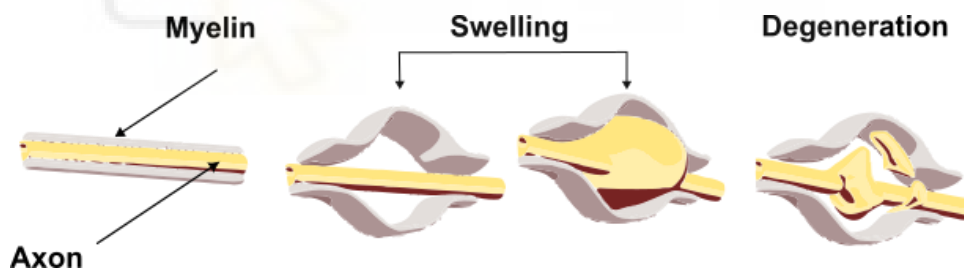


Figure 5.1 Cartoon of the blistering within the axon-myelin unit. Swelling as an early event of axon degeneration in multiple sclerosis, modified from (Luchicchi et al., 2021).

Supportive evidence also arises from a more recent study where acute axonal damage induced by the neurotoxin ibotenic acid injection, subsequently evaluated using the AxCaliber multicompartiment model, exhibited increased axonal diameter and a reduction in the number of axons (Cerdán Cerdá et al., 2024). This same study validated these findings using scanning transmission electron microscopy to assess the injected area against its contralateral part injected with saline, concluding that AxCaliber is sensitive to axonal damage (Cerdán Cerdá et al., 2024). Interestingly, from a different perspective, a study on alcohol-induced axonal damage conducted on dissected optic axons of a rat model of foetal alcohol syndrome demonstrated a significant reduction in optic nerve size and myelinated axon density (Pons-Vázquez et al., 2011).

Mechanisms of alcohol-induced axonal alteration

Alcohol-induced axonal damage and demyelination can occur through multiple mechanisms. For instance, alcohol metabolism generates reactive oxygen species that overwhelm cellular antioxidant defences (Gil-Mohapel et al., 2019). This oxidative stress causes neuronal injury (Haorah et al., 2008), and induces damage to both oligodendrocytes and the myelin sheath, exacerbating demyelination (French et al., 2009). Alcohol also exhibits direct toxic effects on oligodendrocytes, inhibiting their differentiation (Guo et al., 2021) and reducing the expression of mature oligodendrocyte mRNA markers (Darbinian et al., 2021). This disruption of oligodendrocyte function impairs myelin synthesis and maintenance, leading to myelin degradation and loss (Crews and Nixon, 2003; Guo et al., 2021). Additionally, chronic alcohol consumption triggers neuroimmune activation (Erickson et al., 2019), resulting in pro-inflammatory glial responses (Saito et al., 2016). Activated microglia and astrocytes release pro-inflammatory cytokines, which in turn initiate the infiltration of other leukocytes, further activating endogenous glia and sustaining a chronic inflammatory state (Merrill and Benveniste, 1996). This sustained inflammation further damages myelin, impairs remyelination mechanisms, and causes axonal dysfunction (Guo et al., 2021).

Altogether, chronic alcohol consumption significantly disrupts white matter, resulting in distinct changes in axonal structure and myelination. This pattern is comparable to early events in autoimmune diseases like multiple sclerosis (Luchicchi et al., 2021), eventually manifesting as axonal death and demyelination. Such white matter disruption impairs brain communication, thereby affecting both functional and cognitive abilities (Abdullah et al., 2022; Charlton et al., 2006; O'Sullivan et al., 2001), and contributing to the symptomatology of AUD (Baan et al., 2007; Boden and Fergusson, 2011; Malathesh et al., 2021; O'Keefe et al., 2014; Rehm et al., 2019). Notably, white matter integrity has been shown to predict future AUD relapse, with lower integrity indicating a higher likelihood of relapse (Zou et al., 2018). One primary objective of AUD treatment is preventing relapse to heavy drinking, which is particularly challenging in the initial months following abstinence (Sinha, 2011).

All in all, these results open a new horizon into looking at alcohol-induced white matter disruption as a primary contributor to the pathogenesis of AUD, rather than a secondary effect. Thus, novel interventions aimed at protecting against or mitigating this disruption hold a potential for managing the severity of AUD.

5.1.2 Clinical framework

Clinical results yielded fundamental findings demonstrating that patients with AUD exhibit disrupted white matter integrity compared to healthy controls. This disruption, evidenced by decreased FA, and progresses during early abstinence. However, a high-frequency (10 Hz) protocol of Deep TMS targeting midline structures of the frontal lobe halted this progression, resulting in preserved white matter structure in the stimulated area. These preserved structures upheld persistent changes in functional connectivity and were associated with reduced craving and relapse scores. This suggests that maintaining structural integrity by

promoting white matter plasticity, potentially driven by axonal activity and adaptive myelination, may contribute to the therapeutic effects of Deep TMS in AUD.

Consistent microstructural alterations, progression, and relapse

The integrity of white matter in patients with AUD appears disrupted compared to a cohort of healthy subjects matched by age and gender. This disruption in integrity is indicated by an overall reduction in FA, which confirms previous findings from our research group (De Santis et al., 2019). The replication of these results in an independent patient cohort, utilizing a different MRI acquisition approach, demonstrates notable robustness. This robustness is particularly significant given the growing awareness of limited reproducibility commonly observed in MRI studies with conventional sample sizes (Marek et al., 2022).

Previously, we observed that FA decline persisted for at least six weeks after alcohol withdrawal (De Santis et al., 2019). In this study, a similar pattern is observed in the sham-stimulated cohort, where there was a consistent reduction in FA during the three-week stimulation protocol. This observation unveils a process that may either initiate or continue following alcohol cessation, potentially impacting the high relapse rates commonly observed during early abstinence stages (Sinha, 2011). Mathematical modelling of water diffusion in distinct biological compartments suggested that this decline in FA could be attributed to a reduction in myelin content and/or glial reactivity (De Santis et al., 2019), two neurobiological mechanisms likely to occur during the course of AUD (Crews et al., 2017).

Intriguingly, following three weeks of active Deep TMS targeting midline structures of the frontal lobe, the progression of FA reduction observed in the sham-stimulated patients was arrested. The protected white matter regions, integral to both association and commissural pathways in the frontal lobe, were situated in the brain area where Deep TMS was intended to elicit supra-threshold activation for action potential firing (the orange shadow in Figure 4.6, also see Figure 3.4 for power distribution). These findings offer compelling evidence regarding the specificity of the treatment.

White matter changes exhibited right lateralization in patients with AUD compared to healthy subjects, consistent with previous reports (Harris et al., 2008), as well as the protective effect exerted by Deep TMS within the active AUD group. These two phenomena may be related, for instance, potential sensitivity for detecting a positive Deep TMS effect in AUD patients might have been enhanced by the lower FA values observed in the right hemisphere. This is supported by neuroimaging evidence suggesting that inhibitory responses are functionally localized to the right frontal cortex (Aron et al., 2004). While lateralization has also been reported in neuroimaging studies on cue reactivity (Aron et al., 2004; Vollstädt-Klein et al., 2011), including a meta-analysis (Schacht et al., 2013), consistent and full evidence is not yet available.

Positive clinical outcomes are paralleled by interconnected structural and functional changes

In our data-driven approach, we investigated the connectivity of grey matter regions identified as projections of axonal fibres based on Deep TMS outcomes. Four cortical targets were identified, two of these targets, the PCC and dmPFC, were connected via association fibres in the right hemisphere, while the remaining two targets resided in bilateral regions of the dlPFC, connected through commissural fibres. All identified regions have been previously implicated in AUD and are integral to cognitive functions such as cognitive flexibility, inhibitory control, decision-making, planning, and working memory (Cavanna and Trimble, 2006; Ribeiro et al., 2017). Recent research on brain lesions associated with the remission from nicotine or alcohol addiction has identified a network of brain regions and tracts involved in addiction remission (Joutsa et al., 2022). Notably, the brain regions and tracts protected by Deep TMS in our study were confined within this addiction remission network, suggesting that the same mechanism might extend to other addictive disorders.

Our fMRI results, while requiring careful interpretation due to the small sample size, support the notion that microstructural changes in white matter have a functional impact. As previously reported (Harel et al., 2022), the functional connectivity changes observed in the active Deep TMS group differed from those commonly reported in AUD (Camchong et al., 2013; Fede et al., 2019; Kohno et al., 2017; Vergara et al., 2017). Specifically, the active Deep TMS group exhibited a marked increase in functional connectivity between the PCC and a middle frontal gyrus cluster, as well as in the Frontal Eye Field (FEF) region of the premotor cortex. This enhanced connectivity between the PCC (a key node in the default mode network - DMN) and the FEF (a node in the dorsal attention network - DAN) may reflect improved task disengagement (Gusnard and Raichle, 2001) and voluntary response selection (Corbetta and Shulman, 2002). Additionally, a significant increase in functional connectivity was observed between the dmPFC and the pSTS. This connection, central to the social network, is thought to be involved in internalization, strategic planning, and decision-making in social contexts (Adolphs, 2009). Enhanced connectivity between the dmPFC and pSTS may indicate improved social flexibility and adaptability (Jamali et al., 2021; Konovalov et al., 2021; McDonald et al., 2020). It is plausible that the strengthened coupling in this network improves social abilities in patients and contributes to the therapeutic effect of Deep TMS, a hypothesis warranting further investigation.

5.2 Translational findings and their significance

Considering the evidence of disrupted white matter demonstrated by MRI and histological findings in a rat model of AUD, characterised by demyelinated and damaged axons, as well as in patients with AUD who exhibit consistent alterations in microstructural integrity, it is believed that this disrupted white matter mediates dysfunctional neural connections and promotes addiction and relapse in AUD. In this context, we postulate that the mechanism of action of Deep TMS potentially functions as a reparative mechanism to restore damaged axons.

The neurobiological process that mediates the observed clinical improvement

TMS has demonstrated therapeutic benefits for various conditions (Hyde et al., 2022), yet its underlying molecular and cellular mechanisms remain elusive. One proposed mechanism in psychiatric disorders, particularly addiction, involves modulating neuronal activity in relevant addiction circuits, influencing salience, reactivity, and response inhibition to drug-related cues (Gorelick et al., 2014). Additionally, modulation of neurotransmitter activity, specifically dopamine and glutamate, is implicated (Gorelick et al., 2014). Despite some understanding of TMS effects in psychiatric disorders, a definitive mechanism of action remains unclear.

Recent evidence (Cullen and Young, 2016) suggests that mechanisms beyond neuron-centric interpretations may contribute to TMS's therapeutic effects. For instance, high-frequency TMS may enhance neuronal firing rates (Gorelick et al., 2014), potentially increasing activity-dependent myelination, which could improve axonal conduction velocity and transmission reliability between brain areas (Cullen and Young, 2016). Previous research has indicated that TMS treatment can increase FA in patients with MDD (Hong et al., 2020; Seewoo et al., 2022). Our study reveals a rescue in FA values in tracts connecting structures crucial for alcohol addiction, including the dlPFC, dmPFC, and PCC (Beylergil et al., 2017; Klenowski, 2018; Zakiniaez et al., 2017). Notably, our findings also indicate reduced craving and relapse. These observations collectively suggest that Deep TMS efficacy in treating AUD, to some extent, is attributed to rescuing structural connectivity through activity-dependent myelination.

Adaptive myelination, or myelin plasticity, is a process in which the neuronal electrical activity instructs oligodendrocytes to myelinate active axons, and signals oligodendrocyte precursor cells (OPCs) to increase the proliferation of more mature oligodendrocytes. This results in an increase in axonal conduction velocity, as demonstrated by Gibson et al. (Gibson et al., 2014). Repetitive TMS, even at low intensity, has been shown to increase the number of newly born oligodendrocytes without impacting oligodendrogenesis, but rather increasing cell survival and enhancing myelination in the adult mouse cortex (Cullen et al., 2019). This same study also reported an increase in myelin internode length induced by TMS (Cullen et al., 2019), which would lead to faster action potential conduction velocity (Saab and Nave, 2017). These findings suggest TMS could potentially mitigate myelin deficits induced by prolonged alcohol withdrawal (Rice and Gu, 2019). It is noteworthy that the vesicular release of glutamate from axons initiates the signalling cascade that couples neuronal activity to the response of OPCs (Bergles et al., 2000; Kukley et al., 2007). Concurrently, chronic drug use is known to disrupt glutamate homeostasis in the brain (Engblom et al., 2008; Javitt et al., 2011). This disruption suggests that impaired myelin plasticity may represent a common pathophysiological feature of addiction.

Furthermore, TMS may influence white matter microstructure in individuals with AUD by affecting other glial cells. TMS can temporarily increase glial fibrillary acidic protein (GFAP) expression (Rauš et al., 2013) and inhibit neurotoxic astrocyte polarization (Hong et al., 2020). High-frequency, low-intensity TMS after ischemic injury or demyelination appears to promote

a reactive microglia phenotype (Fang et al., 2010; Rauš et al., 2013). Conversely, high-frequency, high-intensity TMS reduces microglial reactivity (Kim et al., 2013). Inflammation is implicated in alcohol addiction pathophysiology (Pascual et al., 2018), with inflammatory markers correlating with lifetime alcohol consumption and age of onset (Crews et al., 2017). Previous research has shown persistent microglial reactivity during early alcohol abstinence in an AUD animal model, characterised by morphological changes indicative of neuroinflammation, as demonstrated by diffusion-weighted MRI parameters (De Santis et al., 2020). This finding extends to patients with AUD (De Santis et al., 2020). Diffusion-based MRI is sensitive to glial morphology changes characteristic of inflammatory conditions, rather than solely myelin content (Garcia-Hernandez et al., 2022). Therefore, TMS treatment benefits may partially stem from reducing pro-inflammatory glial cell activation. A comprehensive understanding of the mechanisms of TMS in AUD necessitates considering both the indirect stimulation of myelin plasticity via increased action potential firing and the direct effects on glial cells, thus warranting further investigation.

5.2 Potential applications and future research directions

Diffusion MRI has demonstrated efficacy in characterising complex microstructural configurations and reflecting global white matter disruptions induced by alcohol, mirroring results obtained through invasive histological methods. These findings underscore the potential of advanced dw-MRI for monitoring AUD progression and evaluating intervention effectiveness. Advanced multicompartiment models, particularly AxCaliber and CHARMED, have proven to be sensitive to axonal structure, capturing intricate white matter organization and revealing additional details beyond basic tensor modelling. However, these advanced methods present challenges in sequence acquisition and reconstruction. In preclinical settings, researchers can adapt acquisition protocols or extend scan times under anaesthesia, offering flexibility. Yet, such adjustments are not typically feasible in clinical settings due to vendor restrictions, patient tolerance, and training limitations. Future research should focus on enhancing data acquired on simpler setups *a posteriori* to meet the requirements of advanced schemes using deep learning (Aja-Fernández et al., 2023) or implementing novel methods for accelerated acquisition to reduce overall scanning time (Hoch et al., 2021), thus improving accessibility for patients and clinical personnel.

While axonal degeneration and demyelination have been primary focuses, it's crucial to acknowledge the multifaceted effects of alcohol on the brain, including glial reactivity (Saba, 2023). Future investigations should enhance diffusion signal modelling by incorporating more anatomy-specific compartments for axons and glial cells separately (Garcia-Hernandez et al., 2022), or utilizing more generalized diffusion models to better understand the interplay between glial activity and axonal alteration (Novikov et al., 2018; Reisert et al., 2017).

Pharmacotherapy for AUD, while evolving over the past 25 years with increased knowledge of the brain, remains limited in efficacy due to genetic, habitual, and epidemiological factors that vary across individuals (Swift and Aston, 2015). Deep TMS therapy, a non-invasive and well-

tolerated treatment, emerges as a promising next-generation approach for AUD management (Swift and Aston, 2015), potentially used alone or in combination with traditional treatments. Its approval for obsessive-compulsive disorders (Tendler et al., 2021), could facilitate direct application to AUD. Future research should investigate Deep TMS alongside existing psychosocial and pharmacotherapies. Ultimately, the goal is to enhance AUD management in healthcare settings (Anderson et al., 2017), leading to improved patient outcomes and broader societal benefits.

5.3 Limitations

Our translational approach, which encompasses both preclinical and clinical setups, has certain limitations that must be acknowledged. First, in the preclinical setup, the control group scanning was scheduled after the experimental group to adhere to the alcohol protocol. However, scanner maintenance issues resulted in data acquisition occurring at different times for both groups, leading to sparse estimation of AxCaliber values due to automatic internal adjustments in the new console software. Despite this, the overall results remained unaffected, as confirmed by the immunohistochemistry group. To improve homogeneity and facilitate cross-sectional and longitudinal analyses, it would be advantageous to acquire the data simultaneously. Nonetheless, accommodating a large number of animals poses challenges due to increased scanning time and an overbooked scanning schedule. The animals were housed individually, eliminating the influence of social interaction on drinking levels (Le et al., 2021; Steele and Southwick, 1985). Implementing a new consumption paradigm would account for this influence (Frie and Khokhar, 2024). Only male rats were used due to the complex relationship between sex hormones and consumption levels, precluding the examination of gender effects. The advanced models employed here are exclusively sensitive to axonal structure. To further delineate the observed disruption subcomponents, the utilization of additional sequences sensitive to other intrinsic cellular properties, as well as more thorough histological investigation, potentially including electron microscopy, would be beneficial.

In the clinical part, to further elucidate the clinical efficacy of Deep TMS, a multicentre study with a larger sample size is warranted. Although both male and female patients were included, the current study's sample size and composition did not permit an analysis of potential sex-specific effects on white matter alterations or clinical outcomes. Additionally, the long-term effects of Deep TMS beyond the follow-up period were not assessed. Furthermore, the stimulation protocol may be subject to further optimization, contingent upon the most critical process for clinical effectiveness. Different neurobiological mechanisms underlying the observed clinical efficacy of Deep TMS, such as activation of specific neural networks, induction of myelin plasticity, or potential anti-inflammatory effects, may necessitate distinct optimization parameters. Further translational research in animal models can potentially dissect the individual contributions to Deep TMS effects and identify the most efficacious stimulation protocols.

5.5 Final remarks

Notwithstanding the aforementioned limitations, the results presented here represent a substantial advancement in the field. Advanced diffusion MRI modelling revealed widespread alterations in white matter microstructure resulting from four weeks of chronic alcohol consumption in a rat model of AUD. Specifically, these alterations indicated early demyelination with signs of axonal degeneration, further corroborated by sensitive histological analysis of myelin and neuronal structure. This finding has significant implications for understanding white matter disruption in AUD patients and opens avenues for novel Deep TMS interventions aimed at preserving neuronal integrity. Moreover, it provides support for understanding the underlying mechanism of action.

Additionally, by combining structural and functional neuroimaging, we demonstrated that Deep TMS can arrest the progression of white matter microstructural changes and exert lasting effects on functional connectivity. A broader implication of our findings is that positive effects on white matter microstructure should be considered as potential mediators of Deep TMS effects, warranting further research to determine the optimal conditions for achieving such effects.



VI. Conclusions

1. Multicompartment diffusion MRI models surpass basic models (e.g., DTI) in characterising axonal structure in both healthy and diseased states.
2. Diffusion MRI and histological data convergently indicate alcohol-induced axonal degeneration and demyelination, aligning with observed white matter integrity loss in patients with AUD.
3. A progressive decline in fractional anisotropy during early withdrawal, indicative of extended white matter disruption in patients with AUD, may be primarily driven by demyelination and axonal degeneration, and potentially exacerbated by inflammatory processes.
4. Deep TMS arrests this progression during early abstinence, influencing both brain structure and function, and leading to positive clinical outcomes, including reduced craving and relapse.
5. Deep TMS safeguards white matter structure through multiple mechanisms, with adaptive myelination potentially playing a primary or contributing role. This positions Deep TMS as a potential next-generation therapy for AUD.



VII. Conclusiones

1. Los modelos de RM-D basados en compartimentos múltiples superan a los modelos básicos (p. ej., DTI) en la caracterización de la estructura axonal tanto en estados sanos como patológicos.
2. Los datos de RM-D e histológicos convergen para indicar degeneración axonal y desmielinización inducidas por el alcohol, lo que se alinea con la pérdida de integridad de la sustancia blanca observada en pacientes con TCA.
3. Una disminución progresiva en la anisotropía fraccional durante la abstinencia temprana, indicativa de una alteración prolongada de la sustancia blanca en pacientes con TCA, puede ser producida principalmente por la desmielinización y la degeneración axonal, potencialmente exacerbada por procesos inflamatorios.
4. La EMT Profunda detiene esta progresión durante la abstinencia temprana, influyendo tanto en la estructura como en la función del cerebro, y conduciendo a resultados clínicos positivos, incluida la reducción del ansia por el consumo y la recaída.
5. La EMT Profunda protege la estructura de la sustancia blanca a través de múltiples mecanismos, con la mielinización adaptativa potencialmente jugando un papel principal o contributivo. Esto posiciona a la EMT Profunda como una posible terapia de nueva generación para TCA.



VIII. References

Abdullah, A.N., Ahmad, A.H., Zakaria, R., Tamam, S., Abd Hamid, A.I., Chai, W.J., Omar, H., Abdul Rahman, M.R., Fitzrol, D.N., Idris, Z., Ghani, A.R.I., Wan Mohamad, W.N.A., Mustafar, F., Hanafi, M.H., Reza, M.F., Umar, H., Mohd Zulkifly, M.F., Ang, S.Y., Zakaria, Z., Musa, K.I., Othman, A., Embong, Z., Sapiai, N.A., Kandasamy, R., Ibrahim, H., Abdullah, M.Z., Amaruchkul, K., Valdes-Sosa, P.A., Bringas Vega, M.L., Biswal, B., Songsiri, J., Yaacob, H.S.,

- Sumari, P., Noh, N.A., Azman, A., Jamir Singh, P.S., Abdullah, J.M., 2022. Disruption of white matter integrity and its relationship with cognitive function in non-severe traumatic brain injury. *Front. Neurol.* 13, 1011304. <https://doi.org/10.3389/fneur.2022.1011304>
- Adolphs, R., 2009. The Social Brain: Neural Basis of Social Knowledge. *Annu. Rev. Psychol.* 60, 693–716. <https://doi.org/10.1146/annurev.psych.60.110707.163514>
- Agartz, I., Momenan, R., Rawlings, R.R., Kerich, M.J., Hommer, D.W., 1999. Hippocampal volume in patients with alcohol dependence. *Arch. Gen. Psychiatry* 56, 356–363. <https://doi.org/10.1001/archpsyc.56.4.356>
- Aja-Fernández, S., Martín-Martín, C., Planchuelo-Gómez, Á., Faiyaz, A., Uddin, M.N., Schifitto, G., Tiwari, A., Shigwan, S.J., Kumar Singh, R., Zheng, T., Cao, Z., Wu, D., Blumberg, S.B., Sen, S., Goodwin-Allcock, T., Slator, P.J., Yigit Avci, M., Li, Z., Bilgic, B., Tian, Q., Wang, X., Tang, Z., Cabezas, M., Rauland, A., Merhof, D., Manzano Maria, R., Campos, V.P., Santini, T., da Costa Vieira, M.A., HashemizadehKolowri, S., DiBella, E., Peng, C., Shen, Z., Chen, Z., Ullah, I., Mani, M., Abdolmotalleby, H., Eckstrom, S., Baete, S.H., Filipiak, P., Dong, T., Fan, Q., de Luis-García, R., Tristán-Vega, A., Pieciak, T., 2023. Validation of deep learning techniques for quality augmentation in diffusion MRI for clinical studies. *NeuroImage Clin.* 39, 103483. <https://doi.org/10.1016/j.nicl.2023.103483>
- Alexander, D.C., Dyrby, T.B., Nilsson, M., Zhang, H., 2019. Imaging brain microstructure with diffusion MRI: practicality and applications. *NMR Biomed.* 32, e3841. <https://doi.org/10.1002/nbm.3841>
- Alexander, D.C., Hubbard, P.L., Hall, M.G., Moore, E.A., Ptito, M., Parker, G.J.M., Dyrby, T.B., 2010. Orientationally invariant indices of axon diameter and density from diffusion MRI. *NeuroImage* 52, 1374–1389. <https://doi.org/10.1016/j.neuroimage.2010.05.043>
- Alexander Leemans, Ben Jeurissen, Jan Sijbers, Derek K. Jones, n.d. ExploreDTI: a graphical toolbox for processing, analyzing, and visualizing diffusion MR data.
- American Psychiatric Association, 2013. Diagnostic and Statistical Manual of Mental Disorders, Fifth Edition. ed. American Psychiatric Association. <https://doi.org/10.1176/appi.books.9780890425596>
- Anderson, P., O'Donnell, A., Kaner, E., 2017. Managing Alcohol Use Disorder in Primary Health Care. *Curr. Psychiatry Rep.* 19, 79. <https://doi.org/10.1007/s11920-017-0837-z>
- Andre, J.B., Bresnahan, B.W., Mossa-Basha, M., Hoff, M.N., Smith, C.P., Anzai, Y., Cohen, W.A., 2015. Toward Quantifying the Prevalence, Severity, and Cost Associated With Patient Motion During Clinical MR Examinations. *J. Am. Coll. Radiol. JACR* 12, 689–695. <https://doi.org/10.1016/j.jacr.2015.03.007>
- Aron, A.R., Robbins, T.W., Poldrack, R.A., 2004. Inhibition and the right inferior frontal cortex. *Trends Cogn. Sci.* 8, 170–177. <https://doi.org/10.1016/j.tics.2004.02.010>
- Assaf, Y., Basser, P.J., 2005. Composite hindered and restricted model of diffusion (CHARMED) MR imaging of the human brain. *NeuroImage* 27, 48–58. <https://doi.org/10.1016/j.neuroimage.2005.03.042>
- Assaf, Y., Blumenfeld-Katzir, T., Yovel, Y., Basser, P.J., 2008. Axcaliber: A method for measuring axon diameter distribution from diffusion MRI. *Magn. Reson. Med.* 59, 1347–1354. <https://doi.org/10.1002/mrm.21577>
- Assaf, Y., Johansen-Berg, H., Thiebaut de Schotten, M., 2019. The role of diffusion MRI in neuroscience. *NMR Biomed.* 32, e3762. <https://doi.org/10.1002/nbm.3762>
- Avants, B., Tustison, N.J., Song, G., 2009. Advanced Normalization Tools: V1.0. *Insight J.* <https://doi.org/10.54294/uvnhin>
- Baan, R., Straif, K., Grosse, Y., Secretan, B., El Ghissassi, F., Bouvard, V., Altieri, A., Coglianò, V., WHO International Agency for Research on Cancer Monograph Working Group, 2007. Carcinogenicity of alcoholic beverages. *Lancet Oncol.* 8, 292–293. [https://doi.org/10.1016/s1470-2045\(07\)70099-2](https://doi.org/10.1016/s1470-2045(07)70099-2)

- Bach, P., Weil, G., Pompili, E., Hoffmann, S., Hermann, D., Vollstädt-Klein, S., Mann, K., Perez-Ramirez, U., Moratal, D., Canals, S., Dursun, S.M., Greenshaw, A.J., Kirsch, P., Kiefer, F., Sommer, W.H., 2020. Incubation of neural alcohol cue reactivity after withdrawal and its blockade by naltrexone. *Addict. Biol.* 25, e12717. <https://doi.org/10.1111/adb.12717>
- Baijot, J., Van Laethem, D., Denissen, S., Costers, L., Cambron, M., D'Haeseleer, M., D'hooghe, M.B., Vanbinst, A.-M., De Mey, J., Nagels, G., Van Schependom, J., 2022. Radial diffusivity reflects general decline rather than specific cognitive deterioration in multiple sclerosis. *Sci. Rep.* 12, 21771. <https://doi.org/10.1038/s41598-022-26204-z>
- Barkhof, F., Scheltens, P., 2002. Imaging of white matter lesions. *Cerebrovasc. Dis. Basel Switz.* 13 Suppl 2, 21–30. <https://doi.org/10.1159/000049146>
- Barrière, D.A., Magalhães, R., Novais, A., Marques, P., Selingue, E., Geffroy, F., Marques, F., Cerqueira, J., Sousa, J.C., Boumezbeur, F., Bottlaender, M., Jay, T.M., Cachia, A., Sousa, N., Mériaux, S., 2019. The SIGMA rat brain templates and atlases for multimodal MRI data analysis and visualization. *Nat. Commun.* 10, 5699. <https://doi.org/10.1038/s41467-019-13575-7>
- Basser, P.J., Mattiello, J., LeBihan, D., 1994. MR diffusion tensor spectroscopy and imaging. *Biophys. J.* 66, 259–267. [https://doi.org/10.1016/S0006-3495\(94\)80775-1](https://doi.org/10.1016/S0006-3495(94)80775-1)
- Basser, P.J., Pajevic, S., Pierpaoli, C., Duda, J., Aldroubi, A., 2000. In vivo fiber tractography using DT-MRI data. *Magn. Reson. Med.* 44, 625–632. [https://doi.org/10.1002/1522-2594\(200010\)44:4<625::aid-mrm17>3.0.co;2-o](https://doi.org/10.1002/1522-2594(200010)44:4<625::aid-mrm17>3.0.co;2-o)
- Beaulieu, C., 2002. The basis of anisotropic water diffusion in the nervous system - a technical review. *NMR Biomed.* 15, 435–455. <https://doi.org/10.1002/nbm.782>
- Becker, H.C., Lopez, M.F., 2004. Increased ethanol drinking after repeated chronic ethanol exposure and withdrawal experience in C57BL/6 mice. *Alcohol. Clin. Exp. Res.* 28, 1829–1838. <https://doi.org/10.1097/01.alc.0000149977.95306.3a>
- Behrens, T.E.J., Woolrich, M.W., Jenkinson, M., Johansen-Berg, H., Nunes, R.G., Clare, S., Matthews, P.M., Brady, J.M., Smith, S.M., 2003. Characterization and propagation of uncertainty in diffusion-weighted MR imaging. *Magn. Reson. Med.* 50, 1077–1088. <https://doi.org/10.1002/mrm.10609>
- Belgers, M., Van Eijndhoven, P., Markus, W., Schene, A.H., Schellekens, A., 2022. rTMS Reduces Craving and Alcohol Use in Patients with Alcohol Use Disorder: Results of a Randomized, Sham-Controlled Clinical Trial. *J. Clin. Med.* 11, 951. <https://doi.org/10.3390/jcm11040951>
- Belin-Paus, A., Daniel, M.-L., Paud, M., Jupp, B., Sawiak, S., Howett, D., McKenzie, C., Caprioli, D., Besson, M., Robbins, T.W., Everitt, B.J., Dalley, J.W., Belin, D., 2016. From impulses to maladaptive actions: the insula is a neurobiological gate for the development of compulsive behavior. *Mol. Psychiatry* 21, 491–499. <https://doi.org/10.1038/mp.2015.140>
- Bergles, D.E., Roberts, J.D.B., Somogyi, P., Jahr, C.E., 2000. Glutamatergic synapses on oligodendrocyte precursor cells in the hippocampus. *Nature* 405, 187–191. <https://doi.org/10.1038/35012083>
- Bertola, A., Mathews, S., Ki, S.H., Wang, H., Gao, B., 2013. Mouse model of chronic and binge ethanol feeding (the NIAAA model). *Nat. Protoc.* 8, 627–637. <https://doi.org/10.1038/nprot.2013.032>
- Beylergil, S.B., Beck, A., Deserno, L., Lorenz, R.C., Rapp, M.A., Schlagenhaut, F., Heinz, A., Obermayer, K., 2017. Dorsolateral prefrontal cortex contributes to the impaired behavioral adaptation in alcohol dependence. *NeuroImage Clin.* 15, 80–94. <https://doi.org/10.1016/j.nicl.2017.04.010>
- Boden, J.M., Fergusson, D.M., 2011. Alcohol and depression. *Addiction* 106, 906–914. <https://doi.org/10.1111/j.1360-0443.2010.03351.x>
- Bohnen, N.I., Albin, R.L., 2011. White matter lesions in Parkinson disease. *Nat. Rev. Neurol.* 7, 229–236. <https://doi.org/10.1038/nrneurol.2011.21>
- Bordier, C., Weil, G., Bach, P., Scuppa, G., Nicolini, C., Forcellini, G., Pérez-Ramirez, U., Moratal, D., Canals, S., Hoffmann, S., Hermann, D., Vollstädt-Klein, S., Kiefer, F., Kirsch, P., Sommer, W.H.,

- Bifone, A., 2022. Increased network centrality of the anterior insula in early abstinence from alcohol. *Addict. Biol.* 27, e13096. <https://doi.org/10.1111/adb.13096>
- Boulanger, J.J., Messier, C., 2014. From precursors to myelinating oligodendrocytes: Contribution of intrinsic and extrinsic factors to white matter plasticity in the adult brain. *Neuroscience* 269, 343–366. <https://doi.org/10.1016/j.neuroscience.2014.03.063>
- Braun, R., Klein, R., Walter, H.L., Ohren, M., Freudenmacher, L., Getachew, K., Ladwig, A., Luelling, J., Neumaier, B., Endepols, H., Graf, R., Hoehn, M., Fink, G.R., Schroeter, M., Rueger, M.A., 2016. Transcranial direct current stimulation accelerates recovery of function, induces neurogenesis and recruits oligodendrocyte precursors in a rat model of stroke. *Exp. Neurol.* 279, 127–136. <https://doi.org/10.1016/j.expneurol.2016.02.018>
- Brunoni, A.R., Sampaio-Junior, B., Moffa, A.H., Aparício, L.V., Gordon, P., Klein, I., Rios, R.M., Razza, L.B., Loo, C., Padberg, F., Valiengo, L., 2019. Noninvasive brain stimulation in psychiatric disorders: a primer. *Rev. Bras. Psiquiatr. Sao Paulo Braz.* 1999 41, 70–81. <https://doi.org/10.1590/1516-4446-2017-0018>
- Budde, M.D., Xie, M., Cross, A.H., Song, S.-K., 2009. Axial diffusivity is the primary correlate of axonal injury in the experimental autoimmune encephalomyelitis spinal cord: a quantitative pixelwise analysis. *J. Neurosci. Off. J. Soc. Neurosci.* 29, 2805–2813. <https://doi.org/10.1523/JNEUROSCI.4605-08.2009>
- Bühler, M., Mann, K., 2011. Alcohol and the human brain: a systematic review of different neuroimaging methods. *Alcohol. Clin. Exp. Res.* 35, 1771–1793. <https://doi.org/10.1111/j.1530-0277.2011.01540.x>
- Buonocore, M.H., Gao, L., 1997. Ghost artifact reduction for echo planar imaging using image phase correction. *Magn. Reson. Med.* 38, 89–100. <https://doi.org/10.1002/mrm.1910380114>
- Burwell, R.D., Saddoris, M.P., Bucci, D.J., Wiig, K.A., 2004. Corticohippocampal contributions to spatial and contextual learning. *J. Neurosci. Off. J. Soc. Neurosci.* 24, 3826–3836. <https://doi.org/10.1523/JNEUROSCI.0410-04.2004>
- Buyanova, I.S., Arsalidou, M., 2021. Cerebral White Matter Myelination and Relations to Age, Gender, and Cognition: A Selective Review. *Front. Hum. Neurosci.* 15, 662031. <https://doi.org/10.3389/fnhum.2021.662031>
- Camchong, J., Stenger, A., Fein, G., 2013. Resting-State Synchrony During Early Alcohol Abstinence Can Predict Subsequent Relapse. *Cereb. Cortex* 23, 2086–2099. <https://doi.org/10.1093/cercor/bhs190>
- Canales-Rodríguez, E.J., Daducci, A., Sotiropoulos, S.N., Caruyer, E., Aja-Fernández, S., Radua, J., Yurramendi Mendizabal, J.M., Iturria-Medina, Y., Melie-García, L., Alemán-Gómez, Y., Thiran, J.-P., Sarró, S., Pomarol-Clotet, E., Salvador, R., 2015. Spherical Deconvolution of Multichannel Diffusion MRI Data with Non-Gaussian Noise Models and Spatial Regularization. *PloS One* 10, e0138910. <https://doi.org/10.1371/journal.pone.0138910>
- Canals, S., Beyerlein, M., Merkle, H., Logothetis, N.K., 2009. Functional MRI Evidence for LTP-Induced Neural Network Reorganization. *Curr. Biol.* 19, 398–403. <https://doi.org/10.1016/j.cub.2009.01.037>
- Canals, S., Beyerlein, M., Murayama, Y., Logothetis, N.K., 2008. Electric stimulation fMRI of the perforant pathway to the rat hippocampus. *Magn. Reson. Imaging* 26, 978–986. <https://doi.org/10.1016/j.mri.2008.02.018>
- Cannella, N., Ubaldi, M., Masi, A., Bramucci, M., Roberto, M., Bifone, A., Ciccocioppo, R., 2019. Building better strategies to develop new medications in Alcohol Use Disorder: Learning from past success and failure to shape a brighter future. *Neurosci. Biobehav. Rev.* 103, 384–398. <https://doi.org/10.1016/j.neubiorev.2019.05.014>
- Carnicella, S., Ron, D., Barak, S., 2014. Intermittent ethanol access schedule in rats as a preclinical model of alcohol abuse. *Alcohol Fayettev.* N 48, 243–252. <https://doi.org/10.1016/j.alcohol.2014.01.006>

- Catani, M., Jones, D.K., ffytche, D.H., 2005. Perisylvian language networks of the human brain. *Ann. Neurol.* 57, 8–16. <https://doi.org/10.1002/ana.20319>
- Cavanna, A.E., Trimble, M.R., 2006. The precuneus: a review of its functional anatomy and behavioural correlates. *Brain* 129, 564–583. <https://doi.org/10.1093/brain/awl004>
- Cerdán Cerdá, A., Toschi, N., Treaba, C.A., Barletta, V., Herranz, E., Mehndiratta, A., Gomez-Sanchez, J.A., Mainero, C., De Santis, S., 2024. A translational MRI approach to validate acute axonal damage detection as an early event in multiple sclerosis. *eLife* 13, e79169. <https://doi.org/10.7554/eLife.79169>
- Chandler, C.M., Hamid, U., Maggio, S.E., Peng, H., Pauly, J.R., Beckmann, J., Nixon, K., Bardo, M.T., 2022. Effects of adolescent alcohol exposure via oral gavage on adult alcohol drinking and co-use of alcohol and nicotine in Sprague Dawley rats. *Drug Alcohol Depend.* 232, 109298. <https://doi.org/10.1016/j.drugalcdep.2022.109298>
- Chang, E.H., Argyelan, M., Aggarwal, M., Chandon, T.-S.S., Karlsgodt, K.H., Mori, S., Malhotra, A.K., 2017. The role of myelination in measures of white matter integrity: Combination of diffusion tensor imaging and two-photon microscopy of CLARITY intact brains. *NeuroImage* 147, 253–261. <https://doi.org/10.1016/j.neuroimage.2016.11.068>
- Chang, L.-C., Jones, D.K., Pierpaoli, C., 2005. RESTORE: Robust estimation of tensors by outlier rejection. *Magn. Reson. Med.* 53, 1088–1095. <https://doi.org/10.1002/mrm.20426>
- Chanraud, S., Martelli, C., Delain, F., Kostogianni, N., Douaud, G., Aubin, H.-J., Reynaud, M., Martinot, J.-L., 2007. Brain morphometry and cognitive performance in detoxified alcohol-dependents with preserved psychosocial functioning. *Neuropsychopharmacol. Off. Publ. Am. Coll. Neuropsychopharmacol.* 32, 429–438. <https://doi.org/10.1038/sj.npp.1301219>
- Chanraud, S., Pitel, A.-L., Pfefferbaum, A., Sullivan, E.V., 2011. Disruption of functional connectivity of the default-mode network in alcoholism. *Cereb. Cortex N. Y. N* 1991 21, 2272–2281. <https://doi.org/10.1093/cercor/bhq297>
- Charlton, R.A., Barrick, T.R., McIntyre, D.J., Shen, Y., O'Sullivan, M., Howe, F.A., Clark, C.A., Morris, R.G., Markus, H.S., 2006. White matter damage on diffusion tensor imaging correlates with age-related cognitive decline. *Neurology* 66, 217–222. <https://doi.org/10.1212/01.wnl.0000194256.15247.83>
- Chen, R., Classen, J., Gerloff, C., Celnik, P., Wassermann, E.M., Hallett, M., Cohen, L.G., 1997. Depression of motor cortex excitability by low-frequency transcranial magnetic stimulation. *Neurology* 48, 1398–1403. <https://doi.org/10.1212/wnl.48.5.1398>
- Chiva-Blanch, G., Badimon, L., 2019. Benefits and Risks of Moderate Alcohol Consumption on Cardiovascular Disease: Current Findings and Controversies. *Nutrients* 12, 108. <https://doi.org/10.3390/nu12010108>
- Christie, I.N., Wells, J.A., Southern, P., Marina, N., Kasparov, S., Gourine, A.V., Lythgoe, M.F., 2013. fMRI response to blue light delivery in the naïve brain: Implications for combined optogenetic fMRI studies. *NeuroImage* 66, 634–641. <https://doi.org/10.1016/j.neuroimage.2012.10.074>
- Ciccocioppo, R., Economidou, D., Cippitelli, A., Cucculelli, M., Ubaldi, M., Soverchia, L., Lourdusamy, A., Massi, M., 2006. Genetically selected Marchigian Sardinian alcohol-preferring (msP) rats: an animal model to study the neurobiology of alcoholism. *Addict. Biol.* 11, 339–355. <https://doi.org/10.1111/j.1369-1600.2006.00032.x>
- Corbetta, M., Shulman, G.L., 2002. Control of goal-directed and stimulus-driven attention in the brain. *Nat. Rev. Neurosci.* 3, 201–215. <https://doi.org/10.1038/nrn755>
- Cosa, A., Moreno, A., Pacheco-Torres, J., Ciccocioppo, R., Hyytiä, P., Sommer, W.H., Moratal, D., Canals, S., 2017. Multi-modal MRI classifiers identify excessive alcohol consumption and treatment effects in the brain: Multi-modal imaging biomarkers. *Addict. Biol.* 22, 1459–1472. <https://doi.org/10.1111/adb.12418>
- Cox, R.W., 1996. AFNI: Software for Analysis and Visualization of Functional Magnetic Resonance Neuroimages. *Comput. Biomed. Res.* 29, 162–173. <https://doi.org/10.1006/cbmr.1996.0014>

- Cox, R.W., Chen, G., Glen, D.R., Reynolds, R.C., Taylor, P.A., 2017. FMRI Clustering in AFNI: False-Positive Rates Redux. *Brain Connect.* 7, 152–171. <https://doi.org/10.1089/brain.2016.0475>
- Crabbe, J.C., Metten, P., Rhodes, J.S., Yu, C.-H., Brown, L.L., Phillips, T.J., Finn, D.A., 2009. A line of mice selected for high blood ethanol concentrations shows drinking in the dark to intoxication. *Biol. Psychiatry* 65, 662–670. <https://doi.org/10.1016/j.biopsych.2008.11.002>
- Crews, F.T., Lawrimore, C.J., Walter, T.J., Coleman, L.G., 2017. The role of neuroimmune signaling in alcoholism. *Neuropharmacology* 122, 56–73. <https://doi.org/10.1016/j.neuropharm.2017.01.031>
- Crews, F.T., Nixon, K., 2009. Mechanisms of neurodegeneration and regeneration in alcoholism. *Alcohol Alcohol. Oxf. Oxf.* 44, 115–127. <https://doi.org/10.1093/alcalc/agn079>
- Crews, F.T., Nixon, K., 2003. Alcohol, neural stem cells, and adult neurogenesis. *Alcohol Res. Health J. Natl. Inst. Alcohol Abuse Alcohol.* 27, 197–204.
- Cullen, C.L., Senesi, M., Tang, A.D., Clutterbuck, M.T., Auderset, L., O'Rourke, M.E., Rodger, J., Young, K.M., 2019. Low-intensity transcranial magnetic stimulation promotes the survival and maturation of newborn oligodendrocytes in the adult mouse brain. *Glia* 67, 1462–1477. <https://doi.org/10.1002/glia.23620>
- Cullen, C.L., Young, K.M., 2016. How Does Transcranial Magnetic Stimulation Influence Glial Cells in the Central Nervous System? *Front. Neural Circuits* 10. <https://doi.org/10.3389/fncir.2016.00026>
- Darbinian, N., Darbinyan, A., Merabova, N., Bajwa, A., Tatevosian, G., Martirosyan, D., Zhao, H., Selzer, M.E., Goetzl, L., 2021. Ethanol-mediated alterations in oligodendrocyte differentiation in the developing brain. *Neurobiol. Dis.* 148, 105181. <https://doi.org/10.1016/j.nbd.2020.105181>
- Daviet, R., Aydogan, G., Jagannathan, K., Spilka, N., Koellinger, P.D., Kranzler, H.R., Nave, G., Wetherill, R.R., 2022. Associations between alcohol consumption and gray and white matter volumes in the UK Biobank. *Nat. Commun.* 13, 1175. <https://doi.org/10.1038/s41467-022-28735-5>
- De Chaumont, F., Dallongeville, S., Chenouard, N., Hervé, N., Pop, S., Provoost, T., Meas-Yedid, V., Pankajakshan, P., Lecomte, T., Le Montagner, Y., Lagache, T., Dufour, A., Olivo-Marin, J.-C., 2012. Icy: an open bioimage informatics platform for extended reproducible research. *Nat. Methods* 9, 690–696. <https://doi.org/10.1038/nmeth.2075>
- De Santis, S., Bach, P., Pérez-Cervera, L., Cosa-Linan, A., Weil, G., Vollstädt-Klein, S., Hermann, D., Kiefer, F., Kirsch, P., Ciccocioppo, R., Sommer, W.H., Canals, S., 2019. Microstructural White Matter Alterations in Men With Alcohol Use Disorder and Rats With Excessive Alcohol Consumption During Early Abstinence. *JAMA Psychiatry* 76, 749. <https://doi.org/10.1001/jamapsychiatry.2019.0318>
- De Santis, S., Cosa-Linan, A., Garcia-Hernandez, R., Dmytrenko, L., Vargova, L., Vorisek, I., Stopponi, S., Bach, P., Kirsch, P., Kiefer, F., Ciccocioppo, R., Sykova, E., Moratal, D., Sommer, W.H., Canals, S., 2020. Chronic alcohol consumption alters extracellular space geometry and transmitter diffusion in the brain. *Sci. Adv.* 6, eaba0154. <https://doi.org/10.1126/sciadv.aba0154>
- De Santis, S., Drakesmith, M., Bells, S., Assaf, Y., Jones, D.K., 2014. Why diffusion tensor MRI does well only some of the time: Variance and covariance of white matter tissue microstructure attributes in the living human brain. *NeuroImage* 89, 35–44. <https://doi.org/10.1016/j.neuroimage.2013.12.003>
- De Santis, S., Jones, D.K., Roebroek, A., 2016. Including diffusion time dependence in the extra-axonal space improves in vivo estimates of axonal diameter and density in human white matter. *NeuroImage* 130, 91–103. <https://doi.org/10.1016/j.neuroimage.2016.01.047>
- De Santis, S., Selim, M.K., Canals, S., 2023. Brain Microstructure in Alcohol Addiction: Characterization of Diffusion-Based MRI Biomarkers, Neuropathological Substrates, and Functional Consequences, in: Mueller, S., Heilig, M. (Eds.), *Alcohol and Alcohol-Related*

- Diseases. Springer International Publishing, Cham, pp. 493–508.
https://doi.org/10.1007/978-3-031-32483-3_27
- Dela Haije, T., Özarslan, E., Feragen, A., 2020. Enforcing necessary non-negativity constraints for common diffusion MRI models using sum of squares programming. *NeuroImage* 209, 116405. <https://doi.org/10.1016/j.neuroimage.2019.116405>
- Devlin, J.T., Watkins, K.E., 2007. Stimulating language: insights from TMS. *Brain J. Neurol.* 130, 610–622. <https://doi.org/10.1093/brain/awl331>
- Dimou, L., Gallo, V., 2015. NG2-glia and their functions in the central nervous system. *Glia* 63, 1429–1451. <https://doi.org/10.1002/glia.22859>
- Droutman, V., Read, S.J., Bechara, A., 2015. Revisiting the role of the insula in addiction. *Trends Cogn. Sci.* 19, 414–420. <https://doi.org/10.1016/j.tics.2015.05.005>
- Dubin, M., 2017. Imaging TMS: antidepressant mechanisms and treatment optimization. *Int. Rev. Psychiatry Abingdon Engl.* 29, 89–97. <https://doi.org/10.1080/09540261.2017.1283297>
- Economidou, D., Cippitelli, A., Stopponi, S., Braconi, S., Clementi, S., Ubaldi, M., Martin-Fardon, R., Weiss, F., Massi, M., Ciccocioppo, R., 2011. Activation of Brain NOP Receptors Attenuates Acute and Protracted Alcohol Withdrawal Symptoms in the Rat: N/OFFQ REDUCES ALCOHOL WITHDRAWAL SYMPTOMS IN RATS. *Alcohol. Clin. Exp. Res.* 35, 747–755.
<https://doi.org/10.1111/j.1530-0277.2010.01392.x>
- Economidou, D., Hansson, A.C., Weiss, F., Terasmaa, A., Sommer, W.H., Cippitelli, A., Fedeli, A., Martin-Fardon, R., Massi, M., Ciccocioppo, R., Heilig, M., 2008. Dysregulation of Nociceptin/Orphanin FQ Activity in the Amygdala Is Linked to Excessive Alcohol Drinking in the Rat. *Biol. Psychiatry* 64, 211–218. <https://doi.org/10.1016/j.biopsych.2008.02.004>
- Einstein, A., 1905. Über die von der molekularkinetischen Theorie der Wärme geforderte Bewegung von in ruhenden Flüssigkeiten suspendierten Teilchen. *Ann. Phys.* 322, 549–560.
<https://doi.org/10.1002/andp.19053220806>
- Engblom, D., Bilbao, A., Sanchis-Segura, C., Dahan, L., Perreau-Lenz, S., Balland, B., Parkitna, J.R., Luján, R., Halbout, B., Mameli, M., Parlato, R., Sprengel, R., Lüscher, C., Schütz, G., Spanagel, R., 2008. Glutamate Receptors on Dopamine Neurons Control the Persistence of Cocaine Seeking. *Neuron* 59, 497–508. <https://doi.org/10.1016/j.neuron.2008.07.010>
- Erickson, E.K., Grantham, E.K., Warden, A.S., Harris, R.A., 2019. Neuroimmune signaling in alcohol use disorder. *Pharmacol. Biochem. Behav.* 177, 34–60.
<https://doi.org/10.1016/j.pbb.2018.12.007>
- Esser, M.B., Pickens, C.M., Guy, G.P., Evans, M.E., 2021. Binge Drinking, Other Substance Use, and Concurrent Use in the U.S., 2016–2018. *Am. J. Prev. Med.* 60, 169–178.
<https://doi.org/10.1016/j.amepre.2020.08.025>
- Everitt, B.J., Belin, D., Economidou, D., Pelloux, Y., Dalley, J.W., Robbins, T.W., 2008. Review. Neural mechanisms underlying the vulnerability to develop compulsive drug-seeking habits and addiction. *Philos. Trans. R. Soc. Lond. B. Biol. Sci.* 363, 3125–3135.
<https://doi.org/10.1098/rstb.2008.0089>
- Fadnavis, S., Chowdhury, A., Batson, J., Drineas, P., Garyfallidis, E., 2022. Patch2Self denoising of Diffusion MRI with Self-Supervision and Matrix Sketching (preprint). *Neuroscience*.
<https://doi.org/10.1101/2022.03.15.484539>
- Fang, Z.-Y., Li, Z., Xiong, L., Huang, J., Huang, X.-L., 2010. Magnetic Stimulation Influences Injury-Induced Migration of White Matter Astrocytes. *Electromagn. Biol. Med.* 29, 113–121.
<https://doi.org/10.3109/15368378.2010.500568>
- Fede, S.J., Grodin, E.N., Dean, S.F., Diazgranados, N., Momenan, R., 2019. Resting state connectivity best predicts alcohol use severity in moderate to heavy alcohol users. *NeuroImage Clin.* 22, 101782. <https://doi.org/10.1016/j.nicl.2019.101782>
- Fields, R.D., 2015. A new mechanism of nervous system plasticity: activity-dependent myelination. *Nat. Rev. Neurosci.* 16, 756–767. <https://doi.org/10.1038/nrn4023>

- Fields, R.D., 2008. White matter in learning, cognition and psychiatric disorders. *Trends Neurosci.* 31, 361–370. <https://doi.org/10.1016/j.tins.2008.04.001>
- Fieremans, E., Jensen, J.H., Helpert, J.A., 2011. White matter characterization with diffusional kurtosis imaging. *NeuroImage* 58, 177–188. <https://doi.org/10.1016/j.neuroimage.2011.06.006>
- Filbey, F.M., Claus, E., Audette, A.R., Niculescu, M., Banich, M.T., Tanabe, J., Du, Y.P., Hutchison, K.E., 2008. Exposure to the taste of alcohol elicits activation of the mesocorticolimbic neurocircuitry. *Neuropsychopharmacol. Off. Publ. Am. Coll. Neuropsychopharmacol.* 33, 1391–1401. <https://doi.org/10.1038/sj.npp.1301513>
- Filippi, M., Bar-Or, A., Piehl, F., Preziosa, P., Solari, A., Vukusic, S., Rocca, M.A., 2018. Multiple sclerosis. *Nat. Rev. Dis. Primer* 4, 43. <https://doi.org/10.1038/s41572-018-0041-4>
- Filippi, M., Rocca, M.A., Ciccarelli, O., De Stefano, N., Evangelou, N., Kappos, L., Rovira, A., Sastre-Garriga, J., Tintorè, M., Frederiksen, J.L., Gasperini, C., Palace, J., Reich, D.S., Banwell, B., Montalban, X., Barkhof, F., MAGNIMS Study Group, 2016. MRI criteria for the diagnosis of multiple sclerosis: MAGNIMS consensus guidelines. *Lancet Neurol.* 15, 292–303. [https://doi.org/10.1016/S1474-4422\(15\)00393-2](https://doi.org/10.1016/S1474-4422(15)00393-2)
- Foster, A.Y., Bujalka, H., Emery, B., 2019. Axoglial interactions in myelin plasticity: Evaluating the relationship between neuronal activity and oligodendrocyte dynamics. *Glia* 67, 2038–2049. <https://doi.org/10.1002/glia.23629>
- Frahm, J., Merboldt, K.D., Hänicke, W., Haase, A., 1985. Stimulated echo imaging. *J. Magn. Reson.* 1969 64, 81–93. [https://doi.org/10.1016/0022-2364\(85\)90033-2](https://doi.org/10.1016/0022-2364(85)90033-2)
- French, H.M., Reid, M., Mamontov, P., Simmons, R.A., Grinspan, J.B., 2009. Oxidative stress disrupts oligodendrocyte maturation. *J. Neurosci. Res.* 87, 3076–3087. <https://doi.org/10.1002/jnr.22139>
- Frie, J.A., Khokhar, J.Y., 2024. FARESHARE: An open-source apparatus for assessing drinking microstructure in socially housed rats. *NPP—Digital Psychiatry Neurosci.* 2, 1. <https://doi.org/10.1038/s44277-024-00002-z>
- Fünfschilling, U., Supplie, L.M., Mahad, D., Boretius, S., Saab, A.S., Edgar, J., Brinkmann, B.G., Kassmann, C.M., Tzvetanova, I.D., Möbius, W., Diaz, F., Meijer, D., Suter, U., Hamprecht, B., Sereda, M.W., Moraes, C.T., Frahm, J., Goebbels, S., Nave, K.-A., 2012. Glycolytic oligodendrocytes maintain myelin and long-term axonal integrity. *Nature* 485, 517–521. <https://doi.org/10.1038/nature11007>
- Gafson, A.R., Barthélemy, N.R., Bomont, P., Carare, R.O., Durham, H.D., Julien, J.-P., Kuhle, J., Leppert, D., Nixon, R.A., Weller, R.O., Zetterberg, H., Matthews, P.M., 2020. Neurofilaments: neurobiological foundations for biomarker applications. *Brain J. Neurol.* 143, 1975–1998. <https://doi.org/10.1093/brain/awaa098>
- Garcia-Hernandez, R., Cerdán Cerdá, A., Trouve Carpena, A., Drakesmith, M., Koller, K., Jones, D.K., Canals, S., De Santis, S., 2022. Mapping microglia and astrocyte activation in vivo using diffusion MRI. *Sci. Adv.* 8, eabq2923. <https://doi.org/10.1126/sciadv.abq2923>
- Garyfallidis, E., Brett, M., Amirbekian, B., Rokem, A., Van Der Walt, S., Descoteaux, M., Nimmo-Smith, I., Dipy Contributors, 2014. Dipy, a library for the analysis of diffusion MRI data. *Front. Neuroinformatics* 8. <https://doi.org/10.3389/fninf.2014.00008>
- George, A., Kuzniecky, R., Rusinek, H., Pardoe, H.R., Human Epilepsy Project Investigators, 2020. Standardized Brain MRI Acquisition Protocols Improve Statistical Power in Multicenter Quantitative Morphometry Studies. *J. Neuroimaging Off. J. Am. Soc. Neuroimaging* 30, 126–133. <https://doi.org/10.1111/jon.12673>
- Gibson, E.M., Purger, D., Mount, C.W., Goldstein, A.K., Lin, G.L., Wood, L.S., Inema, I., Miller, S.E., Bieri, G., Zuchero, J.B., Barres, B.A., Woo, P.J., Vogel, H., Monje, M., 2014. Neuronal Activity Promotes Oligodendrogenesis and Adaptive Myelination in the Mammalian Brain. *Science* 344, 1252304. <https://doi.org/10.1126/science.1252304>

- Gil-Mohapel, J., Bianco, C.D., Cesconetto, P.A., Zamoner, A., Brocardo, P.S., 2019. Ethanol Exposure During Development, and Brain Oxidative Stress, in: *Neuroscience of Alcohol*. Elsevier, pp. 493–503. <https://doi.org/10.1016/B978-0-12-813125-1.00051-9>
- Goldstein, R.Z., Volkow, N.D., 2011. Dysfunction of the prefrontal cortex in addiction: neuroimaging findings and clinical implications. *Nat. Rev. Neurosci.* 12, 652–669. <https://doi.org/10.1038/nrn3119>
- Gonzales, R.A., Job, M.O., Doyon, W.M., 2004. The role of mesolimbic dopamine in the development and maintenance of ethanol reinforcement. *Pharmacol. Ther.* 103, 121–146. <https://doi.org/10.1016/j.pharmthera.2004.06.002>
- Gordon, P.C., Belardinelli, P., Stenroos, M., Ziemann, U., Zrenner, C., 2022. Prefrontal theta phase-dependent rTMS-induced plasticity of cortical and behavioral responses in human cortex. *Brain Stimulat.* 15, 391–402. <https://doi.org/10.1016/j.brs.2022.02.006>
- Gorelick, D.A., Zangen, A., George, M.S., 2014. Transcranial magnetic stimulation in the treatment of substance addiction: TMS as addiction treatment. *Ann. N. Y. Acad. Sci.* n/a-n/a. <https://doi.org/10.1111/nyas.12479>
- Gorgolewski, K., Burns, C.D., Madison, C., Clark, D., Halchenko, Y.O., Waskom, M.L., Ghosh, S.S., 2011. Nipype: A Flexible, Lightweight and Extensible Neuroimaging Data Processing Framework in Python. *Front. Neuroinformatics* 5. <https://doi.org/10.3389/fninf.2011.00013>
- Grant, K.A., Stafford, J., Thiede, A., Kiley, C., Odagiri, M., Ferguson, B., 2008. Who is at risk? Population characterization of alcohol self-administration in nonhuman primates helps identify pathways to dependence. *Alcohol Res. Health J. Natl. Inst. Alcohol Abuse Alcohol.* 31, 289–297.
- Grodin, E.N., Ray, L.A., 2019. The Use of Functional Magnetic Resonance Imaging to Test Pharmacotherapies for Alcohol Use Disorder: A Systematic Review. *Alcohol. Clin. Exp. Res.* 43, 2038–2056. <https://doi.org/10.1111/acer.14167>
- Guo, F., Zhang, Y.-F., Liu, K., Huang, X., Li, R.-X., Wang, S.-Y., Wang, F., Xiao, L., Mei, F., Li, T., 2021. Chronic Exposure to Alcohol Inhibits New Myelin Generation in Adult Mouse Brain. *Front. Cell. Neurosci.* 15, 732602. <https://doi.org/10.3389/fncel.2021.732602>
- Guo, F., Zheng, K., Benedé-Ubieto, R., Cubero, F.J., Nevzorova, Y.A., 2018. The Lieber-DeCarli Diet-A Flagship Model for Experimental Alcoholic Liver Disease. *Alcohol. Clin. Exp. Res.* 42, 1828–1840. <https://doi.org/10.1111/acer.13840>
- Gusnard, D.A., Raichle, M.E., 2001. Searching for a baseline: Functional imaging and the resting human brain. *Nat. Rev. Neurosci.* 2, 685–694. <https://doi.org/10.1038/35094500>
- Halassa, M.M., Kastner, S., 2017. Thalamic functions in distributed cognitive control. *Nat. Neurosci.* 20, 1669–1679. <https://doi.org/10.1038/s41593-017-0020-1>
- Hanlon, C.A., Dowdle, L.T., Austelle, C.W., DeVries, W., Mithoefer, O., Badran, B.W., George, M.S., 2015. What goes up, can come down: Novel brain stimulation paradigms may attenuate craving and craving-related neural circuitry in substance dependent individuals. *Brain Res.* 1628, 199–209. <https://doi.org/10.1016/j.brainres.2015.02.053>
- Haorah, J., Ramirez, S.H., Floreani, N., Gorantla, S., Morsey, B., Persidsky, Y., 2008. Mechanism of alcohol-induced oxidative stress and neuronal injury. *Free Radic. Biol. Med.* 45, 1542–1550. <https://doi.org/10.1016/j.freeradbiomed.2008.08.030>
- Haralick, R.M., Shanmugam, K., Dinstein, I., 1973. Textural Features for Image Classification. *IEEE Trans. Syst. Man Cybern.* SMC-3, 610–621. <https://doi.org/10.1109/TSMC.1973.4309314>
- Harel, M., Perini, I., Kämpe, R., Alyagon, U., Shalev, H., Besser, I., Sommer, W.H., Heilig, M., Zangen, A., 2022. Repetitive Transcranial Magnetic Stimulation in Alcohol Dependence: A Randomized, Double-Blind, Sham-Controlled Proof-of-Concept Trial Targeting the Medial Prefrontal and Anterior Cingulate Cortices. *Biol. Psychiatry* 91, 1061–1069. <https://doi.org/10.1016/j.biopsych.2021.11.020>
- Harmelech, T., Roth, Y., Tendler, A., 2021. Deep TMS H7 Coil: Features, Applications & Future. *Expert Rev. Med. Devices* 18, 1133–1144. <https://doi.org/10.1080/17434440.2021.2013803>

- Harris, G.J., Jaffin, S.K., Hodge, S.M., Kennedy, D., Caviness, V.S., Marinkovic, K., Papadimitriou, G.M., Makris, N., Oscar-Berman, M., 2008. Frontal White Matter and Cingulum Diffusion Tensor Imaging Deficits in Alcoholism. *Alcohol. Clin. Exp. Res.* 32, 1001–1013. <https://doi.org/10.1111/j.1530-0277.2008.00661.x>
- Herberthson, M., Boito, D., Haije, T.D., Feragen, A., Westin, C.-F., Özarlan, E., 2021. Q-space trajectory imaging with positivity constraints (QTI+). *NeuroImage* 238, 118198. <https://doi.org/10.1016/j.neuroimage.2021.118198>
- Hermann, D., Weber-Fahr, W., Sartorius, A., Hoerst, M., Frischknecht, U., Tunc-Skarka, N., Perreaulenz, S., Hansson, A.C., Krumm, B., Kiefer, F., Spanagel, R., Mann, K., Ende, G., Sommer, W.H., 2012. Translational magnetic resonance spectroscopy reveals excessive central glutamate levels during alcohol withdrawal in humans and rats. *Biol. Psychiatry* 71, 1015–1021. <https://doi.org/10.1016/j.biopsych.2011.07.034>
- Hildebrand, C., Hahn, R., 1978. Relation between myelin sheath thickness and axon size in spinal cord white matter of some vertebrate species. *J. Neurol. Sci.* 38, 421–434. [https://doi.org/10.1016/0022-510X\(78\)90147-8](https://doi.org/10.1016/0022-510X(78)90147-8)
- Hoch, M.J., Bruno, M., Pacione, D., Lui, Y.W., Fieremans, E., Shepherd, T.M., 2021. Simultaneous Multislice for Accelerating Diffusion MRI in Clinical Neuroradiology Protocols. *AJNR Am. J. Neuroradiol.* 42, 1437–1443. <https://doi.org/10.3174/ajnr.A7140>
- Hohenfeld, C., Werner, C.J., Reetz, K., 2018. Resting-state connectivity in neurodegenerative disorders: Is there potential for an imaging biomarker? *NeuroImage Clin.* 18, 849–870. <https://doi.org/10.1016/j.nicl.2018.03.013>
- Hong, Y., Liu, Q., Peng, M., Bai, M., Li, J., Sun, R., Guo, H., Xu, P., Xie, Y., Li, Y., Liu, L., Du, J., Liu, X., Yang, B., Xu, G., 2020. High-frequency repetitive transcranial magnetic stimulation improves functional recovery by inhibiting neurotoxic polarization of astrocytes in ischemic rats. *J. Neuroinflammation* 17, 150. <https://doi.org/10.1186/s12974-020-01747-y>
- Hoogendam, J.M., Ramakers, G.M.J., Di Lazzaro, V., 2010. Physiology of repetitive transcranial magnetic stimulation of the human brain. *Brain Stimulat.* 3, 95–118. <https://doi.org/10.1016/j.brs.2009.10.005>
- Höppner, J., Broese, T., Wendler, L., Berger, C., Thome, J., 2011. Repetitive transcranial magnetic stimulation (rTMS) for treatment of alcohol dependence. *World J. Biol. Psychiatry* 12, 57–62. <https://doi.org/10.3109/15622975.2011.598383>
- Hoyer, E.H., Celnik, P.A., 2011. Understanding and enhancing motor recovery after stroke using transcranial magnetic stimulation. *Restor. Neurol. Neurosci.* 29, 395–409. <https://doi.org/10.3233/RNN-2011-0611>
- Huang, C., Titus, J.A., Bell, R.L., Kapros, T., Chen, J., Huang, R., 2012. A mouse model for adolescent alcohol abuse: stunted growth and effects in brain. *Alcohol. Clin. Exp. Res.* 36, 1728–1737. <https://doi.org/10.1111/j.1530-0277.2012.01759.x>
- Huang, Y.-Z., Edwards, M.J., Rounis, E., Bhatia, K.P., Rothwell, J.C., 2005. Theta burst stimulation of the human motor cortex. *Neuron* 45, 201–206. <https://doi.org/10.1016/j.neuron.2004.12.033>
- Huettel, S.A., Song, A.W., McCarthy, G., 2014. *Functional magnetic resonance imaging, Third edition.* ed. Sinauer Associates, Inc., Publishers, Sunderland, Massachusetts, U.S.A.
- Hughes, E.G., Kang, S.H., Fukaya, M., Bergles, D.E., 2013. Oligodendrocyte progenitors balance growth with self-repulsion to achieve homeostasis in the adult brain. *Nat. Neurosci.* 16, 668–676. <https://doi.org/10.1038/nn.3390>
- Huynh, N., Arabian, N.M., Asatryan, L., Davies, D.L., 2019. Murine Drinking Models in the Development of Pharmacotherapies for Alcoholism: Drinking in the Dark and Two-bottle Choice. *J. Vis. Exp. JoVE.* <https://doi.org/10.3791/57027>
- Hyde, J., Carr, H., Kelley, N., Seneviratne, R., Reed, C., Parlatini, V., Garner, M., Solmi, M., Rosson, S., Cortese, S., Brandt, V., 2022. Efficacy of neurostimulation across mental disorders: systematic review and meta-analysis of 208 randomized controlled trials. *Mol. Psychiatry* 27, 2709–2719. <https://doi.org/10.1038/s41380-022-01524-8>

- Hyman, S.E., 2005. Addiction: a disease of learning and memory. *Am. J. Psychiatry* 162, 1414–1422. <https://doi.org/10.1176/appi.ajp.162.8.1414>
- Im, P.K., Wright, N., Yang, L., Chan, K.H., Chen, Y., Guo, Y., Du, H., Yang, X., Avery, D., Wang, Shaojie, Yu, C., Lv, J., Clarke, R., Chen, Junshi, Collins, R., Walters, R.G., Peto, R., Li, L., Chen, Z., Millwood, I.Y., China Kadoorie Biobank Collaborative Group, Wang, Chen, Barnard, M., Bennett, D., Boxall, R., Clarke, J., Mohamed, A.E., Fry, H., Gilbert, S., Iona, A., Kakkoura, M., Kartsonaki, C., Lam, H., Lin, K., Liu, James, Mazidi, M., Morris, S., Nie, Q., Pozarickij, A., Ryder, P., Said, S., Schmidt, D., Stevens, B., Turnbull, I., Wang, B., Wang, L., Yao, P., Han, X., Hou, C., Xia, Q., Liu, C., Pei, P., Sun, D., Chen, Naying, Liu, D., Tang, Z., Chen, Ningyu, Jiang, Q., Lan, J., Li, M., Liu, Yun, Meng, F., Meng, J., Pan, R., Qin, Y., Wang, P., Wang, Sisi, Wei, L., Zhou, L., Dong, C., Ge, P., Ren, X., Li, Z., Mao, E., Wang, T., Zhang, Hui, Zhang, Xi, Chen, Jinyan, Hu, X., Wang, X., Guo, Zhendong, Li, H., Li, Yilei, Weng, M., Wu, S., Yan, S., Zou, M., Zhou, X., Guo, Ziyang, Kang, Q., Li, Yanjie, Yu, B., Xu, Qinai, Chang, L., Fan, L., Feng, S., Zhang, D., Zhou, G., Gao, Y., He, T., He, P., Hu, C., Sun, H., Zhang, Xukui, Chen, B., Fu, Z., Huang, Y., Liu, H., Xu, Qiaohua, Yin, L., Long, H., Xu, X., Zhang, Hao, Zhang, L., Su, J., Tao, R., Wu, M., Yang, J., Zhou, J., Zhou, Y., Hu, Y., Hua, Y., Jin, J., Liu, F., Liu, Jingchao, Lu, Y., Ma, L., Tang, A., Zhang, J., Cheng, L., Du, R., Gao, R., Li, F., Li, S., Liu, Yongmei, Ning, F., Pang, Z., Sun, X., Tian, X., Zhai, Y., Zhang, Hua, Hou, W., Lv, S., Wang, J., Chen, X., Wu, X., Zhang, N., Chang, X., Chen, X., Li, J., Liu, Jiaqiu, Luo, G., Sun, Q., Zhong, X., Gong, W., Hu, R., Wang, H., Wang, M., Yu, M., Chen, L., Gu, Q., Pan, D., Wang, Chunmei, Xie, K., Zhang, Xiaoyi, 2023. Alcohol consumption and risks of more than 200 diseases in Chinese men. *Nat. Med.* 29, 1476–1486. <https://doi.org/10.1038/s41591-023-02383-8>
- Jamali, M., Grannan, B.L., Fedorenko, E., Saxe, R., Báez-Mendoza, R., Williams, Z.M., 2021. Single-neuronal predictions of others' beliefs in humans. *Nature* 591, 610–614. <https://doi.org/10.1038/s41586-021-03184-0>
- Jannati, A., Oberman, L.M., Rotenberg, A., Pascual-Leone, A., 2023. Assessing the mechanisms of brain plasticity by transcranial magnetic stimulation. *Neuropsychopharmacology* 48, 191–208. <https://doi.org/10.1038/s41386-022-01453-8>
- Javitt, D.C., Schoepp, D., Kalivas, P.W., Volkow, N.D., Zarate, C., Merchant, K., Bear, M.F., Umbricht, D., Hajos, M., Potter, W.Z., Lee, C.-M., 2011. Translating Glutamate: From Pathophysiology to Treatment. *Sci. Transl. Med.* 3. <https://doi.org/10.1126/scitranslmed.3002804>
- Jelescu, I.O., Grussu, F., Ianus, A., Hansen, B., Barrett, R.L.C., Aggarwal, M., Michielse, S., Nasrallah, F., Syeda, W., Wang, N., Veraart, J., Roebroek, A., Bagdasarian, A.F., Eichner, C., Sepehrband, F., Zimmermann, J., Soustelle, L., Bowman, C., Tendler, B.C., Hertanu, A., Jeurissen, B., Verhoye, M., Frydman, L., van de Looij, Y., Hike, D., Dunn, J.F., Miller, K., Landman, B.A., Shemesh, N., Anderson, A., McKinnon, E., Farquharson, S., Acqua, F.D., Pierpaoli, C., Drobnjak, I., Leemans, A., Harkins, K.D., Descoteaux, M., Xu, D., Huang, H., Santin, M.D., Grant, S.C., Obenaus, A., Kim, G.S., Wu, D., Bihan, D.L., Blackband, S.J., Ciobanu, L., Fieremans, E., Bai, R., Leergaard, T., Zhang, J., Dyrby, T.B., Johnson, G.A., Cohen-Adad, J., Budde, M.D., Schilling, K.G., 2022. Recommendations and guidelines from the ISMRM Diffusion Study Group for preclinical diffusion MRI: Part 1 -- In vivo small-animal imaging. <https://doi.org/10.48550/ARXIV.2209.12994>
- Jenkinson, M., Beckmann, C.F., Behrens, T.E.J., Woolrich, M.W., Smith, S.M., 2012. FSL. *NeuroImage* 62, 782–790. <https://doi.org/10.1016/j.neuroimage.2011.09.015>
- Johansen-Berg, H., Behrens, T.E.J., 2014. Diffusion MRI: from quantitative measurement to in-vivo neuroanatomy, 2nd ed. ed. Elsevier Science, Amsterdam.
- Jones, D.K., Basser, P.J., 2004. ?Squashing peanuts and smashing pumpkins?: How noise distorts diffusion-weighted MR data. *Magn. Reson. Med.* 52, 979–993. <https://doi.org/10.1002/mrm.20283>

- Jones, D.K., Knösche, T.R., Turner, R., 2013. White matter integrity, fiber count, and other fallacies: The do's and don'ts of diffusion MRI. *NeuroImage* 73, 239–254. <https://doi.org/10.1016/j.neuroimage.2012.06.081>
- Joutsa, J., Moussawi, K., Siddiqi, S.H., Abdolahi, A., Drew, W., Cohen, A.L., Ross, T.J., Deshpande, H.U., Wang, H.Z., Bruss, J., Stein, E.A., Volkow, N.D., Grafman, J.H., van Wijngaarden, E., Boes, A.D., Fox, M.D., 2022. Brain lesions disrupting addiction map to a common human brain circuit. *Nat. Med.* 28, 1249–1255. <https://doi.org/10.1038/s41591-022-01834-y>
- Kähkönen, S., Wilenius, J., Nikulin, V.V., Ollikainen, M., Ilmoniemi, R.J., 2003. Alcohol Reduces Prefrontal Cortical Excitability in Humans: A Combined TMS and EEG Study. *Neuropsychopharmacology* 28, 747–754. <https://doi.org/10.1038/sj.npp.1300099>
- Kato, D., Wake, H., 2019. Activity-Dependent Myelination. *Adv. Exp. Med. Biol.* 1190, 43–51. https://doi.org/10.1007/978-981-32-9636-7_4
- Kim, J.Y., Choi, G.-S., Cho, Y.-W., Cho, H., Hwang, S.-J., Ahn, S.-H., 2013. Attenuation of Spinal Cord Injury-Induced Astroglial and Microglial Activation by Repetitive Transcranial Magnetic Stimulation in Rats. *J. Korean Med. Sci.* 28, 295. <https://doi.org/10.3346/jkms.2013.28.2.295>
- Kister, A., Kister, I., 2023. Overview of myelin, major myelin lipids, and myelin-associated proteins. *Front. Chem.* 10, 1041961. <https://doi.org/10.3389/fchem.2022.1041961>
- Klein, A., Andersson, J., Ardekani, B.A., Ashburner, J., Avants, B., Chiang, M.-C., Christensen, G.E., Collins, D.L., Gee, J., Hellier, P., Song, J.H., Jenkinson, M., Lepage, C., Rueckert, D., Thompson, P., Vercauteren, T., Woods, R.P., Mann, J.J., Parsey, R.V., 2009. Evaluation of 14 nonlinear deformation algorithms applied to human brain MRI registration. *NeuroImage* 46, 786–802. <https://doi.org/10.1016/j.neuroimage.2008.12.037>
- Klenowski, P.M., 2018. Emerging role for the medial prefrontal cortex in alcohol-seeking behaviors. *Addict. Behav.* 77, 102–106. <https://doi.org/10.1016/j.addbeh.2017.09.024>
- Kohno, M., Dennis, L.E., McCready, H., Hoffman, W.F., 2017. Executive Control and Striatal Resting-State Network Interact with Risk Factors to Influence Treatment Outcomes in Alcohol-Use Disorder. *Front. Psychiatry* 8, 182. <https://doi.org/10.3389/fpsy.2017.00182>
- Konovalov, A., Hill, C., Daunizeau, J., Ruff, C.C., 2021. Dissecting functional contributions of the social brain to strategic behavior. *Neuron* 109, 3323–3337.e5. <https://doi.org/10.1016/j.neuron.2021.07.025>
- Koob, G.F., 2009. Neurobiological substrates for the dark side of compulsivity in addiction. *Neuropharmacology* 56 Suppl 1, 18–31. <https://doi.org/10.1016/j.neuropharm.2008.07.043>
- Koob, G.F., Arends, M.A., Le Moal, M., 2014. *Drugs, addiction, and the brain*. Elsevier/AP, Academic Press is an imprint of Elsevier, Amsterdam ; Boston.
- Koob, G.F., Volkow, N.D., 2010. Neurocircuitry of Addiction. *Neuropsychopharmacology* 35, 217–238. <https://doi.org/10.1038/npp.2009.110>
- Koob, G.F., Zimmer, A., 2012. Animal models of psychiatric disorders, in: *Handbook of Clinical Neurology*. Elsevier, pp. 137–166. <https://doi.org/10.1016/B978-0-444-52002-9.00009-7>
- Kubicki, M., Westin, C.-F., McCarley, R.W., Shenton, M.E., 2005. The application of DTI to investigate white matter abnormalities in schizophrenia. *Ann. N. Y. Acad. Sci.* 1064, 134–148. <https://doi.org/10.1196/annals.1340.024>
- Kukley, M., Capetillo-Zarate, E., Dietrich, D., 2007. Vesicular glutamate release from axons in white matter. *Nat. Neurosci.* 10, 311–320. <https://doi.org/10.1038/nn1850>
- Laramee, P., Kusel, J., Leonard, S., Aubin, H.-J., Francois, C., Daepfen, J.-B., 2013. The Economic Burden of Alcohol Dependence in Europe. *Alcohol Alcohol* 48, 259–269. <https://doi.org/10.1093/alcalc/agt004>
- Le, T.M., Wang, W., Zhornitsky, S., Dhingra, I., Chen, Y., Zhang, S., Li, C.-S.R., 2021. The Neural Processes Interlinking Social Isolation, Social Support, and Problem Alcohol Use. *Int. J. Neuropsychopharmacol.* 24, 333–343. <https://doi.org/10.1093/ijnp/pyaa086>
- Lee, Y., Morrison, B.M., Li, Y., Lengacher, S., Farah, M.H., Hoffman, P.N., Liu, Y., Tsingalia, A., Jin, L., Zhang, P.-W., Pellerin, L., Magistretti, P.J., Rothstein, J.D., 2012. Oligodendroglia metabolically

- support axons and contribute to neurodegeneration. *Nature* 487, 443–448.
<https://doi.org/10.1038/nature11314>
- Lefaucheur, J.-P., Aleman, A., Baeken, C., Benninger, D.H., Brunelin, J., Di Lazzaro, V., Filipović, S.R., Grefkes, C., Hasan, A., Hummel, F.C., Jääskeläinen, S.K., Langguth, B., Leocani, L., Londero, A., Nardone, R., Nguyen, J.-P., Nyffeler, T., Oliveira-Maia, A.J., Oliviero, A., Padberg, F., Palm, U., Paulus, W., Poulet, E., Quartarone, A., Rachid, F., Rektorová, I., Rossi, S., Sahlsten, H., Schecklmann, M., Szekely, D., Ziemann, U., 2020. Evidence-based guidelines on the therapeutic use of repetitive transcranial magnetic stimulation (rTMS): An update (2014–2018). *Clin. Neurophysiol. Off. J. Int. Fed. Clin. Neurophysiol.* 131, 474–528.
<https://doi.org/10.1016/j.clinph.2019.11.002>
- Li, L., Velumian, A.A., Samoilova, M., Fehlings, M.G., 2016. A Novel Approach for Studying the Physiology and Pathophysiology of Myelinated and Non-Myelinated Axons in the CNS White Matter. *PLOS ONE* 11, e0165637. <https://doi.org/10.1371/journal.pone.0165637>
- Li, L., Yu, H., Liu, Y., Meng, Y.-J., Li, X.-J., Zhang, C., Liang, S., Li, M.-L., Guo, W., QiangWang, null, Deng, W., Ma, X., Coid, J., Li, T., 2021. Lower regional grey matter in alcohol use disorders: evidence from a voxel-based meta-analysis. *BMC Psychiatry* 21, 247. <https://doi.org/10.1186/s12888-021-03244-9>
- Lipton, M.L., 2008. *Totally accessible MRI: a user's guide to principles, technology, and applications.* Springer, New York ; London.
- Litten, R.Z., Egli, M., Heilig, M., Cui, C., Fertig, J.B., Ryan, M.L., Falk, D.E., Moss, H., Huebner, R., Noronha, A., 2012. Medications development to treat alcohol dependence: a vision for the next decade. *Addict. Biol.* 17, 513–527. <https://doi.org/10.1111/j.1369-1600.2012.00454.x>
- Logothetis, N.K., Pauls, J., Augath, M., Trinath, T., Oeltermann, A., 2001. Neurophysiological investigation of the basis of the fMRI signal. *Nature* 412, 150–157.
<https://doi.org/10.1038/35084005>
- Lopes, R., Betrouni, N., 2009. Fractal and multifractal analysis: A review. *Med. Image Anal.* 13, 634–649. <https://doi.org/10.1016/j.media.2009.05.003>
- Love, S., 2006. Demyelinating diseases. *J. Clin. Pathol.* 59, 1151–1159.
<https://doi.org/10.1136/jcp.2005.031195>
- Luchicchi, A., Hart, B., Frigerio, I., van Dam, A.-M., Perna, L., Offerhaus, H.L., Stys, P.K., Schenk, G.J., Geurts, J.J.G., 2021. Axon-Myelin Unit Blistering as Early Event in MS Normal Appearing White Matter. *Ann. Neurol.* 89, 711–725. <https://doi.org/10.1002/ana.26014>
- Madsen, P.M., Desu, H.L., de Rivero Vaccari, J.P., Florimon, Y., Ellman, D.G., Keane, R.W., Clausen, B.H., Lambertsen, K.L., Brambilla, R., 2020. Oligodendrocytes modulate the immune-inflammatory response in EAE via TNFR2 signaling. *Brain. Behav. Immun.* 84, 132–146.
<https://doi.org/10.1016/j.bbi.2019.11.017>
- Malathesh, B.C., Kumar, C.N., Kandasamy, A., Moirangthem, S., Math, S.B., Murthy, P., 2021. Legal, Social, and Occupational Problems in Persons with Alcohol Use Disorder: An Exploratory Study. *Indian J. Psychol. Med.* 43, 234–240. <https://doi.org/10.1177/0253717620956466>
- Marchant, N.J., McDonald, A.J., Matsuzaki, R., Van Mourik, Y., Schetters, D., De Vries, T.J., 2023. Rats choose alcohol over social reward in an operant choice procedure. *Neuropsychopharmacology* 48, 585–593. <https://doi.org/10.1038/s41386-022-01447-6>
- Marek, S., Tervo-Clemmens, B., Calabro, F.J., Montez, D.F., Kay, B.P., Hatoum, A.S., Donohue, M.R., Foran, W., Miller, R.L., Hendrickson, T.J., Malone, S.M., Kandala, S., Feczko, E., Miranda-Dominguez, O., Graham, A.M., Earl, E.A., Perrone, A.J., Cordova, M., Doyle, O., Moore, L.A., Conan, G.M., Uriarte, J., Snider, K., Lynch, B.J., Wilgenbusch, J.C., Pengo, T., Tam, A., Chen, J., Newbold, D.J., Zheng, A., Seider, N.A., Van, A.N., Metoki, A., Chauvin, R.J., Laumann, T.O., Greene, D.J., Petersen, S.E., Garavan, H., Thompson, W.K., Nichols, T.E., Yeo, B.T.T., Barch, D.M., Luna, B., Fair, D.A., Dosenbach, N.U.F., 2022. Reproducible brain-wide association studies require thousands of individuals. *Nature* 603, 654–660.
<https://doi.org/10.1038/s41586-022-04492-9>

- Marinkovic, K., Rickenbacher, E., Azma, S., Artsy, E., 2012. Acute alcohol intoxication impairs top-down regulation of Stroop incongruity as revealed by blood oxygen level-dependent functional magnetic resonance imaging. *Hum. Brain Mapp.* 33, 319–333. <https://doi.org/10.1002/hbm.21213>
- Martínez-Tazo, P., Santos, A., Selim, M.K., Espinós-Soler, E., De Santis, S., 2024. Sex matters: The MouseX DW-ALLEN Atlas for mice diffusion-weighted MR imaging. *NeuroImage* 292, 120573. <https://doi.org/10.1016/j.neuroimage.2024.120573>
- Martinsen, V., Kursula, P., 2022. Multiple sclerosis and myelin basic protein: insights into protein disorder and disease. *Amino Acids* 54, 99–109. <https://doi.org/10.1007/s00726-021-03111-7>
- Marx, M., Pauly, K.B., Chang, C., 2013. A novel approach for global noise reduction in resting-state fMRI: APPLECOR. *NeuroImage* 64, 19–31. <https://doi.org/10.1016/j.neuroimage.2012.09.040>
- McClintock, S.M., Reti, I.M., Carpenter, L.L., McDonald, W.M., Dubin, M., Taylor, S.F., Cook, I.A., O’Reardon, J., Husain, M.M., Wall, C., Krystal, A.D., Sampson, S.M., Morales, O., Nelson, B.G., Latoussakis, V., George, M.S., Lisanby, S.H., National Network of Depression Centers rTMS Task Group, American Psychiatric Association Council on Research Task Force on Novel Biomarkers and Treatments, 2018. Consensus Recommendations for the Clinical Application of Repetitive Transcranial Magnetic Stimulation (rTMS) in the Treatment of Depression. *J. Clin. Psychiatry* 79, 16cs10905. <https://doi.org/10.4088/JCP.16cs10905>
- McDonald, K.R., Pearson, J.M., Huettel, S.A., 2020. Dorsolateral and dorsomedial prefrontal cortex track distinct properties of dynamic social behavior. *Soc. Cogn. Affect. Neurosci.* 15, 383–393. <https://doi.org/10.1093/scan/nsaa053>
- McFarland, K., Lapish, C.C., Kalivas, P.W., 2003. Prefrontal glutamate release into the core of the nucleus accumbens mediates cocaine-induced reinstatement of drug-seeking behavior. *J. Neurosci. Off. J. Soc. Neurosci.* 23, 3531–3537. <https://doi.org/10.1523/JNEUROSCI.23-08-03531.2003>
- McGovern, P.E., 2009. *Uncorking the past: the quest for wine, beer, and other alcoholic beverages.* University of California Press, Berkeley.
- McGovern, P.E., Mirzoian, A., Hall, G.R., 2009. Ancient Egyptian herbal wines. *Proc. Natl. Acad. Sci.* 106, 7361–7366. <https://doi.org/10.1073/pnas.0811578106>
- McGovern, P.E., Zhang, J., Tang, J., Zhang, Z., Hall, G.R., Moreau, R.A., Nuñez, A., Butrym, E.D., Richards, M.P., Wang, Chen-shan, Cheng, G., Zhao, Z., Wang, Changsui, 2004. Fermented beverages of pre- and proto-historic China. *Proc. Natl. Acad. Sci.* 101, 17593–17598. <https://doi.org/10.1073/pnas.0407921102>
- McKenzie, I.A., Ohayon, D., Li, H., de Faria, J.P., Emery, B., Tohyama, K., Richardson, W.D., 2014. Motor skill learning requires active central myelination. *Science* 346, 318–322. <https://doi.org/10.1126/science.1254960>
- Merrill, J.E., Benveniste, E.N., 1996. Cytokines in inflammatory brain lesions: helpful and harmful. *Trends Neurosci.* 19, 331–338. [https://doi.org/10.1016/0166-2236\(96\)10047-3](https://doi.org/10.1016/0166-2236(96)10047-3)
- Mishra, B.R., Nizamie, S.H., Das, B., Praharaj, S.K., 2010. Efficacy of repetitive transcranial magnetic stimulation in alcohol dependence: a sham-controlled study. *Addict. Abingdon Engl.* 105, 49–55. <https://doi.org/10.1111/j.1360-0443.2009.02777.x>
- Morez, J., Szczepankiewicz, F., Den Dekker, A.J., Vanhevel, F., Sijbers, J., Jeurissen, B., 2023. Optimal experimental design and estimation for q-space trajectory imaging. *Hum. Brain Mapp.* 44, 1793–1809. <https://doi.org/10.1002/hbm.26175>
- Mueller, S., Heilig, M. (Eds.), 2023. *Alcohol and alcohol-related diseases. Volume 2.* Springer Nature, Cham.
- Munyeshyaka, M., Fields, R.D., 2022. Oligodendroglia are emerging players in several forms of learning and memory. *Commun. Biol.* 5, 1148. <https://doi.org/10.1038/s42003-022-04116-y>
- Myrick, H., Anton, R.F., Li, X., Henderson, S., Drobles, D., Voronin, K., George, M.S., 2004. Differential brain activity in alcoholics and social drinkers to alcohol cues: relationship to craving.

- Neuropsychopharmacol. Off. Publ. Am. Coll. Neuropsychopharmacol. 29, 393–402.
<https://doi.org/10.1038/sj.npp.1300295>
- Naqvi, N.H., Bechara, A., 2009. The hidden island of addiction: the insula. *Trends Neurosci.* 32, 56–67. <https://doi.org/10.1016/j.tins.2008.09.009>
- Nardone, R., Höller, Y., Langthaler, P.B., Lochner, P., Golaszewski, S., Schwenker, K., Brigo, F., Trinka, E., 2017. rTMS of the prefrontal cortex has analgesic effects on neuropathic pain in subjects with spinal cord injury. *Spinal Cord* 55, 20–25. <https://doi.org/10.1038/sc.2016.87>
- Nasrabady, S.E., Rizvi, B., Goldman, J.E., Brickman, A.M., 2018. White matter changes in Alzheimer’s disease: a focus on myelin and oligodendrocytes. *Acta Neuropathol. Commun.* 6, 22. <https://doi.org/10.1186/s40478-018-0515-3>
- Nave, K.-A., 2010. Myelination and support of axonal integrity by glia. *Nature* 468, 244–252. <https://doi.org/10.1038/nature09614>
- Nave, K.-A., Werner, H.B., 2014. Myelination of the nervous system: mechanisms and functions. *Annu. Rev. Cell Dev. Biol.* 30, 503–533. <https://doi.org/10.1146/annurev-cellbio-100913-013101>
- Neumann, P.A., Wang, Yicun, Yan, Y., Wang, Yao, Ishikawa, M., Cui, R., Huang, Y.H., Sesack, S.R., Schlüter, O.M., Dong, Y., 2016. Cocaine-Induced Synaptic Alterations in Thalamus to Nucleus Accumbens Projection. *Neuropsychopharmacology* 41, 2399–2410. <https://doi.org/10.1038/npp.2016.52>
- Nimsky, C., Ganslandt, O., Hastreiter, P., Wang, R., Benner, T., Sorensen, A.G., Fahlbusch, R., 2005. Preoperative and intraoperative diffusion tensor imaging-based fiber tracking in glioma surgery. *Neurosurgery* 56, 130–137; discussion 138. <https://doi.org/10.1227/01.neu.0000144842.18771.30>
- Novikov, D.S., Fieremans, E., Jespersen, S.N., Kiselev, V.G., 2019. Quantifying brain microstructure with diffusion MRI: Theory and parameter estimation. *NMR Biomed.* 32, e3998. <https://doi.org/10.1002/nbm.3998>
- Novikov, D.S., Veraart, J., Jelescu, I.O., Fieremans, E., 2018. Rotationally-invariant mapping of scalar and orientational metrics of neuronal microstructure with diffusion MRI. *NeuroImage* 174, 518–538. <https://doi.org/10.1016/j.neuroimage.2018.03.006>
- Ogawa, S., Lee, T., Nayak, A.S., Glynn, P., 1990. Oxygenation-sensitive contrast in magnetic resonance image of rodent brain at high magnetic fields. *Magn. Reson. Med.* 14, 68–78. <https://doi.org/10.1002/mrm.1910140108>
- Ohta, H., Aoki, Y.Y., Itahashi, T., Kanai, C., Fujino, J., Nakamura, M., Kato, N., Hashimoto, R., 2020. White matter alterations in autism spectrum disorder and attention-deficit/hyperactivity disorder in relation to sensory profile. *Mol. Autism* 11, 77. <https://doi.org/10.1186/s13229-020-00379-6>
- Oishi, K. (Ed.), 2011. *MRI atlas of human white matter*, 2. ed. ed. Academic Press, London.
- O’Keefe, J.H., Bhatti, S.K., Bajwa, A., DiNicolantonio, J.J., Lavie, C.J., 2014. Alcohol and cardiovascular health: the dose makes the poison...or the remedy. *Mayo Clin. Proc.* 89, 382–393. <https://doi.org/10.1016/j.mayocp.2013.11.005>
- Olechowski, C., Gener, M., Aiyer, R., Mischel, N., 2023. Transcranial magnetic stimulation for the treatment of chronic low back pain: a narrative review. *Front. Pain Res. Lausanne Switz.* 4, 1092158. <https://doi.org/10.3389/fpain.2023.1092158>
- Olsen, R.W., 2018. GABAA receptor: Positive and negative allosteric modulators. *Neuropharmacology* 136, 10–22. <https://doi.org/10.1016/j.neuropharm.2018.01.036>
- O’Sullivan, M., Jones, D.K., Summers, P.E., Morris, R.G., Williams, S.C.R., Markus, H.S., 2001. Evidence for cortical “disconnection” as a mechanism of age-related cognitive decline. *Neurology* 57, 632–638. <https://doi.org/10.1212/WNL.57.4.632>
- Pando-Naude, V., Toxto, S., Fernandez-Lozano, S., Parsons, C.E., Alcauter, S., Garza-Villarreal, E.A., 2021. Gray and white matter morphology in substance use disorders: a neuroimaging

- systematic review and meta-analysis. *Transl. Psychiatry* 11, 29. <https://doi.org/10.1038/s41398-020-01128-2>
- Pascual, M., Montesinos, J., Guerri, C., 2018. Role of the innate immune system in the neuropathological consequences induced by adolescent binge drinking. *J. Neurosci. Res.* 96, 765–780. <https://doi.org/10.1002/jnr.24203>
- Paulsen, J.S., Zimelman, J.L., Hinton, S.C., Langbehn, D.R., Leveroni, C.L., Benjamin, M.L., Reynolds, N.C., Rao, S.M., 2004. fMRI biomarker of early neuronal dysfunction in presymptomatic Huntington's Disease. *AJNR Am. J. Neuroradiol.* 25, 1715–1721.
- Pawela, C.P., Biswal, B.B., Cho, Y.R., Kao, D.S., Li, R., Jones, S.R., Schulte, M.L., Matloub, H.S., Hudetz, A.G., Hyde, J.S., 2008. Resting-state functional connectivity of the rat brain. *Magn. Reson. Med.* 59, 1021–1029. <https://doi.org/10.1002/mrm.21524>
- Perera, T., George, M.S., Grammer, G., Janicak, P.G., Pascual-Leone, A., Wirecki, T.S., 2016. The Clinical TMS Society Consensus Review and Treatment Recommendations for TMS Therapy for Major Depressive Disorder. *Brain Stimulat.* 9, 336–346. <https://doi.org/10.1016/j.brs.2016.03.010>
- Pérez-Cervera, L., De Santis, S., Marcos, E., Ghorbanzad-Ghaziany, Z., Trouvé-Carpena, A., Selim, M.K., Pérez-Ramírez, Ú., Pfarr, S., Bach, P., Halli, P., Kiefer, F., Moratal, D., Kirsch, P., Sommer, W.H., Canals, S., 2023. Alcohol-induced damage to the fimbria/fornix reduces hippocampal-prefrontal cortex connection during early abstinence. *Acta Neuropathol. Commun.* 11, 101. <https://doi.org/10.1186/s40478-023-01597-8>
- Pfefferbaum, A., Rosenbloom, M., Rohlfing, T., Sullivan, E.V., 2009. Degradation of Association and Projection White Matter Systems in Alcoholism Detected with Quantitative Fiber Tracking. *Biol. Psychiatry* 65, 680–690. <https://doi.org/10.1016/j.biopsych.2008.10.039>
- Pfefferbaum, A., Rosenbloom, M.J., Chu, W., Sassoon, S.A., Rohlfing, T., Pohl, K.M., Zahr, N.M., Sullivan, E.V., 2014. White matter microstructural recovery with abstinence and decline with relapse in alcohol dependence interacts with normal ageing: a controlled longitudinal DTI study. *Lancet Psychiatry* 1, 202–212. [https://doi.org/10.1016/S2215-0366\(14\)70301-3](https://doi.org/10.1016/S2215-0366(14)70301-3)
- Pfefferbaum, A., Sullivan, E.V., 2005. Disruption of Brain White Matter Microstructure by Excessive Intracellular and Extracellular Fluid in Alcoholism: Evidence from Diffusion Tensor Imaging. *Neuropsychopharmacology* 30, 423–432. <https://doi.org/10.1038/sj.npp.1300623>
- Pfefferbaum, A., Sullivan, E.V., Mathalon, D.H., Shear, P.K., Rosenbloom, M.J., Lim, K.O., 1995. Longitudinal Changes in Magnetic Resonance Imaging Brain Volumes in Abstinent and Relapsed Alcoholics. *Alcohol. Clin. Exp. Res.* 19, 1177–1191. <https://doi.org/10.1111/j.1530-0277.1995.tb01598.x>
- Pfefferbaum, A., Zahr, N.M., Mayer, D., Rohlfing, T., Sullivan, E.V., 2015. Dynamic responses of selective brain white matter fiber tracts to binge alcohol and recovery in the rat. *PloS One* 10, e0124885. <https://doi.org/10.1371/journal.pone.0124885>
- Pons-Vázquez, S., Gallego-Pinazo, R., Galbis-Estrada, C., Zanon-Moreno, V., Garcia-Medina, J.J., Vila-Bou, V., Sanz-Solana, P., Pinazo-Durán, M.D., 2011. Combined Pre- and Postnatal Ethanol Exposure in Rats Disturbs the Myelination of Optic Axons†. *Alcohol Alcohol* 46, 514–522. <https://doi.org/10.1093/alcalc/agr063>
- Rahmanzadeh, R., Lu, P.-J., Barakovic, M., Weigel, M., Maggi, P., Nguyen, T.D., Schiavi, S., Daducci, A., La Rosa, F., Schaedelin, S., Absinta, M., Reich, D.S., Sati, P., Wang, Y., Bach Cuadra, M., Radue, E.-W., Kuhle, J., Kappos, L., Granziera, C., 2021. Myelin and axon pathology in multiple sclerosis assessed by myelin water and multi-shell diffusion imaging. *Brain J. Neurol.* 144, 1684–1696. <https://doi.org/10.1093/brain/awab088>
- Raichle, M.E., MacLeod, A.M., Snyder, A.Z., Powers, W.J., Gusnard, D.A., Shulman, G.L., 2001. A default mode of brain function. *Proc. Natl. Acad. Sci.* 98, 676–682. <https://doi.org/10.1073/pnas.98.2.676>
- Rauš, S., Selaković, V., Manojlović-Stojanoski, M., Radenović, L., Prolić, Z., Janać, B., 2013. Response of Hippocampal Neurons and Glial Cells to Alternating Magnetic Field in Gerbils Submitted to

- Global Cerebral Ischemia. *Neurotox. Res.* 23, 79–91. <https://doi.org/10.1007/s12640-012-9333-8>
- Rehm, J., Hasan, O.S.M., Black, S.E., Shield, K.D., Schwarzingler, M., 2019. Alcohol use and dementia: a systematic scoping review. *Alzheimers Res. Ther.* 11, 1. <https://doi.org/10.1186/s13195-018-0453-0>
- Reisert, M., Kellner, E., Dhital, B., Hennig, J., Kiselev, V.G., 2017. Disentangling micro from mesostructure by diffusion MRI: A Bayesian approach. *NeuroImage* 147, 964–975. <https://doi.org/10.1016/j.neuroimage.2016.09.058>
- Ribeiro, E.A., Scarpa, J.R., Garamszegi, S.P., Kasarskis, A., Mash, D.C., Nestler, E.J., 2017. Gene Network Dysregulation in Dorsolateral Prefrontal Cortex Neurons of Humans with Cocaine Use Disorder. *Sci. Rep.* 7, 5412. <https://doi.org/10.1038/s41598-017-05720-3>
- Rice, J., Gu, C., 2019. Function and Mechanism of Myelin Regulation in Alcohol Abuse and Alcoholism. *BioEssays* 41, 1800255. <https://doi.org/10.1002/bies.201800255>
- Rocca, M.A., Schoonheim, M.M., Valsasina, P., Geurts, J.J.G., Filippi, M., 2022. Task- and resting-state fMRI studies in multiple sclerosis: From regions to systems and time-varying analysis. Current status and future perspective. *NeuroImage Clin.* 35, 103076. <https://doi.org/10.1016/j.nicl.2022.103076>
- Rossi, S., Hallett, M., Rossini, P.M., Pascual-Leone, A., Safety of TMS Consensus Group, 2009. Safety, ethical considerations, and application guidelines for the use of transcranial magnetic stimulation in clinical practice and research. *Clin. Neurophysiol. Off. J. Int. Fed. Clin. Neurophysiol.* 120, 2008–2039. <https://doi.org/10.1016/j.clinph.2009.08.016>
- Roth, Y., Pell, G.S., Chistyakov, A.V., Sinai, A., Zangen, A., Zaaroor, M., 2014. Motor cortex activation by H-coil and Figure-8 coil at different depths. Combined motor threshold and electric field distribution study. *Clin. Neurophysiol.* 125, 336–343. <https://doi.org/10.1016/j.clinph.2013.07.013>
- Saab, A.S., Nave, K.-A., 2017. Myelin dynamics: protecting and shaping neuronal functions. *Curr. Opin. Neurobiol.* 47, 104–112. <https://doi.org/10.1016/j.conb.2017.09.013>
- Saba, W., 2023. Glial dysfunction in substance use disorders. New insights from PET and MR imaging. *Addict. Neurosci.* 9, 100135. <https://doi.org/10.1016/j.addicn.2023.100135>
- Saito, Mariko, Chakraborty, G., Hui, M., Masiello, K., Saito, Mitsuo, 2016. Ethanol-Induced Neurodegeneration and Glial Activation in the Developing Brain. *Brain Sci.* 6, 31. <https://doi.org/10.3390/brainsci6030031>
- Salter, M.W., Stevens, B., 2017. Microglia emerge as central players in brain disease. *Nat. Med.* 23, 1018–1027. <https://doi.org/10.1038/nm.4397>
- Sampaio-Baptista, C., Johansen-Berg, H., 2017. White Matter Plasticity in the Adult Brain. *Neuron* 96, 1239–1251. <https://doi.org/10.1016/j.neuron.2017.11.026>
- Sampaio-Baptista, C., Khrapitchev, A.A., Foxley, S., Schlagheck, T., Scholz, J., Jbabdi, S., DeLuca, G.C., Miller, K.L., Taylor, A., Thomas, N., Kleim, J., Sibson, N.R., Bannerman, D., Johansen-Berg, H., 2013. Motor skill learning induces changes in white matter microstructure and myelination. *J. Neurosci. Off. J. Soc. Neurosci.* 33, 19499–19503. <https://doi.org/10.1523/JNEUROSCI.3048-13.2013>
- Schacht, J.P., Anton, R.F., Myrick, H., 2013. Functional neuroimaging studies of alcohol cue reactivity: a quantitative meta-analysis and systematic review: Alcohol cue imaging. *Addict. Biol.* 18, 121–133. <https://doi.org/10.1111/j.1369-1600.2012.00464.x>
- Schneider, C.A., Rasband, W.S., Eliceiri, K.W., 2012. NIH Image to ImageJ: 25 years of image analysis. *Nat. Methods* 9, 671–675. <https://doi.org/10.1038/nmeth.2089>
- Seewoo, B.J., Feindel, K.W., Won, Y., Joos, A.C., Figliomeni, A., Hennessy, L.A., Rodger, J., 2022. White Matter Changes Following Chronic Restraint Stress and Neuromodulation: A Diffusion Magnetic Resonance Imaging Study in Young Male Rats. *Biol. Psychiatry Glob. Open Sci.* 2, 153–166. <https://doi.org/10.1016/j.bpsgos.2021.08.006>

- Segobin, S.H., Chételat, G., Le Berre, A.-P., Lannuzel, C., Boudehent, C., Vabret, F., Eustache, F., Beaunieux, H., Pitel, A.-L., 2014. Relationship between brain volumetric changes and interim drinking at six months in alcohol-dependent patients. *Alcohol. Clin. Exp. Res.* 38, 739–748. <https://doi.org/10.1111/acer.12300>
- Selim, M.K., Harel, M., De Santis, S., Perini, I., Sommer, W.H., Heilig, M., Zangen, A., Canals, S., 2023. Repetitive deep TMS in alcohol dependent patients halts progression of white matter changes in early abstinence. *Psychiatry Clin. Neurosci.* pcn.13624. <https://doi.org/10.1111/pcn.13624>
- Sherman, S.M., 2016. Thalamus plays a central role in ongoing cortical functioning. *Nat. Neurosci.* 19, 533–541. <https://doi.org/10.1038/nn.4269>
- Sinha, R., 2011. New Findings on Biological Factors Predicting Addiction Relapse Vulnerability. *Curr. Psychiatry Rep.* 13, 398–405. <https://doi.org/10.1007/s11920-011-0224-0>
- Skaper, S.D., 2019. Oligodendrocyte precursor cells as a therapeutic target for demyelinating diseases. *Prog. Brain Res.* 245, 119–144. <https://doi.org/10.1016/bs.pbr.2019.03.013>
- Smith, K.S., Tindell, A.J., Aldridge, J.W., Berridge, K.C., 2009. Ventral pallidum roles in reward and motivation. *Behav. Brain Res.* 196, 155–167. <https://doi.org/10.1016/j.bbr.2008.09.038>
- Smith, S.M., Fox, P.T., Miller, K.L., Glahn, D.C., Fox, P.M., Mackay, C.E., Filippini, N., Watkins, K.E., Toro, R., Laird, A.R., Beckmann, C.F., 2009. Correspondence of the brain’s functional architecture during activation and rest. *Proc. Natl. Acad. Sci.* 106, 13040–13045. <https://doi.org/10.1073/pnas.0905267106>
- Smith, S.M., Jenkinson, M., Johansen-Berg, H., Rueckert, D., Nichols, T.E., Mackay, C.E., Watkins, K.E., Ciccarelli, O., Cader, M.Z., Matthews, P.M., Behrens, T.E.J., 2006. Tract-based spatial statistics: Voxelwise analysis of multi-subject diffusion data. *NeuroImage* 31, 1487–1505. <https://doi.org/10.1016/j.neuroimage.2006.02.024>
- Sotiropoulos, S.N., Jbabdi, S., Xu, J., Andersson, J.L., Moeller, S., Auerbach, E.J., Glasser, M.F., Hernandez, M., Sapiro, G., Jenkinson, M., Feinberg, D.A., Yacoub, E., Lenglet, C., Van Essen, D.C., Ugurbil, K., Behrens, T.E.J., 2013. Advances in diffusion MRI acquisition and processing in the Human Connectome Project. *NeuroImage* 80, 125–143. <https://doi.org/10.1016/j.neuroimage.2013.05.057>
- Spanagel, R., 2017. Animal models of addiction. *Dialogues Clin. Neurosci.* 19, 247–258. <https://doi.org/10.31887/DCNS.2017.19.3/rspanagel>
- Spanagel, R., 2009. Alcoholism: a systems approach from molecular physiology to addictive behavior. *Physiol. Rev.* 89, 649–705. <https://doi.org/10.1152/physrev.00013.2008>
- Sperling, R., 2011. The potential of functional MRI as a biomarker in early Alzheimer’s disease. *Neurobiol. Aging* 32, S37–S43. <https://doi.org/10.1016/j.neurobiolaging.2011.09.009>
- Steele, C.M., Southwick, L., 1985. Alcohol and social behavior I: The psychology of drunken excess. *J. Pers. Soc. Psychol.* 48, 18–34. <https://doi.org/10.1037//0022-3514.48.1.18>
- Stejskal, E.O., Tanner, J.E., 1965. Spin Diffusion Measurements: Spin Echoes in the Presence of a Time-Dependent Field Gradient. *J. Chem. Phys.* 42, 288–292. <https://doi.org/10.1063/1.1695690>
- Sullivan, E.V., Marsh, L., Mathalon, D.H., Lim, K.O., Pfefferbaum, A., 1995. Anterior hippocampal volume deficits in nonamnesic, aging chronic alcoholics. *Alcohol. Clin. Exp. Res.* 19, 110–122. <https://doi.org/10.1111/j.1530-0277.1995.tb01478.x>
- Swift, R.M., Aston, E.R., 2015. Pharmacotherapy for alcohol use disorder: current and emerging therapies. *Harv. Rev. Psychiatry* 23, 122–133. <https://doi.org/10.1097/HRP.0000000000000079>
- Tendler, A., Roth, Y., Harmelech, T., 2021. Deep repetitive TMS with the H7 coil is sufficient to treat comorbid MDD and OCD. *Brain Stimulat.* 14, 658–661. <https://doi.org/10.1016/j.brs.2021.04.006>

- Thiele, T.E., Navarro, M., 2014. "Drinking in the dark" (DID) procedures: a model of binge-like ethanol drinking in non-dependent mice. *Alcohol Fayettev. N* 48, 235–241.
<https://doi.org/10.1016/j.alcohol.2013.08.005>
- Thornton, M.A., Hughes, E.G., 2020. Neuron-oligodendroglia interactions: Activity-dependent regulation of cellular signaling. *Neurosci. Lett.* 727, 134916.
<https://doi.org/10.1016/j.neulet.2020.134916>
- Thulborn, K.R., Waterton, J.C., Matthews, P.M., Radda, G.K., 1982. Oxygenation dependence of the transverse relaxation time of water protons in whole blood at high field. *Biochim. Biophys. Acta* 714, 265–270. [https://doi.org/10.1016/0304-4165\(82\)90333-6](https://doi.org/10.1016/0304-4165(82)90333-6)
- Topiwala, A., Ebmeier, K.P., Maullin-Sapey, T., Nichols, T.E., 2022. Alcohol consumption and MRI markers of brain structure and function: Cohort study of 25,378 UK Biobank participants. *NeuroImage Clin.* 35, 103066. <https://doi.org/10.1016/j.nicl.2022.103066>
- Tournier, J.-D., Calamante, F., Connolly, A., 2007. Robust determination of the fibre orientation distribution in diffusion MRI: Non-negativity constrained super-resolved spherical deconvolution. *NeuroImage* 35, 1459–1472.
<https://doi.org/10.1016/j.neuroimage.2007.02.016>
- Tournier, J.-D., Yeh, C.-H., Calamante, F., Cho, K.-H., Connolly, A., Lin, C.-P., 2008. Resolving crossing fibres using constrained spherical deconvolution: Validation using diffusion-weighted imaging phantom data. *NeuroImage* 42, 617–625. <https://doi.org/10.1016/j.neuroimage.2008.05.002>
- Tuch, D.S., 2004. Q-ball imaging. *Magn. Reson. Med.* 52, 1358–1372.
<https://doi.org/10.1002/mrm.20279>
- Tulving, E., Markowitsch, H.J., 1998. Episodic and declarative memory: role of the hippocampus. *Hippocampus* 8, 198–204. [https://doi.org/10.1002/\(SICI\)1098-1063\(1998\)8:3<198::AID-HIPO2>3.0.CO;2-G](https://doi.org/10.1002/(SICI)1098-1063(1998)8:3<198::AID-HIPO2>3.0.CO;2-G)
- Vallat, R., 2018. Pingouin: statistics in Python. *J. Open Source Softw.* 3, 1026.
<https://doi.org/10.21105/joss.01026>
- van der Horn, H.J., Mangina, N.R., Rakers, S.E., Kok, J.G., Timmerman, M.E., Leemans, A., Spikman, J.M., van der Naalt, J., 2021. White matter microstructure of the neural emotion regulation circuitry in mild traumatic brain injury. *Eur. J. Neurosci.* 53, 3463–3475.
<https://doi.org/10.1111/ejn.15199>
- Van Velzen, L.S., Kelly, S., Isaev, D., Aleman, A., Aftanas, L.I., Bauer, J., Baune, B.T., Brak, I.V., Carballedo, A., Connolly, C.G., Couvy-Duchesne, B., Cullen, K.R., Danilenko, K.V., Dannlowski, U., Enneking, V., Filimonova, E., Förster, K., Frodl, T., Gotlib, I.H., Groenewold, N.A., Grotegerd, D., Harris, M.A., Hatton, S.N., Hawkins, E.L., Hickie, I.B., Ho, T.C., Jansen, A., Kircher, T., Klimes-Dougan, B., Kochunov, P., Krug, A., Lagopoulos, J., Lee, R., Lett, T.A., Li, M., MacMaster, F.P., Martin, N.G., McIntosh, A.M., McLellan, Q., Meinert, S., Nenadić, I., Osipov, E., Penninx, B.W.J.H., Portella, M.J., Repple, J., Roos, A., Sacchet, M.D., Sämann, P.G., Schnell, K., Shen, X., Sim, K., Stein, D.J., Van Tol, M.-J., Tomyshev, A.S., Tozzi, L., Veer, I.M., Vermeiren, R., Vives-Gilabert, Y., Walter, H., Walter, M., Van Der Wee, N.J.A., Van Der Werff, S.J.A., Schreiner, M.W., Whalley, H.C., Wright, M.J., Yang, T.T., Zhu, A., Veltman, D.J., Thompson, P.M., Jahanshad, N., Schmaal, L., 2020. White matter disturbances in major depressive disorder: a coordinated analysis across 20 international cohorts in the ENIGMA MDD working group. *Mol. Psychiatry* 25, 1511–1525. <https://doi.org/10.1038/s41380-019-0477-2>
- Vergara, V.M., Liu, J., Claus, E.D., Hutchison, K., Calhoun, V., 2017. Alterations of resting state functional network connectivity in the brain of nicotine and alcohol users. *NeuroImage* 151, 45–54. <https://doi.org/10.1016/j.neuroimage.2016.11.012>
- Verkhatsky, A., Nedergaard, M., 2018. Physiology of Astroglia. *Physiol. Rev.* 98, 239–389.
<https://doi.org/10.1152/physrev.00042.2016>
- Vincent, J.L., Patel, G.H., Fox, M.D., Snyder, A.Z., Baker, J.T., Van Essen, D.C., Zempel, J.M., Snyder, L.H., Corbetta, M., Raichle, M.E., 2007. Intrinsic functional architecture in the anaesthetized monkey brain. *Nature* 447, 83–86. <https://doi.org/10.1038/nature05758>

- Vivian, J.A., Green, H.L., Young, J.E., Majerksy, L.S., Thomas, B.W., Shively, C.A., Tobin, J.R., Nader, M.A., Grant, K.A., 2001. Induction and Maintenance of Ethanol Self-Administration in Cynomolgus Monkeys (*Macaca fascicularis*): Long-Term Characterization of Sex and Individual Differences. *Alcohol. Clin. Exp. Res.* 25, 1087–1097. <https://doi.org/10.1111/j.1530-0277.2001.tb02321.x>
- Vollstädt-Klein, S., Loeber, S., Kirsch, M., Bach, P., Richter, A., Bühler, M., Von Der Goltz, C., Hermann, D., Mann, K., Kiefer, F., 2011. Effects of Cue-Exposure Treatment on Neural Cue Reactivity in Alcohol Dependence: A Randomized Trial. *Biol. Psychiatry* 69, 1060–1066. <https://doi.org/10.1016/j.biopsych.2010.12.016>
- Wang, D., Doddrell, D., 2005. Geometric Distortion in Structural Magnetic Resonance Imaging. *Curr. Med. Imaging Rev.* 1, 49–60. <https://doi.org/10.2174/1573405052953029>
- Wang, Y., Li, X., Zhang, C., Wang, H., Li, Z., Zhu, J., Yu, Y., 2019. Selective micro-structural integrity impairment of the isthmus subregion of the corpus callosum in alcohol-dependent males. *BMC Psychiatry* 19, 96. <https://doi.org/10.1186/s12888-019-2079-6>
- Wansapura, J.P., Holland, S.K., Dunn, R.S., Ball, W.S., 1999. NMR relaxation times in the human brain at 3.0 tesla. *J. Magn. Reson. Imaging JMRI* 9, 531–538. [https://doi.org/10.1002/\(sici\)1522-2586\(199904\)9:4<531::aid-jmri4>3.0.co;2-l](https://doi.org/10.1002/(sici)1522-2586(199904)9:4<531::aid-jmri4>3.0.co;2-l)
- Wattjes, M.P., Rovira, À., Miller, D., Yousry, T.A., Sormani, M.P., de Stefano, M.P., Tintoré, M., Auger, C., Tur, C., Filippi, M., Rocca, M.A., Fazekas, F., Kappos, L., Polman, C., Frederik Barkhof, null, Xavier Montalban, null, MAGNIMS study group, 2015. Evidence-based guidelines: MAGNIMS consensus guidelines on the use of MRI in multiple sclerosis--establishing disease prognosis and monitoring patients. *Nat. Rev. Neurol.* 11, 597–606. <https://doi.org/10.1038/nrneuro.2015.157>
- Weil, M.-T., Möbius, W., Winkler, A., Ruhwedel, T., Wrzos, C., Romanelli, E., Bennett, J.L., Enz, L., Goebels, N., Nave, K.-A., Kerschensteiner, M., Schaeren-Wiemers, N., Stadelmann, C., Simons, M., 2016. Loss of Myelin Basic Protein Function Triggers Myelin Breakdown in Models of Demyelinating Diseases. *Cell Rep.* 16, 314–322. <https://doi.org/10.1016/j.celrep.2016.06.008>
- Wen, W., Sachdev, P., 2004. The topography of white matter hyperintensities on brain MRI in healthy 60- to 64-year-old individuals. *NeuroImage* 22, 144–154. <https://doi.org/10.1016/j.neuroimage.2003.12.027>
- Weston, P.S.J., Poole, T., Nicholas, J.M., Toussaint, N., Simpson, I.J.A., Modat, M., Ryan, N.S., Liang, Y., Rossor, M.N., Schott, J.M., Ourselin, S., Zhang, H., Fox, N.C., 2020. Measuring cortical mean diffusivity to assess early microstructural cortical change in presymptomatic familial Alzheimer's disease. *Alzheimers Res. Ther.* 12, 112. <https://doi.org/10.1186/s13195-020-00679-2>
- Whelan, R., Watts, R., Orr, C.A., Althoff, R.R., Artiges, E., Banaschewski, T., Barker, G.J., Bokde, A.L.W., Büchel, C., Carvalho, F.M., Conrod, P.J., Flor, H., Fauth-Bühler, M., Frouin, V., Gallinat, J., Gan, G., Gowland, P., Heinz, A., Ittermann, B., Lawrence, C., Mann, K., Martinot, J.-L., Nees, F., Ortiz, N., Paillère-Martinot, M.-L., Paus, T., Pausova, Z., Rietschel, M., Robbins, T.W., Smolka, M.N., Ströhle, A., Schumann, G., Garavan, H., IMAGEN Consortium, 2014. Neuropsychosocial profiles of current and future adolescent alcohol misusers. *Nature* 512, 185–189. <https://doi.org/10.1038/nature13402>
- White, A.M., 2003. What happened? Alcohol, memory blackouts, and the brain. *Alcohol Res. Health J. Natl. Inst. Alcohol Abuse Alcohol.* 27, 186–196.
- Wilkins, A., Majed, H., Layfield, R., Compston, A., Chandran, S., 2003. Oligodendrocytes promote neuronal survival and axonal length by distinct intracellular mechanisms: a novel role for oligodendrocyte-derived glial cell line-derived neurotrophic factor. *J. Neurosci. Off. J. Soc. Neurosci.* 23, 4967–4974. <https://doi.org/10.1523/JNEUROSCI.23-12-04967.2003>

- Winklewski, P.J., Sabisz, A., Naumczyk, P., Jodzio, K., Szurowska, E., Szarmach, A., 2018. Understanding the Physiopathology Behind Axial and Radial Diffusivity Changes-What Do We Know? *Front. Neurol.* 9, 92. <https://doi.org/10.3389/fneur.2018.00092>
- Wise, R.A., Koob, G.F., 2014. The Development and Maintenance of Drug Addiction. *Neuropsychopharmacology* 39, 254–262. <https://doi.org/10.1038/npp.2013.261>
- Wood, A.M., Kaptoge, S., Butterworth, A.S., Willeit, P., Warnakula, S., Bolton, T., Paige, E., Paul, D.S., Sweeting, M., Burgess, S., Bell, S., Astle, W., Stevens, D., Koulman, A., Selmer, R.M., Verschuren, W.M.M., Sato, S., Njølstad, I., Woodward, M., Salomaa, V., Nordestgaard, B.G., Yeap, B.B., Fletcher, A., Melander, O., Kuller, L.H., Balkau, B., Marmot, M., Koenig, W., Casiglia, E., Cooper, C., Arndt, V., Franco, O.H., Wennberg, P., Gallacher, J., De La Cámara, A.G., Völzke, H., Dahm, C.C., Dale, C.E., Bergmann, M.M., Crespo, C.J., Van Der Schouw, Y.T., Kaaks, R., Simons, L.A., Lagiou, P., Schoufour, J.D., Boer, J.M.A., Key, T.J., Rodriguez, B., Moreno-Iribas, C., Davidson, K.W., Taylor, J.O., Sacerdote, C., Wallace, R.B., Quiros, J.R., Tumino, R., Blazer, D.G., Linneberg, A., Daimon, M., Panico, S., Howard, B., Skeie, G., Strandberg, T., Weiderpass, E., Nietert, P.J., Psaty, B.M., Kromhout, D., Salamanca-Fernandez, E., Kiechl, S., Krumholz, H.M., Grioni, S., Palli, D., Huerta, J.M., Price, J., Sundström, J., Arriola, L., Arima, H., Travis, R.C., Panagiotakos, D.B., Karakatsani, A., Trichopoulou, A., Kühn, T., Grobbee, D.E., Barrett-Connor, E., Van Schoor, N., Boeing, H., Overvad, K., Kauhanen, J., Wareham, N., Langenberg, C., Forouhi, N., Wennberg, M., Després, J.-P., Cushman, M., Cooper, J.A., Rodriguez, C.J., Sakurai, M., Shaw, J.E., Knuiman, M., Voortman, T., Meisinger, C., Tjønneland, A., Brenner, H., Palmieri, L., Dallongeville, J., Brunner, E.J., Assmann, G., Trevisan, M., Gillum, R.F., Ford, I., Sattar, N., Lazo, M., Thompson, S.G., Ferrari, P., Leon, D.A., Smith, G.D., Peto, R., Jackson, R., Banks, E., Di Angelantonio, E., Danesh, J., Wood, A.M., Kaptoge, S., Butterworth, A., Willeit, P., Warnakula, S., Bolton, T., Paige, E., Paul, D.S., Sweeting, M., Burgess, S., Bell, S., Astle, W., Stevens, D., Koulman, A., Selmer, R.M., Verschuren, M., Sato, S., Njølstad, I., Woodward, M., Veikko, S., Nordestgaard, B.G., Yeap, B.B., Fletcher, A., Melander, O., Kuller, L.H., Balkau, B., Marmot, M., Koenig, W., Casiglia, E., Cooper, C., Arndt, V., Franco, O.H., Wennberg, P., Gallacher, J., Gómez De La Cámara, A., Völzke, H., Dahm, C.C., Dale, C.E., Bergmann, M., Crespo, C., Van Der Schouw, Y.T., Kaaks, R., Simons, L.A., Lagiou, P., Schoufour, J.D., Boer, J.M.A., Key, T.J., Rodriguez, B., Moreno-Iribas, C., Davidson, K.W., Taylor, J.O., Sacerdote, C., Wallace, R.B., Quiros, J.R., Rimm, E.B., Tumino, R., Blazer, D.G., Linneberg, A., Daimon, M., Panico, S., Howard, B., Skeie, G., Salomaa, V., Strandberg, T., Weiderpass, E., Nietert, P.J., Psaty, B.M., Kromhout, D., Salamanca-Fernandez, E., Kiechl, S., Krumholz, H.M., Grioni, S., Palli, D., Huerta, J.M., Price, J., Sundström, J., Arriola, L., Arima, H., Travis, R.C., Panagiotakos, D.B., Karakatsani, A., Trichopoulou, A., Kühn, T., Grobbee, D.E., Barrett-Connor, E., Van Schoor, N., Boeing, H., Overvad, K., Kauhanen, J., Wareham, N., Langenberg, C., Forouhi, N., Wennberg, M., Després, J.-P., Cushman, M., Cooper, J.A., Rodriguez, C.J., Sakurai, M., Shaw, J.E., Knuiman, M., Voortman, T., Meisinger, C., Tjønneland, A., Brenner, H., Palmieri, L., Dallongeville, J.-P., Brunner, E.J., Assmann, G., Trevisan, M., Gillum, R.F., Ford, I.F., Sattar, N., Lazo, M., Thompson, S., Ferrari, P., Leon, D.A., Davey Smith, G., Peto, R., Jackson, R., Banks, E., Di Angelantonio, E., Danesh, J., 2018. Risk thresholds for alcohol consumption: combined analysis of individual-participant data for 599 912 current drinkers in 83 prospective studies. *The Lancet* 391, 1513–1523. [https://doi.org/10.1016/S0140-6736\(18\)30134-X](https://doi.org/10.1016/S0140-6736(18)30134-X)
- World Health Organization, 2018. Global status report on alcohol and health 2018. World Health Organization, Geneva.
- Yeh, P.-H., Simpson, K., Durazzo, T.C., Gazdzinski, S., Meyerhoff, D.J., 2009. Tract-based spatial statistics (TBSS) of diffusion tensor imaging data in alcohol dependence: Abnormalities of the motivational neurocircuitry. *Psychiatry Res. Neuroimaging* 173, 22–30. <https://doi.org/10.1016/j.pscychresns.2008.07.012>

- Yeung, M.S.Y., Zdunek, S., Bergmann, O., Bernard, S., Salehpour, M., Alkass, K., Perl, S., Tisdale, J., Possnert, G., Brundin, L., Druid, H., Frisén, J., 2014. Dynamics of Oligodendrocyte Generation and Myelination in the Human Brain. *Cell* 159, 766–774. <https://doi.org/10.1016/j.cell.2014.10.011>
- Yuan, A., Nixon, R.A., 2021. Neurofilament Proteins as Biomarkers to Monitor Neurological Diseases and the Efficacy of Therapies. *Front. Neurosci.* 15, 689938. <https://doi.org/10.3389/fnins.2021.689938>
- Zakiniæiz, Y., Scheinost, D., Seo, D., Sinha, R., Constable, R.T., 2017. Cingulate cortex functional connectivity predicts future relapse in alcohol dependent individuals. *NeuroImage Clin.* 13, 181–187. <https://doi.org/10.1016/j.nicl.2016.10.019>
- Zangen, A., Moshe, H., Martinez, D., Barnea-Ygael, N., Vapnik, T., Bystritsky, A., Duffy, W., Toder, D., Casuto, L., Grosz, M.L., Nunes, E.V., Ward, H., Tendler, A., Feifel, D., Morales, O., Roth, Y., Iosifescu, D.V., Winston, J., Wirecki, T., Stein, A., Deutsch, F., Li, X., George, M.S., 2021. Repetitive transcranial magnetic stimulation for smoking cessation: a pivotal multicenter double-blind randomized controlled trial. *World Psychiatry Off. J. World Psychiatr. Assoc. WPA* 20, 397–404. <https://doi.org/10.1002/wps.20905>
- Zanon Zotin, M.C., Yilmaz, P., Sveikata, L., Schoemaker, D., Van Veluw, S.J., Etherton, M.R., Charidimou, A., Greenberg, S.M., Duering, M., Viswanathan, A., 2023. Peak Width of Skeletonized Mean Diffusivity: A Neuroimaging Marker for White Matter Injury. *Radiology* 306, e212780. <https://doi.org/10.1148/radiol.212780>
- Zhai, F., Liu, J., Su, N., Han, F., Zhou, L., Ni, J., Yao, M., Zhang, S., Jin, Z., Cui, L., Tian, F., Zhu, Y., 2020. Disrupted white matter integrity and network connectivity are related to poor motor performance. *Sci. Rep.* 10, 18369. <https://doi.org/10.1038/s41598-020-75617-1>
- Zhang, H., Schneider, T., Wheeler-Kingshott, C.A., Alexander, D.C., 2012. NODDI: Practical in vivo neurite orientation dispersion and density imaging of the human brain. *NeuroImage* 61, 1000–1016. <https://doi.org/10.1016/j.neuroimage.2012.03.072>
- Zilverstand, A., Huang, A.S., Alia-Klein, N., Goldstein, R.Z., 2018. Neuroimaging Impaired Response Inhibition and Salience Attribution in Human Drug Addiction: A Systematic Review. *Neuron* 98, 886–903. <https://doi.org/10.1016/j.neuron.2018.03.048>
- Zois, E., Vollstädt-Klein, S., Hoffmann, S., Reinhard, I., Charlet, K., Beck, A., Jorde, A., Kirsch, M., Walter, H., Heinz, A., Kiefer, F., 2017. Orbitofrontal structural markers of negative affect in alcohol dependence and their associations with heavy relapse-risk at 6 months post-treatment. *Eur. Psychiatry* 46, 16–22. <https://doi.org/10.1016/j.eurpsy.2017.07.013>
- Zou, Y., Murray, D.E., Durazzo, T.C., Schmidt, T.P., Murray, T.A., Meyerhoff, D.J., 2018. White matter microstructural correlates of relapse in alcohol dependence. *Psychiatry Res. Neuroimaging* 281, 92–100. <https://doi.org/10.1016/j.psychres.2018.09.004>



IX. Appendices

A. Supplementary data

Supplementary clinical methods

Participants Inclusion Criteria:

- Age 18 – 65.
- Current diagnosis of moderate-severe alcohol use disorder.
- Alcohol use in the past month.
- Right-handed (self-report).
- If female, negative urine pregnancy test.
- If female, must either agree to practice an effective birth control method, agree to abstinence from intercourse, be surgically sterile or postmenopausal for at least one year.

Participants Exclusion Criteria:

- Currently pregnant or breastfeeding.
- More than mild cognitive impairment, as determined by a score on the Montreal Cognitive Assessment (MoCA) <25.¹
- Current DSM-5 diagnosis of schizophrenia, bipolar disorder, or other psychotic disorder.
- Use in the past 2 weeks of medication or illicit drug with known high proconvulsant action, as self-reported or detected using urine toxicology screening and with accordance to the Physician's best judgement.
- Any history of clinically significant neurological disorders, including organic brain disease, epilepsy, stroke, brain lesions, multiple sclerosis, previous neurosurgery, or personal history of head trauma that resulted in loss of consciousness for > 5 minutes and retrograde amnesia for > 30 minutes (self-reported history),
- Any history of seizures other than febrile childhood seizures (self-reported history).
- Clinically significant hearing impairment.
- Presence of ferromagnetic objects in the body that are contraindicated for MRI of the head (pacemakers or other implanted electrical devices, brain stimulators, some types of dental implants, aneurysm clips, metallic prostheses, permanent eyeliner, implanted delivery pump, or shrapnel fragments), or fear of enclosed spaces. Eligibility will be determined by the "MRI Safety Screening Questionnaire" and verified, if necessary, by a radiology consultant. Some of the patients who will be excluded from the imaging part of the study will be included in the clinical part.
- Any psychiatric, medical, or social condition, whether or not listed above, due to which, in the judgement of the investigators and after any consults if indicated, participation in the study is not in the best interest of the patient.

AUD Diagnoses

Participants were diagnosed by an independent psychiatrist to match the current DSM-5 diagnosis of moderate to severe alcohol dependence.

Comorbidities

Anxiety and depression are common comorbidities of AUD; they were measured and reported in the participant's demographics table. There was a reduction in these measures following alcohol detoxification regardless of group.

Medication Regimen

Participants were not provided with new medication prescriptions and were advised to maintain their existing medication regimens that would not interfere with the TMS treatment.

Duration of AUD

The study adhered to the DSM-5 criteria for AUD, indicating that all participants had been dealing with AUD for a minimum of one year.

Abstinence Period

Patients had maintained abstinence for a minimum of 5 days but no longer than one month.

Craving Assessment

Craving was assessed using the Penn Alcohol Craving Scale (PACS) questionnaire, a tool that measures various aspects of craving experienced during the previous week. In the revised version, we have specified it in the text.

Instructions for the rs-fMRI measurements

During resting state, the experimenter instructed the participants to keep their eyes open and "let their mind wander", without pondering on a specific thought, and the scan included a white fixation cross in the middle of the screen. Participants were inquired whether they had fallen asleep at the end of the resting state scan (the responses were always negative) and DTI scan followed resting state.

Supplementary References:

1. Nasreddine, Z. S., Phillips, N. A., Bédirian, V., Charbonneau, S., Whitehead, V., Collin, I., ... & Chertkow, H. (2005). The Montreal Cognitive Assessment, MoCA: a brief screening tool for mild cognitive impairment. *Journal of the American Geriatrics Society*, 53(4), 695-699.

B. Ethical considerations and approvals

Animal Experiments

All animal experiments were authorized by the Animal Care and Use Committee of the Instituto de Neurociencias de Alicante (UMH-CSIC), Alicante, Spain, and conform to the Spanish (law 32/2007) and European regulations (EU directive 86/609, EU decree 2001-486, and EU recommendation 2007/526/EC).

Clinical trial

Data was acquired as part of a double blind, sham-controlled, randomized clinical trial performed at the Ben-Gurion University and the Soroka Medical Centre, Be'er Sheva, Israel. Recruitment occurred between July 2016 and December 2019. The study was conducted in accordance with the Declaration of Helsinki, with approval of the local Institutional Review Board (0404-15) and the Israeli Ministry of Health and was registered at ClinicalTrials.gov (NCT02691390).







C. Peer-reviewed publications integrated into the thesis:





Repetitive deep TMS in alcohol dependent patients halts progression of white matter changes in early abstinence

Mohamed Kotb Selim, MSc ¹, Maayan Harel, PhD ^{2,3}, Silvia De Santis, PhD ¹, Irene Perini, PhD ⁴, Wolfgang H. Sommer, PhD,⁵ Markus Heilig, MD, PhD ⁴, Abraham Zangen, PhD ^{2,3} and Santiago Canals, PhD ^{1*}

Aim: Alcohol use disorder (AUD) is the most prevalent form of addiction, with a great burden on society and limited treatment options. A recent clinical trial reported significant clinical benefits of deep transcranial magnetic stimulations (Deep TMS) targeting midline frontocortical areas. However, the underlying biological substrate remained elusive. Here, we report the effect of Deep TMS on the microstructure of white matter.

Methods: A total of 37 (14 females) AUD treatment-seeking patients were randomized to sham or active Deep TMS. Twenty (six females) age-matched healthy controls were included. White matter integrity was evaluated by fractional anisotropy (FA). Secondary measures included brain functional connectivity and self-reports of craving and drinking units in the 3 months of follow-up period.

Results: White matter integrity was compromised in patients with AUD relative to healthy controls, as reflected by the widespread reduction in FA. This alteration progressed during early

abstinence (3 weeks) in the absence of Deep TMS. However, stimulation of midline frontocortical areas arrested the progression of FA changes in association with decreased craving and relapse scores. Reconstruction of axonal tracts from white-matter regions showing preserved FA values identified cortical regions in the posterior cingulate and dorsomedial prefrontal cortices where functional connectivity was persistently modulated. These effects were absent in the sham-stimulated group.

Conclusions: By integrating brain structure and function to characterize the alcohol-dependent brain, this study provides mechanistic insights into the TMS effect, pointing to myelin plasticity as a possible mediator.

Keywords: Addiction Remission Network, Alcohol Use Disorder, Deep TMS, DTI, fMRI.

<http://onlinelibrary.wiley.com/doi/10.1111/pcn.13624/full>

Among the population aged 15–49 years, alcohol consumption is the leading risk factor for both deaths and disability-adjusted life-years, with 3.8% of female deaths and 12.2% of male deaths attributable to alcohol use, according to recent data.¹ Alcohol use disorder (AUD), the chronic excessive consumption of alcohol, is a chronic illness characterized by cycles of relapse and remission, with several associated co-morbidities and complex neurobiological substrates of alterations. Both psychological and pharmacological interventions have shown efficacy for the treatment of AUD, but a major need for novel treatments with high patient and clinician acceptance remains.²

In a recent double-blind, randomized, sham-controlled clinical trial, we found initial support for the clinical efficacy of deep repetitive transcranial magnetic stimulation (Deep TMS) targeting the anterior cingulate (ACC) and medial prefrontal cortices (mPFC).³ Patients with AUD receiving Deep TMS showed significantly reduced craving and relapse compared to the sham group. Although these results support the continued development of Deep TMS as a non-invasive treatment for AUD, the biological substrates underlying its putative efficacy are not fully understood. A mechanistic understanding of the

observed Deep TMS effects may allow treatment to be optimized and predictive biomarkers to be established.

Non-invasive brain stimulation treatments are based on the notion that abnormal neuronal activity can be retuned by entraining neuronal population activity with specific stimulation patterns.^{4–7} Possible underlying mechanisms include the induction of activity-dependent synaptic plasticity and changes in the intrinsic neuronal excitability.⁸ However, another form of plasticity, less frequently recognized but also activity-dependent and therefore recruited by brain stimulation protocols, is myelin plasticity.^{9–11} Myelin plasticity refers to the dynamic regulation of myelin production by oligodendrocytes in response to increased neuronal firing.⁹ It is associated with increased axonal conduction velocity and transmission reliability.⁹ Interestingly, in *post-mortem* tissue from patients with AUD, demyelination evidence from morphological and molecular alterations have been reported,¹² which likely underlie the white matter alterations repeatedly found in MRI studies as a hallmark of the disease.^{13–15} White matter alterations progress during early abstinence, at least up to 6 weeks after discontinuing alcohol, suggesting a possible contribution to relapse vulnerability.¹⁵ We reasoned that the reduction in

¹ Instituto de Neurociencias, Consejo Superior de Investigaciones Científicas (CSIC) and Universidad Miguel HernándeZ (UMH), Sant Joan d'Alacant, Spain

² Department of Life Sciences, Ben-Gurion University, Beer Sheva, Israel

³ Zlotowski Center for Neuroscience, Ben-Gurion University, Beer Sheva, Israel

⁴ Center for Social and Affective Neuroscience, Department of Biomedical and Clinical Sciences, Linköping University Hospital, Linköping, Sweden

⁵ Department of Addiction Medicine, Department of Clinical Psychology, Medical Faculty Mannheim, Central Institute of Mental Health, University of Heidelberg, Mannheim, Germany

* Correspondence: Email: scanals@umh.es

craving and relapse induced by Deep TMS targeting the ACC and mPFC³ could be in part mediated by myelin plasticity and, if so, should be reflected in the white matter microstructure as measured by diffusion-weighted MRI.

We set out to test the above hypothesis using the same imaging framework as before¹⁵ to elucidate the neurobiological substrate underlying the clinical efficacy of Deep TMS targeting the frontal lobe.³ We first replicated the progression of white matter alterations during early abstinence in the cohort of patients with AUD, and then demonstrated that this progression was arrested by Deep TMS, specifically in active-stimulated but not in sham-stimulated patients, and selectively in the stimulated brain region. Persistent changes in functional connectivity were also found in the brain regions connected by the Deep TMS-protected white matter fiber tracts. By integrating brain structure and function to characterize the alcohol dependent brain, this study provides a mechanistic insight into the effects of TMS, suggesting that its therapeutic efficacy is related to the recovery of white matter microstructure, and pointing to myelin plasticity as a possible mediator.

Materials and Methods

Participants

This was a double blind, sham-controlled, randomized clinical trial performed at the Ben-Gurion University and the Soroka Medical Centre, Be'er Sheva, Israel. Recruitment occurred between July 2016 and December 2019. The study was conducted in accordance with the Declaration of Helsinki, with approval of the local Institutional Review Board (0404–15) and the Israeli Ministry of Health and was registered at [ClinicalTrials.gov](https://clinicaltrials.gov) (NCT02691390). The main clinical outcomes of the original study have been reported previously, where the full recruitment protocol is also described.³ Functional (fMRI) and structural (DTI) data were not available for all subjects in the

trial. From the original study and for this secondary analysis, we derived a subset of 38 patients (19 sham-stimulated/19 active-stimulated) from the initial patients' sample, all of whom possessed DTI data. One patient in the active TMS group did not complete treatment, resulting in 19 patients in the sham TMS group and 18 in the active TMS group. Age-matched controls ($n = 20$) were also included in the trial. Participants provided written informed consent and were instructed to abstain from alcohol for 5 days before commencing treatment. The clinical assessment of the participants included in the DTI analysis is reported in Table 1 (sham vs. active Deep TMS) and Table 2 (AUD vs. Control). More details on the exclusion criteria are provided in the supporting information.

Magnetic resonance imaging

Imaging protocols were coordinated with the SyBil-AA (Systems Biology of Alcohol Addiction) Horizon 2020 Consortium. Imaging was performed using a Philips Ingenia 3 Tesla MRI scanner (Philips Healthcare, Best, The Netherlands) equipped with a 32-channel Philips dS Head head-coil. Blood oxygen-level-dependent (BOLD) data were acquired with an echo-planar imaging (EPI) sequence: TR = 2000 ms; TE = 30 ms; flip angle = 77°; field-of-view = 220 × 220; in-plane resolution = 3.4 × 3.4 mm; slice thickness = 4 mm, no slice gap; number of axial slices (angled with the AC-PC line) = 32; number of volumes = 360. The two collected resting state runs (baseline and follow-up) each lasted for 12 min. A high-resolution 3D T1-weighted Turbo Field Echo scan was acquired before the EPI data acquisitions TR = 7.0 ms; TE = 3.2 ms; flip angle = 8°; field-of-view = 256 mm × 256 mm × 170 mm; voxel resolution = 1 mm × 1 mm × 1 mm; no slice gap; plane: sagittal; number of sagittal slices = 170.

Multi-shell diffusion MRI acquisition protocol consisted of images with 30 uniformly distributed diffusion directions, acquired

Table 1. Demographic characteristics of AUD patients and their group-matched healthy controls

Characteristics	Patients [mean (SD)]	Controls [mean (SD)]	<i>P</i> -value*
Baseline demographic characteristics			
Sample size (<i>n</i> females)	20 (7)	20 (6)	
Age	36.7 (5.8)	35.1 (7.1)	0.45
Education (years)	12.4 (1.5)	13.6 (5.4)	0.01 [†]
Baseline clinical characteristics			
MoCA	28.3 (1.5)	29 (2.1)	0.26
AUDIT	26.5 (5.4)	2.8 (1.9)	<0.001 [†]
ADS	19.05 (7.3)	2.2 (4.3)	<0.001 [†]
TLFB (%pHDD)	32.2% (23.5)	2.4% (6.6)	<0.001 [†]
PACS	17.05 (6.7)	1.4 (1.9)	<0.001 [†]
BDI	14.3 (9.5)	3.3 (4.6)	<0.001 [†]
CPRS-SA			
Depression	5.4 (3.4)	2.1 (2)	0.002
Anxiety	6.9 (5)	3 (2.5)	0.012 [†]
NEO-FFI			
Neuroticism	1.9 (0.9)	1.5 (0.8)	0.15
Extraversion	2.3 (0.6)	2.4 (0.4)	0.68 [†]
Openness	2.1 (0.4)	2.3 (0.3)	0.11
Agreeableness	2.5 (0.6)	2.6 (0.5)	0.83
Conscientiousness	2.6 (0.7)	3.01 (0.4)	0.07 [†]

Abbreviations: ADS, Alcohol Dependence Scale; AUDIT, alcohol use disorder identification test (scores of >20 indicate high-likelihood of dependence); CPRS, Comprehensive Psychopathological Rating Scale; MoCA, Montreal Cognitive Assessment; NEO-FFI, abbreviated five factor personality assessment; SD, standard deviation; TLFB, timeline follow back.

*Two-tailed *P*-value using independent-samples *t*-test.

[†]Mann–Whitney Test.

with b-value of 1000 s/mm², and 60 uniformly distributed diffusion directions, acquired with b-value of 2000 s/mm², in addition to a non-weighted image (b0). Echo Planar Imaging spin-echo diffusion sequence was used with the following parameters: TR = 7 s, TE = 108 ms, matrix size = 224 × 224 × 125, and a spatial resolution of 1.75 mm × 1.75 mm × 2.5 mm. We initially collected fMRI data, followed by the acquisition of diffusion MRI data.

Preprocessing and statistical analysis of resting state data were performed with the Analysis of Functional Neuro Images (AFNI) software v18.3.16.¹⁶ First, a Freesurfer-based parcellation was performed on T1-weighted data using the function *recon-all*, and later used for tissue-based regression to allow for modeling of signal fluctuations not due to BOLD signal. BOLD signal was de-spiked, slice-time and motion-corrected, and then spatially transformed to the Montreal Neurological Institute (MNI) template space, using a combination of linear and non-linear transformations. Motion censoring was set at 3 mm, and outlier fraction was set at 0.05, so that volumes exceeding these values were not included in the time-series regression. A regression on BOLD time-series data was performed using the *3dDeconvolve* function, and head motion effects were accounted for by adding the motion parameters and their derivatives as

regressors of no interest. Afterward, the covarying signals between gray and white matter regions were removed from the residuals using the data-driven APPLECOR method.¹⁷

Microstructural data processing and statistics

All raw data were first denoised using a method based on statistical independence¹⁸ and then converted to ExploreDTI¹⁹ format. Each dataset underwent subject motion and Eddy-current-induced distortions corrections, followed by brain extraction to eliminate non-brain tissue. Images were split according to their b-value. Diffusion-weighted data with b-value = 1000 (30 directions in total) were used for diffusion tensor-DTI estimation, using the robust model fitting.²⁰ After the tensor model was fitted, Fractional Anisotropy (FA) maps were generated for the voxel-wise statistical analyses.

For both cross-sectional and longitudinal analyses, a Tract-based spatial statistics²¹ approach was used. For cross-sectional analysis, FA maps from AUD cohort at the first time point (TP1) and healthy controls were registered to MNI standard template *via* a combination of linear and nonlinear registration implemented in the Advanced Normalization Tools-ANTS²²; then, the FA maps in standard space

Table 2. Demographic characteristics of active and sham Deep TMS groups

Characteristics	Active [mean (SD)]	Sham [mean (SD)]	P-value*
Baseline demographic characteristics			
Sample size (<i>n</i> females)	18 (7)	19 (7)	
Age	42.3 (9.1)	43.8 (9.5)	0.61
Education (years)	12.3 (1.6)	12.2 (3.6)	0.93
Baseline clinical characteristics			
MoCA	28.2 (1.5)	27.5 (1.5)	0.18
AUDIT	25.7 (6.8)	25.6 (6.7)	0.96
ADS	17.9 (7.3)	17.5 (6.7)	0.87
TLFB (%pHDD)	44.6% (33)	32.1% (23)	0.19
Consumption (average g/day)	69.3 (53.2)	55.03 (39.8)	0.35
PACS	15.7 (5.9)	16.5 (7.3)	0.71
BDI	14.4 (9.8)	15.2 (8.1)	0.78
SETS	23 (8.2)	24.6 (8.1)	0.54
CPRS			
Depression	5.9 (3.8)	6.3 (4.05)	0.76
Anxiety	6.9 (5.4)	8.07 (4.6)	0.5
NEO-FFI			
Neuroticism	2.01 (0.8)	1.9 (0.8)	0.74
Extraversion	2.3 (0.6)	2.06 (0.4)	0.25
Openness	2.09 (0.4)	2.1 (0.5)	0.86
Agreeableness	2.6 (0.6)	2.5 (0.5)	0.69
Conscientiousness	2.5 (0.6)	2.6 (0.5)	0.6
Other clinical characteristics			
RMT (% of stimulator power output)	66.1% (7.5)	66.6% (8.1)	0.82
Blinding assessment (% of patients who correctly guessed their treatment arm at the end of follow-up)	(9/17) 527%	(3/15) 20% [†]	0.82 [‡]
Adverse events Headache (moderate to severe)	<i>n</i> = 2	<i>n</i> = 3	0.67 [§]

Abbreviations: ADS, Alcohol Dependence Scale; AUDIT, alcohol use disorder identification test (scores of >20 indicate high-likelihood of dependence); CPRS, Comprehensive Psychopathological Rating Scale; MoCA, Montreal Cognitive Assessment; NEO-FFI, abbreviated five factor personality assessment; RMT, resting motor threshold; SD, standard deviation; SETS, Stanford Expectations of Treatment Scale; TLFB, timeline follow back.

*Two-tailed P-value using independent-samples *t*-test.

[†]Data missing for two participants.

[‡]χ-Test.

[§]Z-Test.

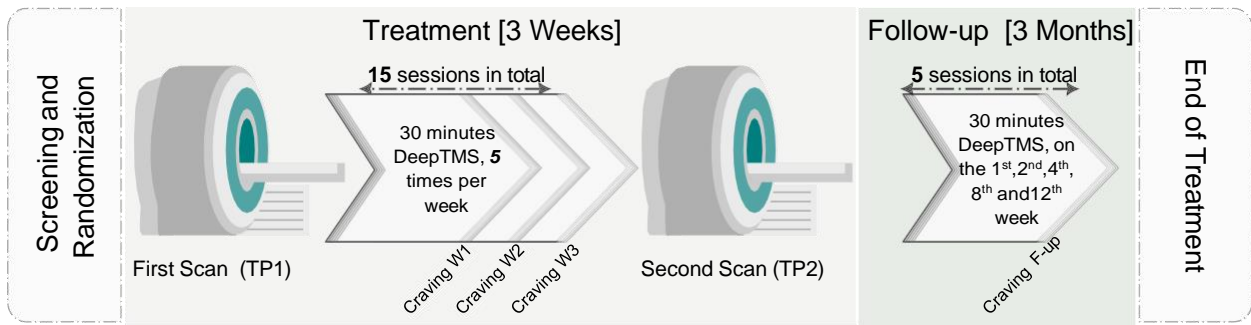


Fig. 1 Study design. Patients with AUD are randomly assigned to sham- or active-stimulated groups. All patients receive two MRI sessions (TP1 and TP2) separated by the 3 weeks of Deep TMS (active or sham) treatment (five daily sessions per week). MRI sessions included functional, anatomical and diffusion-weighted imaging sequences. Additional Deep TMS sessions were applied during the follow up visits taking place 1, 2, 4, 8 and 12 weeks after the end of the acute daily treatment period. Craving and relapse were monitored every week during the acute treatment period and every visit during the follow up period.

were used to generate the white matter skeleton, where the FA images were projected. For longitudinal analysis, for each subject in the AUD cohort, FA maps at the second time point (TP2) were registered to FA maps at TP1 by linear registration, then brought to standard space by applying the same transformation and field warping obtained from nonlinear registration at time point TP1. Then, the FA maps at TP1 in standard space were used to generate the white matter skeleton, where the difference between FA images at the two-time points was projected. Skeletonized FA images were tested using the randomise tool for statistical permutations testing, as part of the FSL package.²³ Using a general linear model (GLM) design, threshold-free cluster enhancement option was used in the statistics.

Three kinds of statistical comparisons were run. To localize differences in FA at TP1 between AUD and control cohorts, a GLM model compared FA maps between groups, while accounting for age and gender. To test the longitudinal evolution of FA between TP1 and TP2, a GLM model tested for positive or negative differences in

FA maps between time points. Finally, to highlight differences in FA progression in sham vs. active Deep TMS, a GLM model tested for group differences in the FA progression between time points (TP2 – TP1), while accounting for age and gender.

Tractography and DTI-driven functional connectivity analysis

The constrained spherical deconvolution²⁴ algorithm incorporated in ExploreDTI was applied to diffusion-weighted data with b-value = 2000 (60 directions in total) to generate whole-brain tractography for each subject belonging to the AUD group. Based on the statistical outcome of the previous voxel-wise analysis, highlighting a significant cluster of voxels contained within the Deep TMS stimulated area in which FA progresses differently in the sham and active groups, we defined a generative seed and selected the white matter tracts passing through this Deep TMS-sensitive spot. All the tracts in individual spaces were registered to standard space and then

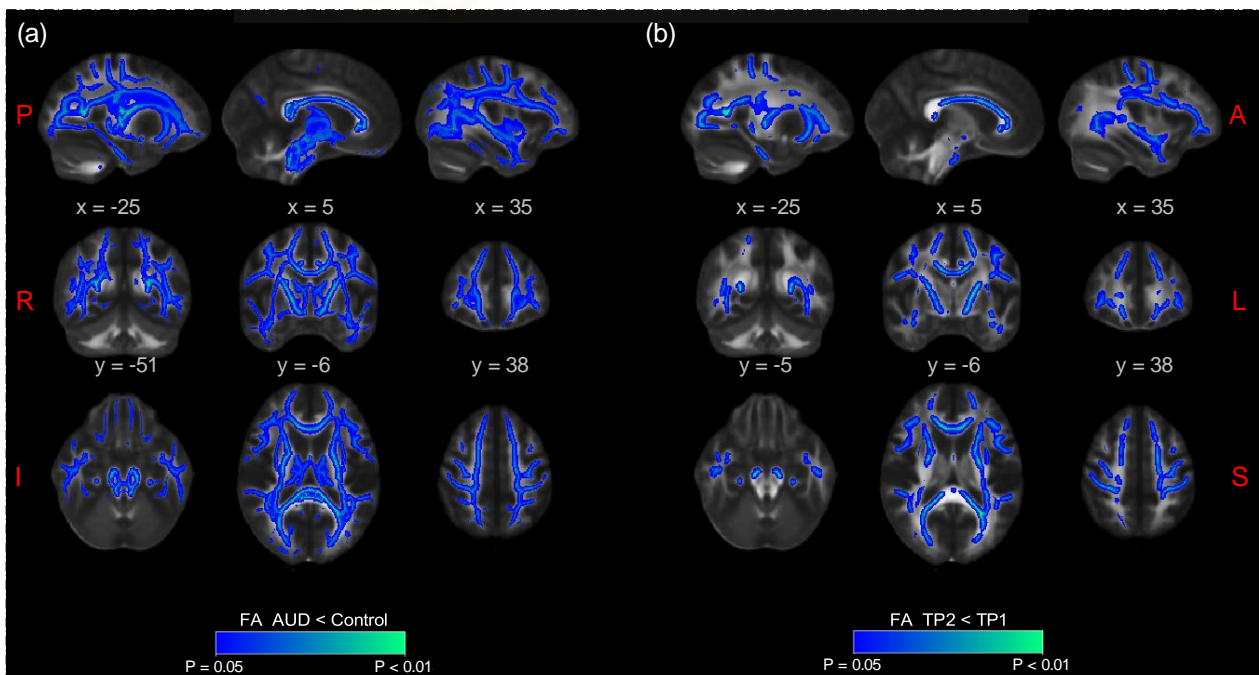


Fig. 2 White matter alterations progress during early abstinence. Tract-based spatial statistics showing in blue the white matter skeleton where FA is reduced in the following conditions: (a) AUD at TP1 ($n = 20$) compared to group-matched healthy controls ($n = 20$; see Table 1 for demographic characteristics), (b) AUD at TP2 compared to TP1 ($n = 19$; longitudinal comparison) from the sham-stimulated group of patients.

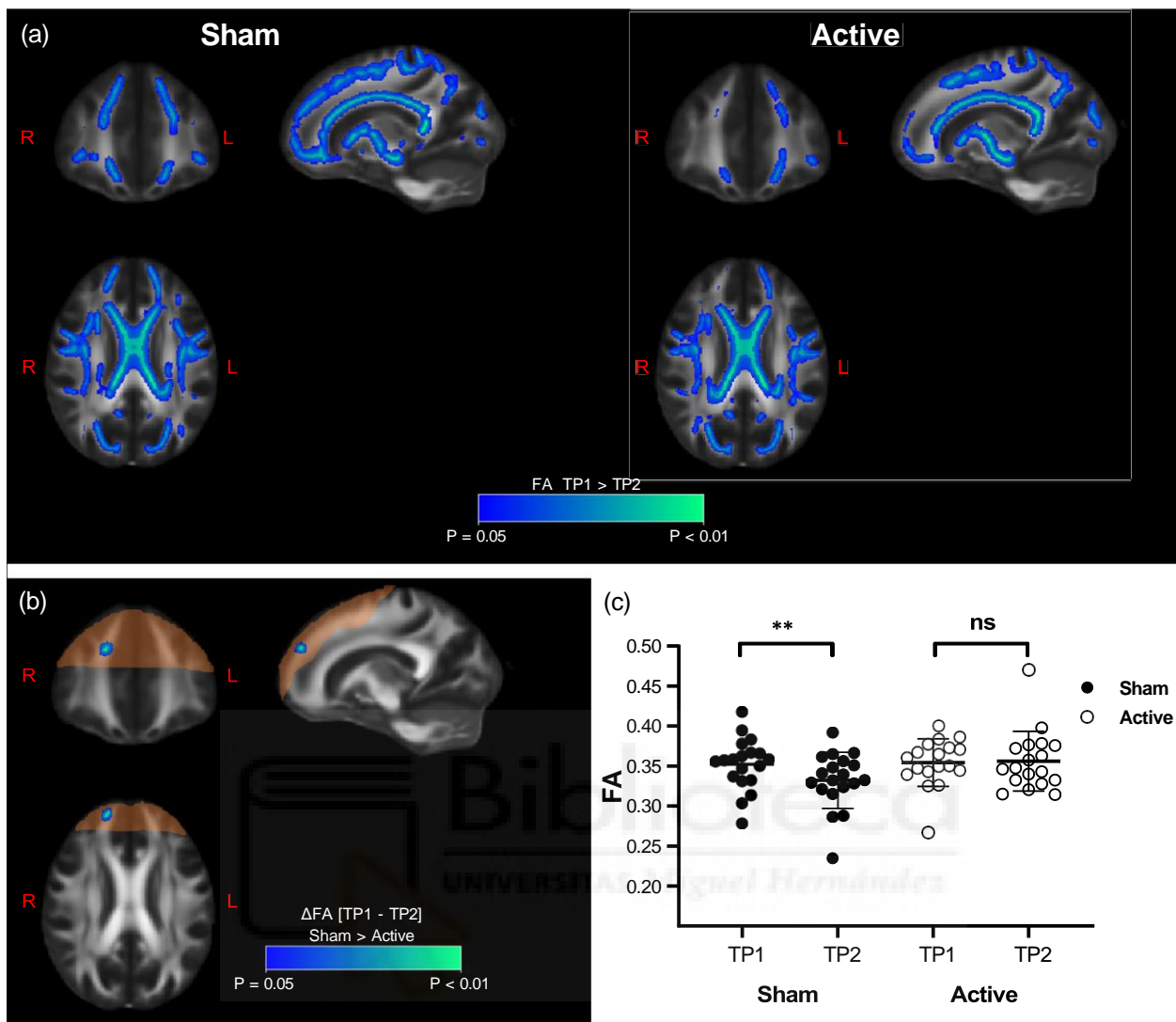


Fig. 3 Progression of white matter alterations are arrested by Deep TMS. (a) Progression of FA between time points calculated separately for sham (left) and active (right) groups. The portion of the brain within the theoretical Deep TMS field intensity above the average threshold for action potential firing is highlighted in orange. (b) Tract-based spatial statistics showing regions of the white matter skeleton with significant differences between active and sham Deep TMS groups in the FA change between TP2 and TP1. (c) Mean FA calculated for the two time points and for the two groups in the area of significant time \times group interaction according to tract-based spatial statistics (shown in b.). Two-way ANOVA yielded significant time \times group interaction $F_{1,35} = 5.3$, $P = 0.027$, then Sidak's multiple comparisons test showed significant change in Sham group only ($P = 0.008$). ns: not statistically significant, $**P < 0.01$.

averaged. A threshold was applied to get tracts that are present in at least 70% of all the subjects. Averaged tracts were masked to get the intersection between generated tracts and the gray matter standard mask. As such, we defined four cortical targets that are connected by tracts passing through the Deep TMS-sensitive spot. These targets were used to define the seed regions for the functional connectivity analysis at post-treatment. Seeds consisted of 5 mm radius spheres centered on the MNI coordinates of the DTI-derived targets. From the original study,³ we utilized fMRI data from subjects that survived motion censoring and completed pre- and post-treatment sessions (sham $n = 18$ and active $n = 19$). In this sample, two subjects from the sham group and two from the active group did not contribute DTI data. However, we retained these individuals in the analysis to maximize statistical power. To assess seed-to-whole brain gray matter connectivity, we conducted a regression analysis, incorporating the seed time course as a predictor variable. The analysis was performed using the *3dDeconvolve* software. The resulting 3D volumes with beta coefficients for each seed location were then compared between groups at post-treatment, using the AFNI function *3dttest++*. Results were

thresholded at a per-voxel $P = 0.002$, and multiple comparisons corrected at $\alpha = 0.05$.²⁵ The cluster size threshold for multiple comparison correction was estimated by entering spatial smoothness parameters of the residuals in the *3dClustsim* simulation function, and as simulation mask, a gray matter mask, which consisted of the union of 80% of the subjects' EPI-masks surviving censoring. In order to assess the potential effects of time, beta coefficients from significant clusters were extracted and entered in a 2×2 repeated measures ANOVA with factors time (pre/post) and group (sham/active Deep TMS).

Results

Progression of FA decrease in early abstinence

When comparing FA maps acquired in the control group and the age- and gender-matched AUD cohort before treatment, we detected significantly lower FA in patients with AUD ($P < 0.05$, mean effect size $d = 1.0$) in most portions of the white matter skeleton, as shown in Fig. 2a. In the AUD cohort receiving sham treatment only, when

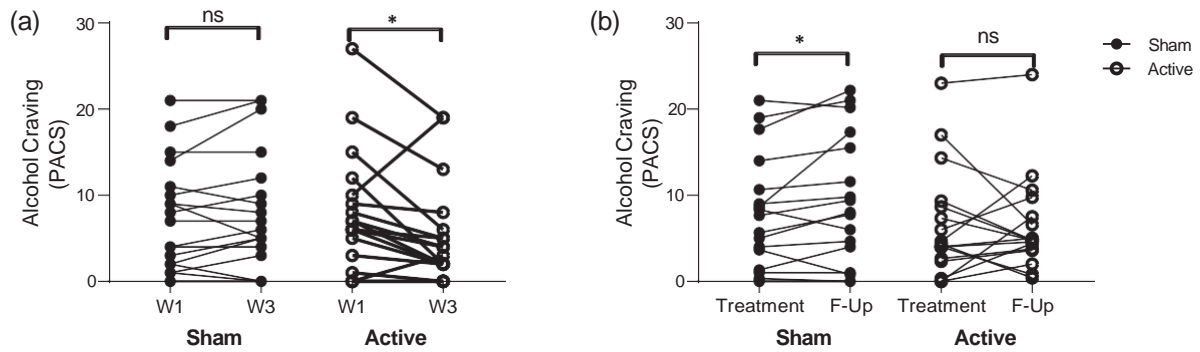


Fig. 4 Deep TMS decreases alcohol craving. (a) Evolution of PACS (Penn Alcohol Craving Scale) values across groups (sham and active) and treatment time points (week 1 and 3). (b) Average PACS values measured during the 3 weeks treatment (“Treatment”) and at 3 months follow up (“F-Up”) for sham and active Deep TMS groups. Wilcoxon rank test. ns: not statistically significant, * $P < 0.05$.

comparing the progression of FA changes between time points TP1 and TP2 (Fig. 1), we detected a significant FA reduction in most areas of the white matter skeleton ($P < 0.05$, mean effect size $d = 0.317$), as shown in (Fig. 2b). These results replicate previous findings on white matter alterations in AUD,^{14,15,26} and its progression during early abstinence.¹⁵

Deep TMS halts the progression of DTI alterations in early abstinence

When comparing FA changes longitudinally in the two groups (TP2 vs. TP1 in active and sham Deep TMS groups independently), we found a strong reduction in the extension of white matter affected by

the progression of FA changes, specifically in the active Deep TMS group, and involving the right frontal lobe (Fig. 3a). We then compared the change in FA (TP2-TP1) between the sham and active Deep TMS groups and found a significant difference in a white matter region belonging to the right frontal lobe (FroL), as shown in (Fig. 3b). In both cases, the regions with preserved FA values in the active group were entirely contained by the volume of brain tissue targeted by the Deep TMS with voltage intensities above 100 V/m, known to be suprathreshold for action potential firing (orange shading in Fig. 3). We then used the mask of the tract-based spatial statistics (TBSS)-defined spot (Fig. 3b) to calculate the mean FA values for each subject and compare the distributions

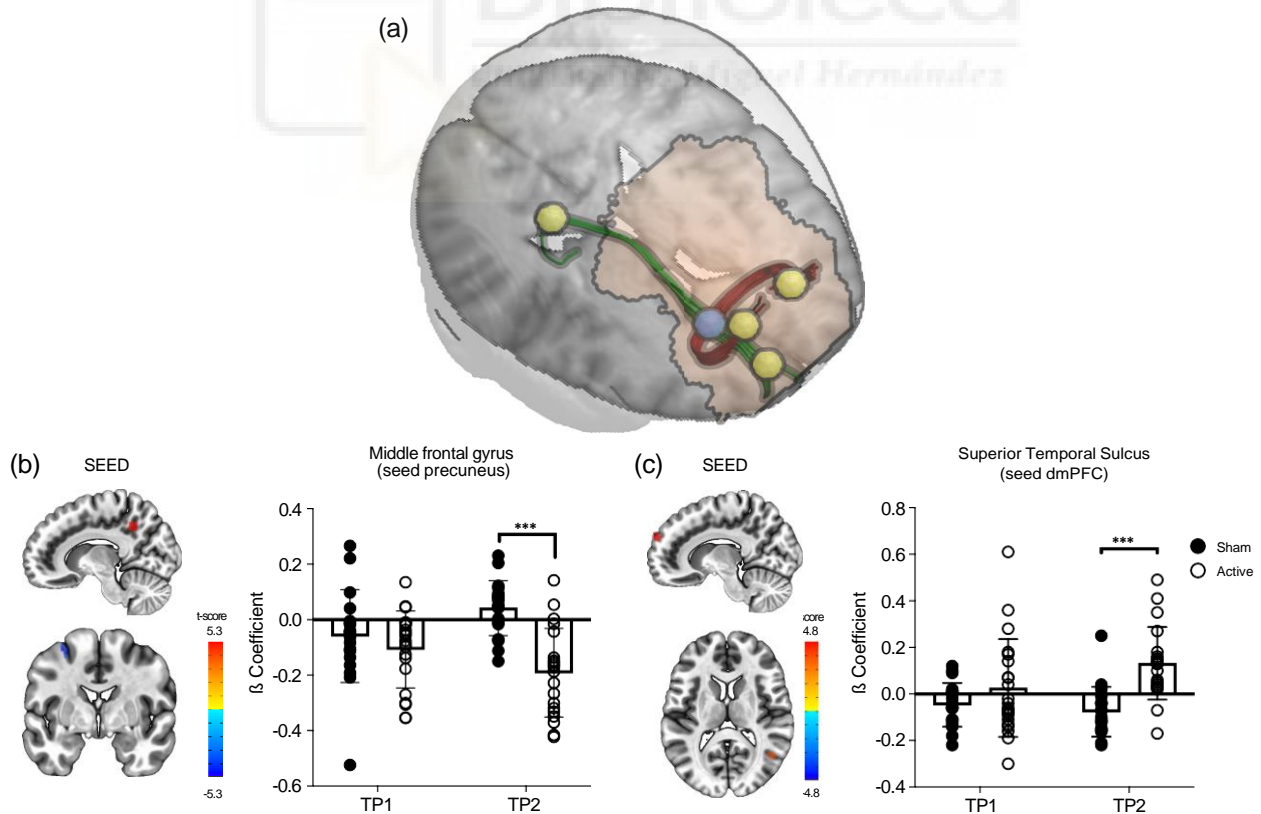


Fig. 5 White matter tracts protected by TMS define terminal fields in the gray matter that show persistent changes in functional connectivity. (a) Cortical targets (yellow spheres) defined by the terminations of white matter streamlines (green: ipsilateral/association; red: bilateral/commissural) passing through the Deep TMS-sensitive spot (blue sphere). Two fiber tracts were consistently identified. (b) Increased negative functional connectivity in the active group at TP2 between the PCCs (defined by the green tract) and middle frontal gyrus. (c) Increased positive functional connectivity in active Deep TMS vs. sham at TP2 between the dmPFC (defined by the green tract) and the pSTS.

across groups. As reported in (Fig. 3c) and (Table S1), FA reduction during abstinence is significant in the sham group ($P < 0.002$), as expected for the progression of microstructural changes, while in the active Deep TMS group, FA is stable after 3 weeks of treatment ($P = 0.82$), indicating that Deep TMS successfully prevented progression. This result remained significant when controlling for baseline differences in FA values.

To obtain insights into the lateralized effect of Deep TMS, we took the area of maximal statistical significance in the right FroL (Fig. 3b) and its counterpart in the left hemisphere (Fig. S1) and calculated the effect size (Cohen's d) of the FA reduction in AUD *vs.* healthy controls. We found significantly larger effect sizes in the right FroL compared to the left (Fig. S1), pointing to a higher vulnerability of white matter microstructure in this hemisphere, at least in the frontal region.

Microstructural changes are paralleled by significant clinical outcome

As indicated above, the sample of subjects used in this study is slightly different from the originally reported cohort,³ due to requirements in the quality of the diffusion-weighted images. Therefore, we reanalyzed the clinical outcome of Deep TMS with the present active and sham Deep TMS groups. As previously reported,³ 3 weeks of Deep TMS treatment reduced craving levels, specifically in the active group (Fig. 4a). Furthermore, craving levels remained lower in the active group 3 months after Deep TMS treatment but not in the sham group, in which craving increased over the follow-up period (Fig. 4b). In good agreement, the average-drinking units (DU) in the follow up period was lower for active *vs.* sham Deep TMS-treated patients (Fig. S2).

Functional connectivity is modulated in the cortical regions defined by the Deep TMS-sensitive axonal tracts

Tractography was used to trace streamlines passing through the white matter spot sensitive to Deep TMS and shown in Fig. 3b. Two fiber tracts were consistently identified across subjects, one of association and one of commissural fibers (green and red tracts, respectively, in Fig. 5a) which were present in at least 70% of the subjects. The terminal fields of these tracts defined four regions of interest in the gray matter. The posterior cingulate cortex (PCC; MNI: 12, -50, 40) and the dorsomedial PFC (dmPFC; MNI: 11, 62, 28), defined by the association fibers and located in posterior and anterior portions of the default mode network, respectively (Fig. 5a); and bilateral regions of the dorsolateral PFC (dlPFC; MNI: 10, 56, 42 and -13, 55, 34), connected by the commissural fibers (Fig. 5a).

Functional connectivity analysis using these regions as seeds showed significant main effects of the group at post-treatment. Follow-up ANOVAs on extracted beta coefficients showed time \times group interactions driven by between-group differences at post-treatment. Specifically, we found increased negative connectivity in active *vs.* sham Deep TMS groups between PCC and the middle frontal gyrus, in the premotor cortex (MNI = -32, -2, 58; 6 voxels; main effect of group $F_{1,35} = 16.5$, $P < 0.001$, $np^2 = 0.32$; time \times group interaction $F_{1,35} = 10.9$, $P = 0.002$, $np^2 = 0.24$; between-group difference at post-treatment, $P < 0.001$, pre-treatment $P = 0.33$). The results were not affected by removal of one outlier (between-group difference at post-treatment, $P < 0.001$, pre-treatment $P = 0.09$; Fig. 5b). Also, we found increased positive connectivity in active *vs.* sham Deep TMS groups between the dmPFC seed and the posterior portion of the superior temporal sulcus (pSTS, MNI = 43, -59, 13; 6 voxels; main effect of group $F_{1,35} = 12.5$, $P = 0.001$, $np^2 = 0.26$; time \times group interaction $F_{1,35} = 5.3$, $P = 0.028$, $np^2 = 0.13$; between-group difference at post-treatment, $P < 0.001$, pre-treatment $P = 0.17$). The results were not affected by the removal of one outlier (between-group difference at post-treatment, $P < 0.001$, pre-treatment $P = 0.33$; Fig. 5c).

Discussion

The fundamental finding of this study is that a protocol of Deep TMS, targeting midline structures of the frontal lobe in patients with AUD to achieve a positive clinical outcome, also had a positive impact on white matter microstructure, which in turn related to persistent changes in functional connectivity. More specifically, we show that the progressive reduction in FA in the white matter of patients with AUD that occurs during early abstinence (see Ref. 15 and confirmed here, Fig. 2) can be arrested by high frequency (10 Hz) Deep TMS applied during 3 weeks of treatment. Furthermore, we show that this structural effect is accompanied by persistent functional changes in the networks connected by the tracts protected by Deep TMS, including the PCC, dmPFC, and dlPFC. Importantly, the same group of actively stimulated patients showed a reduction in craving and relapse scores.³ Our results draw attention to the possibility that induction of white matter plasticity, potentially driven by axonal firing, contributes to the therapeutic effect of Deep TMS in AUD.

Progression of microstructural alterations in white matter

Preventing relapse to heavy drinking is the primary goal of AUD treatment and is particularly challenging in the first months following cessation of use.²⁷ We recently carried out a translational study in patients with AUD and in a rat AUD model, and found a progression of microstructural alterations in white matter that continued for at least 6 weeks after discontinuation of alcohol use.¹⁵ This unexpected result identified a process that appears to be triggered by, or persist after cessation of alcohol use, and that could contribute to the high relapse rates in early abstinence.²⁷ In our previous study,¹⁵ mathematical modeling of water diffusion in distinct biological compartments suggested that this FA reduction could be explained by a decrease in myelin content and/or a glial reactivity in the white matter,¹⁵ two plausible neurobiological mechanisms in AUD.²⁸ We now replicate this result in an independent patient cohort and using a different MRI acquisition protocol. The robustness of this finding is particularly valuable against the background of emerging insights into limited reproducibility in many types of MRI studies with conventional sample sizes.²⁹

The progression of FA changes observed in sham-treated patients was arrested by 3 weeks of active Deep TMS targeting midline structures of the frontal lobe. The Deep TMS-protected white matter regions belonged to frontal lobe fibers, including both association and commissural pathways, and were located in the area of the brain where Deep TMS was expected to produce suprathreshold activation for action potential firing (orange shadow in Fig. 3). Overall, these results provided strong support to the specificity of the finding.

Lateralization of FA changes to the right hemisphere in abstinent AUD subjects has previously been reported in the frontal lobe.³⁰ Here, we replicated this observation, and showed right lateralization of microstructural white matter changes both for the decrease in FA in patients with AUD *vs.* healthy controls (Fig. 2a), and for the protection exerted by Deep TMS within the former group (Fig. 3). The lateralization of these two phenomena may be related. For instance, the lower FA values in the right hemisphere of patients with AUD *vs.* healthy controls (Fig. S1) may have increased the statistical sensitivity to detect a positive TMS effect. Lateralization has also been reported in neuroimaging studies of cue reactivity, including in a meta-analysis,³¹ but fully consistent evidence is not yet available.

What neurobiological process mediates the measured microstructural and clinical improvement?

TMS has demonstrated clinical efficacy on several indications,³² but a mechanistic understanding of these effects is lacking at the level of molecular and cellular physiology. A mechanism of action that has been hypothesized in the context of psychiatric disorders in general, and addiction in particular, is modulation of neuronal activity in brain circuits proposed to be relevant for different psychological processes

(i.e., salience of, and reactivity to drug-associated cues, response inhibition), and modulation of neurotransmitters activity (especially dopamine and glutamate).⁵ However, in addition to neuron-centric interpretations, recent evidence suggests the possibility of other potentially contributing mechanisms.³³ By increasing neuronal firing rates,⁵ high-frequency TMS may recruit activity-dependent increases in myelination, thereby increasing axonal conduction velocity and transmission reliability between brain areas.³³ Previous work has shown increases in FA after TMS treatment in patients with major depression.^{34,35} Our results show a rescue of FA values in white matter tracts connecting structures with a key role in alcohol addiction, such as the dlPFC, dmPFC and PCC,^{36–38} together with signals of decreased craving and relapse. Together, these observations lend support to the possibility that activity-dependent myelination and concomitant rescue of structural connectivity contribute to the therapeutic efficacy of Deep TMS in AUD.

Adaptive myelination, or myelin plasticity, is the process by which electrical activity in axon fibers instructs oligodendrocytes to myelinate active axons, and oligodendrocyte precursor cells (OPCs) to produce more mature oligodendrocytes, increasing axonal conduction velocity.³⁹ Even at low intensity, repetitive TMS has been shown to increase the number of newborn oligodendrocytes in the adult mouse cortex, without altering oligodendrogenesis but rather increasing cell survival and enhancing myelination.⁴⁰ In this study, the authors further reported increases in myelin internode length induced by TMS,⁴⁰ which would translate into faster action potential conduction velocity.⁴¹ In this manner, TMS could serve to repair, at least partially, myelin deficits induced by withdrawal from prolonged alcohol consumption.¹² Of note, the vesicular release of glutamate from the axon within white matter is known to initiate the signaling cascade coupling neuronal activity to OPCs response,^{42,43} while chronic drug use is known to dysregulate glutamate homeostasis in the brain.^{44,45} This opens the possibility that dysfunctional myelin plasticity is a common pathophysiological element of addiction.

In addition, TMS could influence white matter microstructure in patients with AUD by targeting other glial cell types in the stimulated area. TMS has been shown to induce a transient increase in GFAP expression *in vivo*,⁴⁶ and inhibit neurotoxic polarization of astrocytes.³⁴ Application of very low-intensity, but high-frequency TMS following an ischemic injury, or induction of demyelination, appears to induce a reactive microglia phenotype.^{46,47} In contrast, high-intensity, high-frequency TMS attenuates microglial reactivity.⁴⁸ Importantly, inflammation has long been postulated as a contributor to alcohol pathophysiology,⁴⁹ with inflammatory markers correlating with the lifetime of alcohol consumption and age of drinking onset.²⁸ We have reported sustained microglia reactivity during early alcohol abstinence in an animal model of AUD, with a change in cellular morphology consistent with neuroinflammation, and reflected in diffusion-weighted MRI parameters.⁵⁰ The latter finding was translated to patients with AUD.⁵⁰ We recently showed that diffusion-based MRI is sensitive to changes in glia morphology typical of inflammatory conditions, and not only to changes in the myelin content.⁵¹ It is possible that at least part of the benefit of the TMS treatment might be associated with a reduction of pro-inflammatory activation of glial cells. Overall, it seems important to take into account not only the indirect stimulation of myelin plasticity processes *via* heightened action potential firing but also the direct effects of TMS on glial cells.

Linking structural and functional changes to explain positive clinical outcomes

Our previous analysis of functional connectivity in this cohort used hypothesis-driven selection of seed-regions for resting-state fMRI analysis. It found persistent changes in functional connectivity of the mPFC, corresponding to the anterior default mode network, and the dorsal anterior cingulate cortex (ACC), corresponding to the salience network. Connectivity between mPFC and subgenual ACC

was decreased by active Deep TMS, as well as between the dorsal ACC and the caudate.³ In the present study, we analyzed the connectivity of gray matter areas identified as projections of axonal tracts selected based on Deep TMS results. This data-driven approach found four cortical targets. Two of them, the PCC and dmPFC connected through association fibers in the right hemisphere, and the other two corresponded to bilateral regions of the dlPFC connected through commissural fibers. All the regions found in the previous³ as well as the present analysis, have previously been implicated in AUD and are involved in cognitive functions such as inhibitory control, decision-making, planning, cognitive flexibility, and working memory.^{52,53} Recent work studying brain lesions associated with remission of nicotine or alcohol addiction elegantly showed a set of brain regions and tracts conforming an addiction remission network.⁵⁴ Interestingly, the brain regions and tracts protected by Deep TMS stimulation in our study were well contained by this network, linking the structural and functional changes found (Figs 3 and 5) to the observed clinical outcome (Fig. 4 and Ref. 3), and suggesting that the mechanism identified here could generalize to other addictions.

Our fMRI results should be interpreted with caution due to the limited sample size. Nevertheless, they provide support for a functional impact of the identified microstructural changes in white matter. As previously reported,³ functional connectivity changes found in the active Deep TMS group opposed those commonly reported in heavy alcohol users and in AUD.^{55–58} A significant increase in functional connectivity, with negative beta coefficients, was found in active Deep TMS participants between the PCC and a cluster in the middle frontal gyrus and, more specifically, in the frontal eye field (FEF) region of the premotor cortex. The PCC is the posterior node of the default mode network (DMN), a network involved in self-referential processing, task disengagement and “mind-wandering”.⁵⁹ On the contrary, the FEF is one of the nodes of the dorsal attention network (DAN), a network involved in voluntary response selection during attention-demanding tasks.⁶⁰ Typically, the DMN and DAN networks are anti-correlated as they reflect competing cognitive processes, and their spontaneous interaction is crucial in guiding stimulus-independent *versus* attention-driven thought.^{61,62} The increased anticorrelation between DMN and DAN regions in the active group, indicates potential improvement in spontaneous shifting between competing internally *versus* externally oriented states.

We also found an increase in functional connectivity between the dmPFC and pSTS. This is a central connection in the so-called social network, and together with the PCC has been postulated to be involved in internalization, strategic planning, and decision-making in social contexts.⁶³ The dmPFC seems to store longer-term representations of social interactions and guides behavioral strategy, while pSTS integrates visuospatial information, encodes contextual updates and temporary goals.^{64–66} Increased connectivity between these regions may reflect an improvement in social flexibility and the adaptation to contingency changes in social interactions. Whether the strengthened coupling in this network improves social abilities in the patients and contributes to the therapeutic action of Deep TMS, is an appealing interpretation that will deserve further investigation.

Limitations

Our study has several limitations discussed in the previous work.³ First, to definitively establish clinical efficacy of Deep TMS will require replication in a multicenter study with larger sample sizes. Second, although both male and female patients entered the study, the size and sex composition of the sample did not allow for an analysis of potential sex effects, neither on white matter alterations nor the clinical effects. Finally, it is possible that the stimulation protocol could benefit from optimization, depending on the type of process that is most important for the clinical effects. Different neurobiological mechanisms underpinning the observed clinical efficacy of Deep TMS, such as activation of specific neuronal networks, induction of myelin plasticity, or potential anti-inflammatory effects, may benefit from different optimization parameters. Translational work in animal

models may help dissect the different contributions to Deep TMS effects and may help elucidate optimal stimulation protocols.

Conclusions

Despite the limitations discussed above, we believe that the findings presented here represent an important advance. We have combined structural and functional neuroimaging to identify a potential basis for the positive effect of Deep TMS in AUD. We show that Deep TMS is able to arrest the progression of microstructural alterations in white matter with a sustained impact on functional connectivity. A potential broader implication of our findings is that positive effects on white matter microstructure should be considered as potential mediators of Deep TMS effects and that specific effort should be made to identify optimal conditions for achieving this type of effect.

Acknowledgments

This work was supported by the European Union's Horizon 2020 Research and Innovation Program (Grant No. 668863-SyBil-AA [to SC, WHS, AZ and MHe]), the Spanish Ministerio de Ciencia e Innovación, Agencia Estatal de Investigación (PID2021-128158NB-C21 [to SC] and PID2021-128909NA-I00 [to SDS]) and Programs for Centres of Excellence in R&D Severo Ochoa, Agencia Estatal de Investigación (CEX2021-001165-S [to SC and SDS]), the Spanish Generalitat Valenciana Government (PROMETEO Grant CIPROM/2022/15 [to SC] and CIDEAGENT/2021/015 [to SDS]), and the Swedish Research Council (Grant No. 2013-07434 [to MHe]), "la Caixa" Foundation (ID 100010434), fellowship code LCF/BQ/DI18/11660067 and Marie Skłodowska-Curie-COFUND agreement (Grant No. 713673 [to MKS]). We acknowledge support of the publication fee by the CSIC Open Access Publication Support Initiative through its Unit of Information Resources for Research (URICI).

Disclosure statement

AZ is an inventor of deep TMS coils and has a financial interest in BrainsWay, which produces and markets these coils. MHe has received consulting fees, research support, or other compensation from Indivior, Camurus, BrainsWay, Aelis Farma, and Janssen Pharmaceuticals. All other authors report no biomedical financial interests or potential conflicts of interest.

Author contributions

Mohamed Kotb Selim, Silvia De Santis, Irene Perini and Markus Heilig analyzed the data, Markus Heilig, Abraham Zangen, Wolfgang H. Sommer and Santiago Canals supervised the project, Mohamed Kotb Selim, Silvia De Santis and Santiago Canals wrote the first manuscript draft, and all authors reviewed it.

Data availability statement

The data that support the findings of this study are available from the corresponding author, SC, upon a reasonable request.

References

- Griswold MG, Fullman N, Hawley C *et al.* Alcohol use and burden for 195 countries and territories, 1990–2016: A systematic analysis for the global burden of disease study 2016. *Lancet* 2018; 392: 1015–1035.
- Witkiewitz K, Litten RZ, Leggio L. Advances in the science and treatment of alcohol use disorder. *Sci. Adv.* 2019; 5: eaax4043.
- Harel M, Perini I, Kämpe R *et al.* Repetitive transcranial magnetic stimulation in alcohol dependence: A randomized, double-blind, sham-controlled proof-of-concept trial targeting the medial prefrontal and anterior cingulate cortices. *Biol. Psychiatry* 2022; 91: 1061–1069.
- Huerta PT, Volpe BT. Transcranial magnetic stimulation, synaptic plasticity and network oscillations. *J Neuroeng Rehabil.* 2009; 6: 7.
- Gorelick DA, Zangen A, George MS. Transcranial magnetic stimulation in the treatment of substance addiction: TMS as addiction treatment. *Ann. N. Y. Acad. Sci.* 2014; 1327: 79–93.
- Noh NA. Exploring cortical plasticity and oscillatory brain dynamics via transcranial magnetic stimulation and resting-state electroencephalogram. *Malays. J. Med. Sci* 2016; 23: 5–16.
- Pell GS, Roth Y, Zangen A. Modulation of cortical excitability induced by repetitive transcranial magnetic stimulation: Influence of timing and geometrical parameters and underlying mechanisms. *Prog. Neurobiol.* 2011; 93: 59–98.
- Wilson MT, Fulcher BD, Fung PK, Robinson PA, Fornito A, Rogasch NC. Biophysical modeling of neural plasticity induced by transcranial magnetic stimulation. *Clin. Neurophysiol.* 2018; 129: 1230–1241.
- Nave KA. Myelination and support of axonal integrity by glia. *Nature* 2010; 468: 244–252.
- Sampaio-Baptista C, Johansen-Berg H. White matter plasticity in the adult brain. *Neuron* 2017; 96: 1239–1251.
- Fields RD. A new mechanism of nervous system plasticity: Activity-dependent myelination. *Nat. Rev. Neurosci.* 2015; 16: 756–767.
- Rice J, Gu C. Function and mechanism of myelin regulation in alcohol abuse and alcoholism. *Bioessays* 2019; 41: 1800255.
- Pfefferbaum A, Rosenbloom M, Rohlfing T, Sullivan EV. Degradation of association and projection white matter Systems in Alcoholism Detected with quantitative fiber tracking. *Biol. Psychiatry* 2009; 65: 680–690.
- Yeh PH, Simpson K, Durazzo TC, Gazdzinski S, Meyerhoff DJ. Tract-based spatial statistics (TBSS) of diffusion tensor imaging data in alcohol dependence: Abnormalities of the motivational neurocircuitry. *Psychiatry Res.* 2009; 173: 22–30.
- De Santis S, Bach P, Pérez-Cervera L *et al.* Microstructural white matter alterations in men with alcohol use disorder and rats with excessive alcohol consumption during early abstinence. *JAMA Psychiatry* 2019; 76: 749.
- Cox RW. AFNI: Software for analysis and visualization of functional magnetic resonance Neuroimages. *Comput. Biomed. Res.* 1996; 29: 162–173.
- Marx M, Pauly KB, Chang C. A novel approach for global noise reduction in resting-state fMRI: APPECOR. *Neuroimage* 2013; 64: 19–31.
- Fadnavis S, Batson J, Garyfallidis E. Patch2Self: Denoising Diffusion MRI with Self-Supervised Learning. *Advances in Neural Information Processing Systems*, 2020; 33: 16293–16303.
- Leemans A, Jeurissen B, Sijbers J, Jones DK. ExploreDTI: a graphical toolbox for processing, analyzing, and visualizing diffusion MR data.
- Chang LC, Jones DK, Pierpaoli C. RESTORE: Robust estimation of tensors by outlier rejection. *Magn. Reson. Med.* 2005; 53: 1088–1095.
- Smith SM, Jenkinson M, Johansen-Berg H *et al.* Tract-based spatial statistics: Voxelwise analysis of multi-subject diffusion data. *Neuroimage* 2006; 31: 1487–1505.
- Klein A, Andersson J, Ardekani BA *et al.* Evaluation of 14 nonlinear deformation algorithms applied to human brain MRI registration. *Neuroimage* 2009; 46: 786–802.
- Jenkinson M, Beckmann CF, Behrens TEJ, Woolrich MW, Smith SM. FSL. *Neuroimage* 2012; 62: 782–790.
- Tournier JD, Calamante F, Connelly A. Robust determination of the fibre orientation distribution in diffusion MRI: Non-negativity constrained super-resolved spherical deconvolution. *Neuroimage* 2007; 35: 1459–1472.
- Cox RW, Chen G, Glen DR, Reynolds RC, Taylor PA. FMRI clustering in AFNI: False-positive rates Redux. *Brain Connect.* 2017; 7: 152–171.
- Pfefferbaum A, Sullivan EV, Mathalon DH, Shear PK, Rosenbloom MJ, Lim KO. Longitudinal changes in magnetic resonance imaging brain volumes in abstinent and relapsed alcoholics. *Alcohol. Clin. Exp. Res.* 1995; 19: 1177–1191.
- Sinha R. New findings on biological factors predicting addiction relapse vulnerability. *Curr. Psychiatry Rep.* 2011; 13: 398–405.
- Crews FT, Lawrimore CJ, Walter TJ, Coleman LG. The role of neuroimmune signaling in alcoholism. *Neuropharmacology* 2017; 122: 56–73.
- Marek S, Tervo-Clemmens B, Calabro FJ *et al.* Reproducible brain-wide association studies require thousands of individuals. *Nature* 2022; 603: 654–660.
- Harris GJ, Jaffin SK, Hodge SM *et al.* Frontal white matter and cingulum diffusion tensor imaging deficits in alcoholism. *Alcohol. Clin. Exp. Res.* 2008; 32: 1001–1013.
- Schacht JP, Anton RF, Myrick H. Functional neuroimaging studies of alcohol cue reactivity: A quantitative meta-analysis and systematic review: Alcohol cue imaging. *Addict. Biol.* 2013; 18: 121–133.
- Hyde J, Carr H, Kelley N *et al.* Efficacy of neurostimulation across mental disorders: Systematic review and meta-analysis of 208 randomized controlled trials. *Mol. Psychiatry* 2022; 27: 2709–2719.

33. Cullen CL, Young KM. How does transcranial magnetic stimulation influence glial cells in the central nervous system? *Front. Neural Circuits* 2016; 10: 10.
34. Hong Y, Liu Q, Peng M *et al.* High-frequency repetitive transcranial magnetic stimulation improves functional recovery by inhibiting neurotoxic polarization of astrocytes in ischemic rats. *J. Neuroinflammation* 2020; 17: 150.
35. Seewoo BJ, Feindel KW, Won Y *et al.* White matter changes following chronic restraint stress and Neuromodulation: A diffusion magnetic resonance imaging study in Young male rats. *Biol. Psychiatry Glob. Open Sci.* 2022; 2: 153–166.
36. Beylergil SB, Beck A, Deserno L *et al.* Dorsolateral prefrontal cortex contributes to the impaired behavioral adaptation in alcohol dependence. *NeuroImage Clin.* 2017; 15: 80–94.
37. Klenowski PM. Emerging role for the medial prefrontal cortex in alcohol-seeking behaviors. *Addict. Behav.* 2018; 77: 102–106.
38. Zakiniaez Y, Scheinost D, Seo D, Sinha R, Constable RT. Cingulate cortex functional connectivity predicts future relapse in alcohol dependent individuals. *NeuroImage Clin.* 2017; 13: 181–187.
39. Gibson EM, Purger D, Mount CW *et al.* Neuronal activity promotes Oligodendrogenesis and adaptive myelination in the mammalian brain. *Science* 2014; 344: 1252304.
40. Cullen CL, Senesi M, Tang AD *et al.* Low-intensity transcranial magnetic stimulation promotes the survival and maturation of newborn oligodendrocytes in the adult mouse brain. *Glia* 2019; 67: 1462–1477.
41. Saab AS, Nave KA. Myelin dynamics: Protecting and shaping neuronal functions. *Curr. Opin. Neurobiol.* 2017; 47: 104–112.
42. Bergles DE, Roberts JDB, Somogyi P, Jahr CE. Glutamatergic synapses on oligodendrocyte precursor cells in the hippocampus. *Nature* 2000; 405: 187–191.
43. Kukley M, Capetillo-Zarate E, Dietrich D. Vesicular glutamate release from axons in white matter. *Nat. Neurosci.* 2007; 10: 311–320.
44. Javitt DC, Schoepp D, Kalivas PW *et al.* Translating glutamate: From pathophysiology to treatment. *Sci. Transl. Med.* 2011; 3: 102mr2–102mr.
45. Engblom D, Bilbao A, Sanchis-Segura C *et al.* Glutamate receptors on dopamine neurons control the persistence of cocaine seeking. *Neuron* 2008; 59: 497–508.
46. Raus S, Selaković V, Manojlović-Stojanoski M, Radenović L, Prolić Z, Janać B. Response of hippocampal neurons and glial cells to alternating magnetic field in gerbils submitted to global cerebral ischemia. *Neurotox. Res.* 2013; 23: 79–91.
47. Fang ZY, Li Z, Xiong L, Huang J, Huang XL. Magnetic stimulation influences injury-induced migration of white matter astrocytes. *Electromagn. Biol. Med.* 2010; 29: 113–121.
48. Kim JY, Choi GS, Cho YW, Cho H, Hwang SJ, Ahn SH. Attenuation of spinal cord injury-induced Astroglial and microglial activation by repetitive transcranial magnetic stimulation in rats. *J. Korean Med. Sci.* 2013; 28: 295.
49. Pascual M, Montesinos J, Guerri C. Role of the innate immune system in the neuropathological consequences induced by adolescent binge drinking. *J. Neurosci. Res.* 2018; 96: 765–780.
50. De Santis S, Cosa-Linan A, Garcia-Hernandez R *et al.* Chronic alcohol consumption alters extracellular space geometry and transmitter diffusion in the brain. *Sci. Adv.* 2020; 6: eaba0154.
51. Garcia-Hernandez R, Cerd'án Cerd'a A, Trouve Carpena A *et al.* Mapping microglia and astrocyte activation in vivo using diffusion MRI. *Sci. Adv.* 2022; 8: eabq2923.
52. Cavanna AE, Trimble MR. The precuneus: A review of its functional anatomy and behavioural correlates. *Brain* 2006; 129: 564–583.
53. Ribeiro EA, Scarpa JR, Garamszegi SP, Kasarskis A, Mash DC, Nestler EJ. Gene network dysregulation in dorsolateral prefrontal cortex neurons of humans with cocaine use disorder. *Sci. Rep.* 2017; 7: 5412.
54. Joutsa J, Moussawi K, Siddiqi SH *et al.* Brain lesions disrupting addiction map to a common human brain circuit. *Nat. Med.* 2022; 28: 1249–1255.
55. Camchong J, Stenger A, Fein G. Resting-state synchrony during early alcohol abstinence can predict subsequent relapse. *Cereb. Cortex* 2013; 23: 2086–2099.
56. Fede SJ, Grodin EN, Dean SF, Diazgranados N, Momenan R. Resting state connectivity best predicts alcohol use severity in moderate to heavy alcohol users. *NeuroImage Clin.* 2019; 22: 101782.
57. Kohno M, Dennis LE, McCready H, Hoffman WF. Executive control and striatal resting-state network interact with risk factors to influence treatment outcomes in alcohol-use disorder. *Front. Psych.* 2017; 8: 182.
58. Vergara VM, Liu J, Claus ED, Hutchison K, Calhoun V. Alterations of resting state functional network connectivity in the brain of nicotine and alcohol users. *Neuroimage* 2017; 151: 45–54.
59. Gusnard DA, Raichle ME. Searching for a baseline: Functional imaging and the resting human brain. *Nat. Rev. Neurosci.* 2001; 2: 685–694.
60. Corbetta M, Shulman GL. Control of goal-directed and stimulus-driven attention in the brain. *Nat. Rev. Neurosci.* 2002; 3: 201–215.
61. Fox MD, Snyder AZ, Vincent JL, Corbetta M, Van Essen DC, Raichle ME. The human brain is intrinsically organized into dynamic, anticorrelated functional networks. *Proc. Natl. Acad. Sci. U. S. A.* 2005; 102: 9673–9678.
62. Anderson JS, Ferguson MA, Lopez-Larson M, Yurgelun-Todd D. Connectivity gradients between the default mode and attention control networks. *Brain Connect.* 2011; 1: 147–157.
63. Adolphs R. The social brain: Neural basis of social knowledge. *Annu. Rev. Psychol.* 2009; 60: 693–716.
64. McDonald KR, Pearson JM, Huettel SA. Dorsolateral and dorsomedial prefrontal cortex track distinct properties of dynamic social behavior. *Soc. Cogn. Affect. Neurosci.* 2020; 15: 383–393.
65. Konovalov A, Hill C, Daunizeau J, Ruff CC. Dissecting functional contributions of the social brain to strategic behavior. *Neuron* 2021; 109: 3323–3337.e5.
66. Jamali M, Grannan BL, Fedorenko E, Saxe R, B'aez-Mendoza R, Williams ZM. Single-neuronal predictions of others' beliefs in humans. *Nature* 2021; 591: 610–614.

Supporting Information

Additional supporting information can be found online in the Supporting Information section at the end of this article.

Chapter 27

Brain Microstructure in Alcohol Addiction: Characterization of Diffusion-Based MRI Biomarkers, Neuropathological Substrates, and Functional Consequences

Silvia De Santis, Mohamed Kotb Selim, and Santiago Canals

Abstract Alcohol consumption is associated with structural alterations in the brain parenchyma. Understanding the longitudinal brain transformations that occur from an alcohol naïve state to alcohol addiction, through cycles of consumption, abstinence and relapse, is crucial to progress towards effective treatments. Magnetic Resonance Imaging, and in particular diffusion-weighted approaches, have been a breakthrough for neuroscience, neurology and psychiatry due to their ability to access different aspects of brain anatomy in a non-invasive and longitudinal way. In the last 20 years, this technique has been instrumental in characterizing brain alterations associated to alcohol consumption.

In this chapter, we will first introduce diffusion-weighted Magnetic Resonance Imaging and its most widely adopted formulation, Diffusion Tensor Imaging, describing its utility to look at brain microstructure and its most used biomarkers, mean diffusivity and fractional anisotropy; we will then focus on the importance of diffusion tensor imaging in alcohol use disorders, describing the most salient aspects of the pathology that can be captured and dissected; next, we will discuss several recent advances in the field that were possible thanks to the use of diffusion tensor imaging. Finally, we will disclose important limitations of the technique that must be taken into account in the interpretation of alcohol-driven alterations, challenging the conventional view that diffusion tensor imaging can discern between “healthy” and “damaged” microstructure under all circumstances.

Keywords Alcohol use disorder · Diffusion-weighted MRI · Mean diffusivity · Fractional anisotropy · Microstructural integrity · Extracellular space

S. De Santis · M. K. Selim · S. Canals (✉)
Instituto de Neurociencias, CSIC/UMH, San Juan de Alicante, Alicante, Spain
e-mail: dsilvia@umh.es; mselem@umh.es; scanals@umh.es

Introduction

Magnetic Resonance Imaging (MRI), and particularly diffusion weighted approaches, were a breakthrough for neuroscience, neurology and psychiatry due to their ability to access distinct aspects of brain anatomy non-invasively and without the use of ionizing radiation and/or contrast agents. Being non-invasive and translational, diffusion-weighted MRI can be used to monitor brain changes over time *in vivo* in humans and in animal models, giving access to fine microstructural properties of the brain parenchyma, and has proven pivotal to characterize brain changes associated with alcohol consumption.

In this chapter, we will first introduce diffusion-weighted MRI and its most widely adopted formulation, diffusion-tensor imaging (DTI), describing its utility to look at brain microstructure; we will then focus on the importance of DTI in alcohol use disorders, describing the most salient aspects of the pathology that DTI can capture and dissect; next, we will discuss several recent advances in the field that were possible thanks to the use of DTI. Finally, we will disclose important limitations of the technique which need to be taken into account in the interpretation of alcohol-driven DTI alterations, challenging the conventional view that DTI can discern between “healthy” and “damaged” microstructure under all circumstances. Throughout the chapter, we will focus on the so-called uncomplicated alcohol use disorder, i. e., in absence of other degenerative conditions associated with alcohol, like the Wernicke-Korsakoff syndrome.

Measuring Water Diffusivity Non-invasively Through Diffusion-Weighted MRI

At absolute temperatures higher than zero Kelvin, water molecules are in constant motion due to their intrinsic thermal energy, colliding with each other and with the obstacles they find in their path. Due to such collisions, the trajectories followed by the particles are random, so their motion is referred to as “random walk”. Within living organisms, soft tissues like the brain contain a high percentage of water, and the diffusion trajectories of the water molecules are influenced by the shape and orientation of the structures in which they are embedded (e.g., axons, cell bodies, glia, . . .). Through the diffusion-weighted MRI sequence, a label is imparted to hydrogen nuclei (by manipulating the phase of the transverse magnetization), and the displacement of the water molecules is characterized by reading this label at a later time; normally, in the milliseconds range. The larger the signal attenuation recorded between the two time points, the larger the motion that has occurred. In this way, the diffusion of water during the allowed diffusion time can be quantified.

One of the main advantages of diffusion-weighted MRI is the ability to highlight what is known as diffusion *anisotropy*, that is, when molecules exhibit different diffusion properties along different orientations in space. For example, the axonal

bundles that constitute the white matter of the brain present a structure dominated mostly by cylindrical elements, the axons. Since the cell membranes are largely impermeable to water, the movement of water in these structures is less hindered parallel to the fiber bundle than in the perpendicular direction. If one were to measure water diffusion parallel to the fibers, this would appear much faster than perpendicular to them.

To quantify anisotropy, as well as the average water diffusion in the tissue, several indices can be extracted from the diffusion-weighted MRI measurements; the most popular are the *fractional anisotropy*, FA, and the *mean diffusivity*, MD. While MD quantifies the average water displacement in the tissue and is measured in square meters per second (m²/s), FA is a dimensionless index ranging from 0 (no anisotropy) to 1 (maximum anisotropy). The mathematical framework used to define FA and MD is detailed in Box 27.1.

Box 27.1

The simplest mathematical structure capable of accounting for diffusion anisotropy in a 3D environment is a tensor. In the diffusion-tensor imaging (DTI) framework, water diffusion in each voxel is modeled with a 3 × 3 diffusion tensor D .

$$D = \begin{bmatrix} D_{xx} & D_{xy} & D_{xz} \\ D_{yx} & D_{yy} & D_{yz} \\ D_{zx} & D_{zy} & D_{zz} \end{bmatrix}$$

D is constituted by 9 components, but only 6 of them are independent, due to the tensor symmetry. For this reason, to measure the diffusion tensor, a minimum of 6 measures along different orientation, plus one measure without diffusion weighting, are needed, although to have a better signal-to-noise ratio it is highly recommended to use more [1]. From the eigen-decomposition of D , different scalar indices can be obtained, like the mean diffusivity (MD) and the fractional anisotropy (FA), as defined in the following expressions:

$$MD = \frac{\lambda_1 + \lambda_2 + \lambda_3}{3}.$$

$$FA = \sqrt{\frac{3}{2} \frac{\sqrt{(\lambda_1 - MD)^2 + (\lambda_2 - MD)^2 + (\lambda_3 - MD)^2}}{\sqrt{\lambda_1^2 + \lambda_2^2 + \lambda_3^2}}}.$$

The mean diffusivity is the mean of the three diffusivities measured along the eigenvectors and is interpreted as the average water diffusivity in the measured volume (the voxel in MRI). Fractional anisotropy is proportional to the standard deviation of the diffusivities measured along the eigenvectors divided by their root mean squared; importantly, fractional anisotropy quantifies the

degree of anisotropy of the media. Anisotropic tissues have fractional anisotropy values closer to 1, meaning that the diffusion of water molecules in such environments occurs predominantly in one orientation, and can be visualized as an ellipsoid, while isotropic tissues have fractional anisotropy values closer to 0, meaning that the diffusion is similar in all directions, and can be visualized as a sphere [2]. These scalars are translationally invariant, meaning that they do not depend on the specific orientations along which the diffusion is measured. This makes their use ideal as quantitative biomarkers of brain microstructure.

Among the diffusion-based indices extracted from MRI, fractional anisotropy has probably become the most popular in neurology and psychiatry, with its reduction commonly interpreted as a marker of loss of white matter integrity [3]. However, many factors contribute to determining the value of the resulting fractional anisotropy, such as the amount of myelin, axonal diameter, axonal density and fiber dispersion. Therefore, it is not straightforward to assign a specific tissue configuration or biological state to a measured fractional anisotropy change, as discussed below. Figure 27.1 illustrates a typical diffusion-weighted MRI acquisition and processing pipeline.

It is important to note that the direction of the greatest diffusivity, i.e., the orientation of the principal eigenvector, can be interpreted as an estimate of the fiber orientation in the white matter under the assumption that when a number of neuronal axons are aligned along a common axis, the diffusion of water molecules will be hindered to a greater extent across this axis than along it [7]. By integrating these estimates across the whole brain white matter, it is possible to generate a 3D representation of the major axonal bundles. These are the basis of the technique called *tractography*, which quickly became a powerful tool to look at brain anatomy. Several more advanced non-tensor approaches have been introduced in recent years to extract the fiber orientation distribution; each of these models has its own strengths and pitfalls, nevertheless, a comparative discussion is outside the scope of this chapter.

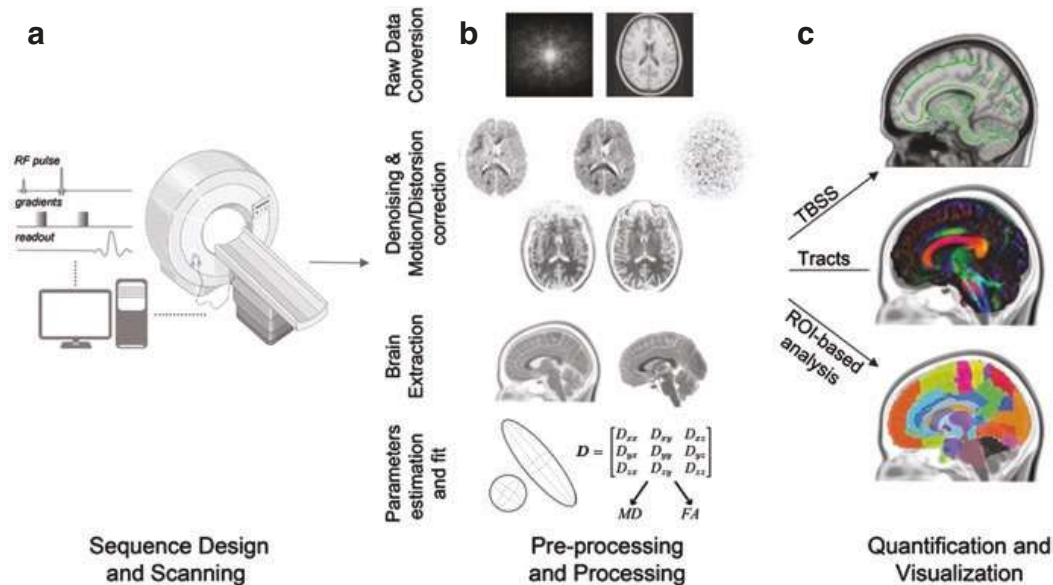


Fig. 27.1 Diffusion-weighted MRI acquisition and processing pipeline. **(a)** Diffusion-weighted MRI experiments normally encompass several acquisition and processing steps. The diffusion-weighted MRI sequence is tuned according to the specific need of the experiment in terms of diffusion weighting (quantified by the *b-value*) which, by defining the time allowed for the labeled water molecule to diffuse and the range of diffusivities on which the sequence focuses, weights the contribution of the different tissue compartments to the diffusion measurement (e.g., diffusion in the intracellular vs. extracellular space). Other important parameters are the number of gradient orientations, which define the directions in which diffusion will be quantified; or the image resolution, which is a compromise between the capabilities of the MRI system to acquire data with good signal-to-noise ratio and the time devoted to acquiring them, and which determines the voxel size. **(b)** After the desired diffusion-weighted MRI sequence is defined and acquired, the preprocessing might involve denoising, motion and distortion corrections, brain extraction and normalization to other contrasts. Then, the desired diffusion model is applied, and the data are visualized, ready for the statistics of choice. **(c)** Statistical analysis normally involves voxel-wise approaches like the widely adopted tract-based spatial statistics [4], or region-of-interest approaches like those based on parcellated brains in standard space [5], or on tractography in single subject space [6]

Neuropathological Substrate and Utility of DTI Biomarkers in Alcohol Use Disorders

Difficulty walking and talking, blurred vision, slowed reactivity: clearly, alcohol affects the brain, but while some of these impairments quickly resolve when alcohol is discontinued, chronic drinking produces the accumulation of deficits that persist into sobriety, generating a disability with great impact on society. As such, alcohol neurotoxicity has been widely investigated, with the goal of achieving a mechanistic understanding of this complex behavioral and medical condition.

The histopathological substrate underlying the well-characterized brain shrinkage in alcohol use disorder (AUD) patients involves changes in both myelination and axonal integrity, as well as region-selective neuronal loss [8]. Dendritic and

synaptic changes have also been well documented in people with alcohol addiction [9]. Importantly, alcohol exposure not only affects neurons, but also the development, morphology, physiology and gene expression in astrocytes, oligodendrocytes and microglia cells [10].

In this context, neuroimaging techniques like DTI-based approaches represent a unique tool to assess alcohol-induced brain alterations, being sensitive to fine details of the brain parenchyma's microstructure. DTI can detect changes in both myelination and axonal integrity in white matter with high sensitivity [11]. While the technique is preferentially used to look at white matter microstructure, there are also numerous applications to grey matter morphology, where the diffusion of water molecules is expected to sense and reflect the complex geometry of a tissue containing neurons, their dendrites and axons with different levels of myelination and orientations, and glial cells of different morphologies [12, 13].

A major feature of DTI is that it affords relatively high resolution compared to other whole brain imaging techniques, going from 2–3 mm in humans, to few hundreds of microns in animals. Furthermore, being non-invasive, the technique allows for longitudinal studies. In the context of alcoholism, this means that the dynamic course of the disease, going through periods of drinking, sobriety, and relapse, can be followed [14].

Another important feature of DTI, shared with the other MRI-based techniques and sometimes underestimated, is the possibility to perform translational studies. DTI can be applied across species, in humans and animal models. This important feature allows scientists to interrogate the causality of alcohol-related brain alterations in well-controlled animal experiments, something that is difficult to achieve in studies with AUD patients where alcohol-induced damage almost inevitably coexists with that produced by tobacco and other drugs of abuse, medication and other comorbid factors. A reverse translational approach, in which alterations found with DTI in patients find an equivalent counterpart in animal models, and the latter are used to investigate the underlying neurobiological mechanism, has proven successful in bringing causality to AUD [15, 16].

Multiple DTI metrics can be combined, and they can also be combined with other imaging and non-imaging measures, using machine learning frameworks. Pioneer work in this field has shown that multi-parametric approaches including DTI have high potential to serve as valuable biomarkers for early diagnosis and response to treatment in AUD, by demonstrating high accuracy and precision in classifying baseline, alcohol drinking and abstinence states, and even the effect of medication with naltrexone in an animal model [17]. Those multimodal studies pointed to water diffusion measures as the more informative feature to differentiate between AUD associated states. Recently, machine learning algorithms using structural MRI data have also been able to predict in adolescents future patterns of alcohol binge-drinking, providing important information of the substrate that may favor the development of alcohol addiction [18].

Regional Specificity of Altered Diffusivity in AUD: Frontal White Matter Vulnerability

By mapping DTI parameters in AUD versus age- and sex-matched controls, a pattern of region-specific vulnerability emerged. In white matter, frontal and dorsal tracts consistently show the greatest abnormalities in people with alcohol addiction relative to controls, while more posterior and ventral bundles were relatively spared [19, 20]. A recent meta-analysis including over 900 subjects identified four significant clusters of convergent microstructural white matter alterations in AUD patients that were assigned to the genu and body of the corpus callosum, anterior and posterior cingulum, fornix, and the right posterior limb of the internal capsule [21]. Genu and fornix seem to be particularly vulnerable tracts in alcohol use disorder, showing alterations after a single episode of binge drinking and suggesting potential for rapid neuroplasticity [22]. Importantly, these same axonal bundles are also preferentially affected in rat models of AUD longitudinally investigated with DTI [15, 20], which in addition to attributing a causal role to alcohol (see above), suggest the existence of some fundamental biological principle, generalizable across species, that determines heterogeneous white matter vulnerability to alcohol. White matter tracts showing alterations in the AUD population compared to controls are shown in Fig. 27.2.

The described microstructural alterations are expected to have functional implications. Abnormalities in the white matter tracts connecting regions of the

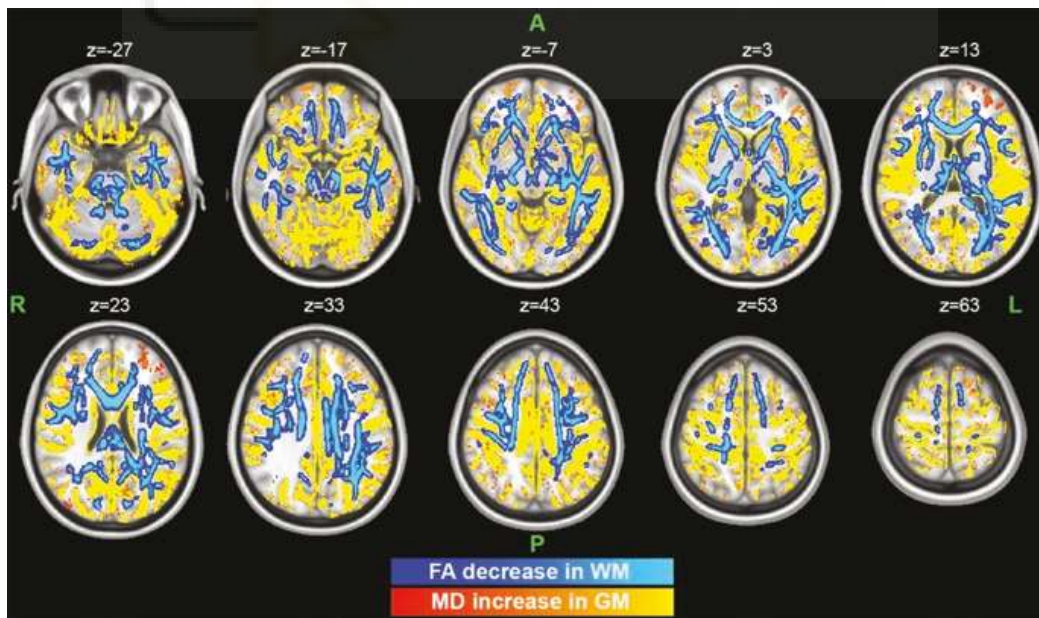


Fig. 27.2 White matter regions of significantly reduced fractional anisotropy (FA) in AUD vs. controls (blue, filled with the `tbss_fill` routine) according to the cohort in [15], and grey matter regions of significantly increased mean diffusivity (MD) in AUD vs. controls (red-yellow, $p < 0.05$) in the same cohort [23]

mesolimbic pathway, known to play an important role in the rewarding effects of drugs, are associated with higher impulsivity and alterations of the reward network [24]. The fimbria, for instances, is the main pathway connecting the hippocampus and the prefrontal cortex and plays a fundamental role in memory formation and extinction, executive function and emotional processing [25]; thus, the high vulnerability of the fimbria white matter to alcohol drinking might be an important contribution to the observed inability of AUD patients to suppress maladaptive memories, and the display of behavioral inflexibility [20]. More generally, the fact that alcohol consumption causes heterogeneous alterations of white matter tracts could be interpreted in functional terms as the basis for the observed imbalances between fMRI brain networks, some of them showing decreases in functional coupling and others increases, possibly reflecting a new functional equilibrium characteristic of an AUD state (allostasis).

Finally, the patterns of region-specific white matter vulnerability are not limited to AUD; negative associations between alcohol intake and brain microstructure are already apparent in individuals consuming an average of only one to two daily alcohol units, and become stronger as alcohol intake increases, in a region-specific manner, with the fornix and the corpus callosum featuring prominently as areas associated to the largest effect sizes [26].

DTI in Grey Matter: Functional Consequences

While DTI has traditionally been used to assess white matter integrity, it can be also used to look at microstructure in grey matter. The preferred biomarker in grey matter is the mean diffusivity, due to the low degree of anisotropy which characterizes grey matter microstructure. Microstructural information has the potential to complement and, most importantly, anticipate macroscopic alterations like volume and cortical thickness changes, which are normally employed as surrogate markers of neuronal degeneration, but which are believed to pick up alterations only when these are in a relatively advanced state [27].

Higher mean diffusivity was detected in frontal, temporal and parahippocampal grey matter, and in the cerebellum of alcohol dependent patients compared to controls. Low verbal episodic memory performance was associated with higher mean diffusivity but not shrinkage in parahippocampal areas, in frontal cortex and in the left temporal cortex, suggesting that regional microstructural but not macrostructural alteration of the brain parenchyma might be responsible, at least in part, for episodic memory deficits in alcohol dependence [28]. Another study measured increased mean diffusivity in the medial prefrontal cortex of rats exposed to chronic intermittent ethanol vapor, associated to deficits in retrieval and recall of fear memories, and whose neuropathological substrate included demyelination and mitochondrial damage [29].

A recent study comparing water diffusivity in the grey matter of AUD patients and a rat model of chronic voluntary drinking in a two-bottle free-choice paradigm

[23], showed widespread increases in mean diffusivity in both species. Grey matter areas showing alterations in the AUD population compared to controls are shown in Fig. 27.2. The authors demonstrated that 1 month of chronic alcohol drinking (4–6 g/kg/day) is sufficient to trigger the mean diffusivity effect in the rat model and in both, humans and rats, higher mean diffusivity persisted during abstinence. However, as we have mentioned already and will discuss further in the last section, interpreting DTI findings in biological terms is challenging, as all water compartments (i.e., intracellular and extracellular) contribute to determine mean diffusivity. To answer this question, the authors turned into the animal model and, using an invasive technique called iontophoresis, they quantified with high precision the diffusion in the extracellular space of the brain. Together with a small decrease in the total volume fraction, they found a large and significant reduction in the extracellular space tortuosity triggered by alcohol drinking, this is, a reduction in the diffusion barriers. The reduction in tortuosity was sufficient to explain the increase in mean diffusivity measured with DTI and suggested a significant change in the manner in which solutes can diffuse through the extracellular space of the brain.

To study the possible functional impact of the increased mean diffusivity in the grey matter of alcohol-exposed individuals, a mathematical model was used to investigate how the above tortuosity change might influence the diffusion of extrasynaptically released neurotransmitters, such as dopamine [23]. The authors found a marked increase in the spatial reach of the released neurotransmitter, a potentiation of volume neurotransmission, so that a same amount of dopamine will diffuse farther and in greater concentration in the same amount of time [23]. The authors speculated that a synergistic combination of a primarily weak reinforcer like ethanol, which is known to raise dopamine levels (albeit modestly), with progressively enhanced volume neurotransmission due to increased extracellular diffusivity, might comprise a novel mechanism to explain the slow onset but potent addictive effect of alcohol. Further experimental work will be necessary to confirm or refute this hypothesis. The impact of mean diffusivity changes on other important biochemical processes heavily relying on extracellular space diffusivity, like the clearance of metabolic byproducts, might also be interesting to investigate. This result already serves as an example to illustrate the mechanistic insight that can be gained from investigating the neurobiological basis of DTI biomarkers.

Progression of Diffusivity Alterations During Early Abstinence

Longitudinal DTI acquisitions have been used to measure microstructural integrity in the white matter of abstinent AUD patients from 1 to a few years after the last drinking episode [30, 31]. These studies reported the recovery of DTI values towards control levels in long-term abstinent subjects, providing a microstructural substrate for the observed clinical improvement. However, AUD is associated with a chronically relapsing-remitting course over lifetime, and most individuals treated for AUD are known to relapse to hazardous alcohol

consumption within just 6 months of treatment [32]. What happens then with the microstructure of the brain during the most critical early phase of alcohol abstinence? To answer this question, a recent DTI study acquired longitudinal DTI data in AUD patients and rat models thereof at different time intervals from 2 to 6 weeks, during early abstinence [15]. Interestingly, in both species it was shown during this period that, far from recovering, the reduction in fractional anisotropy measured in the white matter tracts progressed, becoming reduced after 3 weeks of abstinence, and even further reduced at 6 vs. 3 weeks of abstinence. The progression during early abstinence suggests the existence of an underlying process that evolves soon after cessation of alcohol consumption, challenging the conventional idea that the microstructural damage starts to repair immediately after discontinuing alcohol drinking.

What might this process be? Answering this question will require further experimental work, but a first clue can perhaps be seen in the change in extracellular space tortuosity found in the grey matter [23]. In that study, it was shown that the reduction in tortuosity explaining the increased water mean diffusivity in the grey matter was associated with a microglial response. Microglial cells retracted their cellular processes and engrossed the cell body acquiring an amoeboid morphology. This change did not affect other glial subtypes, extracellular matrix proteins or neuronal density. The morphological change in microglia explained the decrease in diffusion barriers and the increased mean diffusivity. Indeed, reactivation of microglia independently of alcohol drinking with lipopolysaccharide, or their elimination with the CSF1R inhibitor PLX5622, provided causal evidence to support their effect on diffusion [23]. A role of microglial cells and neuroinflammation in the neurotoxic effects of alcohol has long been proposed [33]. Taken together, these results suggest that the biological process underlying the progression of microstructural alterations during early abstinence could be an inflammatory response, maybe triggered by alcohol withdrawal.

Overall, this result, besides proving that DTI can provide unique information to understand the neuroadaptations occurring during abstinence, puts this critical phase in the spotlight as a central target for therapeutic interventions [16].

Sex Differences in Alcohol Use Disorder

While alcohol neuroimaging investigation has been affected, like many other fields, by the systematic underrepresentation of female subjects, especially in basic research, there is a remarkable convergence of evidence pointing towards a sex effect in AUD, confirmed by DTI studies. In addition, over the last 10 years, rates of alcohol use disorder have increased in women by 84%, while they have increased by 35% in men [34], highlighting even more the importance of including both sexes in AUD studies. The drawback of this necessary change of paradigm is that including an additional factor might further reduce power in neuroimaging studies, many of which have by design small sample size.

Pioneer work showed that AUD women have more DTI features of white matter degradation than men of the same age in several fiber bundles [19]. Also in animal models, female rats have been reported to be more affected in a chronic intermittent ethanol paradigm, as shown by greater reduction of fractional anisotropy in the fornix. This vulnerability was explained by higher initial blood alcohol levels in females [35]. In women but not in men, more frequent binge drinking was associated with lower fractional anisotropy values, a result that was interpreted as evidence of higher vulnerability to alcohol in females [36]. However, a recent study using multimodal brain imaging in a large general population (36,678 generally healthy middle-aged and older adults from the UK Biobank) [26], found consistent associations between daily alcohol units consumed and lower fractional anisotropy values in several white matter tracts, with the strongest effects in the fornix, but no significant or weak association to sex. Therefore, while sex seems to be an important factor to develop brain damage in AUD, the interaction between sex and less severe levels of alcohol drinking will require further clarification. Furthermore, women and men's white matter microstructure is affected differently by age [37], suggesting that longitudinal studies involving larger cohorts than those normally employed in neuroimaging studies might be necessary to characterize the complex interaction between AUD and age in a sex-specific manner.

Finally, the reported difference in DTI features across sexes in AUD are not limited to differences in effect size. Indeed, opposite patterns of DTI changes between sexes have been also reported. Fractional anisotropy is systematically reduced in AUD males compared to controls but, interestingly, seems to be increased in some fiber tracts in AUD women [38, 39]. Before going into interpreting these apparent discrepancies, it is important to remember what is being measured with DTI and how it relates to the underlying neurobiological substrate. While the classical view of DTI associates a reduced fractional anisotropy to impaired microstructure (demyelination and axonal damage), as discussed in the next paragraph, other factors are contributing; according to this rationale, it is not possible to univocally associate an increase in fractional anisotropy to an improvement in the quality of microstructure.

DTI Limitations and Caveats in the Interpretation of DTI Biomarkers in AUD

DTI-derived measures are affected by at least two limitations: the lack of specificity to sub-compartments of the tissue, meaning that very different neuroanatomical configurations can result in the same measured values of water diffusion [40], and the limited utility in structures like grey matter lacking macroscopic anisotropy.

Given the lack of specificity of DTI measures, interpreting the underlying neurobiological substrate that is causing the observed change is challenging. As mentioned earlier, postmortem studies consistently report compromised white matter

integrity in AUD that could explain, at least in part, the observed DTI changes. In these patients, the reduction in white matter volume is normally explained as a process of demyelination and axonal loss produced by the regional neuronal loss that can occur especially in the dorsal frontal cortex [41]. Alcohol drinking induces loss of mainly small fibers, myelin irregularity and segmental de/remyelination [42], accompanied by neuroinflammation. Also, the possibility of excessive intracellular and extracellular fluids accumulation has been proposed to explain some DTI changes in AUD vs. age matched controls [43].

However, recent *in silico* data challenged the idea that it is possible to infer the specific microstructural alteration causing the observed pattern of DTI changes. It was shown that a different balance between the restricted, hindered and isotropic water pools in the tissue can explain the DTI alterations found in AUD patients with totally different neurobiological underpinnings, simply depending on the underlying geometry [15]. Importantly, the increase in the proportion of the isotropic water pool, which can be a model for both an accumulation of fluids in the extra-cellular space as well as a glial reaction, results in an increase of fractional anisotropy in areas of white matter with single fibers, and a decrease of fractional anisotropy in areas of crossing fibers. Overall, the observed changes in fractional anisotropy across the different phases of AUD can thus be equally explained by progressive myelin damage, axonal loss, and/or a glial/cellular reaction, for instance, during an ongoing inflammatory process. In addition, the same biological phenomenon can impact with opposite trends in DTI (fractional anisotropy either increasing or decreasing) depending on the affected brain region (areas of predominantly single fiber vs. areas of crossing fibers). Possible neuropathological substrates generating fractional anisotropy alterations are illustrated in Fig. 27.3.

All in all, DTI is non-specific to neurobiological correlates of brain tissue, and needs to be complemented with other approaches to dissect cell-specific patterns of alterations in AUD. For example, diffusion-weighted MRI has been shown to be sensitive to axonal density [44] and diameter in white matter [45]; DTI measures can be complemented with myelin specific sequences like those based on magnetization transfer [46].

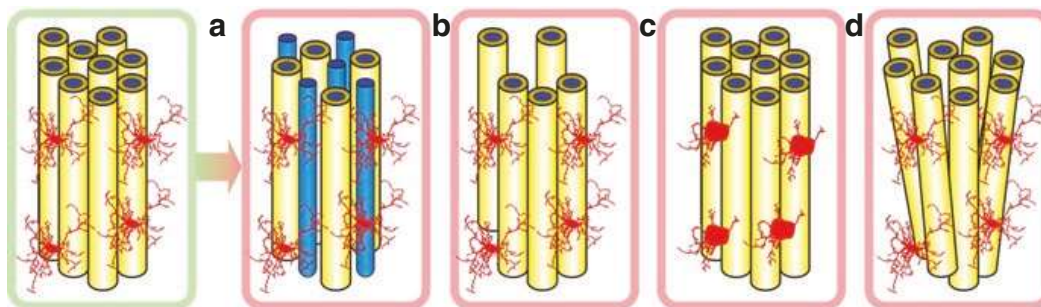


Fig. 27.3 Possible biological substrates driving changes in fractional anisotropy: demyelination (a), axonal loss (b), glia morphological changes (c) and increased fiber dispersion (d). Myelin is shown in yellow, axons in blue and microglial cells in red

The other major limitation of DTI is that, given the low anisotropy of grey matter tissue, fractional anisotropy is a poor predictor of microstructural integrity in grey matter. As detailed earlier in the chapter, mean diffusivity has been successfully used to highlight grey matter alterations in AUD; however, it suffers from the same lack of specificity of other DTI parameters. A recent approach based on stereotaxic injections of neurotoxins affecting selectively glia, myelin and neuronal compartments showed that mean diffusivity is highly sensitive to changes, but poorly specific [13], with similar effect sizes in demyelination, inflammation and degeneration. As such, to achieve augmented specificity, it is advisable to choose more advanced, grey-matter specific diffusion-weighted MRI sequences focusing on neurite morphology [47] or inflammation [13]. The drawback here is that, for the time being, such advanced techniques entail longer and more complex data acquisitions.

References

1. Jones DK, Basser PJ. Squashing peanuts and smashing pumpkins? How noise distorts diffusion-weighted MR data. *Magn Reson Med*. 2004;52:979–93. <https://doi.org/10.1002/mrm.20283>.
2. Beaulieu C. The basis of anisotropic water diffusion in the nervous system—a technical review. *NMR Biomed*. 2002;15:435–55. <https://doi.org/10.1002/nbm.782>.
3. Jones DK, Knösche TR, Turner R. White matter integrity, fiber count, and other fallacies: The do's and don'ts of diffusion MRI. *NeuroImage*. 2013;73:239–54. <https://doi.org/10.1016/j.neuroimage.2012.06.081>.
4. Smith SM, Jenkinson M, Johansen-Berg H, Rueckert D, Nichols TE, Mackay CE, Watkins KE, Ciccarelli O, Cader MZ, Matthews PM, Behrens TEJ. Tract-based spatial statistics: voxelwise analysis of multi-subject diffusion data. *NeuroImage*. 2006;31:1487–505. <https://doi.org/10.1016/j.neuroimage.2006.02.024>.
5. Mori S, Oishi K, Jiang H, Jiang L, Li X, Akhter K, Hua K, Faria AV, Mahmood A, Woods R, Toga AW, Pike GB, Neto PR, Evans A, Zhang J, Huang H, Miller MI, van Zijl P, Mazziotta J. Stereotaxic white matter atlas based on diffusion tensor imaging in an ICBM template. *NeuroImage*. 2008;40:570–82. <https://doi.org/10.1016/j.neuroimage.2007.12.035>.
6. Chamberland M, Genc S, Tax CMW, Shastin D, Koller K, Raven EP, Cunningham A, Doherty J, van den Bree MBM, Parker GD, Hamandi K, Gray WP, Jones DK. Detecting microstructural deviations in individuals with deep diffusion MRI tractometry. *Nat Comput Sci*. 2021;1:598–606. <https://doi.org/10.1038/s43588-021-00126-8>.
7. Johansen-Berg H, Behrens TE. *Diffusion MRI*. London: Elsevier; 2013.
8. Harper C. The neuropathology of alcohol-specific brain damage, or does alcohol damage the brain? *J Neuropathol Exp Neurol*. 1998;57:101–10. <https://doi.org/10.1097/00005072-199802000-00001>.
9. Harper C, Corbett D. Changes in the basal dendrites of cortical pyramidal cells from alcoholic patients—a quantitative Golgi study. *J Neurol Neurosurg Psychiatry*. 1990;53:856–61. <https://doi.org/10.1136/jnnp.53.10.856>.
10. Miguel-Hidalgo JJ. Molecular neuropathology of astrocytes and oligodendrocytes in alcohol use disorders. *Front Mol Neurosci*. 2018;11:78. <https://doi.org/10.3389/fnmol.2018.00078>.
11. Assaf Y, Pasternak O. Diffusion tensor imaging (DTI)-based white matter mapping in brain research: a review. *J Mol Neurosci*. 2008;34:51–61. <https://doi.org/10.1007/s12031-007-0029-0>.

12. Pfefferbaum A, Adalsteinsson E, Rohlfing T, Sullivan EV. Diffusion tensor imaging of deep gray matter brain structures: effects of age and iron concentration. *Neurobiol Aging*. 2010;31:482–93. <https://doi.org/10.1016/j.neurobiolaging.2008.04.013>.
13. Garcia-Hernandez R, Cerdán Cerdá A, Trouve Carpena A, Drakesmith M, Koller K, Jones DK, Canals S, De Santis S. Mapping microglia and astrocyte activation in vivo using diffusion MRI. *Sci Adv*. 2022;8:eabq2923. <https://doi.org/10.1126/sciadv.abq2923>.
14. Sullivan EV, Pfefferbaum A. Neurocircuitry in alcoholism: a substrate of disruption and repair. *Psychopharmacology*. 2005;180:583–94. <https://doi.org/10.1007/s00213-005-2267-6>.
15. De Santis S, Bach P, Perez-Cervera L, Cosa-Linan A, Weil G, Vollstadt-Klein S, Hermann D, Kiefer F, Kirsch P, Ciccocioppo R, Sommer WH, Canals S. Microstructural white matter alterations in men with alcohol use disorder and rats with excessive alcohol consumption during early abstinence. *JAMA Psychiatry*. 2019a;76:749–58. <https://doi.org/10.1001/jamapsychiatry.2019.0318>.
16. De Santis S, Sommer WH, Canals S. Detecting alcohol-induced brain damage noninvasively using diffusion tensor imaging. *ACS Chem Neurosci*. 2019b;10:4187–9. <https://doi.org/10.1021/acchemneuro.9b00481>.
17. Cosa A, Moreno A, Pacheco-Torres J, Ciccocioppo R, Hyytiä P, Sommer WH, Moratal D, Canals S. Multi-modal MRI classifiers identify excessive alcohol consumption and treatment effects in the brain: multi-modal imaging biomarkers. *Addict Biol*. 2017;22:1459–72. <https://doi.org/10.1111/adb.12418>.
18. Rane RP, de Man EF, Kim J, Görgen K, Tschorn M, Rapp MA, Banaschewski T, Bokde AL, Desrivieres S, Flor H, Grigis A, Garavan H, Gowland PA, Brühl R, Martinot J-L, Martinot M-LP, Artiges E, Nees F, Papadopoulos Orfanos D, Lemaitre H, Paus T, Poustka L, Fröhner J, Robinson L, Smolka MN, Winterer J, Whelan R, Schumann G, Walter H, Heinz A, Ritter K, IMAGEN Consortium. Structural differences in adolescent brains can predict alcohol misuse. *eLife*. 2022;11:e77545. <https://doi.org/10.7554/eLife.77545>.
19. Pfefferbaum A, Rosenbloom M, Rohlfing T, Sullivan EV. Degradation of association and projection white matter systems in alcoholism detected with quantitative fiber tracking. *Biol Psychiatry*. 2009;65:680–90. <https://doi.org/10.1016/j.biopsych.2008.10.039>.
20. Pérez-Ramírez Ú, López-Madrona VJ, Pérez-Segura A, Pallarés V, Moreno A, Ciccocioppo R, Hyytiä P, Sommer WH, Moratal D, Canals S. Brain Network Allostasis after Chronic Alcohol Drinking Is Characterized by Functional Dedifferentiation and Narrowing. *J Neurosci*. 2022;42(21):4401–13. <https://doi.org/10.1523/JNEUROSCI.0389-21.2022>. Epub 2022 Apr 18. PMID: 35437279; PMCID: PMC9145238.
21. Spindler C, Mallien L, Trautmann S, Alexander N, Muehlhan M. A coordinate-based meta-analysis of white matter alterations in patients with alcohol use disorder. *Transl Psychiatry*. 2022;12:40. <https://doi.org/10.1038/s41398-022-01809-0>.
22. Pfefferbaum A, Zahr NM, Mayer D, Rohlfing T, Sullivan EV. Dynamic responses of selective brain white matter fiber tracts to binge alcohol and recovery in the rat. *PLoS One*. 2015;10:e0124885. <https://doi.org/10.1371/journal.pone.0124885>.
23. De Santis S, Cosa-Linan A, Garcia-Hernandez R, Dmytrenko L, Vargova L, Vorisek I, Stopponi S, Bach P, Kirsch P, Kiefer F, Ciccocioppo R, Sykova E, Moratal D, Sommer WH, Canals S. Chronic alcohol consumption alters extracellular space geometry and transmitter diffusion in the brain. *Sci Adv*. 2020;6:eaba0154. <https://doi.org/10.1126/sciadv.aba0154>.
24. Wang J, Fan Y, Dong Y, Ma M, Ma Y, Dong Y, Niu Y, Jiang Y, Wang H, Wang Z, Wu L, Sun H, Cui C. Alterations in brain structure and functional connectivity in alcohol dependent patients and possible association with impulsivity. *PLoS One*. 2016;11:e0161956. <https://doi.org/10.1371/journal.pone.0161956>.
25. Ji J, Maren S. Hippocampal involvement in contextual modulation of fear extinction. *Hippocampus*. 2007;17:749–58. <https://doi.org/10.1002/hipo.20331>.
26. Daviet R, Aydogan G, Jagannathan K, Spilka N, Koellinger PD, Kranzler HR, Nave G, Wetherill RR. Associations between alcohol consumption and gray and white matter volumes in the UK Biobank. *Nat Commun*. 2022;13:1175. <https://doi.org/10.1038/s41467-022-28735-5>.

27. Kantarci K, Petersen RC, Boeve BF, Knopman DS, Weigand SD, O'Brien PC, Shiung MM, Smith GE, Ivnik RJ, Tangalos EG, Jack CR. DWI predicts future progression to Alzheimer disease in amnesic mild cognitive impairment. *Neurology*. 2005;64:902–4. <https://doi.org/10.1212/01.WNL.0000153076.46126.E9>.
28. Chanraud S, Leroy C, Martelli C, Kostogianni N, Delain F, Aubin H-J, Reynaud M, Martinot J-L. Episodic memory in detoxified alcoholics: contribution of grey matter microstructure alteration. *PLoS One*. 2009;4:e6786. <https://doi.org/10.1371/journal.pone.0006786>.
29. Somkuwar SS, Villalpando EG, Quach LW, Head BP, McKenna BS, Scadeng M, Mandyam CD. Abstinence from ethanol dependence produces concomitant cortical gray matter abnormalities, microstructural deficits and cognitive dysfunction. *Eur Neuropsychopharmacol*. 2021;42:22–34. <https://doi.org/10.1016/j.euroneuro.2020.11.010>.
30. Alhassoon OM, Sorg SF, Taylor MJ, Stephan RA, Schweinsburg BC, Stricker NH, Gongvatana A, Grant I. Callosal white matter microstructural recovery in abstinent alcoholics: a longitudinal diffusion tensor imaging study. *Alcohol Clin Exp Res*. 2012;36:1922–31. <https://doi.org/10.1111/j.1530-0277.2012.01808.x>.
31. Pfefferbaum A, Rosenbloom MJ, Chu W, Sassoon SA, Rohlfing T, Pohl KM, Zahr NM, Sullivan EV. White matter microstructural recovery with abstinence and decline with relapse in alcohol dependence interacts with normal ageing: a controlled longitudinal DTI study. *Lancet Psychiatry*. 2014;1:202–12. [https://doi.org/10.1016/S2215-0366\(14\)70301-3](https://doi.org/10.1016/S2215-0366(14)70301-3).
32. Witkiewitz K, Marlatt GA. Modeling the complexity of post-treatment drinking: it's a rocky road to relapse. *Clin Psychol Rev*. 2007;27:724–38. <https://doi.org/10.1016/j.cpr.2007.01.002>.
33. He J, Crews FT. Increased MCP-1 and microglia in various regions of the human alcoholic brain. *Exp Neurol*. 2008;210(2):349–58. <https://doi.org/10.1016/j.expneurol.2007.11.017>. Epub 2007 Dec 3. PMID: 18190912; PMCID: PMC2346541.
34. Verplaetse TL, Cosgrove KP, Tanabe J, McKee SA. Sex/gender differences in brain function and structure in alcohol use: a narrative review of neuroimaging findings over the last 10 years. *J Neurosci Res*. 2021;99:309–23. <https://doi.org/10.1002/jnr.24625>.
35. Zahr NM, Lenart AM, Karpf JA, Casey KM, Pohl KM, Sullivan EV, Pfefferbaum A. Multimodal imaging reveals differential brain volumetric, biochemical, and white matter fiber responsivity to repeated intermittent ethanol vapor exposure in male and female rats. *Neuropharmacology*. 2020;170:108066. <https://doi.org/10.1016/j.neuropharm.2020.108066>.
36. Monnig MA, Yeo RA, Tonigan JS, McCrady BS, Thoma RJ, Sabbineni A, Hutchison KE. Associations of white matter microstructure with clinical and demographic characteristics in heavy drinkers. *PLoS One*. 2015;10:e0142042. <https://doi.org/10.1371/journal.pone.0142042>.
37. Toschi N, Gisbert RA, Passamonti L, Canals S, De Santis S. Multishell diffusion imaging reveals sex-specific trajectories of early white matter degeneration in normal aging. *Neurobiol Aging*. 2020;86:191–200. <https://doi.org/10.1016/j.neurobiolaging.2019.11.014>.
38. Rivas-Grajales AM, Sawyer KS, Karmacharya S, Papadimitriou G, Camprodon JA, Harris GJ, Kubicki M, Oscar-Berman M, Makris N. Sexually dimorphic structural abnormalities in major connections of the medial forebrain bundle in alcoholism. *Neuroimage*. 2018;19:98–105. <https://doi.org/10.1016/j.nicl.2018.03.025>.
39. Sawyer KS, Maleki N, Papadimitriou G, Makris N, Oscar-Berman M, Harris GJ. Cerebral white matter sex dimorphism in alcoholism: a diffusion tensor imaging study. *Neuropsychopharmacology*. 2018;43:1876–83. <https://doi.org/10.1038/s41386-018-0089-6>.
40. De Santis S, Drakesmith M, Bells S, Assaf Y, Jones DK. Why diffusion tensor MRI does well only some of the time: variance and covariance of white matter tissue microstructure attributes in the living human brain. *NeuroImage*. 2014;89:35–44. <https://doi.org/10.1016/j.neuroimage.2013.12.003>.
41. Harper C, Kril J. Patterns of neuronal loss in the cerebral cortex in chronic alcoholic patients. *J Neurol Sci*. 1989;92:81–9. [https://doi.org/10.1016/0022-510X\(89\)90177-9](https://doi.org/10.1016/0022-510X(89)90177-9).

42. Koike H, Mori K, Misu K, Hattori N, Ito H, Hirayama M, Sobue G. Painful alcoholic polyneuropathy with predominant small-fiber loss and normal thiamine status. *Neurology*. 2001;56:1727–32. <https://doi.org/10.1212/WNL.56.12.1727>.
43. Pfefferbaum A, Sullivan EV. Disruption of brain white matter microstructure by excessive intracellular and extracellular fluid in alcoholism: evidence from diffusion tensor imaging. *Neuropsychopharmacology*. 2005;30:423–32. <https://doi.org/10.1038/sj.npp.1300623>.
44. Assaf Y, Basser PJ. Composite hindered and restricted model of diffusion (CHARMED) MR imaging of the human brain. *NeuroImage*. 2005;27:48–58. <https://doi.org/10.1016/j.neuroimage.2005.03.042>.
45. Barazany D, Basser PJ, Assaf Y. In vivo measurement of axon diameter distribution in the corpus callosum of rat brain. *Brain*. 2009;132:1210–20. <https://doi.org/10.1093/brain/awp042>.
46. Cercignani M, Symms MR, Schmierer K, Boulby PA, Tozer DJ, Ron M, Tofts PS, Barker GJ. Three-dimensional quantitative magnetisation transfer imaging of the human brain. *NeuroImage*. 2005;27:436–41. <https://doi.org/10.1016/j.neuroimage.2005.04.031>.
47. Zhang H, Schneider T, Wheeler-Kingshott CA, Alexander DC. NODDI: practical in vivo neurite orientation dispersion and density imaging of the human brain. *NeuroImage*. 2012;61:1000–16. <https://doi.org/10.1016/j.neuroimage.2012.03.072>.

